PB-230 842

MATHEMATICAL MODELING OF SORPTION KINETICS IN FINITE AND INFINITE-BATH SYSTEMS

Francis A. DiGiano, et al

Michigan University
Ann Arbor, Michigan

April 1969

DISTRIBUTED BY:

NTIS
National Technical Information Service
U. S. DEPARTMENT OF COMMERCE
5285 Port Royal Road, Springfield Va. 22151

WP-00706

PB 230 842
T-69-1

THE UNIVERSITY OF MICHIGAN

DEPARTMENT OF CIVIL ENGINEERING
Division of Sanitary and Water Resources Engineering

Mathematical Modeling of Sorption Kinetics in Finite and Infinite-Bath Systems

FRANCIS A. DI GIANO
and
WALTER J. WEBER, JR.

April 1969
Technical Publication
Research Project WP-00706
Federal Water Pollution Control Administration
United States Department of Interior

OFFICE OF RESEARCH ADMINISTRATION · ANN ARBOR

Reproduced by
NATIONAL TECHNICAL
INFORMATION SERVICE
U. S. Department of Commerce
Springfield VA 22151

207

THE UNIVERSITY OF MICHIGAN
DEPARTMENT OF CIVIL ENGINEERING

Mathematical Modeling of Sorption Kinetics in Finite and Infinite-Bath Systems

Francis A. DiGiano
and
Walter J. Weber, Jr.

Federal Water Pollution Control Administration
United States Department of Interior
Grant No. WP-00706
Washington, D.C.

TABLE OF CONTENTS

Page

ACKNOWLEDGMENTS.................................... ii

LIST OF TABLES..................................... vi

LIST OF ILLUSTRATIONS.............................. vii

NOMENCLATURE....................................... xiv

LIST OF APPENDICES................................. xix

I. INTRODUCTION.................................... 1

2. ADSORPTION EQUILIBRIA AND MASS TRANSFER IN FIXED-BED ABSORBERS........................... 4

  Equilibrium Model................................ 6

  Mass Transfer Coefficients....................... 9

  Chemical Reaction Model.......................... 11

  Summary of Column Calculations................... 14

3. MODELING CONSIDERATIONS IN BATCH REACTORS....... 16

  Adsorption Reaction.............................. 17

  Boundary Conditions.............................. 18

  Summary of Batch Reactor Modeling................ 20

4. EQUILIBRIUM ADSORPTION.......................... 22

  Experimental Materials........................... 22

  Experimental Procedure........................... 27

  Results and Discussion........................... 28

  Phenol, PNP, DNP Anion Equilibria................ 30

TABLE OF CONTENTS (continued)

Page

Accompanying pH Increases.................... 35

DNOSBP Equilibria - Effect of Phosphate Buffer and $NaHCO_3$.......................... 37

DNOCHP and 2-Octylbenzenesulfonate Equilibria. 40

Summary.................................... 43

5. FINITE-BATH KINETICS...................... 45

Pore Resistance Controlling Model-Isotherm Approximation............................. 45

Combined Internal and External Resistance Controlling................................ 52

Limitations of Irreversible Immobilization and Quasi-Steady State Assumptions........... 58

Sensitivity Test for Simplified Kinetic Model. 68

Experimental Materials and Procedure.......... 71

Experimental Results - Alkylbenzenesulfonates. 72

Experimental Results - DNOCHP and DNOSBP...... 85

Experimental Results - DNP (A) and DNP (N).... 92

Experimental Results - Phenol and PNP......... 99

Initial Carbon-Solute Interaction and Stirring Speed Studies.............................. 105

Simple Film Diffusion Model.................. 105

Summary of Finite-Bath Kinetics.............. 112

TABLE OF CONTENTS (continued)

Page

6. INFINITE-BATH KINETICS........................ 117

Experimental Apparatus........................ 117

Experimental Procedure........................ 119

Solutes.................................... 120

Sensitivity of Apparatus...................... 121

Film and Pore Resistances in Series with Simultaneous Non-Linear Adsorption........... 121

Selection of Grid Size........................ 125

Experimental Results - PNP (N)................ 128

Experimental Results - PNP (A)................ 137

Experimental Results - DNP (N)................ 148

Experimental Results - DNP (A)................ 153

Summary of Infinite-Bath Kinetics............. 156

7. CONCLUSIONS AND FURTHER RESEARCH.............. 162

Further Research.............................. 164

LIST OF REFERENCES............................. 185

LIST OF TABLES

Table	Title	Page
4-1	Properties of Columbia LC Carbon	23
4-2	Analytical Data and Ionization Constants for Solutes Investigated	25
4-3	Langmuir Constants, b and Q, for the Neutral and Anion Species of Phenol, PNP and DNP	34
4-4	Summary of Equilibrium Adsorption Data for the Anions of DNP, DNOSBP, DNOCHP and 2-Octylbenzenesulfonate	44
5-1	Calculated Values of V_p for Selected Isotherms and Equilibrium Positions	63
5-2	Results of Alkylbenzenesulfonate Investigations	83
5-3	Calculated Film and Pore Diffusion Model Parameters from DNOSBP Experiment	88
5-4	Results of DNOCHP and DNOSBP Investigations	91
5-5	Results of DNP Investigations	100
5-6	The Effect of Stirring Speed on the Transfer Coefficient, k_f, and Fractional Approach to Equilibrium	110
5-7	The Effect of External Particle Surface Area on the Transfer Coefficient, k_f, for PNP (N)	110
5-8	Application of Simple Film Diffusion Model to Phenol (N) and DNP (N) Rates of Adsorption	111
6-1	Results of Infinite-Bath Investigations	159

LIST OF ILLUSTRATIONS

Figure	Title	Page
2-1	Activity Within Column Segment ΔV_1 of Fixed-Bed Adsorber.	5
4-1	Pore Size Distribution for Columbia LC Carbon.	24
4-2	Equilibrium Adsorption of Neutral Species of Phenol, PNP and DNP.	29
4-3	Determination of Langmuir Model Parameters for DNP (N).	31
4-4	Equilibrium Adsorption of Anion Species of Phenol, PNP and DNP	32
4-5	Effect of Carbon Dosage on Equilibrium pH for DNP (A).	36
4-6	Effect of pH and Phosphate Buffer on Equilibrium Adsorption of DNP (A).	38
4-7	Effect of Phosphate Buffer and $NaHCO_3$ on Equilibrium Adsorption DNOSBP.	39
4-8	Equilibrium Adsorption of DNOCHP.	40
4-9	Equilibrium Adsorption of 2-Octylbenzenesulfonate.	42
5-1	Frontal Position (r_o/a) as a Function of Dimensionless Time, T.	50
5-2	Dimensionless Solution Concentration, ϕ, as a Function of Dimensionless Time, T, for ϕ_e Values of 0.5, 0.2 and 0.0.	51
5-3	Frontal Position (r_o/a) as a Function of Film Diffusion Parameter $G(r_o/a)$ for ϕ_e Values of 0.5, 0.2 and 0.0.	55

LIST OF ILLUSTRATIONS (continued)

Figure	Title	Page
5-4	Dimensionless Solution Concentration, ϕ, as a Function of Film Diffusion Parameter $G(r_o/a)$ for ϕ_e Values of 0.5, 0.2 and 0.0.	56
5-5	Effect of Transfer Coefficient, k_f, on Dimensionless Rate of Adsorption for Combined Film and Pore Diffusion Model.	57
5-6	Hypothetical Isotherms to Test Simplified Kinetic Model. $\alpha = 10000$ and $\beta = 5$, 30 and 50.	61
5-7	Hypothetical Isotherms to Test Simplified Kinetic Model. $\alpha = 20000$ and $\beta = 5$, 30 and 50.	62
5-8	Comparison of Models Using Irreversible Immobilization and Actual Non-Linear Isotherm for $\alpha = 10000$ and $\phi_e = 0.1$.	65
5-9	Comparison of Models Using Irreversible Immobilization and Actual Non-Linear Isotherm for $\alpha = 20000$ and $\phi_e = 0.1$.	66
5-10	Comparison of Models Using Irreversible Immobilization and Actual Non-Linear Isotherm for $\phi_e = 0.2$ and $\beta = 30$.	67
5-11	Sensitivity of Simplified Model for $\alpha = 10000$, $\phi_e = 0.1$ and $\beta = 5$, 30 and 50.	70
5-12	Simplified Pore Diffusion Model. Data for 2-Octylbenzenesulfonate. ($C_{F_o} = 0.4 \times 10^{-4}$ $\underline{M}$, W = 0.1 gm/l, a = 0.0136 cm, 1250 rpm)	73
5-13	Model for Pore Diffusion with Simultaneous Non-Linear Adsorption. Data for 2-Octylbenzenesulfonate.	74

LIST OF ILLUSTRATIONS (continued)

Figure	Title	Page
5-14	Simplified Film and Pore Diffusion Model. Data for 2-Octylbenzenesulfonate.	76
5-15	Comparison of Models Using Irreversible Immobilization and Non-Linear Isotherm. Data for 2-Octylbenzenesulfonate.	77
5-16	Linearized Form of Film and Pore Diffusion Model. Data for 2-Hexyl- and 2-Decylbenzenesulfonate. ($C_{F_o} = 0.4 \times 10^{-4}$ $\underline{M}$, W = 0.1 gm/l, a = 0.0136 cm, 1250 rpm)	78
5-17	Model for Pore Diffusion with Simultaneous Non-Linear Adsorption. Data for 2-Hexyl- and 2-Decylbenzenesulfonate.	80
5-18	Calculated Rate Curves for Film and Pore Diffusion Model. Data for 2-Hexyl- and 2-Decylbenzenesulfonate.	81
5-19	Linearized Form of Film and Pore Diffusion Model. Data for DNOCHP. ($C_{F_o} = 1.0 \times 10^{-4}$ $\underline{M}$, $\phi_e = 0.2$, a = 0.0105 cm, 1250 rpm)	86
5-20	Linearized Form of Film and Pore Diffusion Model. Data for DNOSBP. ($C_{F_o} = 1.0 \times 10^{-4}$ $\underline{M}$, $\phi_e = 0.2$, a = 0.0105 cm, 1250 rpm)	87
5-21	Model for Pore Diffusion with Simultaneous Non-Linear Adsorption. Data for DNOCHP and DNOSBP.	89
5-22	Linearized Form of Film and Pore Diffusion Model. Data for DNP (A). ($C_{F_o} = 1.0 \times 10^{-4}$ $\underline{M}$, $\phi_e = 0.2$, a = 0.0105 cm, 1250 rpm)	93
5-23	Model for Pore Diffusion with Simultaneous Non-Linear Adsorption. Data for DNP (A).	93

LIST OF ILLUSTRATIONS (continued)

Figure Title Page

5-24 Calculated Rate Curves for Film and Pore Diffusion Model. Data for DNOCHP, DNOSBP and DNP (A). 94

5-25 Effect of Phosphate Buffer System on the Rate of Adsorption for DNP (A). (C_{F_o} = 1.0×10^{-4} M , W = 0.16 gm/l, a = 0.0136 cm, 1250 rpm) 95

5-26 Linearized Form of Film and Pore Diffusion Model. Data for Buffered and Unbuffered DNP (A) Systems. 95

5-27 Rates of Adsorption for DNP (N). (C_{F_o} = 1.0×10^{-4} M , a = 0.025 cm, 1250 rpm) 97

5-28 Linearized Form of Film and Pore Diffusion Model. Data for DNP (N) with ϕ_e of 0.5 and 0.2. 98

5-29 Rate of Adsorption for Phenol (A). (C_{F_o} = 1.0×10^{-4} M , ϕ_e = 0.3, a = 0.0.25 cm, 1250 rpm) 102

5-30 Model for Pore Diffusion with Simultaneous Non-Linear Adsorption. Data for Phenol (A). 102

5-31 Rate of Adsorption for PNP (A). (C_{F_o} = 1.0×10^{-4} M , ϕ_e = 0.3, a = 0.025 cm, 1250 rpm) 103

5-32 Rates of Adsorption for Phenol (N) and PNP (N). (C_{F_o} = 1.0×10^{-4} M , ϕ_e = 0.2, a = 0.025 cm, 1250 rpm) 104

5-33 Simple Film Diffusion Model. Data for DNP (N), PNP (N) and Phenol (N). (C_{F_o} = 1.0×10^{-4} M , ϕ_e = 0.2, a = 0.025 cm, 1250 rpm) 107

LIST OF ILLUSTRATIONS (continued)

Figure	Title	Page
5-34	Simple Film Diffusion Model. Data for PNP (A). ($C_{F_o} = 1.0 \times 10^{-4}$ $\underline{M}$, ϕ_e = 0.3, a = 0.025 cm, 1250 rpm)	113
6-1	Schematic Diagram of Infinite-Bath Apparatus.	118
6-2	Comparison of Finite Difference and Analytical Solutions for $R = 10^4$ and $R = 10^5$.	127
6-3	Dimensionless Surface Flux - Dimensionless Time Profiles for PNP (N) and γ Values of 2.5, 5, 7.5 and 10.	129
6-4	Dimensionless Uptake, $M\theta$, as a Function of Dimensionless Time, θ , for PNP (N) and γ Values of 2.5, 5, 7.5 and 10.	131
6-5	Selection of γ for PNP (N) - Experiment A ($C_{F_o} = 1.0 \times 10^{-4}$ $\underline{M}$, W = 0.15 gm/l, a = 0.025 cm, 1250 rpm)	132
6-6	Calculated and Experimental Surface Flux Versus Time. Data for PNP (N) - Experiment A and γ Values of 5 and 2.5.	134
6-7	Calculated and Experimental Fractional Uptakes of PNP (N) - Experiments A, B and C.	136
6-8	Calculated and Experimental Fractional Uptakes of PNP (N). ($C_{F_o} = 1.0 \times 10^{-4}$ $\underline{M}$, W = 0.15 gm/l, a = 0.0136 cm, 1250 rpm)	138
6-9	Calculated and Experimental Surface Flux Versus Time. Data for PNP (N). (C_{F_o} = 1.0×10^{-4} $\underline{M}$, W = 0.15 gm/l, a = 0.0136 cm, 1250 rpm)	139

LIST OF ILLUSTRATIONS (continued)

Figure	Title	Page
6-10	Effect of Stirring Speed on the Rate of Uptake of PNP. ($C_{F_0} = 1.0 \times 10^{-4}$ $\underline{M}$, a = 0.025 cm)	140
6-11	Dimensionless Surface Flux - Dimensionless Time Profiles for PNP (A) and γ Values of 12, 35 and 40.	141
6-12	Dimensionless Uptake, $M\theta$, as a Function of Dimensionless Time, θ, for PNP (A) and γ Values of 12, 25 and 40.	142
6-13	Comparison of Dimensionless Surface Flux - Dimensionless Time Profiles for PNP (N) and PNP (A).	144
6-14	Calculated and Experimental Surface Flux Versus Time. Data for PNP (A). ($C_{F_0} = 0.5 \times 10^{-4}$ $\underline{M}$, W = 0.25 gm/l, a = 0.0136 cm, 1250 rpm)	145
6-15	Calculated and Experimental Fractional Uptakes of PNP (A). Comparison of $\gamma = 17$ and $\gamma = 25$.	146
6-16	Selection of γ. Data for PNP (A). ($C_{F_0} = 0.5 \times 10^{-4}$ $\underline{M}$, W = 0.25 gm/l, a = 0.025 cm, 1250 rpm)	147
6-17	Effect of Stirring Speed on the Rate of Uptake of PNP (A). ($C_{F_0} = 0.5 \times 10^{-4}$ $\underline{M}$, W = 0.25 gm/l, a = 0.025 cm)	149
6-18	Calculated and Experimental Surface Flux Versus Time. Data for PNP (A). ($C_{F_0} = 0.5 \times 10^{-4}$ $\underline{M}$, W = 0.025 gm/l, a = 0.025 cm, 600 rpm)	150
6-19	Dimensionless Surface Flux - Dimensionless Time Profiles for DNP (N) and γ Values of 4, 8 and 12.	151

LIST OF ILLUSTRATIONS (continued)

Figure	Title	Page
6-20	Dimensionless Uptake, M_θ, as a Function of Dimensionless Time, θ, for DNP (N) and γ Values of 4, 8 and 12.	152
6-21	Calculated and Experimental Fractional Uptakes of DNP (N). ($C_{F_o} = 1.0 \times 10^{-4}$ $\underline{M}$, W = 0.06 gm/l, a = 0.0136 cm, 1250 rpm)	154
6-22	Effect of Stirring Speed on the Rate of Uptake of DNP (N). ($C_{F_o} = 1.0 \times 10^{-4}$ $\underline{M}$, W = 0.15 gm/l, a = 0.025 cm)	155
6-23	Calculated and Experimental Uptakes of DNP (A), Buffered and Unbuffered Systems. ($C_{F_o} = 0.5 \times 10^{-4}$ $\underline{M}$, W = 0.25 gm/l, a = 0.0136 cm, 1250 rpm)	157

NOMENCLATURE

ROMAN

Symbol	Description and Units
a	Particle Radius (cm)
a'	Dummy Variable
A	Cross Sectional Area of Fixed Bed Adsorber (cm^2)
A_o	Particle Surface Area (cm^2)
A^o	Angstrom (10^{-8}cm)
b	Langmuir Equilibrium Energy Constant (liters/mole)
C_F	Fluid Phase Concentration (moles/liter)
C_{F_e}	Equilibrium Fluid Phase Concentration (moles/liter)
C_{F_i}	Interfacial Fluid Phase Concentration (moles/liter)
C_{F_o}	Initial or Inlet Feed Fluid Phase Concentration (moles/liter)
C_{F_1}	Fluid Phase Concentration in Finite Bath (moles/liter)
C_F^*	Imaginary Moving Phase Concentration in Equilibrium with C_S (moles/liter)
C^*	Limiting Fluid Phase Concentration for Application of Simple Film Model (moles/liter)
C_S	Solid Phase Concentration (moles/liter)
$\overline{C}_S$	Average Solid Phase Concentration (moles/liter)
C_{S_i}	Interfacial Solid Phase Concentration (moles/liter)

NOMENCLATURE (continued)

Symbol	Description and Units
C_{S_o}	Solid Phase Concentration in Equilibrium with Inlet Fluid Phase Concentration, C_{F_o}, (Moles/Liter)
D	Pore Diffusion Coefficient (cm^2/sec)
D_A	Apparent Diffusivity (cm^2/sec)
D_G	Ratio of Solid Phase and Fluid Phase Concentrations at Saturation $\frac{C_{S_o}(1-\varepsilon)}{C_{F_o}\varepsilon}$
D_p	Particle Diameter (cm)
F	Rate of Movement of Solute in moles/sec
$F(\frac{r_o}{a})$	Simplified Pore Diffusion Model Function
$G(\frac{r_o}{a})$	Film Diffusion Parameter for Simplified and Pore Diffusion Model
k	Langmuir Forward Rate Constant [cm^3/(mole-sec)]
k_f	Liquid Phase Mass Transfer Coefficient (cm/sec)
k_s	Stationary Phase Mass Transfer Coefficient (cm/sec)
K_f	Overall Mass Transfer Coefficient (cm/sec)
m	Average Slope of Adsorption Isotherm
$m\mu$	Millimicrons
M_θ	Dimensionless Uptake of Solute
M_t	Uptake of Solute (μ moles/cm^2)
M_∞	Equilibrium Solute Uptake (μ moles/cm^2)

NOMENCLATURE (continued)

Symbol	Description and Units
M_t/M_∞	Fractional Approach to Equilibrium
N	Diffusion Flux [moles/(cm^2 - sec)]
N_o	Surface Diffusion Flux [moles/(cm^2 - sec)]
pK_a	Dissociation Constant
Q	Ultimate Capacity of the Adsorbent Langmuir "monolayer" Capacity Constant (m mol/gm)
r	Radius Parameter (cm)
R	Dimensionless Slope of Linear Isotherm or Instantaneous Slope of Non-Linear Isotherm
$\frac{r_o}{a}$	Dimensionless Frontal Position
r_o	Frontal Position (cm)
S	Surface Concentration (moles/liter)
S_o	Surface Area to Volume Ratio (cm^{-1})
t	Time
t^*	Limiting Experimental Time for Application of Simple Film Model
T	Dimensionless Time Parameter $T = \frac{C_{F_o} Dt}{Sa^2}$
v_o	Volumetric Flow Rate (cm^3/sec)
V_1	Volume Position in Fixed Bed Absorber (cm^3)
V	Volume Served Per Particle $V = \frac{\rho}{w} \frac{4}{3} \pi a^3$
V_p	Dimensionless Inverse Volume Served per Particle $V_p = 3 \frac{w}{\rho}$
w	Freundlich Isotherm constant

NOMENCLATURE (continued)

Symbol	Description and Units
W	Carbon Dosage (gm/liter)
X	Solid Phase Concentration (m mol/gm)
y	Exponential Factor of Freundlich Isotherm
z	Distance Position on Fixed Bed Absorber (cm)
Greek Symbol	
α	Dimensionless Langmuir "monolayer coverage" $\alpha = Q \frac{\rho}{C_{F_o}}$
β	Dimensionless Langmuir Equilibrium Energy Constant
γ	Dimensionless Ratio of Film to Pore Diffusion Parameter $\gamma = \frac{k_f a}{D}$
$\Delta \theta$	Finite Difference Time Step
$\Delta \xi$	Finite Difference Distance Step
ϵ	Fractional Void Space
η	Assumed Concentration Function
θ	Dimensionless Time Parameter $\theta = \frac{Dt}{a^2}$
κ	Generalized Rate Coefficient (sec^{-1})
λ	Dimensionless Equilibrium Modulus $\lambda = (1 + bC_{F_o})^{-1}$
ξ	Dimensionless Radial Distance $\xi = (\frac{r}{a})$
ρ	Particle Density (gm/cm^3)

NOMENCLATURE (continued)

Symbol	Description and Units
σ	Dimensionless Solid Phase Concentration $\sigma = \frac{\alpha \beta \phi}{1 + \beta \phi}$
σ_e	Dimensionless Equilibrium Solid Phase Concentration
σ_m	Dimensionless Solid Phase Concentration at Distance Step m
τ	Dimensionless Time Parameter $\tau = \frac{\kappa}{D_G} t$
ϕ	Dimensionless Fluid Phase Concentration C_F/C_{F_o}
ϕ_m	Dimensionless Fluid Phase Concentration at Distance Step m
ϕ_e	Dimensionless Equilibrium Fluid Phase Concentration
ϕ^*	Lowest Observed Experimental Dimensionless Fluid Phase Concentration
ψ_m	Roots of Triginometric Function
ω	Dimensionless Solid Phase Concentration C_S/C_{S_o}
∇^2	Scalar Laplacian Operator

LIST OF APPENDICES

Appendix	Title	Page
A	IMPLICIT FINITE DIFFERENCE SOLUTION TO TRANSIENT DIFFUSION WITH NON LINEAR ADSORPTION...............................	168
B	COMPUTER PROGRAM FOR EXPLICIT FINITE DIFFERENCE SOLUTION TO FILM AND PORE DIFFUSION WITH NON LINEAR ADSORPTION - INFINITE BATH............................	174
C	CORRELATION OF MASS TRANSFER COEFFICIENTS	176

CHAPTER I

INTRODUCTION

The Advanced Waste Treatment (AWTR) Program was initiated in 1960 (33) for the purpose of developing new wastewater treatment methods which would permit direct wastewater reuse. To date, the practical impact of this program has been limited; however, its objectives will surely be more fully recognized as the needs for pollution control and clean water supplies rapidly converge. Among the methods of treatment being investigated is adsorption on activated carbon. Research efforts, ranging from laboratory to pilot plant scale, have shown this to be a feasible way for removing organic contaminants which escape conventional wastewater treatment (3,5,14,21,28).

For the adsorption process to become an effective and integral part of wastewater treatment, design parameters must be defined. Ideally, as in other unit operations familiar to the chemical engineer, mathematical modeling of the adsorption reactor would enable optimization of design. But unfortunately, mathematical description in an actual wastewater treatment operation is beset with difficulties originating from unknown and varied waste composition. That is, a rather complex boundary condition exists at the inlet to the adsorber unit. Moreover, the rate controlling step of mass transfer and equilibrium phase distributions of waste components are difficult to analyze for the same reason.

The logical approach, then, to process evaluation is to systematically study the less complicated sub-systems involved. More specifically, an investigation of the adsorption of sorbates differing in size and charge could yield valuable information concerning the overall reactor performance when an unknown mixture of components is present.

Another system simplification results from examining sorbate-sorbent interaction in a batch rather than continuous flow reactor. Hydraulic complications, both experimental and theoretical are deemed unnecessary since the objective is to study the effect of sorbate character on mass transport through the internal carbon structure. In this sub-system, mathematical models for sorption kinetics may easily be developed. Adsorption equilibrium is necessarily involved since the observed rate of adsorption is really the result of simultaneous pore diffusion and adsorption on adjacent carbon surfaces. The latter process is usually considered to be controlled by local equilibrium conditions.

Experimental kinetic and equilibrium data for any sorbate can then be applied to the selected model. If data conforms to the model, a system constant, such as an effective pore diffusion coefficient, D, may be calculated. Thus, variations in adsorption rates, for molecules differing in size and charge, can be quantitatively established. Pore diffusion coefficients obtained for each sorbate may then be used as input to a model for a continuous flow system in which intraparticle diffusion is known to be all or part of the controlling resistance to mass transfer. Such a model, as applied recently by Keinath and Weber (22) in a study of fluidized carbon beds for removal of a pesticide waste, will be discussed in the next chapter.

Although a non-competing sorbate system has been considered thus far, extension of process evaluation to the more complicated, heterogeneous sorbate system may follow in a similar fashion. For example, total organic carbon (TOC) could be used as a measure of reactor performance. In addition, a common rate limiting mass transfer step for all components and a competitive equilibrium adsorption factor would have to be included in the model.

In this study, diffusion coefficients were obtained for a variety of sorbates differing in size and charge. But the methodology used, both experimental and mathematical, is actually more significant. Preliminary experimental observations confirmed the importance of mass transfer resistance at the liquid-solid interface in a rapidly stirred batch reactor. Thus, attention was focused on developing a model in which external mass transfer and pore diffusion, acting in series control the rate of adsorption.

A finite-bath system, in which bulk solution concentration decreases with time, offers the advantage of expedient data collection. However, it also complicates mathematical analysis, especially when non-linear adsorption and a film-pore diffusion mechanism of mass transfer are considered. This led to the application of irreversible immobilization and quasi-steady state assumptions in order to simplify the mathematical model.

In contrast, mathematical analysis is more straightforward in an infinite rather than a finite-bath system since bulk solution concentration remains constant throughout the kinetic experiment. However, a special apparatus is required to maintain this condition. When non-linear adsorption cannot be approximated by irreversible immobilization, and resistance to mass transfer at the surface of the particle and in the pores must be considered, the infinite-bath system provides the necessary simplifying condition.

Hopefully, mathematical modeling techniques presented in this study, for both finite and infinite-bath systems, will aid in the systematic study of adsorption behavior. Moreover, information gained from these sub-systems can then be applied to actual process design.

CHAPTER 2

ADSORPTION EQUILIBRIA AND MASS TRANSFER IN FIXED-BED ADSORBERS

Before discussing batch reactor kinetics, it is informative to briefly examine the general mathematical modeling formulations which may be used in a flow through system. Of particular interest are the predictions of concentration profiles and effluent curves for a fixed-bed adsorber. In this manner, the importance of both adsorption equilibria and mass transfer resistances, which in part are determined from batch reactor tests, become more apparent.

Beginning with the simplest model, which is commonly used to describe chromotographic separations in a sorption column or bed, the general mass balance for a given solute may be written:

RATE IN - RATE OUT + RATE OF REACTION = RATE OF ACCUMULATION

$$F\Big|_{V_1} - F\Big|_{V_1 + \Delta V_1} + 0 = \frac{d}{dt}\left(\epsilon C_F + (1 - \epsilon)C_S\right)\Delta V_1 \qquad (2\text{-}1)$$

Figure 2-1 illustrates the column segment over which the mass balance is made. In Equation 2-1, F is the total rate of movement of the solute in the mobile phase, V_1 the volume position in the bed, ΔV_1 the incremental volume over which the mass balance is made, ϵ the fractional void space, C_F, the fluid phase concentration of solute, C_S, the solid phase concentration and t, of course, is time. As indicated from Figure 1, the movement of solute in the mobile phase can occur by two mechanisms: convection and diffusion as shown by Equation 2-2.

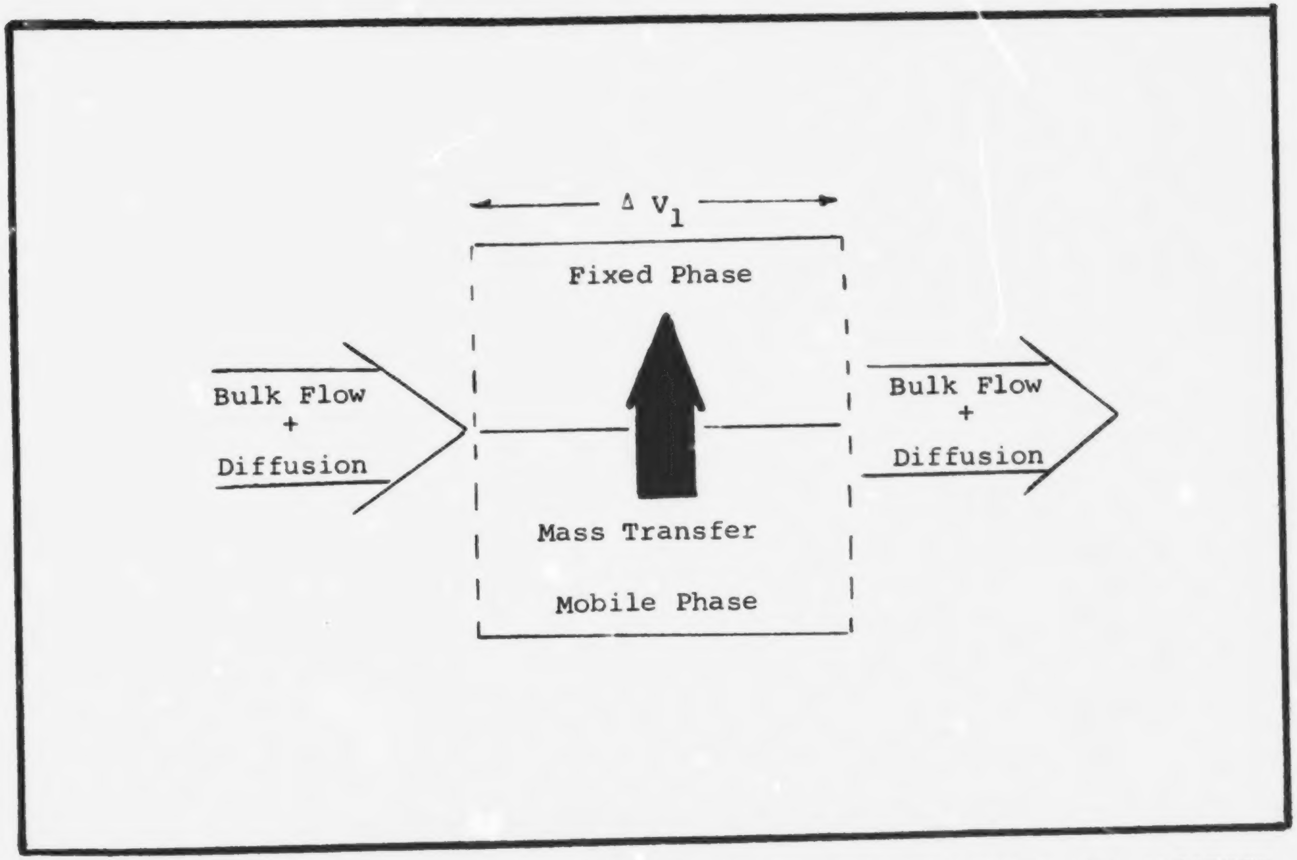
ΔV_1
Fixed Phase
Bulk Flow
+
Diffusion
Bulk Flow
+
Diffusion
Mass Transfer
Mobile Phase

FIGURE 2-1. ACTIVITY WITHIN COLUMN SEGMENT ΔV_1 OF FIXED-BED ADSORBER

$$F = v_o C_F - D_A A \frac{\partial C_F}{\partial z} \qquad (2\text{-}2)$$

where v_o is the volumetric flow rate, A the cross sectional area of the column, z the distance from the column inlet and D_A the apparent diffusivity of the solute in the system. As described by Lightfoot, et al. (26), the term D_A is actually a combination of molecular diffusivity and a dispersion coefficient accounting for back mixing and non-uniform velocity distribution.

Substituting Equation 2-2 into Equation 2-1, dividing through by ΔV_1 and taking the limit as ΔV_1 approaches zero yields Equation 2-3.

$$- v_o \frac{\partial C_F}{\partial V_1} + D_A A \frac{\partial^2 C_F}{\partial V_1^2} = \frac{\partial}{\partial t} (\epsilon C_F + (1 - \epsilon) C_S) \qquad (2\text{-}3)$$

Examination of this equation reveals that it is necessary to somehow express the dependent variable C_S in terms of C_F. Herein lies the essence of the modeling problem and the need for equilibrium and rate data.

EQUILIBRIUM MODEL

The simplest case to consider is that in which the effects of longitudinal dispersion and the resistance to transport across the interface between the solid and liquid phases are neglected. Thus, column behavior can be defined in terms of adsorption equilibrium relationships. Using the chain rule for derivatives, the right hand side of Equation 2-3 may be written for this case as

$$\frac{\partial}{\partial t} [\epsilon C_F + (1 - \epsilon) C_S] = \frac{\epsilon \partial C_F}{\partial t} + (1 - \epsilon) \frac{\partial C_S}{\partial C_F} \cdot \frac{\partial C_F}{\partial t} \qquad (2\text{-}4)$$

The term $\frac{\partial C_S}{\partial C_F}$ is thus the slope of the equilibrium curve, $f'(C_F)$. To solve for C_F as a function of time, t, and distance, z, the function is assumed to be of the form:

$$C_F = g\ (z - a't) \tag{2-5}$$

where a' is a constant which must be further defined. From Equation 2-5, the derivatives of C_F with respect to t and z are determined as follows:

$$\frac{\partial C_F}{\partial z} = \frac{\partial g}{\partial z} = \frac{\partial g}{\partial \eta} \cdot \frac{\partial \eta}{\partial z} \tag{2-6}$$

where $$\eta = z - a't \tag{2-7}$$

$$\frac{\partial \eta}{\partial z} = 1 \tag{2-8}$$

Therefore, $$\frac{\partial C_F}{\partial z} = g'\ (\eta) \tag{2-9}$$

$$\frac{\partial C_F}{\partial t} = g'\ (\eta) \cdot (-a') \tag{2-10}$$

Neglecting longitudinal dispersion and allowing the independent variable to be z, $(V_1 = Az)$, Equation 2-3 becomes:

$$v_o \frac{\partial C_F}{\partial z} = A\ [\ \epsilon + (1-\epsilon)\ f'(C_F)]\ \frac{\partial C_F}{\partial t} \tag{2-11}$$

Substituting Equations 2-9 and 2-10 into 2-11 eliminates g' and thus yields a':

$$a' = \frac{v_o}{A[\ \epsilon + (1-\epsilon)\ f'\ (C_F)]} \tag{2-12}$$

A time-distance variable may be defined for each value of concentration, C_F, by letting η be zero, or:

$$z = \frac{v_o \quad t}{A[\epsilon + (1-\epsilon)\ f'\ (C_F)]} \tag{2-13}$$

Taking the derivative of z with respect to t then gives the velocity of the particular concentration C_F moving down the column:

$$\left.\frac{dz}{dt}\right|_{C_F} = \frac{v_o}{A[\epsilon + (1-\epsilon)\ f'\ (C_F)]} \tag{2-14}$$

The Langmuir equilibrium adsorption expression is given in Equation 2-15

$$C_S = \frac{Q \rho b C_F}{1 + b C_F} \tag{2-15}$$

where Q represents the ultimate "monolayer" coverage of solute on the solid phase and b the ratio of the adsorption to the desorption rate constants, i.e., a measure of energy of adsorption. Taking the derivative of C_S with respect to C_F yields:

$$\frac{dC_S}{dC_F} = \frac{Q \rho b}{(1 + b C_F)^2} \tag{2-16}$$

It may be observed that $d^2 C_F/d C^2_S$ is negative which is inherently true for a "favorable" or "convex" isotherm. Hence with reference to the time-distance relationship given by Equation 2-14, the velocity increases with increasing mobile phase concentration causing a "pile up" into a front as the capacity of the bed becomes exhausted. Consequently, for this model the first "breakthrough" of solute exiting the column will be of inlet concentration. A simple mass balance at the front gives

$$v_o C_{F_o} = [\,\epsilon C_{F_o} + (1-\epsilon)\, C_{S_o}]\, \frac{dz}{dt} \cdot A \qquad (2\text{-}17)$$

and thus

$$\left.\frac{dz}{dt}\right|_{\text{Front}} = \frac{v_o}{\left[\epsilon + (1-\epsilon)\,\dfrac{C_{S_o}}{C_{F_o}}\right] \cdot A} \qquad (2\text{-}18)$$

where C_{F_o} denotes the inlet feed concentration and C_{S_o} the solid phase concentration in equilibrium with that inlet concentration. Therefore, from Equation 2-18, the breakthrough time for a given flow rate and bed volume can be calculated provided that the equilibrium relationship is known. Equation 2-14 can then be used to determine the shape of the elution tail for a discontinuous feed concentration.

This mathematical technique as described above may also be applied to the "concave" or "unfavorable" isotherm, with the net result being the reversal of the elution tail and adsorption front. Of course, the linear isotherm can be shown to produce an ideal, nondispersed wave front in a similar manner.

As pointed out by Lightfoot (26), the equilibrium model, although least likely to be realistic, is the simplest to handle and can give approximations to column capacity. In addition, it is the only one generally useable for multicomponent solutions of competitive solutes.

MASS TRANSFER COEFFICIENTS

Several types of models have been formulated (36) to include the effects of mass transfer resistances. Two of the more commonly used of these are presented here for purposes of illustration. Again with reference to Equation 2-3, it is desired to express the change in solid phase concentration, C_S, in terms of C_F, the liquid phase concentration. Local mass transfer coefficients may be defined for the steady state condition as follows:

$$\frac{\partial C_S}{\partial t} = k_f \; S_o \; (C_F - C_{F_i}) \qquad (2\text{-}19)$$

$$= k_s \; S_o \; (C_{S_i} - C_S) \qquad (2\text{-}20)$$

$$= K_F \; S_o \; (C_F - C_F^{*}) \qquad (2\text{-}21)$$

$$K_f = \left[\frac{1}{k_f} + \frac{1}{m\,k_s}\right]^{-1} \qquad (2\text{-}22)$$

where k_f is the liquid phase mass transfer coefficient, k_s, the stationary phase mass transfer coefficient, K_F, the overall mass transfer coefficient, C_{F_i}, the interfacial concentration in the moving phase, C_{S_i}, the interfacial concentration in the stationary phase, C_F^{*}, the imaginary moving phase concentration in equilibrium with C_S, S_O, the surface area to volume ratio for the particle and m, the average slope of dC_S/dC_F of the equilibrium distribution. It may be noted that m becomes the actual slope dC_S/dC_F for a linear isotherm; but for the general case, m is the "average" slope given by

$$m = \frac{(C_S - C_{S_i})}{(C_F^{*} - C_{F_i})} \qquad (2\text{-}23)$$

It is then necessary to evaluate the two mass transfer coefficients k_f and k_s. The moving phase or external film resistance k_f may be evaluated by several empirical correlation techniques involving dimensionless groupings such as the Colburn factor, j_D, the Reynolds number, N_{Re} and the Schmidt number, N_{Sc} (19,20). However, the internal resistance, k_s, must be evaluated by considering the movement of the solute within the solid phase. This entails calculating an effective diffusion coefficient, D, if transport phenomena is assumed to be described by Fick's second "law" of transient diffusion.

Such information can be obtained by appropriate batch reactor experiments, providing the mathematical model for the batch system is adequate. As previously stressed, the research work to be reported deals specifically with this problem. Upon evaluation of D, k_s for spherical particles can be expressed empirically by

$$k_s = 10 \cdot \frac{D}{D_p} \qquad (2\text{-}24)$$

where D_p is the particle diameter (26).

CHEMICAL REACTION MODEL

Mass transfer resistances may also be included in Equation 2-3 via the Thomas or chemical reaction model (26,34). The basis for application to fixed-bed adsorbers is to be able to relate mass transfer models to a generalized second order kinetics expression derived from the Langmuir adsorption model. Equation 2-25 describes the Langmuir model for adsorption

$$\frac{\partial C_S}{\partial t} = k\ [C_F\ (Q_\rho - C_S) - \frac{C_S}{b}] \qquad (2\text{-}25)$$

where k is the forward rate constant, and b the ratio of the forward to backward rate constants. The Langmuir equilibrium adsorption model is obtained by setting dC_s/dt equal to zero. The term, Q, in Equation 2-25 can be eliminated by introducing the constant C_{S_O}, representing that solid phase concentration which will exist in equilibrium with the inlet fluid phase concentration C_{F_O}, according to the Langmuir equilibrium relationship to give

$$\frac{d\omega}{dt} = k\left[\frac{1}{b} + C_{F_O}\right] \cdot \left[\phi - \frac{b\, C_{F_O}}{(1 + b\, C_{F_O})}\omega\phi - \frac{\omega}{(1 + b\, C_{F_O})}\right] \tag{2-26}$$

The dimensionless variables ω and ϕ are given by:

$$\omega = \frac{C_S}{C_{S_O}} \tag{2-27}$$

$$\phi = \frac{C_F}{C_{F_O}} \tag{2-28}$$

In addition, substitution of the so-called equilibrium modulus, λ , given by

$$\lambda = \frac{1}{1 + b\, C_{F_O}} = 1 - \frac{C_{S_O}}{Q^o} \tag{2-29}$$

reduces Equation 2-26 to a dimensionless form:

$$\frac{d\,\omega}{d\,\tau} = \phi\,[1 - \omega] - \lambda\omega\,[1 - \phi] \tag{2-30}$$

The dimensionless time parameter, τ , is

$$\tau = k\left[\frac{1}{b} + C_{F_O}\right] t \tag{2-31}$$

Thus, Equation 2-30 can provide the necessary input for dC_s/dt in the mass balance given by Equation 2-3.

In order to relate Equation 2-30 to a chosen mass transfer controlling step, a generalized rate coefficient, κ , and a dimensionless coefficient D_G are first introduced in place of $k\ (1/b + C_{F_o})$ in Equation 2-31.

$$\tau = \frac{\kappa}{D_G}\, t \tag{2-32}$$

The coefficient D_G represents the ratio of the limiting distribution of solute between the solid and liquid phase:

$$D_G = \frac{C_{S_o}}{C_{F_o}} \cdot \frac{(1-\epsilon)}{\epsilon} \tag{2-33}$$

For any mechanism postulated to describe the controlling mass transfer resistance, it is then necessary to arrive at a second order kinetic expression. This can be accomplished by involving the equilibrium concentration of solute in the driving force equation and using the Langmuir equilibrium model.

For example, a film diffusion model may be written as

$$\frac{\partial C_S}{\partial t} = k_f\, S_o\, (C_F - C_F^*) \tag{2-34}$$

where C_F^* represents the fluid phase concentration on the inside of the liquid film in equilibrium with the average solid phase concentration. Thus C_F^* is given by the Langmuir model, Equation 2-15. Carrying out the same substitution procedure as described above, Equation 2-30, the general second order kinetic expression is obtained with

$$\tau = \frac{k_f \quad S_o \quad C_{F_o}}{C_{S_o}\left[1 + (\lambda - 1)\frac{C_S}{C_{S_o}}\right]}\, t = \frac{\kappa}{D_G}\, t \tag{2-35}$$

Therefore, the general rate coefficient, κ , can be expressed in terms of k_f.

In a similar, but somewhat less straightforward manner, a transient diffusion model describing the pore resistance controlling case leads to a second order kinetic expression which involves D, the effective diffusion coefficient. Batch reactor kinetics can provide this value for subsequent use in the generalized Thomas model.

Recent work by Keinath and Weber (22) involved the application of the Thomas model for evaluating effluent concentration profiles in a fluid bed adsorber. This study concerned the adsorption of a pesticide, dinitro-o-sec-butylphenol (DNOSBP) on granular activated carbon with equilibrium being described by the Langmuir model. However, no convenient mathematical model was available to describe batch reactor kinetics in order to calculate a pore diffusion coefficient. This problem originates from a combination of complicating factors, both experimental and mathematical, which, as briefly discussed in Chapter I, form the basis for the study to be reported.

SUMMARY OF COLUMN CALCULATIONS

In summary, the objective in mathematical modeling of fixed- or fluid-bed adsorbers is to be able to predict the non-steady state effluent concentration profile. In order to formulate such a model it is necessary to understand the nature of the mass transfer resistances which control, and the nature of the equilibrium involved. From correlation procedures, as briefly discussed, it is possible to estimate a film transfer coefficient, while batch reactor kinetics yield a pore diffusion coefficient. Therefore it is conceivable that adsorber design can be accomplished with a minimum of experimental effort, without resorting to time consuming column testing. For the sake of completeness, however, the reader may refer to the recent work of Allen and Joyce (2) in which an emperical approach is taken to process design calculations for an activated carbon adsorber. Such a method necessarily involves obtaining actual column effluent profiles and back-calculating an artificial transfer coefficient.

It has been shown in this chapter that mass transfer considerations at the surface and within the sorbent particle may be included by use of a film model or general second order kinetic expression. However, several other models have been formulated and are discussed by Vermuelen (36). All of these inherently involve the equilibrium adsorption relationship and produce varying degrees of mathematical difficulty in describing the effluent concentration profile of a fixed- or fluid-bed adsorber.

CHAPTER 3

MODELING CONSIDERATIONS IN BATCH REACTORS

Investigators seeking a mathematical model to describe the rate of removal of a solute on activated carbon in a batch reactor are immediately confronted with numerous system complications, including solvent-solute interactions, undefined carbon pore structure, surface heterogeneity, and other complex factors. A mathematical model can only represent a predetermined conceptual model. The conceptual-mathematic model should closely describe the actual kinetic process; however, its mathematical complexity should not outweigh its usefulness as an applied research and design intermediary. Alternative empirical equations and relationships prevent a mechanistic interpretation of the process and thus sometimes fail to adequately respond to changes in system variables.

Certain simplifying assumptions are required in kinetic models in order to make them workable; nonetheless, these models should be so developed as to closely represent the controlling rate mechanisms. An electrical analog provides a convenient means for visualizing the interplay of the various mechanisms involved in the movement of sorbate from the liquid into the solid phase in the adsorption process. The resistances to movement may be categorized as 1) diffusion of solute through solution, 2) diffusion across the solid-liquid interface, 3) diffusion through the internal pore structure, 4) adsorption on internal surfaces, and 5) migration of adsorbed molecules along the solid phase, i.e., surface diffusion. These resistances act both in parallel and in series and hence the overall rate of adsorption may be controlled by a combination of them.

Assuming radial movement of the solute within a sphericle particle, Equation 3-1 represents the mass balance for a given incremental radius, Δr.

RATE IN - RATE OUT + RATE OF RX = RATE OF ACCUMULATION [1]

$$N \cdot 4\pi r^2\Big|_r - N \cdot 4\pi r^2\Big|_{r+\Delta r} = \frac{\partial}{\partial t}\left(\varepsilon C_F + (1-\varepsilon)C_S\right) 4\pi r^2 \Delta r \qquad (3\text{-}1)$$

If diffusional movement is assumed within the particle, N the superficial flux, is given by Fick's first law as

$$N = -D\frac{\partial C_F}{\partial r} \qquad (3\text{-}2)$$

Dividing Equation 3-1 by Δr and letting Δr approach zero yields

$$D\left[\frac{\partial^2 C_F}{\partial r^2} + \frac{2}{r}\frac{\partial C_F}{\partial r}\right] = \frac{\partial}{\partial t}\left(\varepsilon C_F + (1-\varepsilon)C_S\right) \qquad (3\text{-}3)$$

ADSORPTION REACTION

The nature of surface diffusion and internal surface adsorption reaction resistances are open to question. Although surface diffusion is generally restricted to gases, Dedrick and Beckman (15) and Brecher, et al., (4), have both indicated that in aqueous systems solutes of low adsorption energy may exhibit surface migration. This resistance would act in parallel to pore diffusion and would necessitate evaluation of another characteristic system constant, further complicating a mechanistic interpretation. Usually, the adsorption reaction itself is considered to be so rapid (1) that local equilibrium is always maintained and the term $\partial C_S/\partial t$ in Equation 3-3 is determined by differentiation of the equilibrium relationship with respect to time. A non-equilibrium case has been considered by Edeskuty and Amundson (16) in which an external film resistance is also included in series. The mathematical solution to this case, however, is rather formidable, demanding the evaluation of three system constants. A similar problem, subject to the same difficulties, has been solved by Crank (12).

---

[1] $C_S = X \cdot \rho_{Solid}$ having units of moles/unit volume of solid

Actually, the surface adsorption reaction, usually represented by a solid-liquid phase equilibrium expression, in itself offers modeling difficulties. Adsorption isotherm models can be classified as irreversible, non-linear and linear according to the following general forms:

$$\text{Irreversible} \qquad C_S = \text{Constant} \qquad (3\text{-}4)$$

$$\text{Non-Linear} \qquad C_S = w\, C_F^{\,y} \qquad (3\text{-}5)$$

$$\text{Linear} \qquad C_S = R\, C_F \qquad (3\text{-}6)$$

The non-linear Langmuir isotherm model for monolayer coverage encompasses all three classifications depending on the magnitude of the adsorption energy term, b, in Equation 2-15. As b increases, Equation 3-4 is approached; as b decreases, Equation 3-6 can be approximated for a given region of the isotherm. The value of C_F, equilibrium fluid phase concentration of sorbate, at which half surface coverage ($C_S = Q/2$) is attained, is equal to $1/b$. Thus the larger the value of b, the lower the fluid phase concentrations at which $C_S = Q/2$ and hence the more closely Equation 3-4 is approximated.

BOUNDARY CONDITIONS

With reference to the electrical analog, resistances 3) and 4) have been combined in parallel in the mass balance relationship given by Equation 3-3. Usually, experimental conditions minimize the resistance offered by the solute diffusing through bulk solution, leaving only film diffusion resistance to be included as a boundary condition at the surface of the carbon particles, acting in series with the internal resistances. In addition, depending on experimental conditions, a boundary condition of either constant or changing concentration of solute in solution is implied, the latter being a finite-bath and the former an infinite-bath condition. Thus, for each case, the following corresponding boundary equations may be written

Finite-Bath:

$$V \frac{\partial C_F}{\partial t} = -4 \pi a^2 D \frac{\partial C_{F_i}}{\partial r} \qquad r = a,\ t \geq 0 \qquad (3\text{-}7)$$

$$D \frac{\partial C_{F_i}}{\partial r} = k_f \left(C_F - C_{F_i}\right) \qquad r = a,\ t \geq 0 \qquad (3\text{-}8)$$

Infinite-Bath:

$$C_F = C_{F_o} \qquad r \geq a,\ t \geq 0 \qquad (3\text{-}9)$$

$$D \frac{\partial C_{F_i}}{\partial r} = k_f \left(C_{F_o} - C_{F_i}\right) \qquad r = a,\ t \geq 0 \qquad (3\text{-}10)$$

The terms V and a refer to the volume of solution served per particle and particle radius respectively.

The mathematical complexity of the model used to describe the rate of uptake of solute in a batch reactor is thus the end product of several model inputs. Clearly, the simplest model would involve a linear adsorption isotherm (Equation 3-6), negligible film resistance and unchanging solution concentration, i.e., an infinite-bath (Equation 3-9). However, the most common complication is the non-linear adsorption isotherm given by Equations 3-5 or 2-15, which forces the use of a numerical methods technique for convenient solution to Equation 3-3. The infinite-bath condition usually must be artificially produced by employing a special experimental apparatus. This fact may outweigh the benefits derived from the mathematical simplication which results for an unchanging solute concentration in solution.

On the other hand, use of the finite-bath boundary condition, with external resistance included, leads to a rather unmanageable mathematical solution, even when the simplest, linear isotherm is applied. Edeskuty and Amundson (16,17) have presented analytical solutions for models of this type using both cylindrical and spherical particle geometry. Roots of a Bessel and a triginometric equation are required for particles of these two geometrys, respectively, in order to obtain a solution to Equation 3-3. In either case, the magnitude of the isotherm slope, R, influences the nature of the roots calculated, and hence the existence of a solution. Several other investigators (6,15,29,41) have indicated rates of adsorption in finite-bath systems to be controlled by pore diffusion. However, in most instances (6,15,29), this conclusion was intuitive since consideration of a non-linear isotherm prevented a straightforward mathematical solution.

SUMMARY OF BATCH REACTOR MODELING

It may be restated that the description of the mass transfer mechanism is often a compromise between mathematical simplicity and major modeling objectives. From the preceeding discussion, non-linear adsorption isotherms complicate the solution of Equation 3-3 regardless of the combination of resistances assumed to be controlling. However, between the extremes of strong and weak adsorption——i.e., irreversible and linear adsorption——Weisz (42) has indicated a limited area of kinetic behavior . His conclusion was based on solution to Equation 3-3 using in turn an irreversible and linear adsorption equilibrium model with a constant external concentration boundary condition, and no film resistance. With the use of a universal time parameter, including an uncertainty factor to account for error introduced by not considering the shape of the isotherm, Weisz and Hicks (43) tested the model for a range of system properties and found that it effectively described uptake rates for fractional coverages of up to one half in general. The important point to be noted from their investigation is that adsorption isotherms may be approximated to facilitate a mathematical solution to the sorption-diffusion process.

Further, the physical boundary condition imposed by the experimental system, i.e., finite or infinite-bath, influences the mathematical and experimental complexity encountered in modeling. The simplicity of kinetic data collection in a finite-bath may be an advantage, providing non-linear adsorption isotherms can be approximated by either linear or irreversible adsorption. On the other hand, it may be necessary to use the infinite-bath system, with its experimental complications, when non-linear isotherms can not be approximated. This method may be especially advantageous when both film[1] and pore diffusion in series control the rate of mass transfer.

---

[1] Film, penetration, boundary layer and other theories have been postulated to explain mass transfer in the region separating a turbulent bulk solution and a solid surface. However, the fluid mechanics of this region are not well defined. Boundary layer theory accounts for a velocity distribution and is more realistic than film theory, which assumes a laminar film surrounding the particle. The term "film diffusion" will be used throughout to generally describe the resistance to mass transfer at the surface of the particle. However, use of this term is not intended to imply the existence of a definable film nor is it meant to restrict treatment of the data to the film theory. The correlation of k_f with hydrodynamics, fluid properties and free-liquid diffusivities will be discussed in Appendix C.

CHAPTER 4

EQUILIBRIUM ADSORPTION

The equation describing equilibrium adsorption is an important model input for description of batch reactor kinetics, as discussed in Chapter 3. In this chapter, experimental equilibrium data will be presented for organic sorbates of different molecular size and charge characteristics. The major objective is to focus attention on the variations encountered in adsorption isotherms, since the kinetic model given by Equation 3-3 must use Equations 3-4, 3-5, or 3-6 to describe the equilibrium solid-liquid phase distribution of solute.

EXPERIMENTAL MATERIALS

Columbia LC Carbon (Union Carbide Corp., New York, N.Y.), a petroleum base carbon, was the adsorbent used in all the experimental work. Table 1 lists the properties given by the manufacturer (9) and the Brunauer-Emmet-Teller N_2-(BET) surface area determined in the laboratory using a Sor-BET device (Aminco Instrument Co.). The percentage loss in weight of the new carbon after heating for six hours at 150°C is one per cent as shown in Table 4-1. The percent by weight of CCl_4 adsorbed at 25°C from dry air saturated with this vapor at 0°C is 67 per cent and is used as a relative standard of adsorptive capacity for concentrated vapors. Hardness is determined by measuring the change in screen analysis observed after mechanical abrasion of the carbon. Thus Columbia LC retains 95 per cent of its original "abrasive strength". The amount of inorganic materials contained in the carbon is given as two per cent, measured as total ash content. A BET surface area of 1170 M^2/gm is fairly typical of various commercial activated carbons.

TABLE 4-1

PROPERTIES OF COLUMBIA LC CARBON

Moisture %	1.0
CCl_4 Activity %	67
Hardness	95
Total Ash %	2
BET Surface Area m^2/gm	1170

Figure 4-1 represents the pore size distribution given by the manufacturer (9). The total pore volume is about 0.676 cc/gm with .50 cc/gm contained in pores of smaller than 20 angstrom (A^o) diameter.

Uniform particle size fractions were obtained by sieving with a set of United States Standard Sieves. Equilibrium experiments were carried out using the size fraction 30/40 (particles passing a 30 mesh but retained on a 40 mesh sieve) which has a mean diameter of 0.503 cm. All carbon was washed with distilled water to remove fines and leachable impurities and dried at 105°C for 24 hours.

For each solute, Table 4-2 lists the wavelength of maximum absorption, corresponding molar absorptivity used for analysis and the negative log of the ionization constant (pK_a). All solutes investigated have a benzene ring structure in common. The first five listed, phenol, p-nitrophenol (PNP), 2,4-dinitrophenol (DNP), 2,4-dinitro-o-sec-butylphenol (DNOSBP) and 2,4-dinitro-o-cyclo-hexylphenol (DNOCHP) are

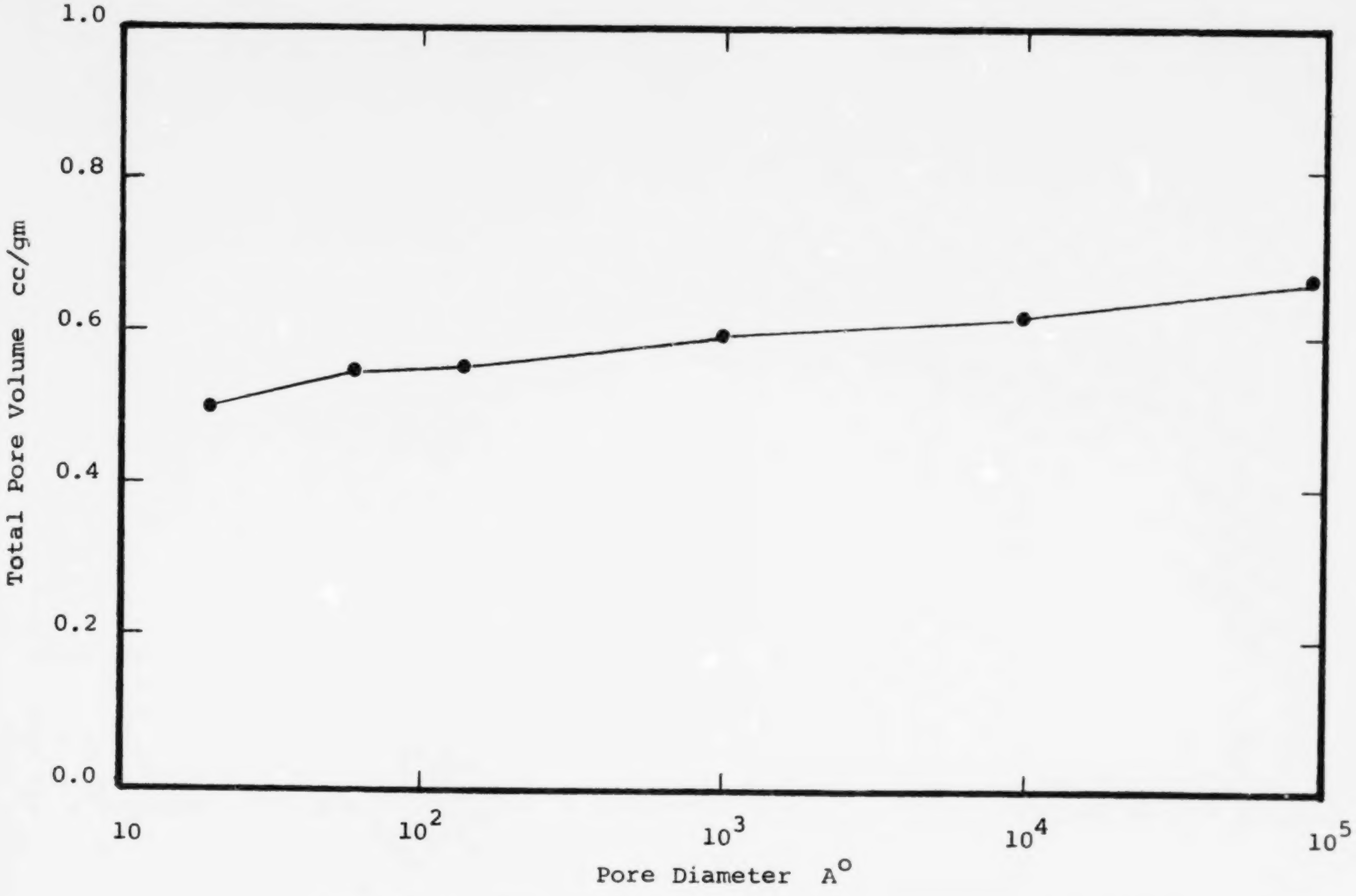

FIGURE 4-1. PORE SIZE DISTRIBUTION FOR COLUMBIA LC CARBON

TABLE 4-2

ANALYTICAL DATA AND IONIZATION CONSTANTS FOR SOLUTES INVESTIGATED

Solute	Wavelength of Maximum Absorptivity		Molar Absorptivity 1/ mol-cm	pK_a
phenol	274	Neutral	1370	9.89
	287	Anion	2500	
p-nitrophenol (PNP)	315	Neutral	9690	7.17
	400	Anion	18376	
2,4-dinitrophenol (DNP)	260	Neutral	11500	4.09
	360	Anion	14300	
2,4-dinitro-o-sec-butylphenol (DNOSBP)	375	Anion	14780	4.37
2,4-dinitro-o-cyclo hexylphenol (DNOCHP)	375	Anion	14510	3.77
2-hexylbenzene-sulfonate	226	Anion	12850	~1.5
2-octylbenzene-sulfonate	226	Anion	12850	~1.5
2-decylbenzene-sulfonate	226	Anion	12850	~1.5

phenolic compounds which release hydrogen ions to yield the -o⁻ group. The anions thus formed are highly soluble in water. However, the corresponding neutral molecules decrease in solubility with the addition of the nitro and alkyl groups. Snoeyink and Weber (30) reported solubilities of 0.8 and 0.1 M for phenol and PNP respectively at pH 4 and 25°C. A value of 0.024 M was experimentally found in this study for DNP at pH 2 and 25°C. Both DNOSBP and DNOCHP are only very slightly soluble as the neutral molecules and therefore were not investigated. The last three solutes listed in Table 4-2 are 2-hexyl-, 2-octyl- and 2-decylbenzenesulfonate respectively. These were obtained as their sodium salts and investigated in only the anion forms.

In addition to the variation in molecular size, structure and charge afforded by the choice of these solutes, there is also a practical significance associated with each. Phenol is often found in industrial wastes, particularly steel mills and many chemical companies; the compounds DNOSBP and DNOCHP are both used as insecticides thus making it apparent that nitrated phenols such as PNP and DNP could occur as decomposition products of these and other pesticides. Finally, 2-hexyl and 2-decylbenzenesulfonate are exemplary of the more surface active compounds found in wastewaters.

Phenol, PNP and DNP were obtained as the chemically pure compounds from chemical companies. (Phenol from Allied Chemical, PNP and DNP from Matheson, Coleman and Bell). Dow Chemical Company supplied technical grade DNOSBP and DNOCHP, which were then recrystallized in the laboratory. Atlantic Refining Company furnished the 2-decyl-, 2-octyl- and 2-hexylbenzenesulfonate as the sodium salts. These were specified as 98 to 99% pure in terms of structure of the alkyl group and location of the benzene ring.

EXPERIMENTAL PROCEDURE

Adsorption equilibria were determined for the neutral and anionic species of phenol, PNP and DNP, and the anions of DNOSBP and DNOCHP. Data obtained by Keinath (23), using the same Columbia LC carbon and 2-octylbenzenesulfonate was used due to the lack of sufficient quantities of each alkylbenzenesulfonate compound to perform both equilibrium and kinetic studies.

To obtain a large number of equilibrium points for each system, 100-ml aliquots of a given solution were pipetted into 125-ml, French-Square, wide mouth bottles containing a carefully weighed amount of carbon. Upwards of twenty bottles were filled with varying quantities of carbon along with three blanks containing no carbon. Laboratory built tumblers, each having a capacity for 72 bottles, were used to provide agitation. Following the method of Snoeyink and Weber (30), approximately one month was allowed for equilibrium to be attained at room temperature. Equilibrium solution concentration in each bottle was then determined using a Beckman DU spectrophotometer. The solid phase concentration, X(mmol/gm), was then calculated from the experimental data using Equation 4-1

$$X = \frac{C_{F_o} - C_{F_e}}{W} \qquad (4\text{-}1)$$

where C_{F_o} is the initial fluid phase concentration (mol/l) C_{F_e}, the final equilibrium fluid phase concentration (mol/l) and W, the carbon dosage (gm/l).

A Langmuir equilibrium adsorption model was used to fit the data obtained. Values of the Langmuir parameters Q and b in Equation 2-15 were determined from the linearized form given in Equation (4-2)

$$\frac{C_{F_e}}{X} = \frac{1}{Q} C_{F_e} + \frac{1}{Qb} \qquad (4\text{-}2)$$

RESULTS AND DISCUSSION

Adsorption equilibria obtained for the neutral species of phenol, PNP and DNP are shown in Figure 4-2. The pH was adjusted to 4 with HCl for both the phenol and PNP isotherms while a pH of 2 was needed for DNP. It may be observed from examination of Table 4-2 that the molecules are almost completely undissociated at these values of pH. For the practical consequences of this research only those equilibrium concentrations, C_{F_e}, less than 10^{-4} M are of interest.

The most striking feature observed in Figure 4-2 is that the steepness of the adsorption isotherms increased in the order phenol, PNP, DNP. The concept of reduced concentrations can be used to normalize for the amount of energy needed to bring the solute molecule from bulk solution to the surface of the carbon. As previously given, the solubilities for phenol and PNP at pH4 and 25°C are 0.8 M and 0.1 M respectively (30). Thus it is apparent that the PNP isotherm is still much higher than that of phenol even when the equilibrium concentrations are divided by the solubility limits of the respective molecules. Such a phenomenon was also observed by Snoeyink and Weber (30) and Mattson, et al., (27). This argument may be extended to the results obtained for the DNP isotherm. Mattson, et al., (27) postulated that the mechanism of adsorption involves the formation of a donor-acceptor complex with surface carbonyl oxygen groups. The ability to form the complex depends on the electron density in the pi-system of the benzene ring. Nitro groups act as strong electron withdrawing agents and thus enhance the acceptance of electrons from surface carbonyl oxygens, forming stronger donor acceptor complexes.

Although an understanding of the mechanism of adsorption is important, the main thrust of the research reported herein

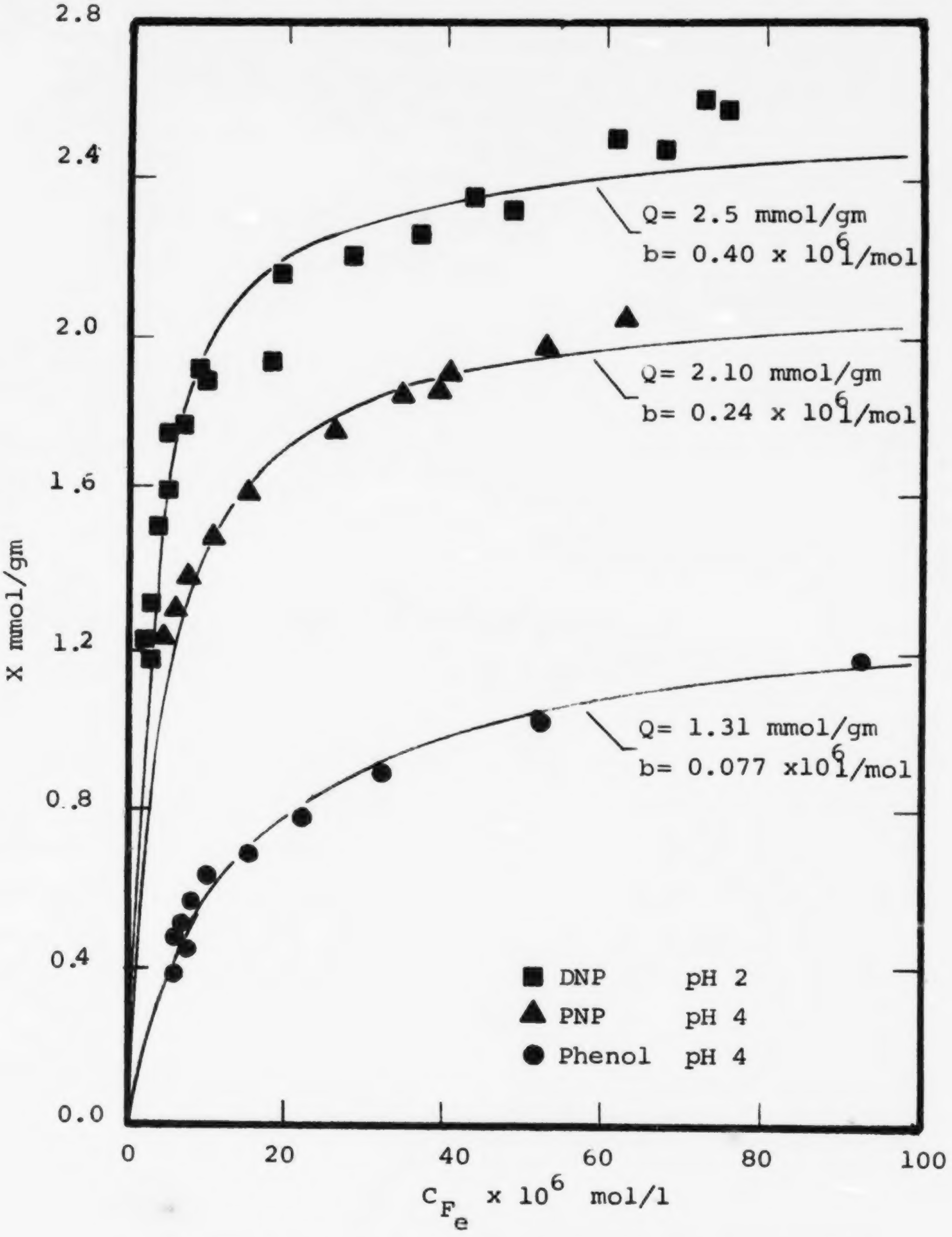

FIGURE 4-2. EQUILIBRIUM ADSORPTION OF NEUTRAL SPECIES OF PHENOL, PNP AND DNP

is to develop mathematical models that describe the rate of adsorption. It has been assumed that equilibrium is attained instantaneously at the surface sites and thus it is only necessary to mathematically describe the equilibrium relationships for subsequent model input.

The calculated curves shown in Figure 4-2 derive from plotting C_{F_e}/X versus C_{F_e} in Equation 4-2 to obtain the Langmuir constants, Q and b. Recent work by Snoeyink and Weber (30) and Dedrick and Beckman (15), using similar systems, has shown that a Langmuir model is not adequate for a large range of equilibrium concentrations. This conclusion is also evident from the results shown in Figure 4-3 in which the data for DNP (N) has been plotted according to Equation 4-2. For higher equilibrium concentrations another straight line could be drawn intersecting the first at some arbitrary value. As explained by Weber and Morris (40) and Snoeyink and Weber (30), such behavior is indicative of a continuous spectrum of site energies due to the surface heterogeneity of activated carbon. The important point to be noted from the calculated curves is that the shape of the isotherm is reflected in the b and Q values. Thus the steepest isotherm, that of DNP, has the largest b value and this in turn reflects a more favorable interaction with surface sites.

PHENOL, PNP, DNP ANION EQUILIBRIA

Figure 4-4 comparitively describes the adsorption for the anionic species of phenol, PNP and DNP. Solution pH for the equilibrium studies was initially adjusted to pH 12, 10 and 8, respectively, for each solute. No significant change in pH was noted after the equilibration time in the case of phenol and PNP. However, for DNP——as will be discussed in more detail——the pH at equilibrium adsorption had increased

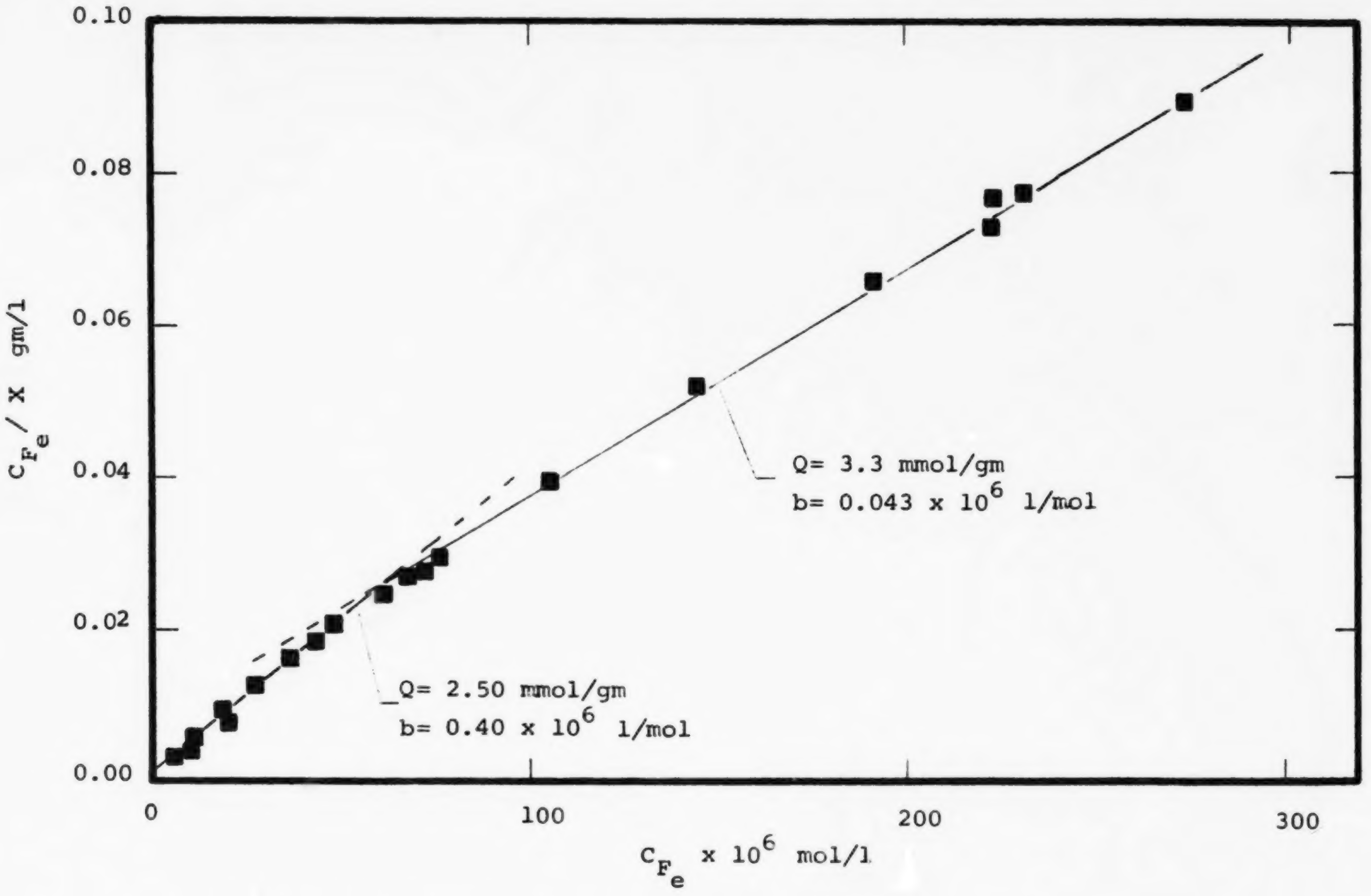

FIGURE 4-3. DETERMINATION OF LANGMUIR MODEL PARAMETERS FOR DNP (N).

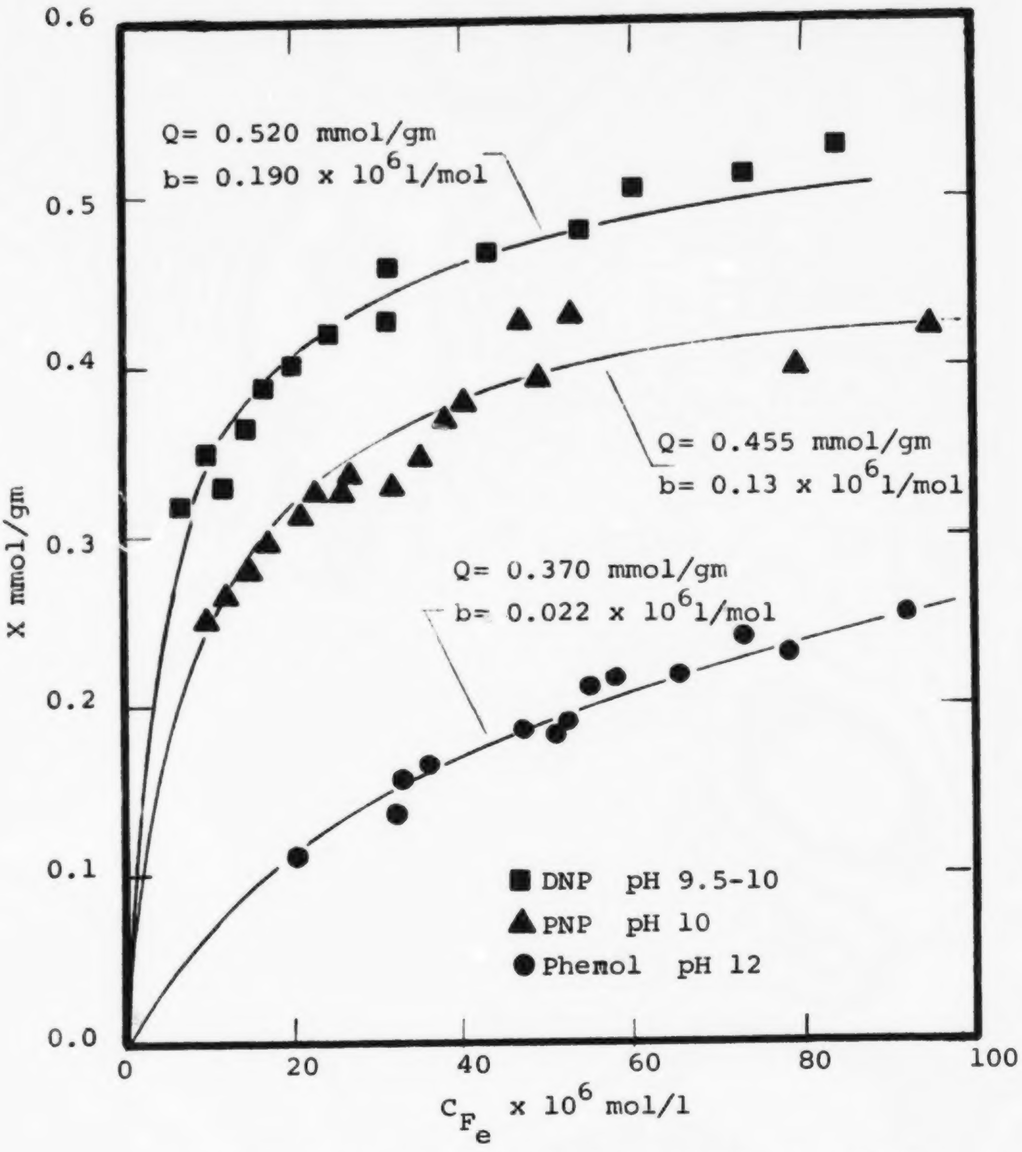

FIGURE 4-4. EQUILIBRIUM ADSORPTION OF ANION SPECIES OF PHENOL, PNP AND DNP.

significantly. Thus, the isotherm data points shown in Figure 4-4 for DNP were selected because equilibrium pH fell between 9.5 and 10.

The same relative isotherm shapes were obtained for the anionic species of phenol, PNP and DNP as for the corresponding neutral species (See Figure 4-2); however, for each anion the amounts adsorbed were greatly reduced. Such behavior was also noted by Snoeyink and Weber (30) in studies of phenol and PNP adsorption on activated carbon. These authors postulated that repulsive forces between the anionic sorbate and the negative carbon surface were responsible. The mechanism of electron donor-acceptor complexes is also consistent with the observations since the resonance structures for the anion species of PNP and DNP have a more dense electron cloud within the ring than do the corresponding neutral species. Consequently, there is less tendency to accept electrons from carbonyl oxygen groups on the surface which then results in a decrease in adsorption.

Again, it is difficult to perceive that the increased solubility of the anionic species could account for the observed decrease in adsorption. An unsuccessful attempt was made to determine the solubility of DNP (A) by adding an excess of DNP (N) crystals to distilled water, adjusting the pH to 7, at which anionic species would prevail, and measuring the saturated solution concentration. It is necessary to essentially titrate the dissociating weak acid with a strong base (NaOH) since as dissolution occurs, hydrogen ions are released. However, before an end point can be reached, corresponding to the solubility limit of the anion, sodium 2-4-dinitrophenolate first begins to precipitate. Therefore, the solubility product dictates the solubility of DNP (A), and DNP (N) continues to dissolve only to be precipitated as sodium 2,4-dinitrophenolate. An alternative method would be to add an excess of sodium 2,4-dinitrophenolate to distilled water giving a predominance of DNP (A), which could then be measured.

Suffice it to say that although the anion of DNP is much more soluble than the neutral species, comparison of Figures 4-2 and 4-4 shows that anion solubility would have to be many orders of magnitude greater than could be anticipated in order to account for such a marked decrease in adsorption.

The b values obtained for the anion species were also lower than those calculated for the corresponding neutral species in the same range of equilibrium concentrations. This is consistent with the postulation of lower adsorption energies. Table 4-3 summarizes the results of fitting a Langmuir equation to isotherm data obtained for each solute, both anion and neutral.

TABLE 4-3

LANGMUIR CONSTANTS, b AND Q, FOR THE NEUTRAL AND ANIONIC SPECIES OF PHENOL, PNP AND DNP

Solute	b $1/mol \times 10^{-6}$	Q mmol/gm	Equilibrium Concentration range $mol/l \times 10^{6}$
Phenol (N)	0.077	1.31	5 - 100
Phenol (A)	0.022	0.37	30 - 100
PNP (N)	0.24	2.10	5 - 100
PNP (A)	0.13	0.455	5 - 100
DNP (N)	0.40	2.50	2 - 75
DNP (A)	0.19	0.52	5 - 84

ACCOMPANING pH INCREASES

The pH shift in the equilibrium studies reported for DNP anionic species uncovers a rather interesting and perplexing phenomena. Further study was required since the rate of adsorption for this solute was to be investigated and thus equilibrium relationships would be involved. In Figure 4-5, the effect of carbon dosage on the equilibrium pH obtained in the DNP anion equilibrium studies is shown. The amount of carbon placed in each bottle was varied from 0.003 gm to 0.15 gm per 100 ml. For the lower carbon dosages, the initial concentration, C_{F_o}, of DNP (A) was 10^{-4} M while for the higher carbon dosages, C_{F_o} was 5×10^{-4} M. The original intent was to use the higher carbon dosages to avoid experimental error in weighing. However, as illustrated in Figure 4-5, equilibrium pH rose sharply as carbon dosages increased to a level of 0.4 gm/l and then tapered off at higher dosages.

One explanation may be that weak, acidic functional groups on the surface of the carbon (10,30) are being ionized. Another may be that hydrolytic adsorption is taking place and thus, the negatively charged DNP (A) is being used to cleave surface functional groups rather than OH^- ions from dissociation of water. This causes a release of OH^- ions in proportion to the amount of DNP (A) hydrolytically adsorbed and would account for the increase in pH as carbon dosage increased.

At higher initial pH such as used for the PNP and phenol anion equilibrium studies, the release of OH^- ions was possibly masked by the swamping OH^--ion concentration.

Figure 4-6 illustrates adsorption equilibria for DNP (A) at three different pH levels. Equilibrium pH values, which

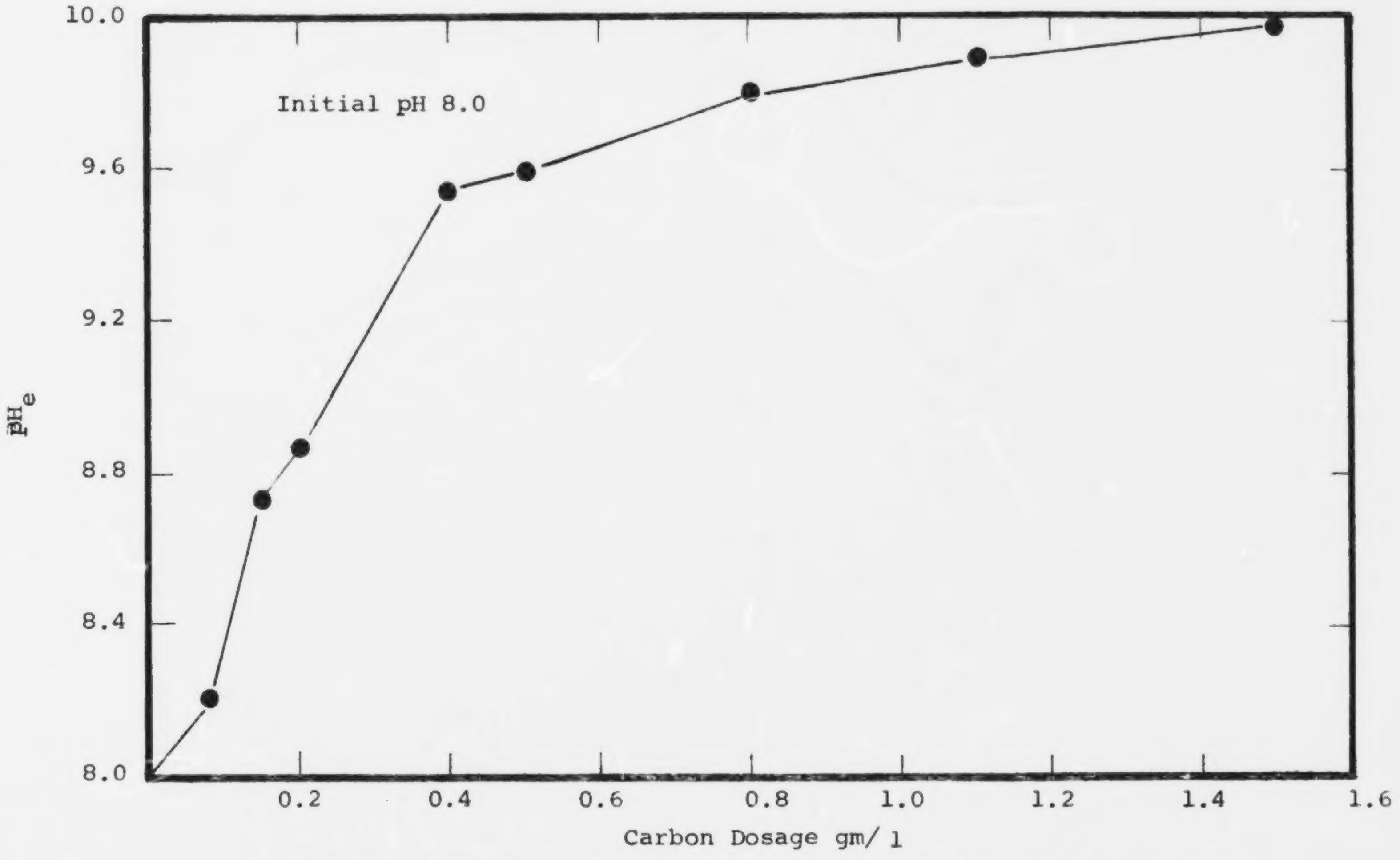

FIGURE 4-5. EFFECT OF CARBON DOSAGE ON EQUILIBRIUM pH FOR DNP (A).

were between 8.0 and 8.8 resulted from experiments in which the lower carbon dosages were used as discussed above. It may be noted that the resulting adsorption isotherm is higher than that for the pH range of 9.5 to 10 and is evidence for some alteration in carbon surface-solute interaction. More striking, however, is the increase in adsorption capacity observed when a 10^{-2} $\underline{M}$ phosphate buffer was added to maintain a pH of 7.2 (10^{-2} $\underline{M}$ $K_2H\ PO_4$ and 10^{-2} $\underline{M}$ KH_2PO_4).

DNOSBP EQUILIBRIA - EFFECT OF PHOSPHATE BUFFER AND $NaHCO_3$

Figure 4-7 shows the comparitive equilibrium behavior of the anion of DNOSBP in systems containing a 10^{-2} $\underline{M}$ phosphate buffer, 10^{-2} $\underline{M}$ $NaHCO_3$ and no added ionic strength. Although the same increase in equilibrium pH was observed as in studies with DNP (A) in a system containing no additional buffer, the differences in adsorption equilibrium between the low and high pH were not as significant. Again, addition of a 10^{-2} $\underline{M}$ phosphate buffer almost doubled adsorptive capacity. Moreover, addition of 10^{-2} $\underline{M}$ $NaHCO_3$ produced the same affect. In this case, a conjugate acid-base system was not added, but buffer capacity existed as a result of the amphoteric HCO_3^- ion, and gave a system pH of approximately 8.4. Therefore, the lower range of equilibrium pH for the unbuffered system fell within that of the 10^{-2} $\underline{M}$ $NaHCO_3$ system.

It appears then, that the lower system pH of 7.2 in contrast to 8.4 is not responsible for the increased adsorption capacities. Further investigations are required, however, before any positive conclusion may be reached regarding the observed phenomena. Interestingly enough, Keinath (22), in investigating adsorption equilibria of

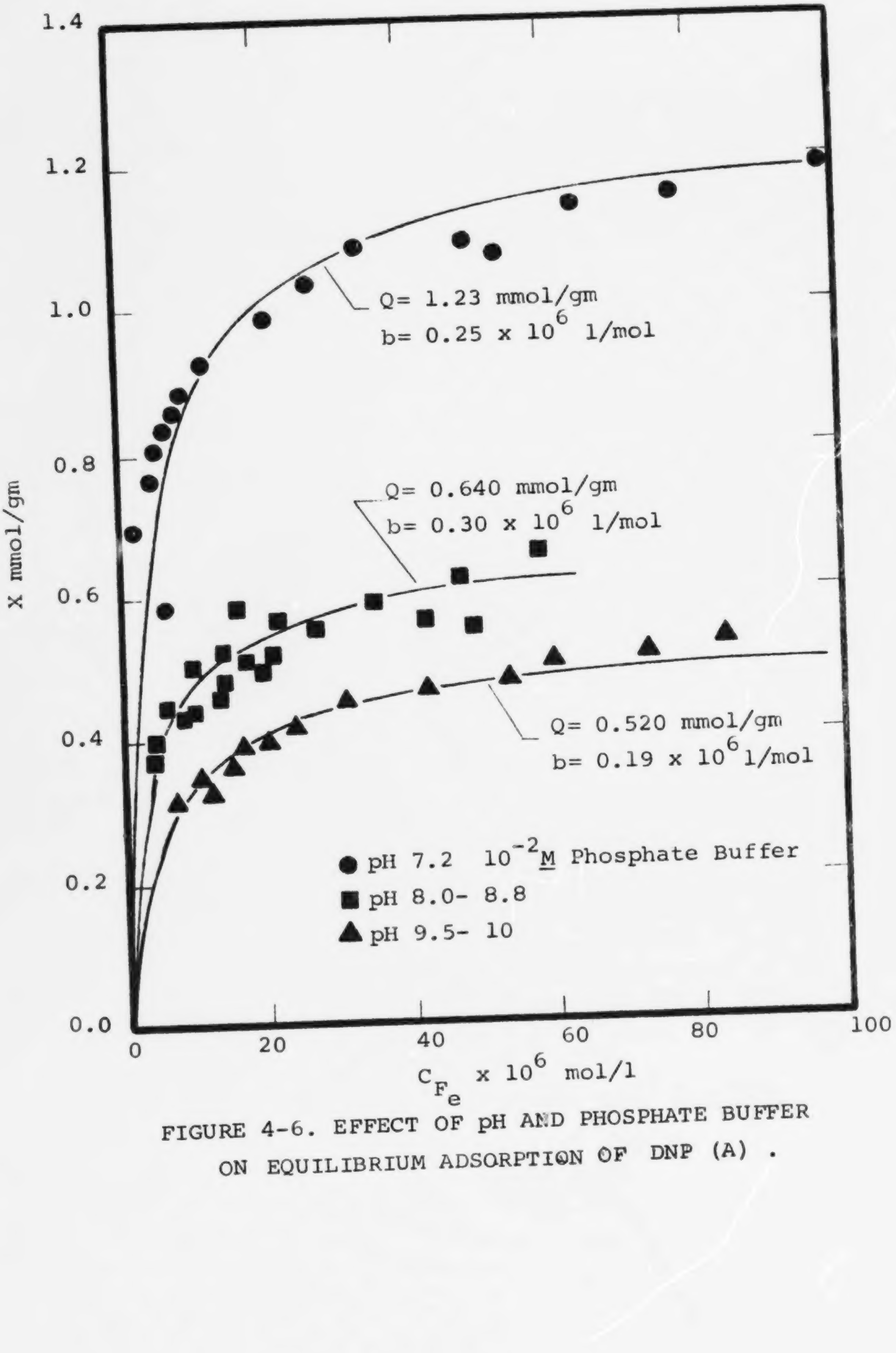

FIGURE 4-6. EFFECT OF pH AND PHOSPHATE BUFFER ON EQUILIBRIUM ADSORPTION OF DNP (A) .

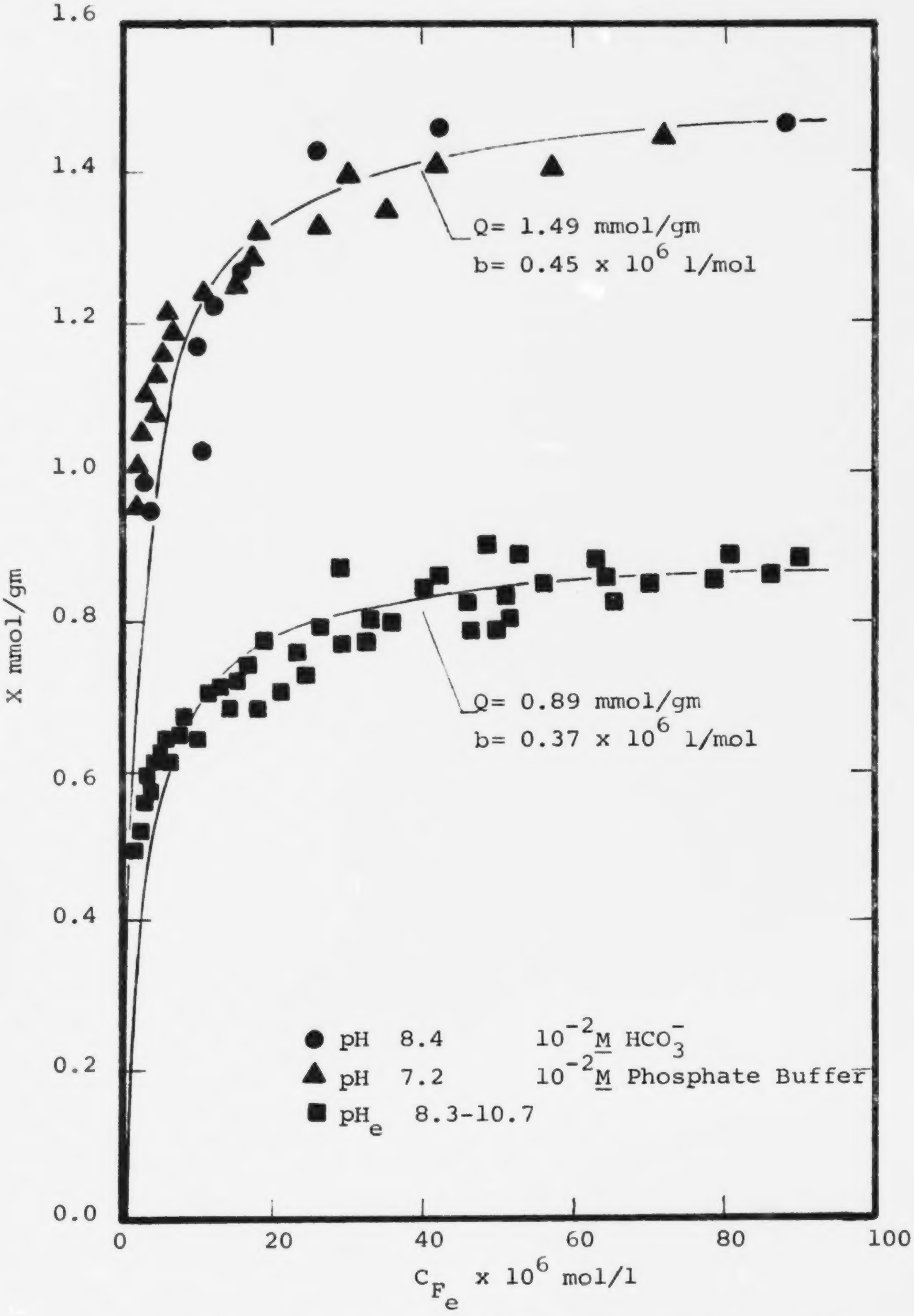

FIGURE 4-7. EFFECT OF PHOSPHATE BUFFER AND $NaHCO_3^-$ ON EQUILIBRIUM ADSORPTION OF DNOSBP .

DNOSBP on Columbia Carbon, used a 10^{-2} M $NaHCO_3$ - 10^{-2} M Na_2CO_3 buffer system at pH 10.4 and observed a similar isotherm to that obtained for the unbuffered system reported herein. Therefore, increased ionic strength apparently was not entirely responsible for the increased adsorption capacities observed using phosphate buffer and $NaHCO_3$ systems; perhaps alterations of carbon surface groups at higher pH override this affect. As noted by Kipling (24), ion exchange may occur with small quantities of inorganic material present in the carbon and also with chemically bound complexes, such as acidic groups, on the surfaces; thus, either the phosphate or bicarbonate system could in this way influence adsorption behavior.

DNOCHP AND 2-OCTYLBENZENESULFONATE EQUILIBRIA

As shown in Figure 4-8, the adsorption equilibrium obtained for DNOCHP was quite similar to that of DNOSBP except for the initial portion which is somewhat steeper for DNOCHP. This is reflected in the larger b of 0.5 x 10^6 l/mol calculated for DNOCHP. As noted before, equilibrium pH again shifted upward as a function of carbon dosage, but all data were fitted to a single calculated isotherm.

Keinath (23), a co-worker, obtained the adsorption equilibrium data for 2-octylbenzenesulfonate shown in Figure 4-9. His experiments were performed in exactly the same manner, using the same batch of Columbia Carbon. A pH of 6 was initially set and the same increase in pH was noted at equilibrium. As seen from Figure 4-9, adsorption behavior was quite similar to that of DNOSBP and DNOCHP. Adsorption equilibrium studies were not performed with 2-hexyl- and 2-decylbenzenesulfonate, but previous work of Weber and Morris

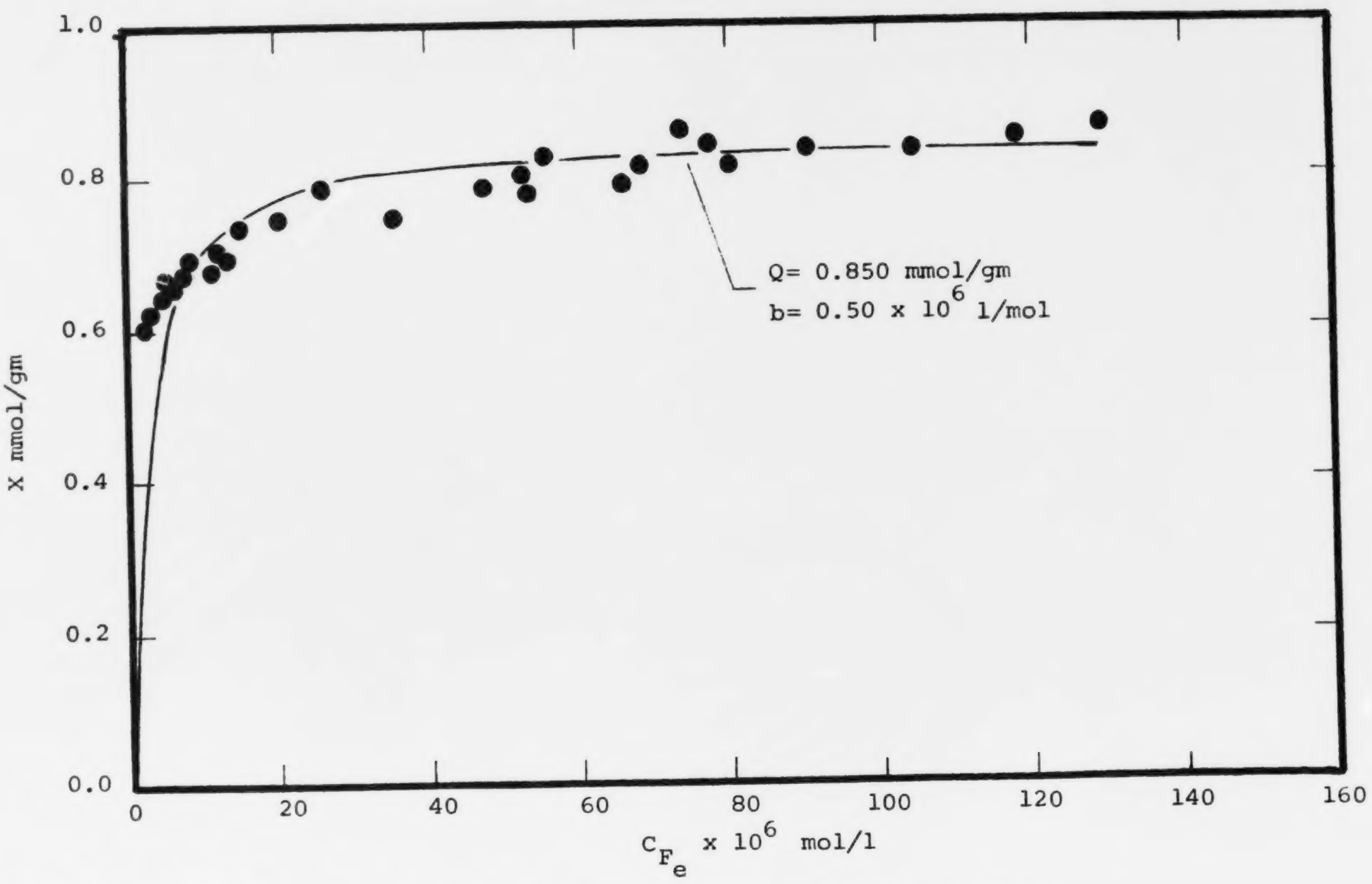

FIGURE 4-8. EQUILIBRIUM ADSORPTION OF DNOCHP .

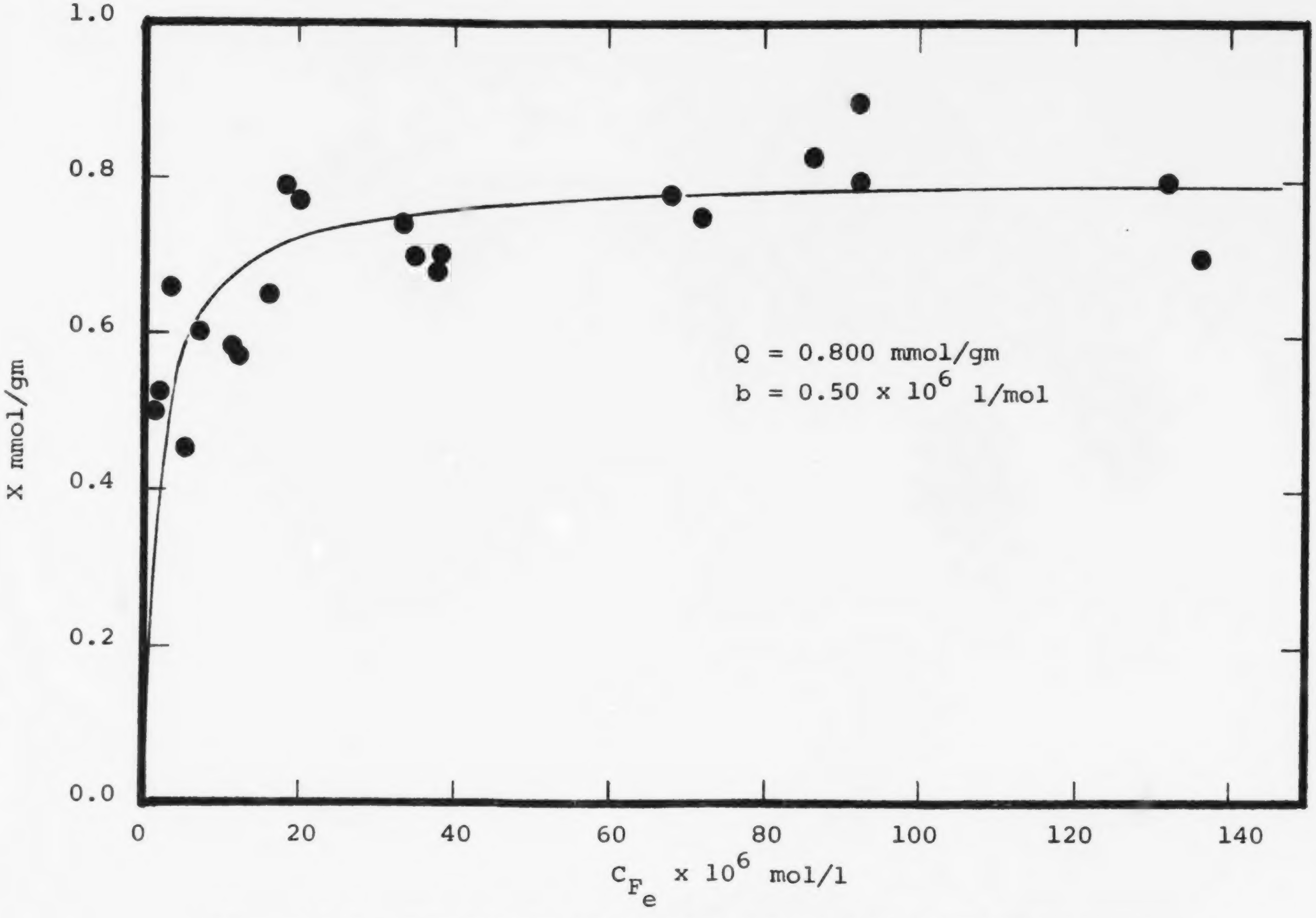

FIGURE 4-9. EQUILIBRIUM ADSORPTION OF 2-OCTYLBENZENESULFONATE

(40) with these three sorbates has indicated that their adsorption behaviors are very similar.

SUMMARY

Table 4-4 provides a summary of the results obtained for the anions of DNP, DNOSBP, DNOCHP and 2-octylbenzenesulfonate. Of particular interest are the values of Q and b obtained for DNP and DNOSBP, with and without the addition of phosphate buffer. For each solute, the shape of the isotherm, as given by b, remained relatively constant. However, the value of Q approximately doubled with addition of phosphate buffer. Moreover, addition of $NaHCO_3$ produced the same effect on the DNOSBP adsorption equilibria. It is also evident that DNOSBP, DNOCHP and 2-octylbenzenesulfonate each exhibited a much sharper rise to a relatively constant level of adsorption than the neutral or anion species of phenol and PNP; and although somewhat less noticeable, than either species of DNP.

TABLE 4-4

SUMMARY OF EQUILIBRIUM ADSORPTION DATA FOR THE ANIONS OF DNP, DNOSBP, DNOCHP AND 2-OCTYLBENZENESULFONATE

Solute	Langmuir Constants Q mmol/gm	b $1/\text{mol} \times 10^{-6}$	C_{F_e} Range $\text{mol}/1 \times 10^{6}$	pH	Buffer System
DNP	0.520	0.19	6-84	9.5-10	-
DNP	0.640	0.30	4-60	8-8.8	-
DNP	1.23	0.25	2-100	7.2	Phosphate
DNOSBP	0.89	0.37	1-90	8.3-10.7	-
DNOSBP	1.49	0.45	1-70	7.2	Phosphate
DNOSBP	1.49	0.45	1-90	8.4	Bicarbonate
DNOCHP	0.85	0.50	1-130	8.3-10-7	-
2-Octylbenzenesulfonate	0.80	0.50	1-136	6-8	-

CHAPTER 5

FINITE-BATH KINETICS

As indicated in Chapter 4, the adsorption equilibria being considered in the present research can all be classified as non-linear; however, the shape of the initial portion of the isotherm is indeed variable for different solutes ranging from the gentle slope of the phenol isotherm to the steep slopes of the DNOSBP, DNOCHP and alkylbenzenesulfonate isotherms. In this chapter, finite-bath kinetics will be discussed and applied to the solutes chosen for investigation. An approximation to replace the non-linear adsorption equilibrium model will be developed and used in a kinetic model.

Solution to Equation 3-3, the mass balance describing pore diffusion with simultaneous adsorption, can be accomplished by finite difference equations (11,12,35) when non-linear adsorption is assumed. But, dimensionless parameter inputs are such that only limited flexibility is allowed in choosing values of system parameters for a given output of C_F/C_{F_O} or ϕ as a function of time. Consequently, system investigation can be laborious, even with the aid of a digital computer.

PORE RESISTANCE CONTROLLING MODEL-ISOTHERM APPROXIMATION

Weber and Rumer (41) applied the Crank-Nicholson finite difference technique (12) to Equation 3-3 for a non-linear isotherm with a finite-bath boundary condition in order to test a pore diffusion model for description of the rates of adsorption for various alkylbenzenesulfonates on activated carbon. The data obtained from their investigation conformed very well to the proposed model. Snoeyink and Weber (31), used the same numerical technique and found the rate of adsorption of strong acids on activated carbon to also be described quite closely by a pore diffusion model.

An alternative to the use of a non-linear isotherm model is the approximation to an irreversible isotherm as previously mentioned (see Equation 3-4). The case of irreversible immobilization coupled with pore diffusion has been considered by Crank (13). The usual diffusion equation, given by Equation 5-1

$$D \nabla^2 C_F = \frac{\partial C_F}{\partial t} \qquad (5\text{-}1)$$

is to be solved with the following initial and boundary conditions applied to a spherical particle:

$$C_F = 0, \qquad t = 0,\ 0 < r < a \qquad (5\text{-}2)$$

$$V \frac{\partial C_F}{\partial t} = -4 \pi a^2 D \frac{\partial C_F}{\partial r}, \qquad r = a,\ t \geq 0 \qquad (5\text{-}3)$$

$$S \frac{\partial r_o}{\partial t} = -D \frac{\partial C_F}{\partial r}, \qquad r = r_o,\ t \geq 0 \qquad (5\text{-}4)$$

In Equation 5-4, r_o represents the position of the moving boundary. For $r \geq r_o$, all sites are occupied, while for $r < r_o$, all sites are unoccupied, since the concentration of molecules immobilized on the sites is zero if C_F is zero and equal to S when C_F is non zero. Equation 5-4 states that the rate at which the boundary advances, i.e., the number of sites occupied per unit time, is determined by the rate of supply of molecules by the diffusion flux. When r_o reaches the center of the sphere, Equation 5-4 is replaced by Equation 5-5.

$$\frac{\partial C_F}{\partial r} = 0, \qquad r = 0, \quad t \geq 0 \qquad (5\text{-}5)$$

The solution to such a moving boundary problem is analytical but quite complicated for all but the most simple boundary conditions. With the assumption of quasi-steady state, however, a straightforward solution is attainable for various boundary conditions and particle geometries. The quasi-steady state approximation entails the assumption that the rate of motion of the front is slow compared to the rate of immobilization and thus a steady state concentration gradient is established for $r_o \leq r \leq a$. As implied by Crank (13), the larger the ratio of S/C_{F_o}, the closer the steady state approximation approaches the formal mathematical solution.

A mass balance, written for a spherical particle, considering diffusion flux, N, only, yields Equation 5-6.

$$-\frac{\partial (N r^2)}{r^2 \partial r} = \frac{\partial C_F}{\partial t} \qquad (5\text{-}6)$$

The quasi-steady state assumption sets $\partial C_F / \partial t$ equal to zero and thus the product $r^2 N$ is always constant.

$$- r^2 D \frac{\partial C_F}{\partial r} = a^2 N_o \qquad (5\text{-}7)$$

Flux at the surface of the sphere, N_o, can be related to the frontal position, r_o, by integrating Equation 5-7 between $r = r_o$, $C_F = 0$ and $r = a$, $C_F = C_{F_1}$ to yield

$$N_o = - \frac{D C_{F_1}}{a} \left[\frac{r_o}{a - r_o} \right] \qquad (5\text{-}8)$$

Using Equation 5-7, the concentration gradient can be found by substituting for N_o and integrating between $r = r$, $C_F = C_F$ and $r = r_o$, $C_F = 0$ to yield Equation 5-9.

$$C_F = \frac{a C_{F_1}}{r} \left[\frac{r_o - r}{r_o - a} \right] \qquad (5\text{-}9)$$

Differentiation of Equation 5-9 at $r = r_o$ and $r = a$ and substitution into the respective boundary condition equations 5-4 and 5-3, results in an expression that relates the change in solution concentration, C_{F_1}, to the change in frontal position, r_o.

$$V \, d \, C_{F_1} = 4 \pi \, S \, r_o^2 \, d \, r_o \qquad (5\text{-}10)$$

Integration of Equation 5-10 between $r_o = a$, $C_{F_1} = C_{F_o}$ at $t = 0$ and $r_o = r_o$, $C_{F_1} = C_{F_1}$ at time t yields

$$\phi = \frac{C_{F_1}}{C_{F_o}} = 1 + \frac{4\pi}{3V} \frac{S}{C_{F_o}} a^3 \left[\left(\frac{r_o}{a}\right)^3 - 1 \right] \qquad (5\text{-}11)$$

Substitution of $C_{F_1} = f\,(r_o)$ from Equation 5-11 into Equation 5-9 followed by substitution into the frontal boundary condition (Equation 5-4) gives the advancement of the front as a function only of frontal position.

$$S \frac{d \, r_o}{dt} = \frac{a \, D \, C_{F_o}}{r_o \, (r_o - a)} \left[1 + \frac{4\pi}{3V} \frac{S}{C_{F_o}} a^3 \left[\left(\frac{r_o}{a} \right)^3 - 1 \right] \right] \qquad (5\text{-}12)$$

Finally, frontal position as a function of time is obtained from integration of Equation 5-12 between $t = 0$, $r_o = a$ and $t = t$, $r_o = r_o$.

$$\int_1^{\left(\frac{r_o}{a}\right)} \frac{\left(\frac{r_o}{a}\right) \left(\frac{r_o}{a} - 1\right) d \left(\frac{r_o}{a}\right)}{1 + \frac{4\pi}{3V} \frac{S}{C_{F_o}} a^3 \left[\left(\frac{r_o}{a}\right)^3 - 1 \right]} = \frac{C_{F_o}}{S} \frac{D \, t}{a^2} = T \qquad (5\text{-}13)$$

Equation 5-13, employing a dimensionless frontal position parameter, (r_o/a), can then be used in conjunction with Equation 5-11 to produce a dimensionless rate of adsorption plot (ϕ versus $T = [C_{F_o}/S] \cdot D \, t/a^2$).

It may be noted that the denominator of the integrand in Equation 5-13 is equal to C_{F_1}/C_{F_o} as given by Equation 5-11 thereby relating C_{F_1}/C_{F_o} to the numerical integration in a direct manner. Furthermore, the coefficient of $\left[\left(\frac{r_o}{a}\right)^3 - 1\right]$ may be considerably simplified by expressing S, the surface site concentration, in moles/cm^3, as

$$S = (C_{F_o} - C_{F_e})\frac{\rho}{W} \qquad (5\text{-}14)$$

from the adsorption equilibrium. The term V, is actually the inverse of the number of particles per unit volume of solution where

$$\text{No. of particles} = \frac{W}{\rho \cdot \frac{4}{3} \pi a^3} \qquad (5\text{-}15)$$

or,

$$V = \frac{\rho}{W} \frac{4}{3} \pi a^3 \qquad (5\text{-}16)$$

Substituting for S and V in Equation 5-11 gives

$$\phi = 1 + (1 - \phi_e) \left[\left(\frac{r_o}{a}\right)^3 - 1\right] \qquad (5\text{-}17)$$

where

$$\phi_e = \frac{C_{F_e}}{C_{F_o}}$$

This simplification, applied to the integrand of Equation 5-13, allows calculation of a family of integrals for values of ϕ_e between 0 and 1 which can then be used for any system combination of initial solute concentration and carbon dosage. In Figure 5-1, frontal position (r_o/a) is plotted versus the integral, represented by $F\ (r_o/a)$, for ϕ_e of 0.0, 0.2 and 0.5. The corresponding values of ϕ, from Equation 5-11, are shown versus T in Figure 5-2 for the same assumed dimensionless equilibrium positions.

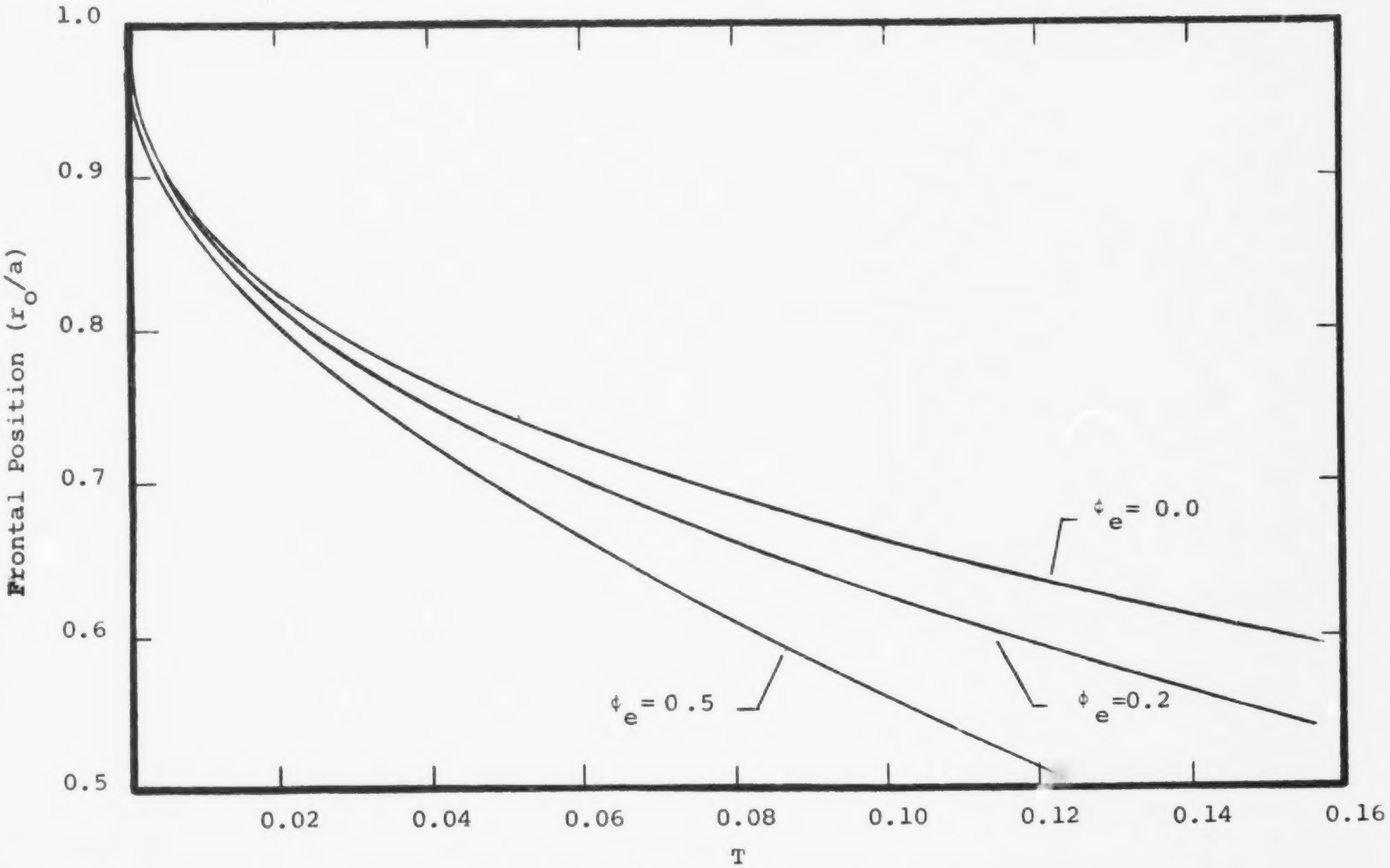

FIGURE 5-1. FRONTAL POSITION (r_o/a) AS A FUNCTION OF DIMENSIONLESS TIME, T.

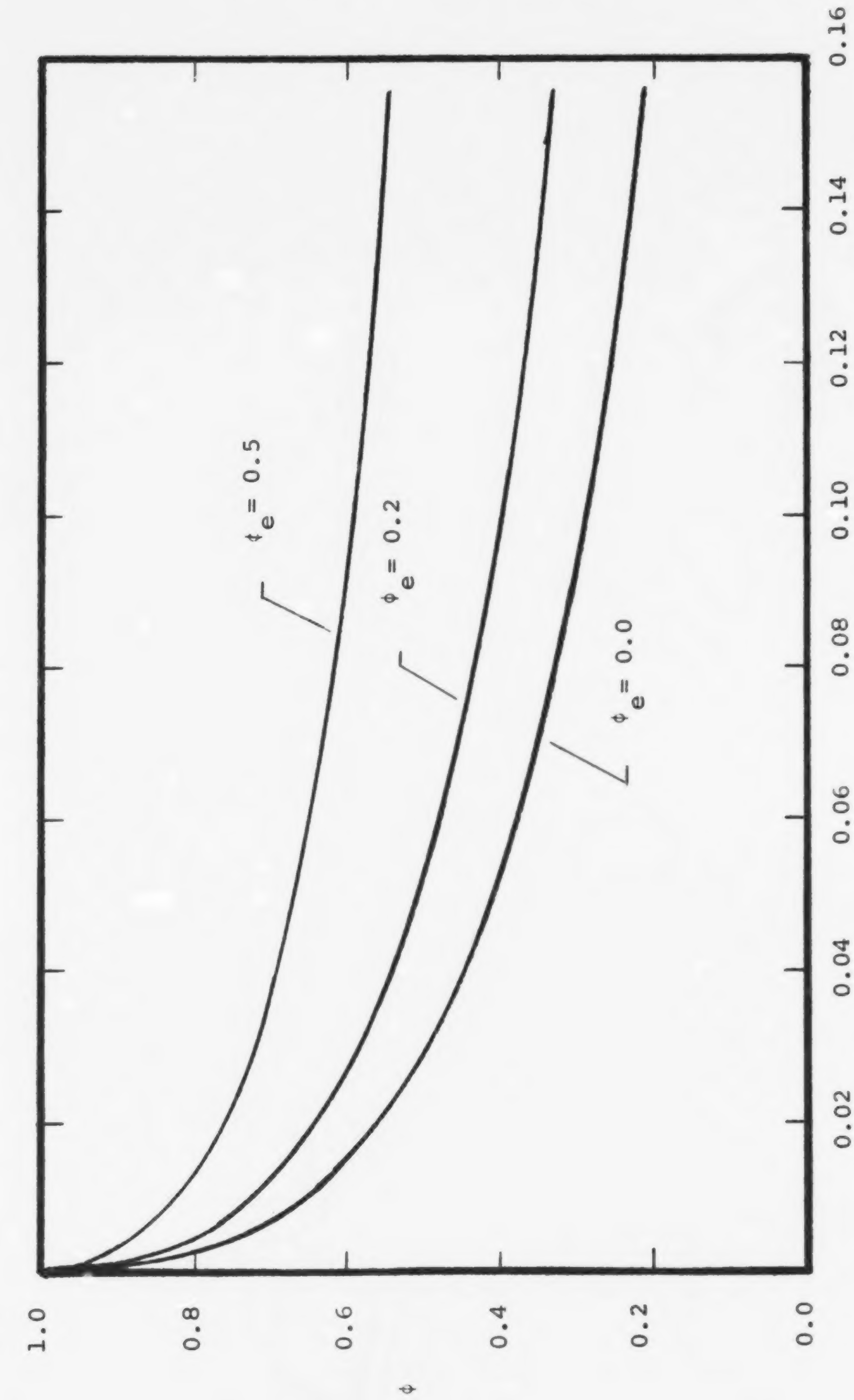

FIGURE 5-2. DIMENSIONLESS SOLUTION CONCENTRATION, ϕ, AS A FUNCTION OF DIMENSIONLESS TIME, T, FOR ϕ_e VALUES OF 0.5, 0.2 AND 0.0 .

COMBINED INTERNAL AND EXTERNAL RESISTANCE CONTROLLING

For the case of film diffusion in series with internal pore diffusion and adsorption, a new surface boundary condition is introduced.

$$- D \frac{\partial C_{F_i}}{\partial r} = k_f \; (C_{F_i} - C_{F_1}), \; r = a, \; t \geq 0 \qquad (5\text{-}18)$$

In Equation 5-18, k_f is the transfer coefficient (cm/sec) characterizing the mass transfer resistance at the particle surface, C_{F_i} the concentration on the inside of the film and C_{F_1}, the concentration on the outside, i.e., solution concentration.

The approximation to an irreversible isotherm model can provide a very manageable solution to the case of combined external and internal resistance controlling. With the assumption of quasi-steady state, the surface fluxes given by Equations 5-8 (with C_{F_1} replaced by C_{F_i}) and 5-18 may be equated and the internal concentration C_{F_i} eliminated to yield Equation 5-19.

$$N_o = - \frac{C_{F_1}}{\left[\frac{1}{D} \frac{(a - r_o)}{r_o} + \frac{1}{k_f}\right]} \qquad (5\text{-}19)$$

Replacement of the flux given in Equation 5-3 by that in Equation 5-19 yields

$$V \frac{d \; C_{F_1}}{d \; t} = - \frac{4 \; \pi \; a^2 \; C_{F_1}}{\left[\frac{a}{D} \frac{(a - r_o)}{r_o} + \frac{1}{k_f}\right]} \qquad (5\text{-}20)$$

Equation 5-10 generally relates the change in solution concentration to the movement of the front, r_o, and therefore remains valid for the new surface boundary condition. As a result, Equation 5-11, giving C_{F_1} as a function of r_o, may be substituted into Equation 5-20 which then yields an expression similar to Equation 5-12 and describes the rate of change of frontal position as a function of frontal position only. Thus,

$$V \frac{d}{dt}\left[C_{F_o}\left[1 + \frac{4\pi}{3V}\frac{S}{C_{F_o}}\, a^3 \left[\left(\frac{r_o}{a}\right)^3 - 1\right]\right]\right] =$$

$$\frac{-\,4\pi a^2 \left[C_{F_o}\left[1+\frac{4}{3V}\frac{S}{C_{F_o}}\, a^3\left[\left(\frac{r_o}{a}\right)^3-1\right]\right]\right]}{\left[\frac{a}{D}\,\frac{(a-r_o)}{r_o}+\frac{1}{k_f}\right]} \qquad (5\text{-}21)$$

simplifying,

$$\frac{\left[\frac{a}{D}\,\frac{(a-r_o)}{r_o}+\frac{1}{k_f}\right]\cdot S\; a\left(\frac{r_o}{a}\right)^2 \frac{d\left(\frac{r_o}{a}\right)}{d\,t}}{-\,C_{F_o}\left[1+\frac{4\pi S}{3V}\,\frac{a^3}{C_{F_o}}\left[\left(\frac{r_o}{a}\right)^3-1\right]\right]} = 1 \qquad (5\text{-}22)$$

or,

$$-\frac{\left(\frac{r_o}{a}\right)^2\left[\frac{a}{D}\,\frac{(a-r_o)}{r_o}+\frac{1}{k_f}\right] d\left(\frac{r_o}{a}\right)}{1+\frac{4\pi S}{3V}\,\frac{a^3}{C_{F_o}}\left[\left(\frac{r_o}{a}\right)^3-1\right]} = \frac{C_{F_o}}{a\;S}\,d\,t \qquad (5\text{-}23)$$

Multiplying both sides by D/a gives

$$\frac{\left(\frac{r_o}{a}\right)\left(\frac{r_o}{a}-1\right) d\left(\frac{r_o}{a}\right) - \left(\frac{r_o}{a}\right)^2 \frac{D}{k_f\,a}\, d\left(\frac{r_o}{a}\right)}{1+\frac{4\pi S}{3V}\,\frac{a^3}{C_{F_o}}\left[\left(\frac{r_o}{a}\right)^3-1\right]} = \qquad (5\text{-}24)$$

$$\frac{C_{F_o}}{S}\,\frac{D}{a^2}\,d\,t$$

Integration of Equation 5-24, having the same integrand denominator as Equation 5-13, then expresses frontal position as a function of the dimensionless time parameter, T.

$$\int_{\left(\frac{r_o}{a}\right)}^{1} \frac{\left(\frac{r_o}{a}\right)\left(1 - \frac{r_o}{a}\right) d\left(\frac{r_o}{a}\right)}{1 + (1 - \phi_e)\left(\left(\frac{r_o}{a}\right)^3 - 1\right)} + \frac{D}{k_f a} \int_{\left(\frac{r_o}{a}\right)}^{1} \frac{\left(\frac{r_o}{a}\right)^2 d\left(\frac{r_o}{a}\right)}{1 + (1 - \phi_e)\left(\left(\frac{r_o}{a}\right)^3 - 1\right)} = T \tag{5-25}$$

It may be noted that the first integral on the left hand side of Equation 5-25 is exactly the same as that obtained for the pore diffusion resistance model given by Equation 5-13. The second integral, which will be designated as $G(r_o/a)$, is the result of considering film resistance in series with pore resistance. Figures 5-3 and 5-4 show the calculated curves obtained for $G(r_o/a)$ as a function of frontal position (r_o/a) and dimensionless solution concentration ϕ respectively, using the same three values of ϕ_e for which the function $F(r_o/a)$ was plotted in Figures 5-1 and 5-2.

For $k_f \rightarrow \infty$, Equation 5-25 reduces to Equation 5-13, the pore diffusion model. A further comparison with Equation 5-13 reveals that for any finite value of k_f, the combined film-pore diffusion model gives a larger value of T at any (r_o/a), or correspondingly, at any value of ϕ. Values of k_f of .001, .005, .01 and ∞ cm/sec produce the calculated curves of ϕ versus T shown in Figure 5-5. For each curve, the other model inputs, D, $S/C_{F_o} a^2$ and $(1 - \phi_e)$ were arbitrarily chosen to be 1×10^{-5} cm^2/sec, 3.6 and 0.9

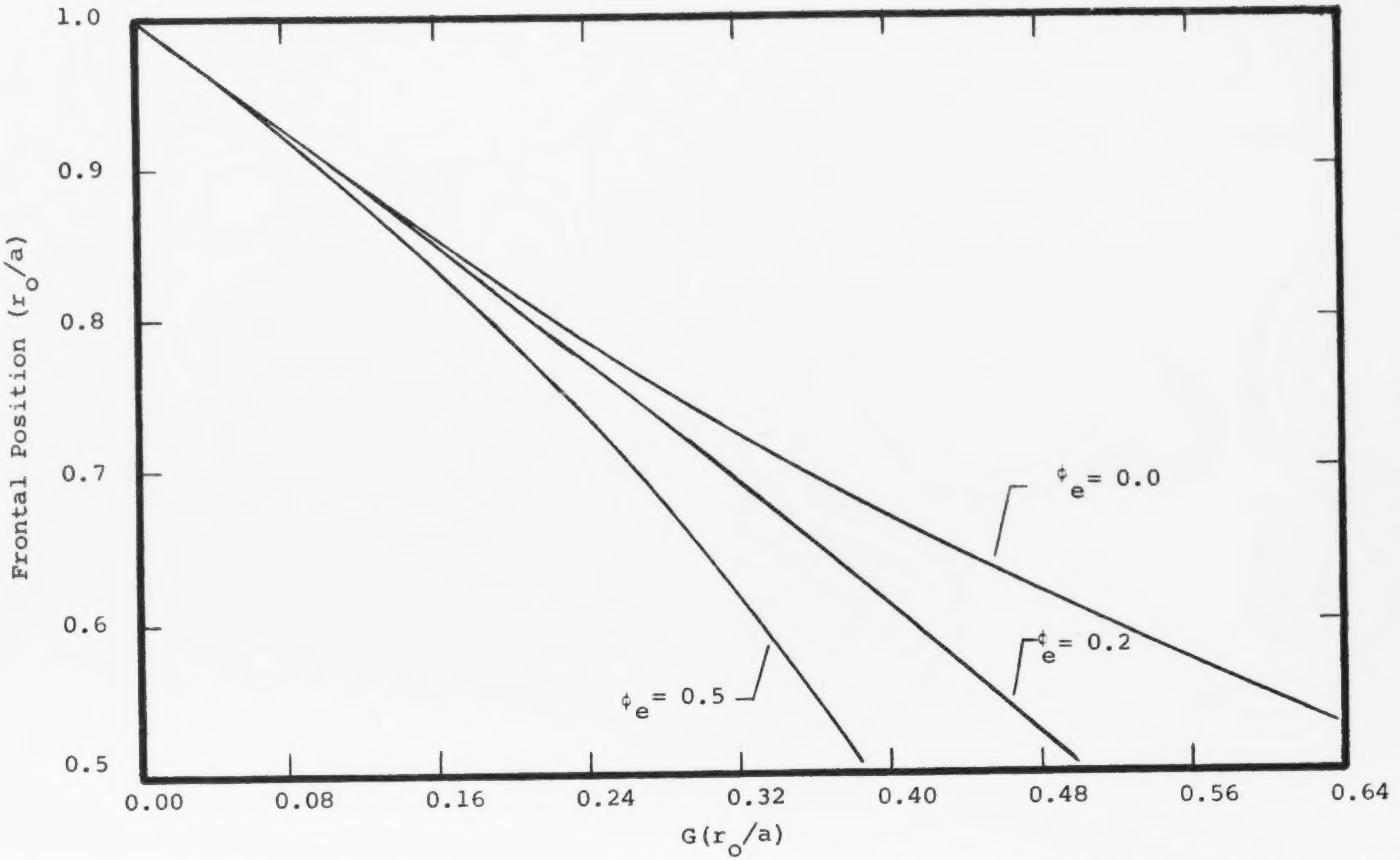

FIGURE 5-3. FRONTAL POSITION (r_o/a) AS A FUNCTION OF FILM DIFFUSION PARAMETER $G(r_o/a)$ FOR ϕ_e VALUES OF 0.5, 0.2 AND 0.0 .

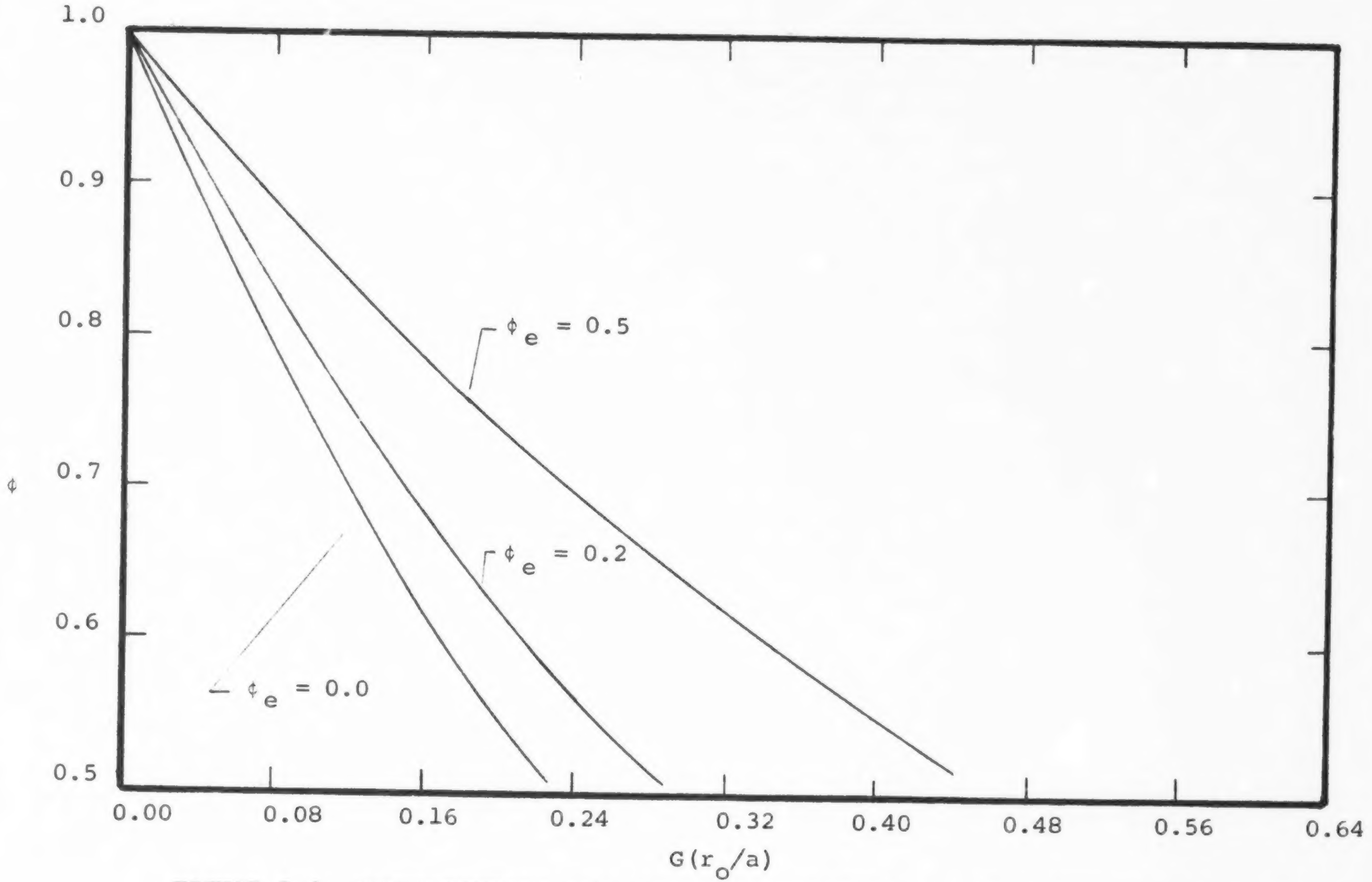

FIGURE 5-4. DIMENSIONLESS SOLUTION CONCENTRATION, ϕ , AS A FUNCTION OF FILM DIFFUSION PARAMETER $G(r_o/a)$ FOR ϕ_e VALUES OF 0.5, 0.2 AND 0.0 .

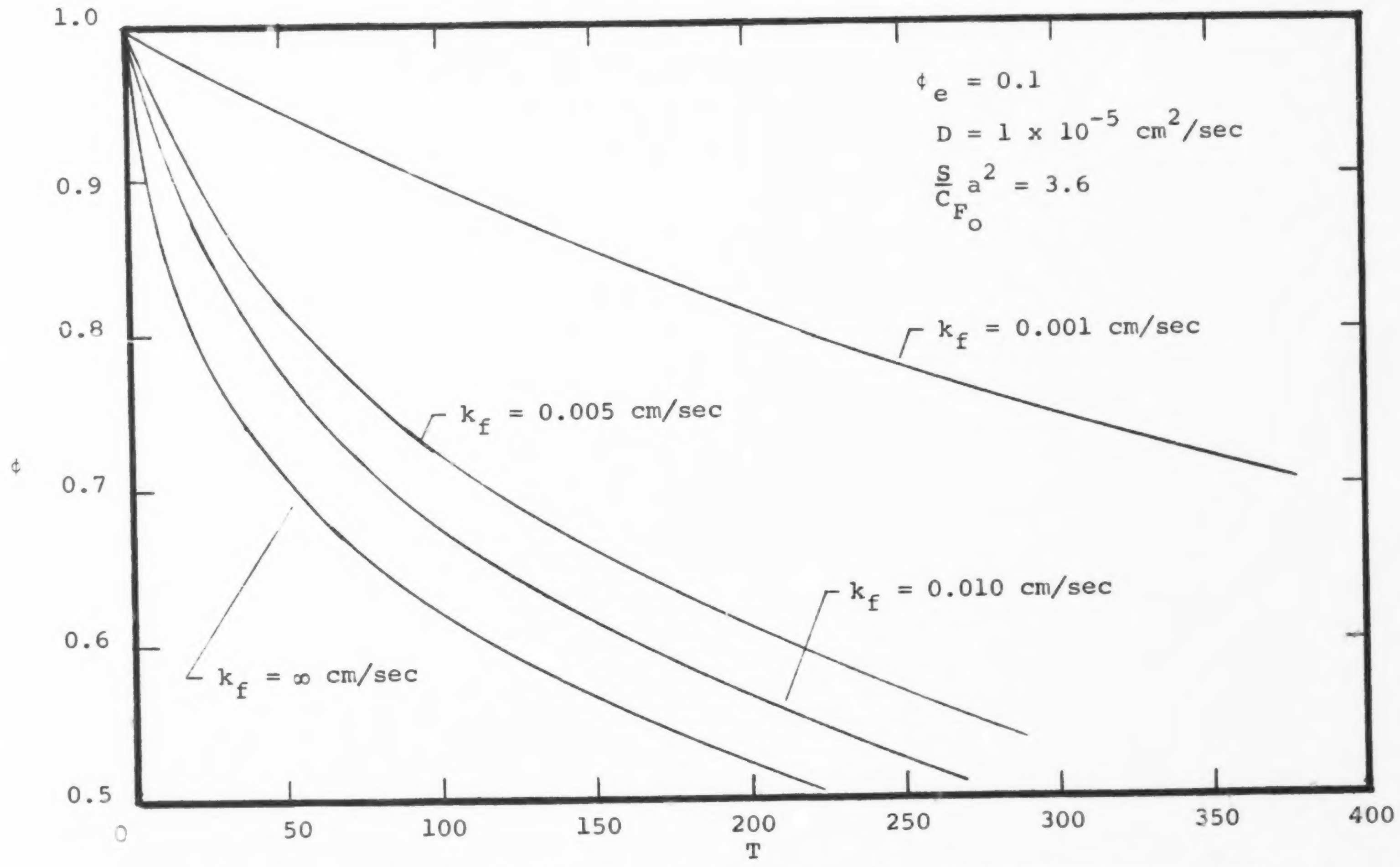

FIGURE 5-5. EFFECT OF TRANSFER COEFFICIENT, k_f, ON DIMENSIONLESS RATE OF ADSORPTION FOR COMBINED FILM AND PORE DIFFUSION MODEL.

respectively. As the value of k_f decreases, the initial rate of adsorption is continually retarded. Theoretically, the slope of ϕ versus T at $t = 0$ is infinite in a pore diffusion model while finite in a combined film-pore diffusion model.

LIMITATIONS OF IRREVERSIBLE IMMOBILIZATION AND QUASI-STEADY STATE ASSUMPTIONS

The preceeding section dealt with the formulation of a simplified kinetic model for a finite-bath system in which film and pore diffusion were controlling in series. This difficult set of boundary conditions, in addition to a non-linear isotherm, would have made a solution prohibitive if the assumptions of irreversible immobilization and quasi-steady state were not used. However, there will clearly be limitations to the model. Actually, two types of constraints must be considered. First, the shape of the isotherm will affect the assumption of irreversible immobilization. Secondly, the equilibrium distribution ratio of solid to liquid phase will affect the assumption of quasi-steady state since the lower the ratio, the greater the time rate of change in liquid phase concentration at any location within the pores.

As previously mentioned, a model may be formulated for finite-bath kinetics in which a non-linear isotherm is considered. A numerical methods technique is required and only the pore diffusion controlling case can be easily solved. However, such a model provided the basis for defining the limitations of the simplified model given by Equation 5-13. The procedure was to select a given isotherm shape, calculate a solution concentration-time profile and compare the result with that calculated from the simplified model using an irreversible instead of a non-linear isotherm. Moreover, the case of film diffusion acting in series with pore diffusion (Equation 5-25) was examined indirectly by considering $k_f \rightarrow \infty$.

The transient diffusion and simultaneous adsorption model, Equation 3-3, with C_s given by the Langmuir isotherm equation, may be solved by using the Crank-Nicholson implicit finite difference technique (11, 12). The details of the approximations used for the first and second derivatives with respect to distance, r, and first derivative with respect to time, t, are given in Appendix A together with a description of solution technique. Although Snoeyink and Weber (31) used a similar model, improvements have been made which considerably decreased the computer time required. For example, it was found much more expedient to use 50 rather than 8 to 12 distance steps as proposed by Snoeyink and Weber (31). Of these 50 steps, only the first 6 to 10 were actually calculated since the fluid phase concentration gradient decreased very rapidly with distance from the exterior of the particle.

As given in Appendix A, the following dimensionless parameters were used for time, and the Langmuir isotherm constants:

$$\theta = \frac{D\ t}{a^2} \tag{5-26}$$

$$\alpha = Q \frac{\rho}{C_{F_o}} \tag{5-27}$$

$$\beta = b\ C_{F_o} \tag{5-28}$$

In addition to α and β, the volume served per particle, V, must also be specified as input to the model since the boundary condition given by Equation 5-29 must be applied.

$$V(1-\phi) = 4\pi a^3 \int_0^1 (\varepsilon\phi + \sigma)\xi^2 d\xi \quad (5\text{-}29)$$

The dimensionless term σ refers to the solid phase concentration given by[1]

$$\sigma = \frac{\alpha\beta\phi}{1+\beta\phi} \quad (5\text{-}30)$$

and ξ is the dimensionless distance variable. Since Equation 5-16 defines V, the actual model input may be simplified to

$$V_p = \frac{4\pi a^3}{V} = 3 \cdot \frac{W}{\rho} \quad (5\text{-}31)$$

The value of ρ/W depends on the equilibrium position being approached. This may be calculated for a given value of equilibrium concentration, ϕ_e, since the corresponding σ_e may be expressed as

$$\sigma_e = \frac{(C_{F_o} - C_{F_e})}{C_{F_o}} \cdot \frac{\rho}{W} \quad (5\text{-}32)$$

or,

$$\frac{\rho}{W} = \frac{\sigma_e}{1-\phi_e} \quad (5\text{-}33)$$

Figures 5-6 and 5-7 show the hypothetical isotherms to be tested. The values of β chosen were 5, 30, and 50 since these are representative of the range encountered when considering adsorption equilibria given in Chapter 4 and initial concentrations, C_{F_o}, used in rate studies; that is, the range of C_{F_o} of interest was between 0.4 and 1.0 x 10^{-4} M and the values of b varied from 0.022 to 0.5 x 10^{+6} l/mol. Values of Q obtained from adsorption equilibrium studies ranged from 2.5 x 10^{-3} M/gm for DNP (N) to .37 x 10^{-3} M/gm for phenol (A). Representative values of α were therefore selected to be 10,000 and 20,000, assuming the same range of

[1] The term σ includes $(1-\epsilon)\rho_{Solid}$ in calculation of α.

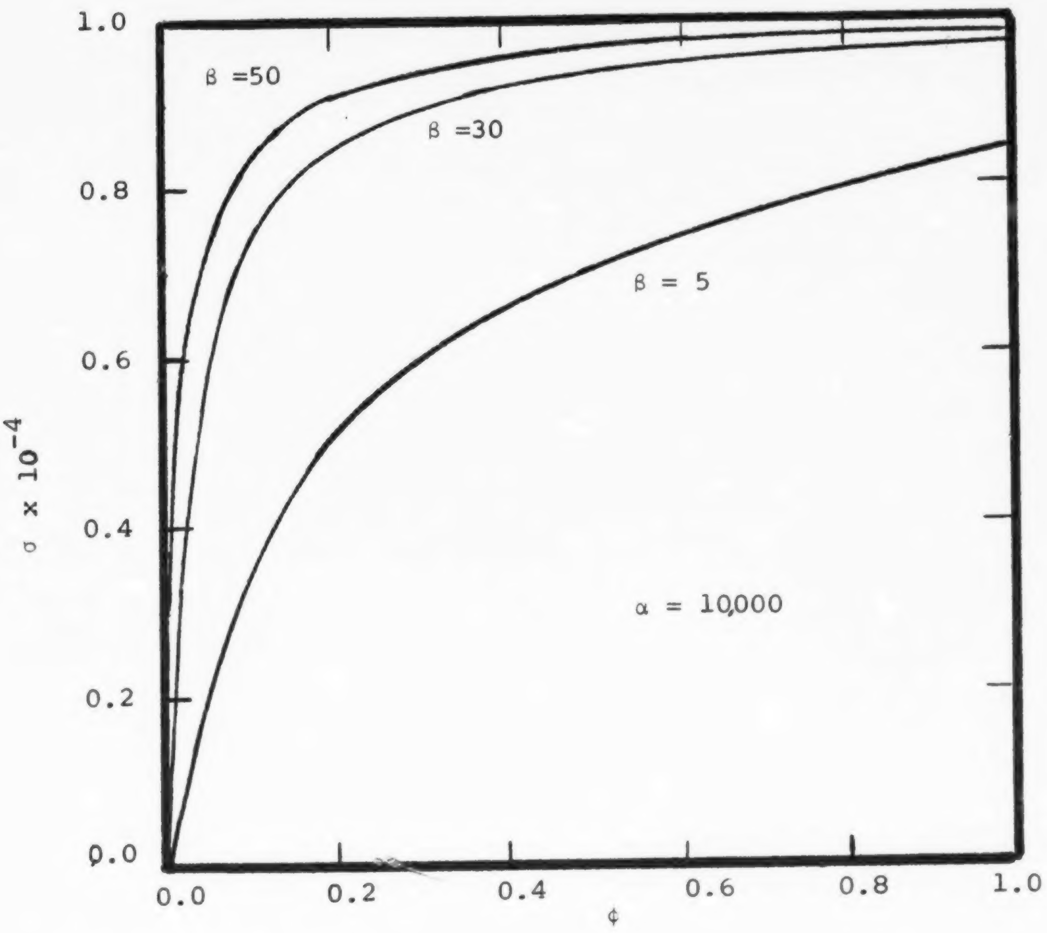

FIGURE 5-6. HYPOTHETICAL ISOTHERMS TO TEST SIMPLIFIED KINETIC MODEL. $\alpha = 10{,}000$ AND $\beta = 5, 30$ AND 50 .

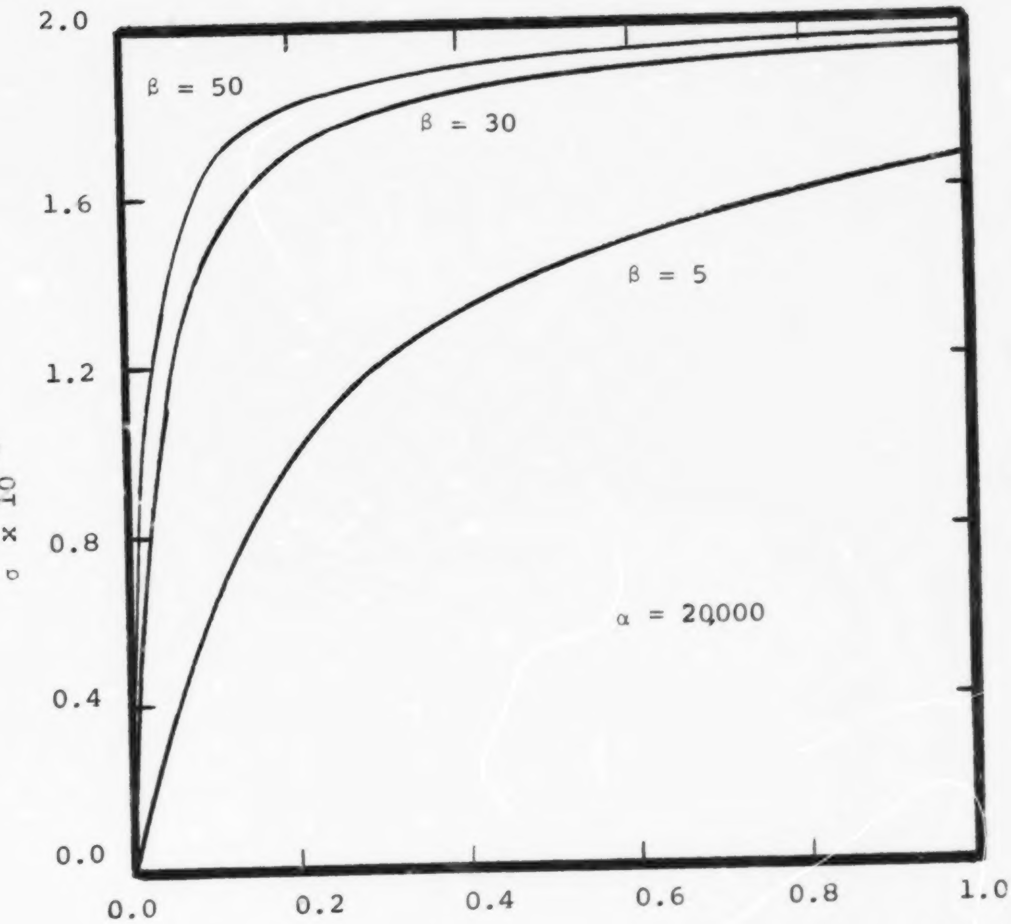

FIGURE 5-7. HYPOTHETICAL ISOTHERMS TO TEST SIMPLIFIED KINETIC MODEL. α = 20,000 AND β =5,30 AND 50.

C_{F_o} as above and an apparent particle density, ρ , of 0.750 gm/cc. This value is actually $(1-\varepsilon)\cdot\rho_{solid}$ which also applies to Equation 3-3 for calculating C_S and to Equation 5-31 for calculating V_p. An apparent density of 0.750 gm/cc is given by the Calgon Company for a similar carbon (7). Dedrick and Beckman (15), using a Columbia Carbon, were able to measure dry particle density quite accurately since they used much larger particles than employed in this study. The resulting densities reported were quite close to 0.750 gm/cc. As given on page 23, the total pore volume is about 0.676 cc/gm which yields a porosity, ε , of 0.5.

The entries in Table 5-1 are the values of V_p calculated for each isotherm and selected value of equilibrium, ϕ_e. An additional isotherm, with α and β values of 2000 and 2.2 respectively, will be discussed in a later section of this chapter dealing with the kinetic behavior of phenol (A).

TABLE 5-1

CALCULATED VALUES OF V_p FOR SELECTED ISOTHERMS AND EQUILIBRIUM POSITIONS

α	10,000			20,000		
β / ϕ_e	5	30	50	5	30	50
.1	7.80×10^{-4}	5.40×10^{-4}	3.6×10^{-4}	4.35×10^{-4}	2.70×10^{-4}	1.80×10^{-4}
.2		2.78×10^{-4}			1.40×10^{-4}	

The calculated curves obtained by a finite difference solution to the pore diffusion with simultaneous non-linear adsorption model are shown in Figure 5-8 for α = 10,000, Φ_e = 0.1, and β = 5, 30 and 50. Comparison to the irreversible immobilization model is accomplished by converting dimensionless time, T, of Equation 5-13 to dimensionless time, θ, of Equation 5-26 as follows:

$$\theta = \frac{S}{C_{F_o}} T \qquad (5\text{-}34)$$

where S/C_{F_o}, as previously defined, is equivalent to σ_e of Equation 5-32. Therefore, after selecting the desired Φ_e, curves of Φ versus θ may be plotted for the simplified pore diffusion model, since Φ is given as a function of T as shown in Figure 5-2.

The calculated curves obtained from the simplified model are shown in Figure 5-8. As expected, the assumptions of irreversible immobilization and quasi-steady state yield better approximations to the actual rate of adsorption as the value of β increases. It may also be observed that the rate of adsorption decreases as β increases. The obvious reason for this behavior is that carbon dosage W, decreases and hence volume of solution served per particle, V, increases with increasing β if the final equilibrium position remains the same.

The results obtained when α was increased to 20,000 are shown in Figure 5-9. For each value of β, a slower rate of adsorption than that for α of 10,000 was calculated, since the higher solid to liquid phase distribution, as measured by α, increases the value of V. Comparison of the two models again indicates that irreversible immobilization becomes a more valid assumption as β increases from 5 to 50.

Figure 5-10 illustrates the effect of increasing Φ_e from 0.1 to 0.2 for a β value of 30 and α of 10,000, and

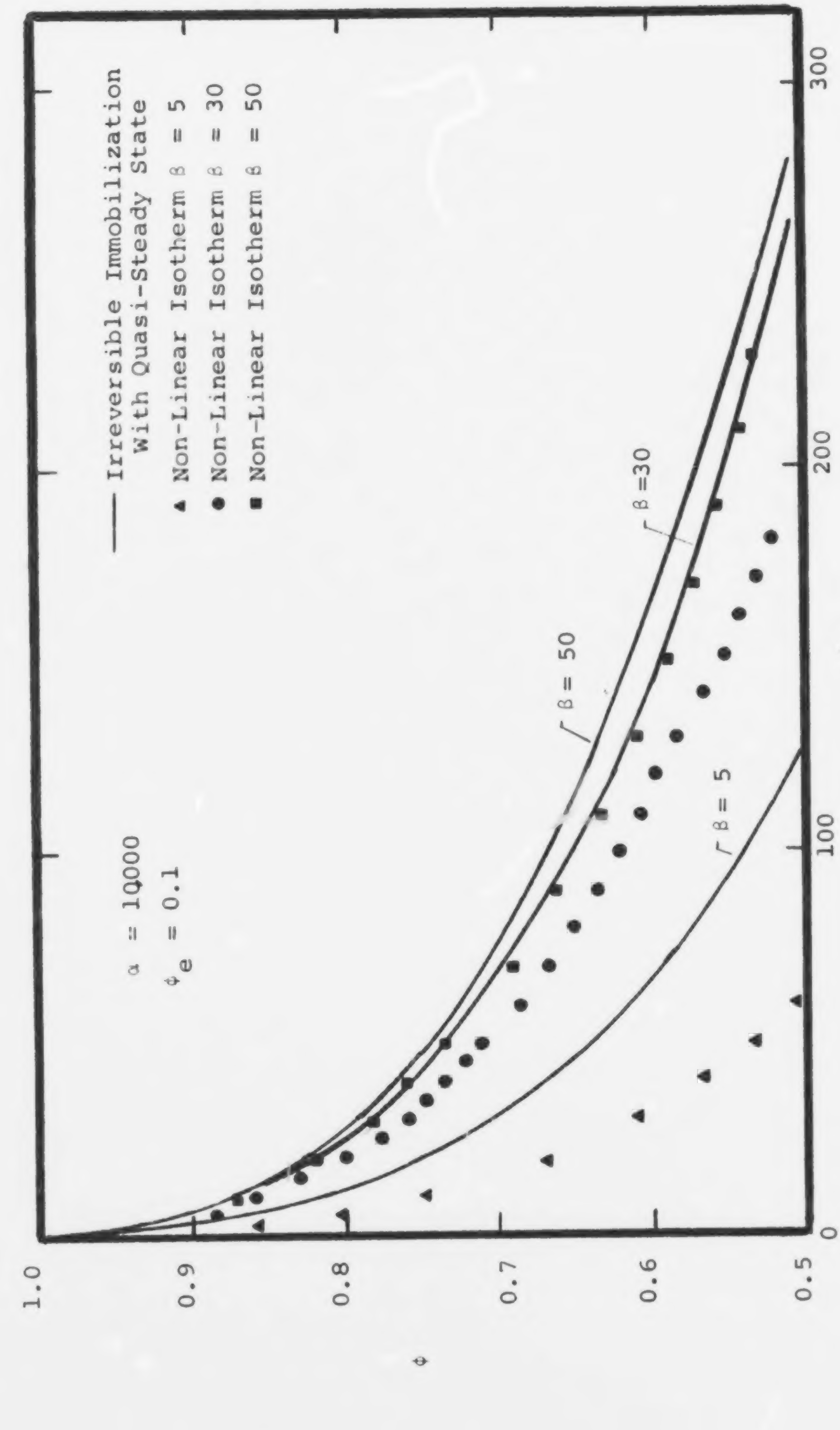

FIGURE 5-8. COMPARISON OF MODELS USING IRREVERSIBLE IMMOBILIZATION AND ACTUAL NON-LINEAR ISOTHERM FOR α = 10,000 AND $\phi_e = 0.1$.

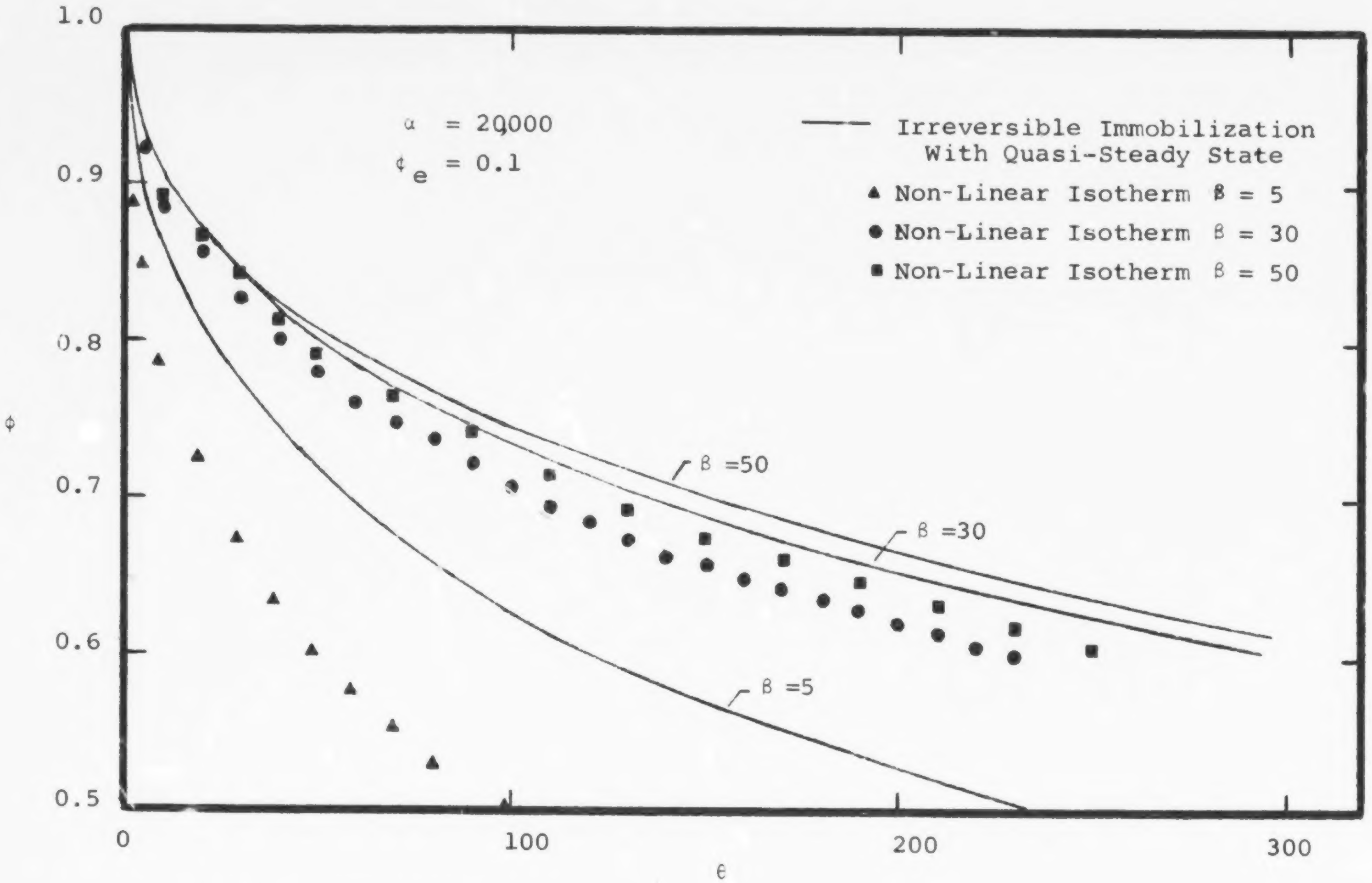

FIGURE 5-9. COMPARISON OF MODELS USING IRREVERSIBLE IMMOBILIZATION AND ACTUAL NON-LINEAR ISOTHERM FOR α = 20,000 AND ϕ_e = 0.1 .

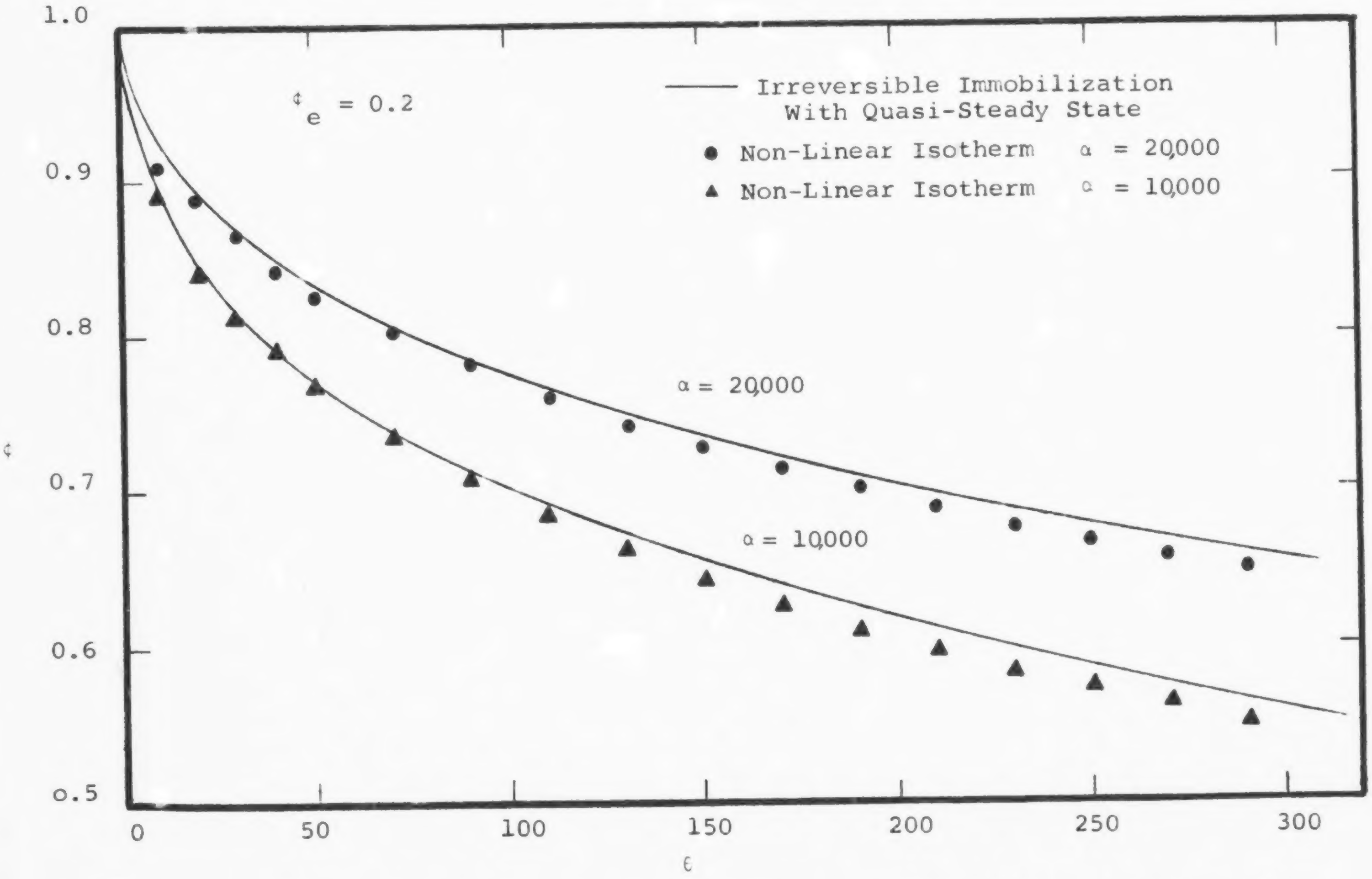

FIGURE 5-10. COMPARISON OF MODELS USING IRREVERSIBLE IMMOBILIZATION AND ACTUAL NON-LINEAR ISOTHERM FOR $\phi_e = 0.2$ AND $\beta = 30$.

20,000. This result could be predicted since less of the highly non-linear region of the isotherm is of significance.

SENSITIVITY TEST FOR SIMPLIFIED KINETIC MODEL

Fitting experimental data to Equations 5-13 and 5-25, the simplified pore and film-pore diffusion models respectively, should yield a system constant, D, if model assumptions are valid. That is, a linear plot of $F(r_o/a)$ versus t should follow from experimental data if the model adequately describes the pore diffusion controlled case and external film resistance is negligible. Moreover, the combined film and pore diffusion model should also yield a linear function since the pore diffusion model results from letting $k_f \to \infty$. If the second integral on the left of Equation 5-25 is denoted by $G(r_o/a)$ and the first again by $F(r_o/a)$, then

$$F\left(\frac{r_o}{a}\right) + \frac{D}{k_f a} G\left(\frac{r_o}{a}\right) = T \tag{5-35}$$

or,

$$\frac{F\left(\frac{r_o}{a}\right)}{G\left(\frac{r_o}{a}\right)} + \frac{D}{k_f a} = \frac{T}{G\left(\frac{r_o}{a}\right)} = \frac{C_{F_o}\ D\ t}{S\ a^2\ G\left(\frac{r_o}{a}\right)} \tag{5-36}$$

Thus, a linear plot of $F(r_o/a)/G(r_o/a)$ versus $C_{F_o}\ t/\ (Sa^2 G(\frac{r_o}{a}))$ should be obtained from experimental data with D given by the slope and $D/k_f a$ by the intercept, from which k_f can be calculated. If pore diffusion alone controls, then the origin is the intercept.

To test the sensitivity of the combined resistance model, the calculated model points of ϕ versus θ, for the pore diffusion model incorporating the non-linear isotherm, may be considered as data input to the simplified model. As before, T may be related to θ to yield Equation 5-37.

$$\frac{F(\frac{r_o}{a})}{G(\frac{r_o}{a})} + \frac{D}{k_f a} = \frac{\theta}{\sigma_e \; G(\frac{r_o}{a})} \qquad (5\text{-}37$$

A plot of $F(r_o/a)/G(r_o/a)$ versus $\theta / \sigma_e G(r_o/a)$ should therefore give a slope of one and an intercept of zero.

The results of applying this test are shown in Figure 5-11, for a value of α of 10,000 and ϕ_e of 0.1 with β equal to 5, 30 and 50. The discrepancy between the two calculated model functions as previously shown in Figure 5-8 is also apparent from Figure 5-11. Since both were designed to approach the same value of ϕ_e, convergence of the models is expected as θ increases. Therefore, a convex curve, returning to the theoretical slope line of one is predicted for each set of data points shown in Figure 5-11. If curvature is mistakenly ignored as experimental error, the value of D calculated would be about 1.25 times greater than the actual for β equal to 30. In contrast, D would be about twice the actual for β equal to 5.

From the above discussion, it may be generally concluded that the simplified model, although somewhat bounded, may be applied for a variety of isotherm shapes. This then allows consideration of a model for the combined film and pore resistance controlling case in a finite-bath system by a rather straightforward calculating procedure. The two most critical dimensionless system parameters are ϕ_e and β. As both become larger, the simplified kinetic model better approximates the model incorporating the actual non-linear isotherm. Since β is the product of b times C_{F_o}, the value of β may be experimentally controlled, providing adsorption equilibrium information is available. Moreover, ϕ_e is also the result of experimental design; but increasing ϕ_e has the effect of increasing V, the volume served per particle (see Equations 5-33 and 5-11), thereby reducing the observed

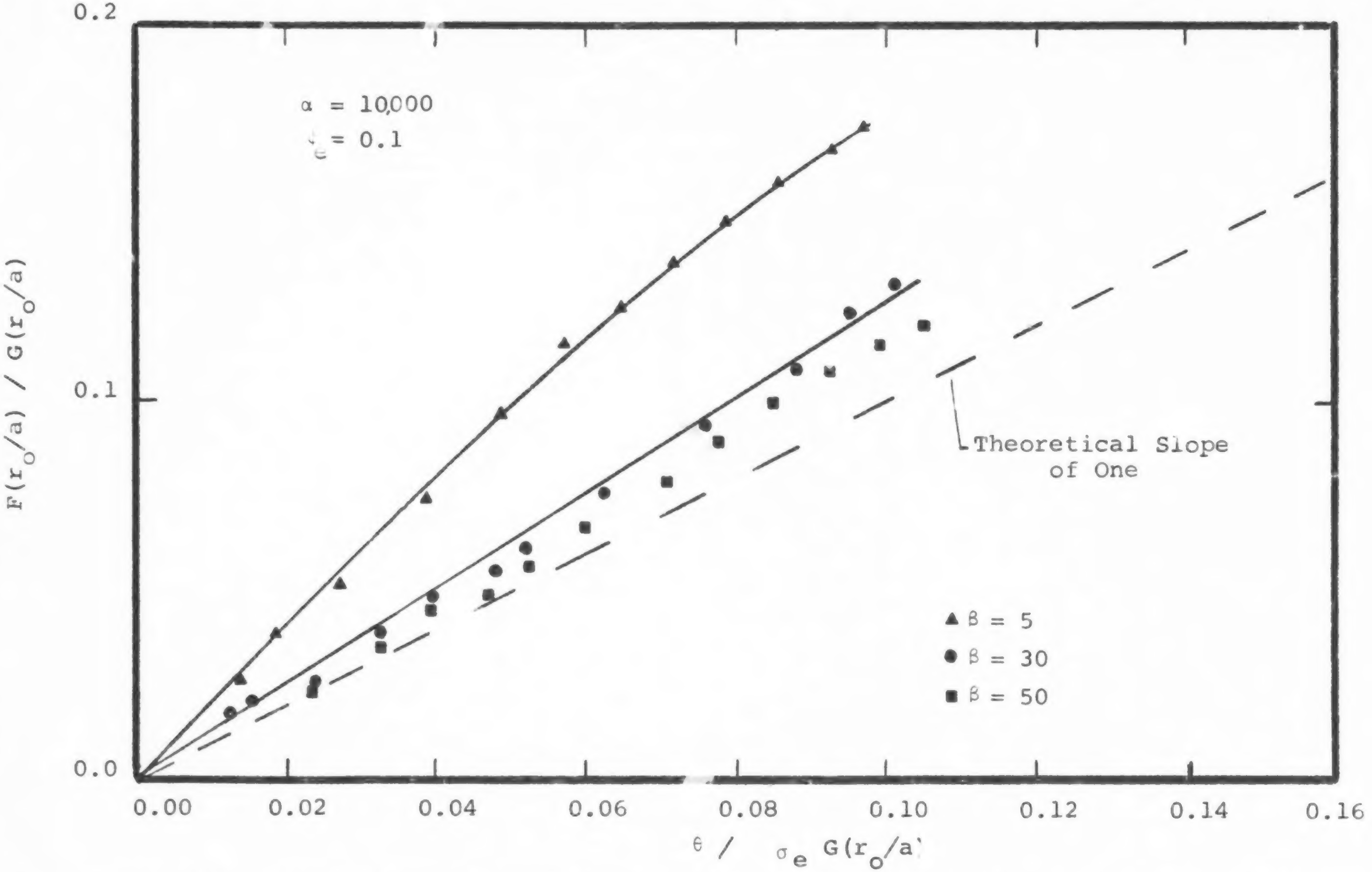

FIGURE 5-11. SENSITIVITY OF SIMPLIFIED MODEL FOR $\alpha = 10{,}000$, $\phi_e = 0.1$ AND $\beta = 5$, 30 AND 50

rate of adsorption and lengthening experimental observation time.

EXPERIMENTAL MATERIALS AND PROCEDURE

The solutes under investigation have been discussed in Chapter 4. In addition to the 30/40 size fraction of activated carbon employed in the equilibrium studies, 16/20, 20/30, 40/50, 50/60, and 60/80 fractions, having mean diameters of 0.100, 0.0710, 0.0350, 0.0273 and 0.0211 cm respectively, were used in the kinetic experiments to be reported.

All experiments were carried out at room temperature in 3.5 liter widemouth jars, each fitted with two plexiglass baffles, 2 centimeters wide, extending to within 1 centimeter of the bottom. A finite-bath technique was applied, with agitation provided by a variable speed, electric motor driven, polyethylene stirring blade, the rpm of which was adjusted with the aid of a strobe light. Initial investigation showed that no measurable adsorption occurred on either the baffles or stirring blade. Solution pH was initially adjusted and no significant changes were noted during the tests.

Each experiment was performed in duplicate with experimental error in spectrophotometric readings consistently less than one per cent. A three-liter test solution was used and stirring stopped to allow carbon to settle before drawing a sample. Since no sample dilution was required in most experiments, the sample aliquot was returned to the reaction vessel to prevent volume loss. In all systems investigated, the rate of adsorption was observed for a minimum of six hours.

EXPERIMENTAL RESULTS - ALKYLBENZENESULFONATES

The simplified pore diffusion model, given by Equation 5-13, was applied to kinetic data obtained for 2-octylbenzenesulfonate. Data points shown in Figure 5-12 represent experimental data with C_{F_o} of 0.4×10^{-4} M. carbon dosage, W, of 0.100 gm/l and stirring speed of 1250 rpm. The resulting dimensionless Langmuir parameters α and β were 15,000 and 20 respectively, and ϕ_e was approximately zero. Using a 50/60 sieve fraction particle size (a = 0.0136 cm), it was necessary to follow the rate of adsorption for 2100 minutes, or 35 hours, before a fractional solution concentration, ϕ, of 0.25 was reached.

The method of obtaining values for $F(r_o/a)$ from experimental values of ϕ has been discussed in a previous section. From Figure 5-12, convex curvature of data plotting points is somewhat apparent; however, fitting a straight line yields a value of 1.43×10^{-6} cm^2/sec for the diffusion coefficient.

Since the rate controlling step appeared to be solely pore diffusion, the model for pore diffusion with simultaneous non-linear adsorption was also applied to the rate data as illustrated in Figure 5-13. From the finite difference solution to Equation 3-3, dimensionless concentration, ϕ, is obtained as a function of dimensionless time, θ. Hence, for each experimental point (ϕ, t) there is a corresponding model value (ϕ, θ). If data conforms to the model, then a plot of θ versus t should yield a straight line with slope of D/a^2. Figure 5-13 indicates that a reasonable fit was obtained, yielding a D of 0.84×10^{-6} cm^2/sec, as opposed to 1.43×10^{-6} cm^2/sec obtained from the simplified model.

In Figure 5-14, the above rate data was plotted according to the simplified film and pore diffusion model given by

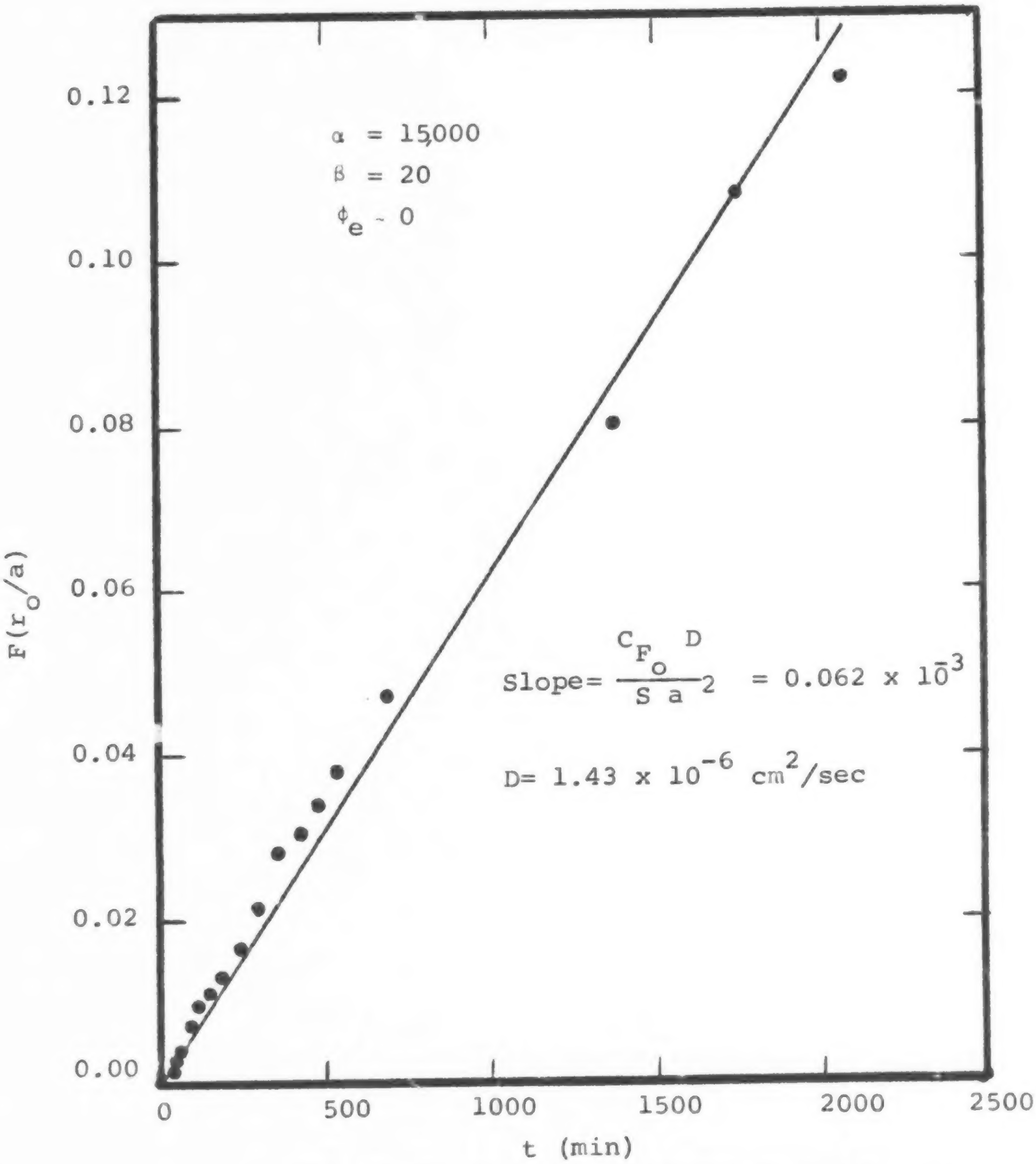

FIGURE 5-12. SIMPLIFIED PORE DIFFUSION MODEL. DATA FOR 2-OCTYLBENZENESULFONATE. (C_{F_o} = 0.4 x 10^{-4} M , W= 0.1 gm/l, a= 0.0136 cm, 1250 rpm)

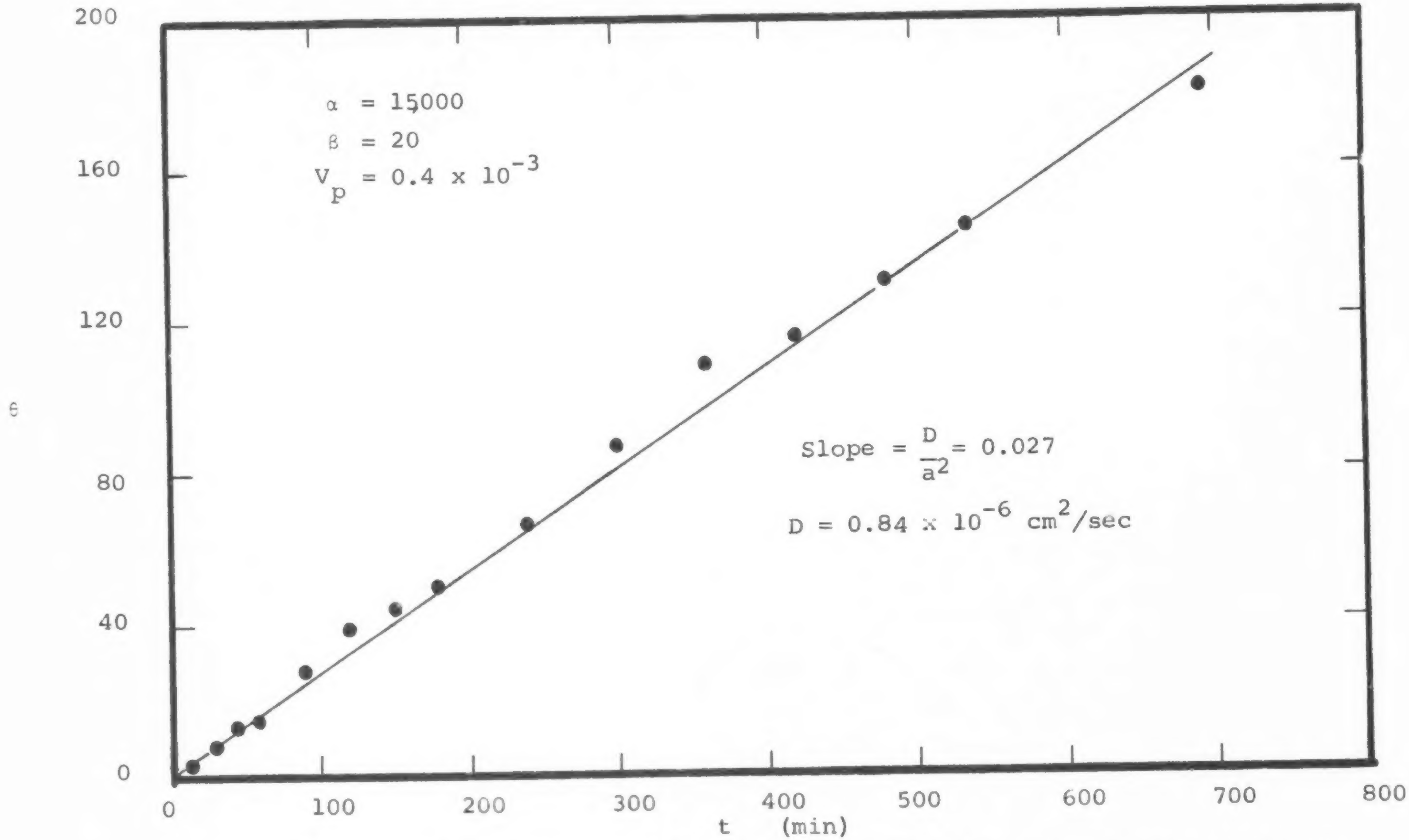

FIGURE 5-13. MODEL FOR PORE DIFFUSION WITH SIMULTANEOUS NON-LINEAR ADSORPTION. DATA FOR 2-OCTYLBENZENESULFONATE.

Equation 5-25. The linearized form given by Equation 5-37 was used to test the data. As expected, the plotted points formed a convex curve since β and ϕ_e were both rather small. However, the intercept was close to the origin, indicating that film diffusion is not a significant part of the rate-controlling mechanism. The model solutions for values of D obtained from the simple pore diffusion and non-linear adsorption models have been superimposed for comparative purposes. In accord with the results of sensitivity analysis shown in Figure 5-11, data recorded to equilibrium would thus form a convex curve intercepting the "theoretical" model solution given by considering the actual non linear isotherm.

Calculated adsorption rate curves for both pore diffusion with irreversible immobilization and non-linear adsorption are shown in Figure 5-15, along with experimental data. It may be observed that while diffusion coefficients differed by a factor of about 1.7, the calculated curves remained quite similar. This was anticipated because rate data, as shown in Figures 5-12 and 5-13, fitted both models. Moreover, as discussed in reference to Figures 5-11 and 5-14, a plot of the linearized form of the irreversible immobilization model will always give higher values of diffusivity when convex curvature is ignored. As expected, the calculated curves shown in Figure 5-15 indicate that the non linear model gives a better fit to the data points.

The results of applying the simplified film and pore diffusion model to rate data for 2-hexyl- and 2-decylbenzenesulfonate are shown in Figure 5-16. Experimental conditions were as described for 2-octylbenzenesulfonate. Rates of adsorption were followed for 7 hours to a value of ϕ of about 0.5. Hence, although α and β values were the

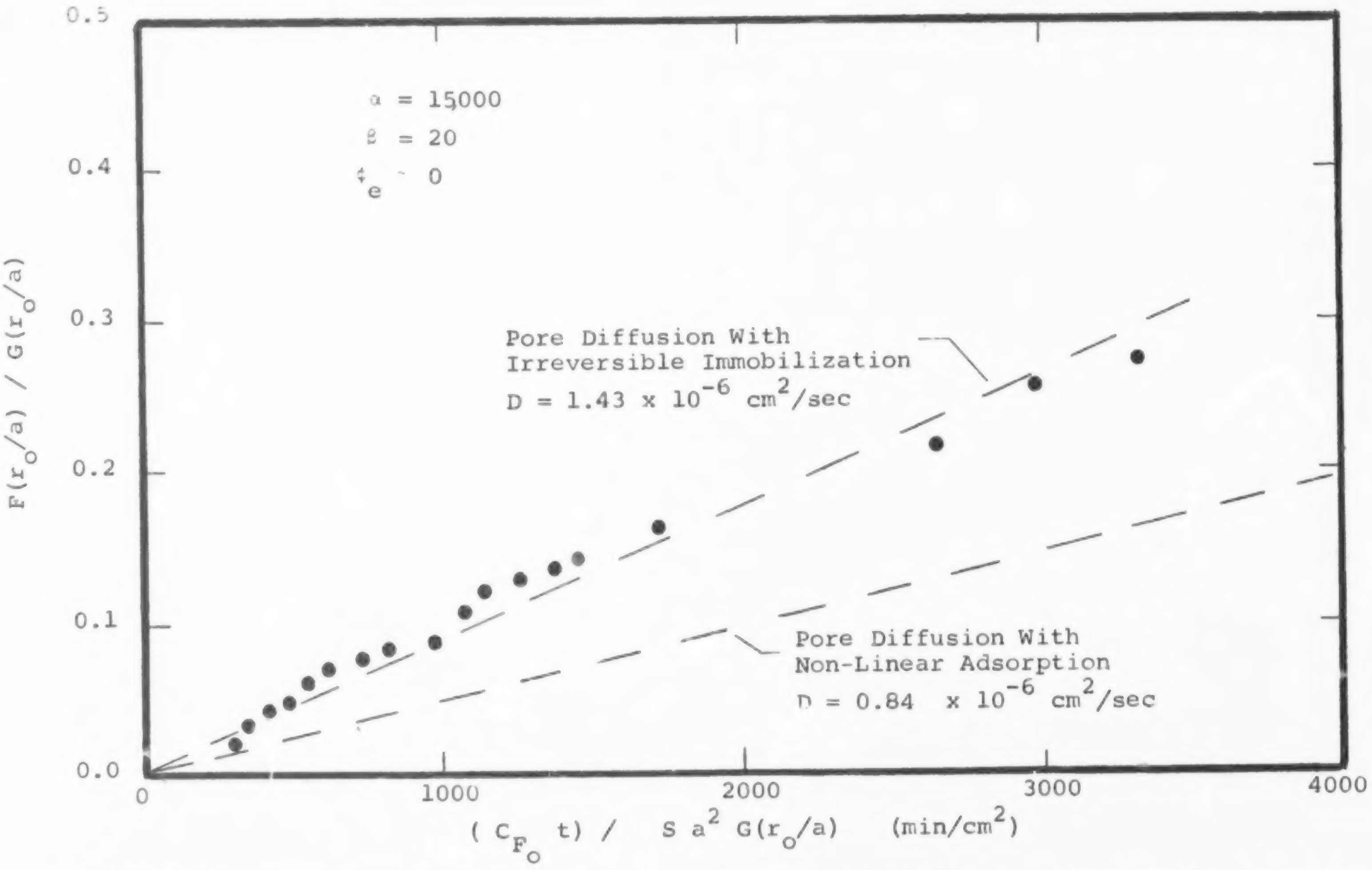

FIGURE 5-14. SIMPLIFIED FILM AND PORE DIFFUSION MODEL. DATA FOR 2-OCTYLBENZENESULFONATE.

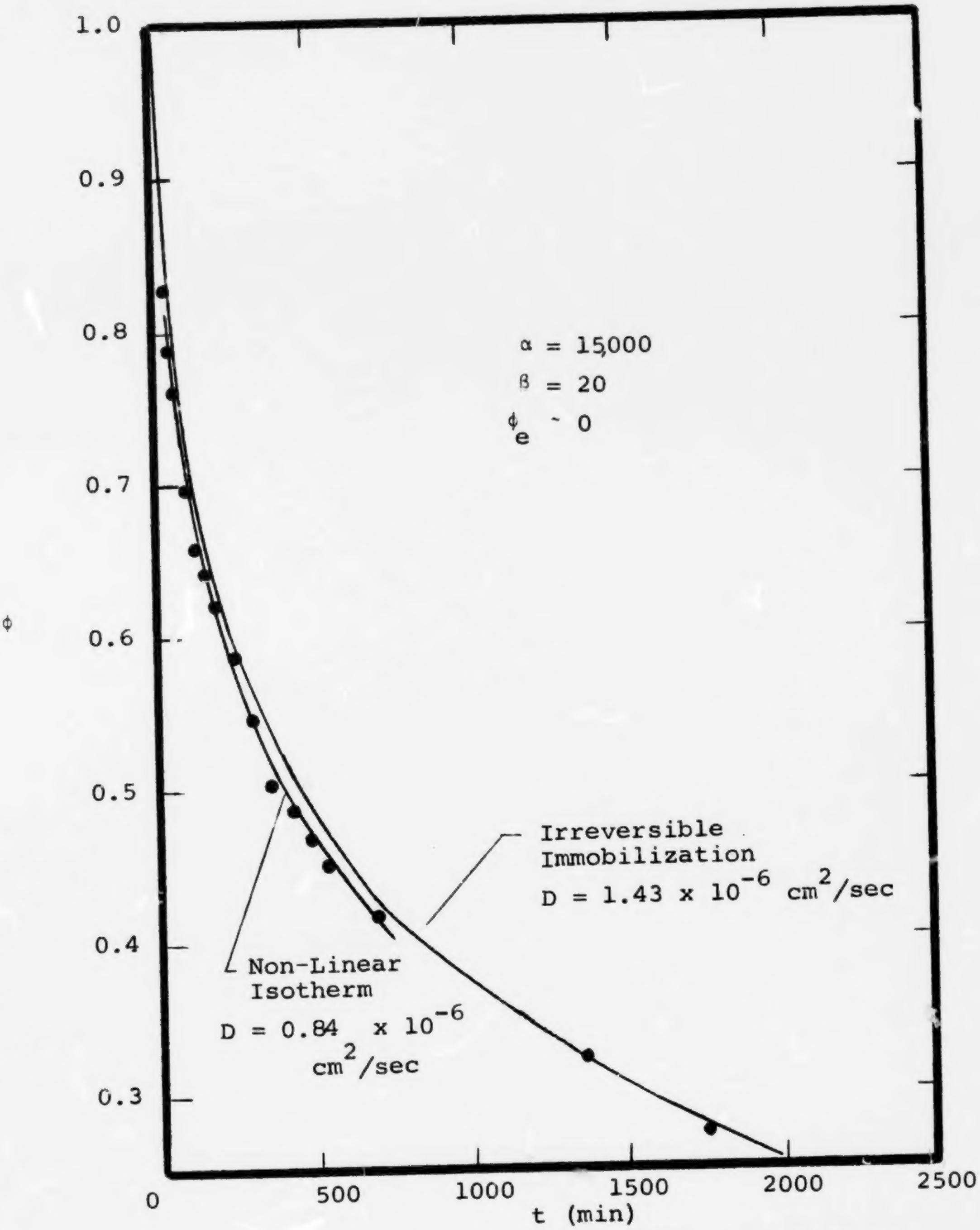

FIGURE 5-15. COMPARISON OF MODELS USING IRREVERSIBLE IMMOBILIZATION AND NON-LINEAR ISOTHERM DATA FOR 2-OCTYLBENZENESULFONATE

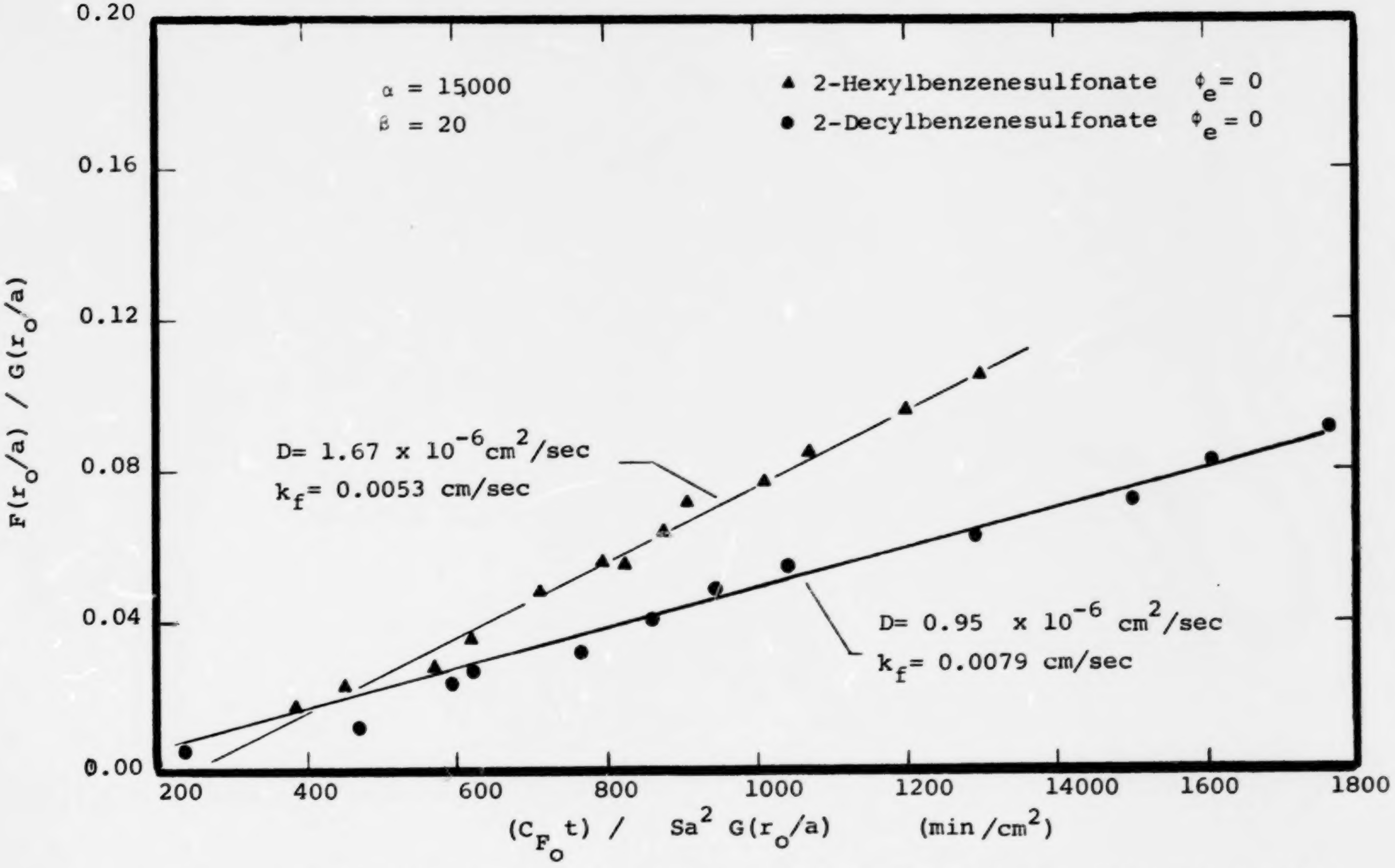

FIGURE 5-16. LINEARIZED FORM OF FILM AND PORE DIFFUSION MODEL. DATA FOR 2-HEXYL- AND 2-DECYLBENZENESULFONATE. (C_{F_o} = 0.4 x 10^{-4} M , W= 0.1 gm/1, a= 0.0136 cm, 1250 rpm)

same as given above, the convex curvature of the model plot was not apparent. Values of D obtained by least squares fit were 0.95 x 10^{-6} cm^2/sec and 1.67 x 10^{-6} cm^2/sec for 2-decyl- and 2-hexylbenzenesulfonate respectively. Both sets of data gave ordinate intercepts slightly below the origin from which film transfer coefficients of .0079 and 0.0053 cm/sec were calculated.

Reasonable conformity to the model for pore diffusion with non-linear adsorption was also indicated. As shown in Figure 5-17, initial data for 2-hexylbenzenesulfonate showed more scatter than that for 2-decylbenzenesulfonate, which may be evidence of rate limiting film transfer. The D values of 0.68 x 10^{-6} and 0.40 x 10^{-6} cm^2/sec for 2-hexyl- and 2-decylbenzenesulfonate were both smaller than those calculated from the simplified model by about a factor of two.

Using the results of the film and pore diffusion model, calculated curves have been superimposed on adsorption rate data in Figure 5-18 for 2-hexyl- and 2-decylbenzenesulfonate. Because both sorbates were assumed to have the same adsorption isotherm, differences in adsorption rates may be attributed to differences in diffusion coefficients.

This assumption was necessary because equilibrium adsorption experiments were not performed with these two sorbates due to lack of sufficient quantities. Weber and Morris (40) have shown all three alkylbenzenesulfonates discussed herein to exhibit similar equilibrium adsorption curves. However, they noted that the Langmuir energy constant, b, and the Langmuir "monolayer" coverage, Q, both increased with addition of the methyl group in the series 2-hexyl-, 2-octyl- and 2-decylbenzenesulfonate. Nonetheless, they found the value of Q for 2-hexylbenzenesulfonate to be about 80 per cent of that for 2-decylbenzenesulfonate.

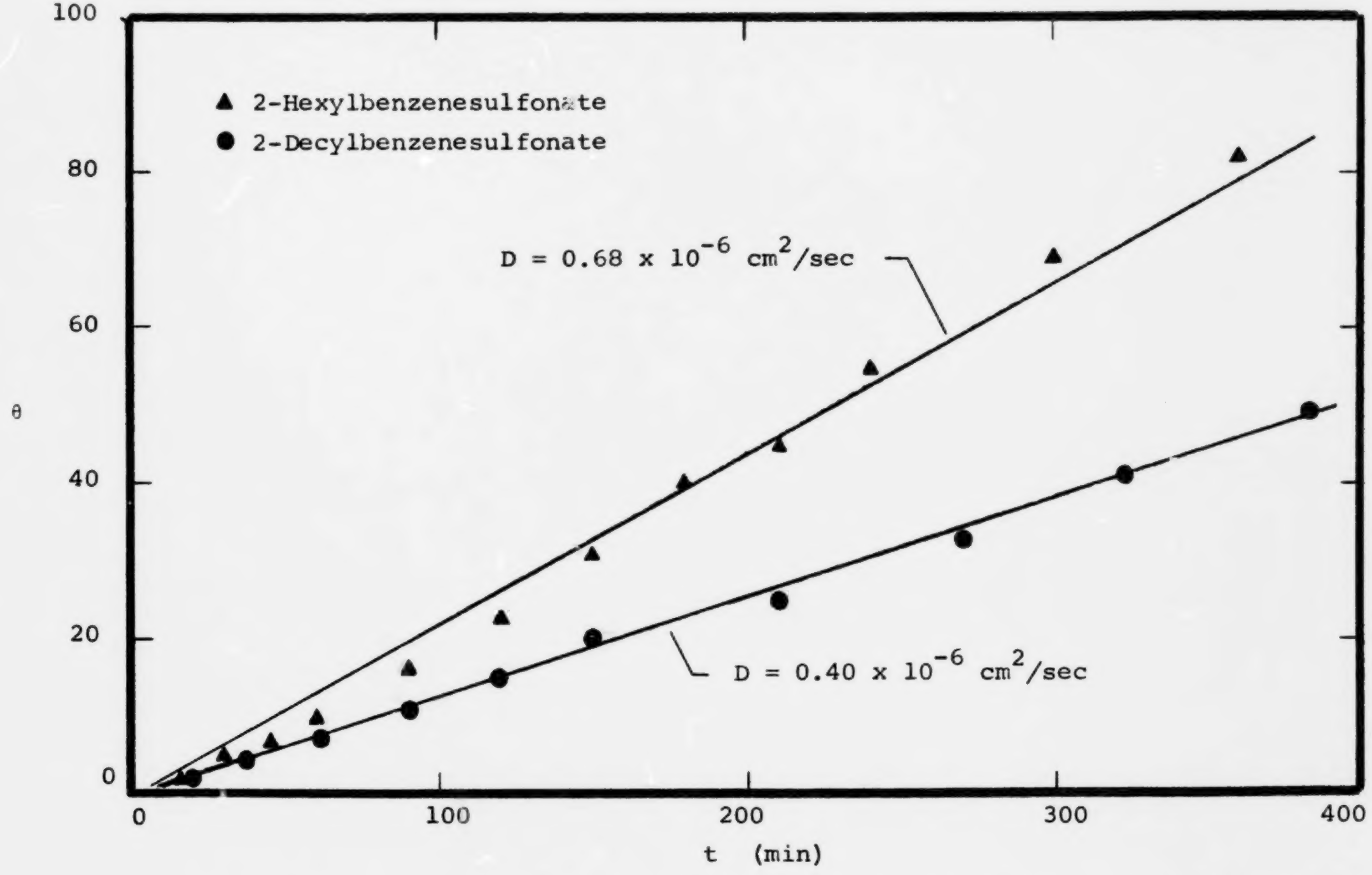

FIGURE 5-17. MODEL FOR PORE DIFFUSION WITH SIMULTANEOUS NON-LINEAR ADSORPTION. DATA FOR 2-HEXYL- AND 2-DECYLBENZENESULFONATE .

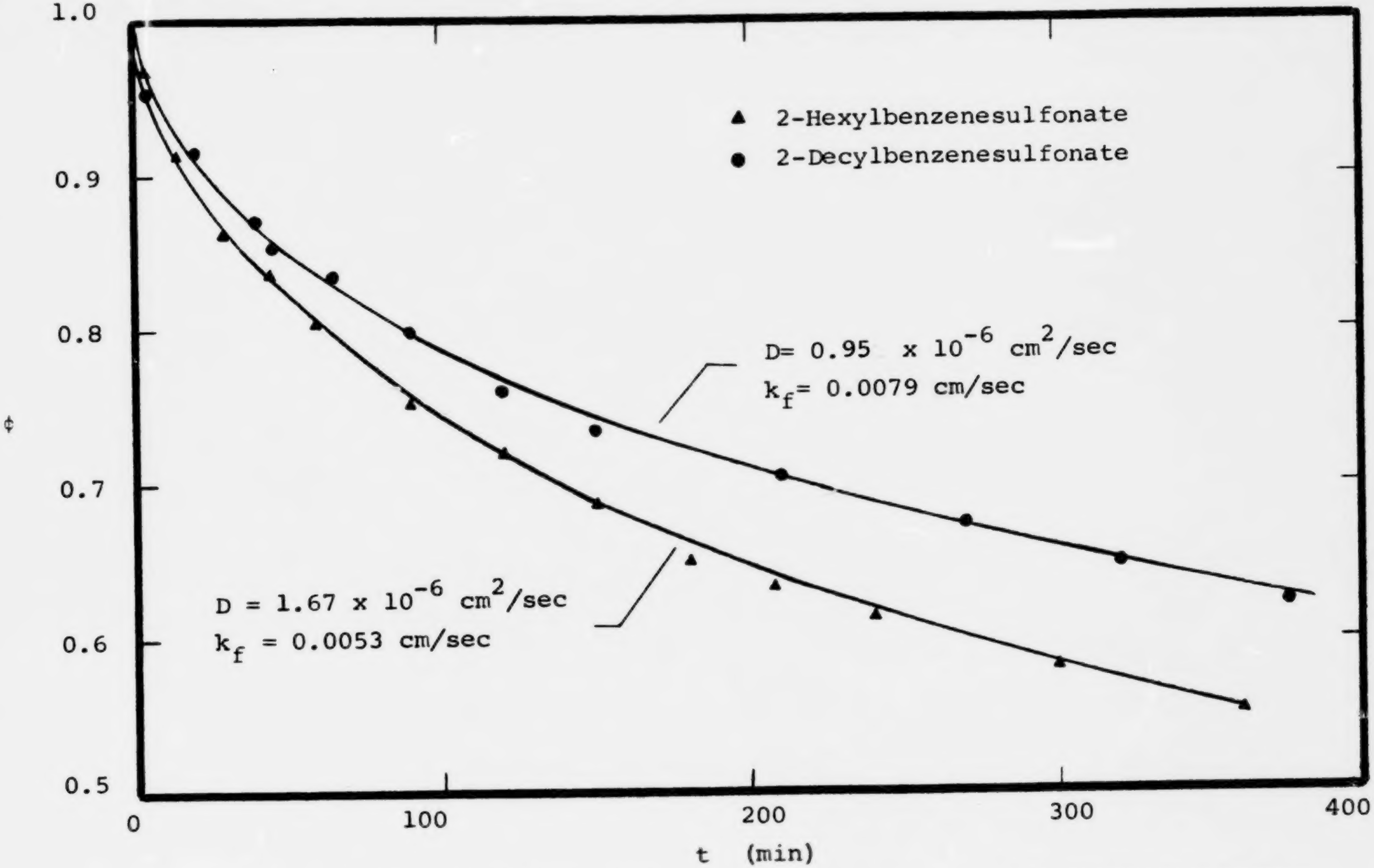

FIGURE 5-18. CALCULATED RATE CURVES FOR FILM AND PORE DIFFUSION MODEL. DATA FOR 2-HEXYL- AND 2-DECYLBENZENESULFONATE .

Furthermore, adsorption of all alkylbenzenesulfonates was noted to be close to "monolayer" coverage at C_{F_e} values of about 1×10^{-6} $\underline{M}$.

For the purposes of this research, the equilibrium adsorption relationship is only necessary to estimate the final equilibrium position, ϕ_e, from which the value of S can be calculated according to Equation 5-14. In addition, ϕ_e, is needed for selection of model functions of ϕ versus $F(r_o/a)$ and ϕ versus $G(r_o/a)$ (See Figures 5-2 and 5-4). Therefore, slight differences in equilibrium positions for these three compounds should not greatly effect the final results if ϕ_e is assumed constant.

Experiments conducted with a stirring speed of 800 rpm rather than 1250 rpm produced no discernable difference in kinetic data. Weber and Morris (38) also found, in a similar system, that rates of adsorption of alkylbenzenesulfonates (ABS) were not affected by stirring speeds above a few hundred rpm. A series mechanism, however, involving external film diffusion is still probable, since it is difficult to determine the change in hydrodynamics[1] required to significantly decrease film thickness. The mathematical analysis of diffusion to a free falling solid particle (25), a somewhat analogous system, indicates film thickness to be inversely proportional to the cube root of velocity. Hence, unless a large change in local velocities is produced by altering stirring speed, the rate of mass transfer may not be measureably affected.

Table 5-2 lists the experimental findings for the three alkylbenzenesulfonates investigated. The α and β values of 15,000 and 20 respectively, correspond to a C_{F_o} of 0.4×10^{-4} $\underline{M}$, while 30,000 and 10 correspond to a C_{F_o} of

---

[1] See Appendix C for correlation of transfer coefficient with hydrodynamics.

TABLE 5-2

RESULTS OF ALKYLBENZENESULFONATE INVESTIGATIONS

Sorbate	α	β	ϕ^*	Film-Pore Diffusion Model			Non Linear Model	Wilke-Chang Equation
				$D\pm$ $\times 10^6$ cm^2/sec	$D/k_f a\pm$ $-\times 10^3$	$^*k_f$ $\times 10^3$cm/sec	$D \times 10^6$ cm^2/sec	$D \times 10^6$ cm^2/sec
2-decyl-	15000	20	0.61	0.95±.03	9±3	7.9	0.40	5.3
" "	30000	10	0.68	1.30±.01	17±5	8.4	-	-
2-octyl-	15000	20	0.25	1.43±.1	1±1	10.5	0.84	5.5
" "	30000	10	0.63	1.60±.2	10±7	11.0	-	-
2-hexyl-	15000	20	0.50	1.67±.2	23±6	5.3	0.68	5.6

* See Appendix C for correlation of transfer coefficient, k_f , with hydrodynamics, fluid properties and free-liquid diffusivities.

0.2×10^{-4} M . In each experiment, ϕ_e was very close to zero and the table value ϕ^* designates the lowest value of ϕ actually observed. For each experiment, the method of least squares was used to fit a straight line to Equation 5-37, the combined film and pore diffusion model. For both slope and intercept, 95 per cent confidence intervals were calculated. The value of k_f given in the table was calculated from the least squares value of intercept. The following column lists the diffusion coefficients obtained from the model of pore diffusion with non-linear adsorption. Lastly, free liquid diffusivities, calculated by the Wilke-Chang equation (44) are tabulated. A particle size of 50/60 ($a = 0.0136$ cm) and stirring speed of 1250 rpm were used in each experiment reported.

From Table 5-2, it may be seen that D values calculated from the simplified model were approximately twice those obtained using the actual non-linear isotherm in the kinetic model. Although selection of a higher C_{F_0} or ϕ_e would have improved these results, it would also have greatly increased experimental observation time. As expected, modeling error increased as β decreased from 20 to 10. It may also be noted that the intercept values, D/ka, was much smaller for the 2-octylbenzenesulfonate experiment carried out to a ϕ^* of 0.25. This is probably because slope values in other experiments were taken from the initial portion of the convex curve, giving slopes that were steeper than actual and thus resulting in larger negative intercepts.

Free-liquid diffusivities for 2-decyl-, 2-octyl- and 2-hexylbenzenesulfonate were found to be about five times larger than the experimental values; however, the difference in D values between 2-hexyl- and 2-decylbenzenesulfonate was 0.3×10^{-6} cm^2/sec which is comparable to that obtained experimentally, using the non-linear model. The calculated pore diffusivity, using superficial flux, N, should be lower than the free-liquid diffusivity by a factor of two corresponding to the assumed value of porosity of 0.5 . Increased diffusion path length due to tortuousity effects also decreases the apparent value of pore diffusivity. In addition, Weber and Rumer (41) have suggested that steric and electrokinetic interactions may be responsible for the smaller values obtained for pore diffusivity.

The importance of diffusional path length, a, and particle density, ρ , in calculating the diffusion coefficient can be seen from inspection of the abscissa of Figure 5-11. The slope obtained from plotting the film and pore diffusion model (Equation 5-37) increases directly with the square of particle radius, a. Thus a tortuousity factor of two would give a four-fold increase in the value of D. Moreover, the diffusion coefficient increases directly with assumed particle density, since ρ is used to calculate σ_e which appears in the denominator of the abscissa parameter.

EXPERIMENTAL RESULTS - DNOCHP AND DNOSBP

Figures 5-19 and 5-20 illustrate results obtained for DNOCHP and DNOSBP rate data when applied to the film and pore diffusion model. An initial concentration, C_{F_0}, of 1.0×10^{-4} M produced α and β values of 6400 and 50 respectively for DNOCHP, and 6700 and 37 respectively for DNOSBP. Carbon dosage was selected such that ϕ_e was 0.2 in both experiments. Rates of adsorption were monitored for the first 1250 minutes at which ϕ was 0.521 for DNOCHP and 0.303 for DNOSBP.

It may be observed that data for both sorbates conformed reasonably well to the simplified model with convex curvature noticeably absent. Values of D and k_f were calculated to be 0.4×10^{-6} cm^2/sec and 0.0192 cm/sec respectively for DNOCHP and 1.9×10^{-6} cm^2/sec and 0.0087 cm/sec respectively for DNOSBP. It may also be noticed that the intercept on the

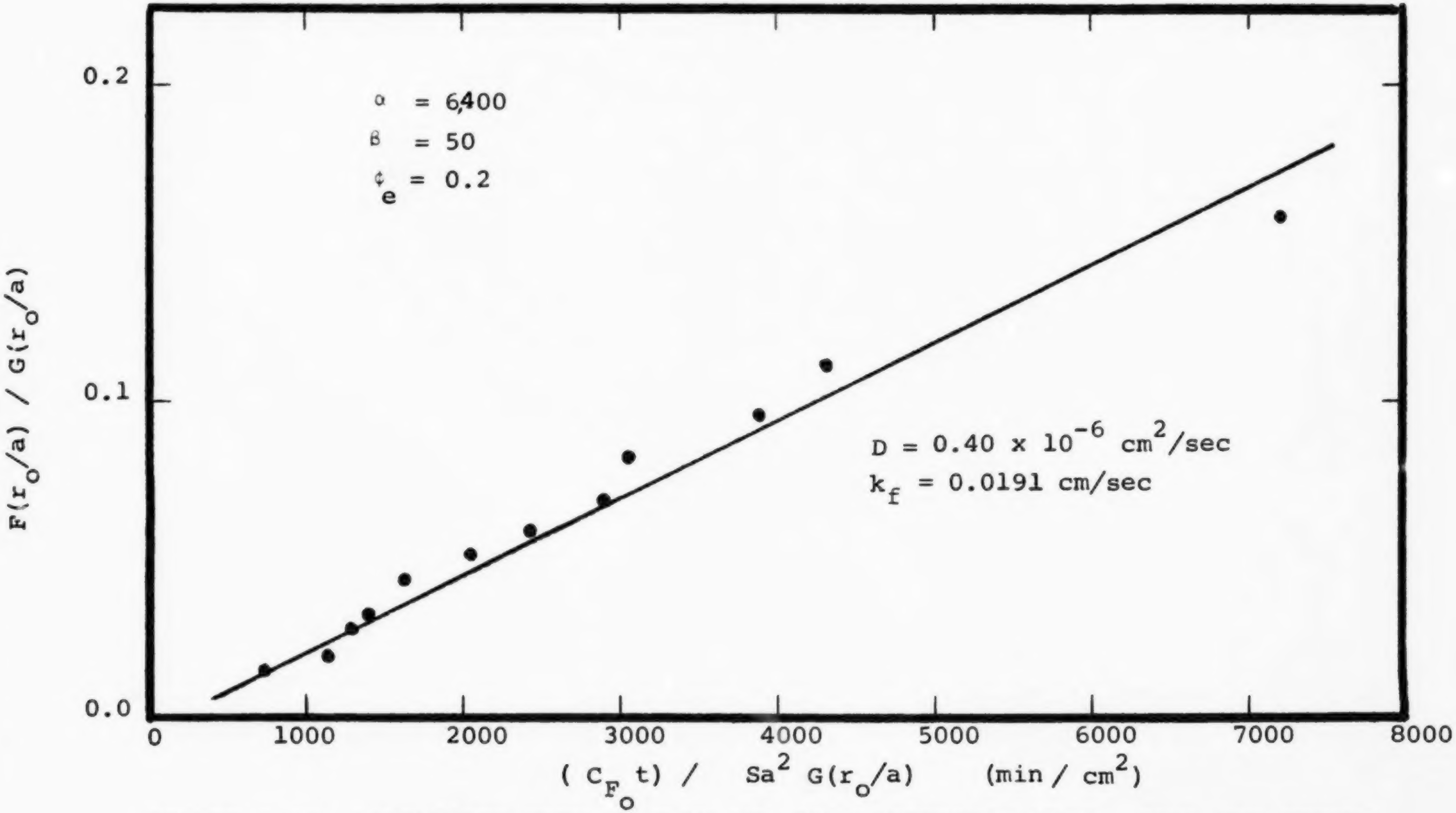

FIGURE 5-19. LINEARIZED FORM OF FILM AND PORE DIFFUSION MODEL. DATA FOR DNOCHP. ($C_{F_o} = 1.0 \times 10^{-4}$ $\underline{M}$, $\phi_e = 0.2$, a= 0.0105 cm, 1250 rpm)

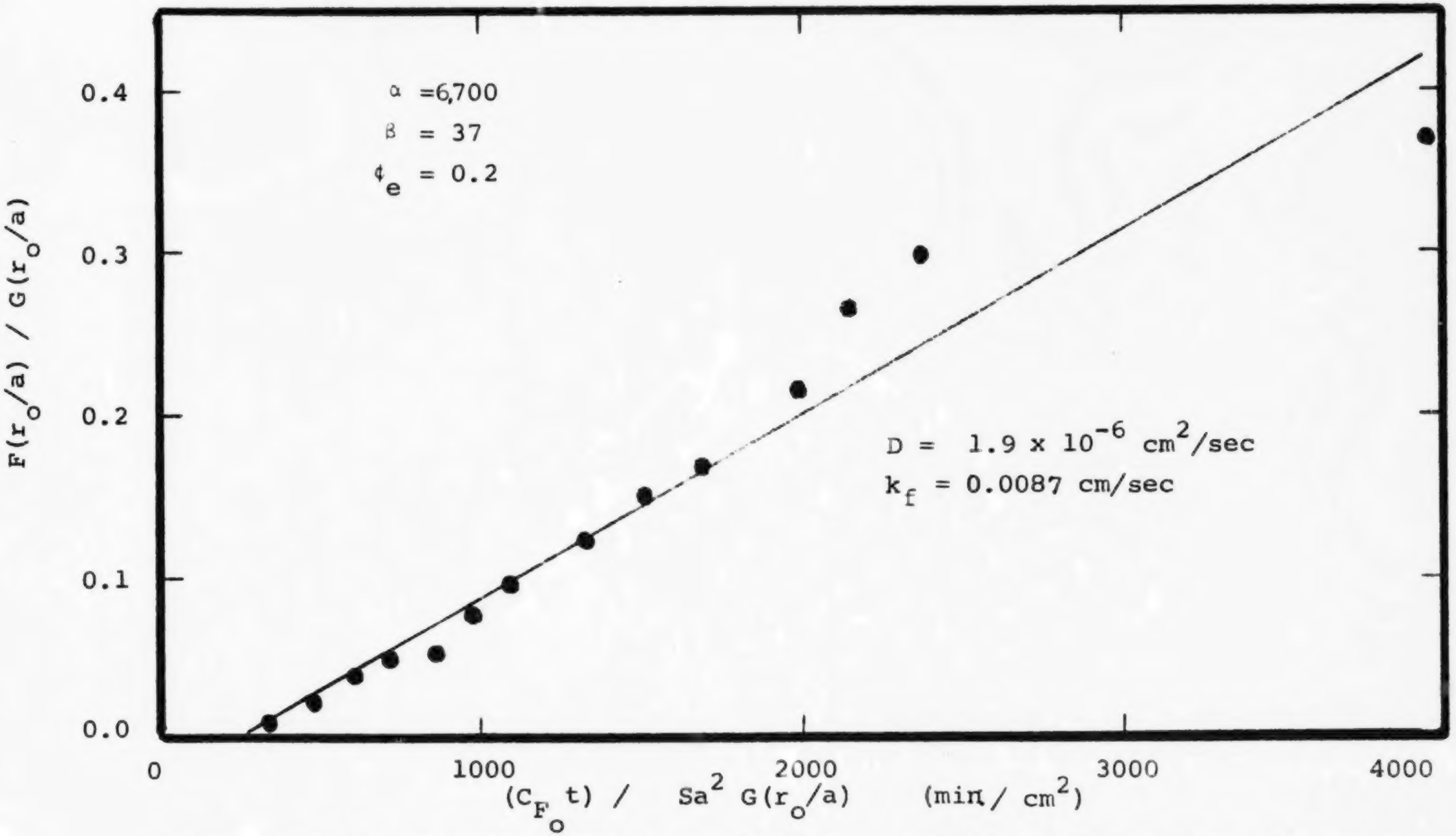

FIGURE 5-20. LINEARIZED FORM OF FILM AND PORE DIFFUSION MODEL. DATA FOR DNOSBP. (C_{F_o} = 1.0 x 10-4 M , ϕ_e= 0.2, a= 0.0105 cm, 1250 rpm)

ordinate for the DNOSBP data is somewhat more displaced from the origin than that of the DNOCHP data.

Applying the model for pore diffusion with non-linear adsorption produced the results shown in Figure 5-21. Rate data for DNOCHP conformed to the model while that of DNOSBP did not. Moreover, the value of D for DNOCHP obtained from the slope was the same as calculated from the simplified model. The poor fit of the rate data for DNOSBP seems to support the notion that film transfer is controlling initially.

The calculated values of $F(r_o/a)$, $(D/k_f a)G(r_o/a)$ and t, obtained from the film and pore diffusion model for DNOSBP, are shown in Table 5-3 with the corresponding values of ϕ.

TABLE 5-3

CALCULATED FILM AND PORE DIFFUSION MODEL PARAMETERS FROM DNOSBP EXPERIMENT

ϕ	Pore Diffusion Parameter $F(r_o/a)$	Film Diffusion Parameter $(D/k_f a)G(r_o/a)$	t (min)
0.945	0.0003	0.00053	5
0.890	0.0012	0.00111	13
0.831	0.0031	0.00175	27
0.790	0.0050	0.00222	41
0.705	0.0114	0.00326	82

As seen from Equation 5-25, addition of the terms $F(r_o/a)$ and $(D/k_f a)G(r_o/a)$ gives dimensionless time, T, for each value of ϕ, from which t can be calculated. Examination of the entries in Table 5-3 shows that film diffusion was significant for at least the first 41 minutes of adsorption in the DNOSBP experiment. Of course, as time

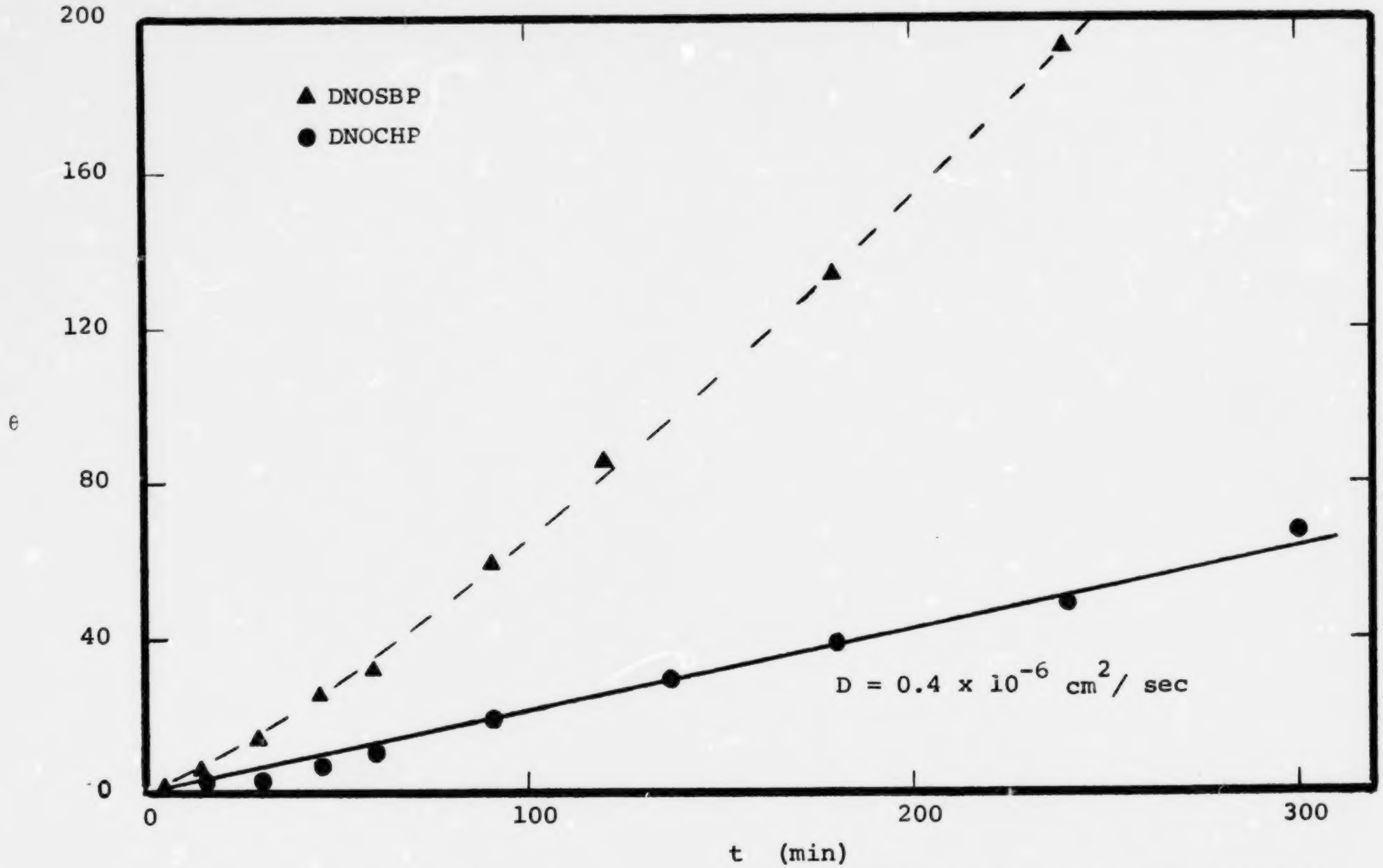

FIGURE 5-21. MODEL FOR PORE DIFFUSION WITH SIMULTANEOUS NON-LINEAR ADSORPTION DATA FOR DNOCHP AND DNOSBP .

progresses, internal pore diffusion gradually becomes entirely rate controlling.

Table 5-4 summarizes results of DNOCHP and DNOSBP experiments performed with a stirring speed of 1250 rpm and a pH of 8. For both sorbates, the larger values of α given in the table refer to experiments conducted with a C_{F_O} of 0.6×10^{-4} M while the smaller values refer to a C_{F_O} of 1.0×10^{-4} M. Particle sizes of 50/60 and 60/80 were used ($a = 0.0136$ cm, 0.0105 cm respectively). The combination of lower β and ϕ_e values in experiments conducted with C_{F_O} of 0.6×10^{-4} M produced more error in the simplified model as evidenced by the approximate doubling of calculated diffusion coefficient. However, experimental observation time was only about 7 hours and thus convex curvature of the plot of data points had not yet been noticed. As noted in Table 5-2, 95 per cent confidence intervals for slope and intercept have been calculated. The larger negative intercept for experiments with lower values of β again is due to the fact that a steeper than actual slope was calculated along the initial portion of the convex curve.

Calculation of free-liquid diffusivities yielded values of 6.4×10^{-6} cm^2/sec for DNOCHP and 7.0×10^{-6} cm^2/sec for DNOSBP. These values, as also noted for studies with the alkylbenzenesulfonates were larger than the experimental pore diffusivities of 0.4×10^{-6} cm^2/sec for DNOCHP and 1.9×10^{-6} cm^2/sec for DNOSBP. The five fold increase in D when comparing DNOCHP with DNOSBP may be partially explained from molecular structure considerations. That is, the rather rigid cyclohexyl group of DNOCHP in contrast to the flexible sec-butyl group of DNOSBP, may actually restrict diffusion to smaller pores (37).

TABLE 5-4

RESULTS OF DNOCHP AND DNOSBP INVESTIGATIONS

					Film-Pore Diffusion Model			Wilke-Chang Equation
Sorbate	a cm	α	β	ϕ_e	D± $\times10^6$ cm^2/sec	$D/k_f a$± $-\times10^3$	* k_f $\times10^3$ cm/sec	$D\times10^6$ cm^2/sec
DNOCHP	0.0136	10600	30	0	1.0±.1	15±9	6.2	6.4
" "	0.0105	6400	50	0.2	0.4±.05	2±8	19.1	-
DNOSBP	0.0136	11100	22	0	4.7±1.0	50±21	3.7	7.0
" "	0.0105	11100	22	0	4.1±.45	82±21	4.8	-
" "	0.0105	6700	37	0.2	1.9±.03	22±29	8.7	-

*See Appendix C for correlation of k_f with hydrodynamics, fluid properties and free-liquid diffusivities.

EXPERIMENTAL RESULTS - DNP (A) AND DNP (N)

Rate data obtained for DNP (A) with a C_{F_o} of 1.0 x 10^{-4} $\underline{M}$, ϕ_e of 0.2, particle radius of 0.0105 cm, stirring speed of 1250 rpm and pH of 8 was tested using the simplified film and pore diffusion model. The rate of adsorption was followed to a ϕ^* of 0.214 at a time of 637 minutes. As seen from Figure 5-22, convex curvature of the trace of data points was absent and a least squares fit yielded D and k_f values of 5.0 x 10^{-6} cm^2/sec and 0.0252 cm/sec respectively.

Figure 5-23 illustrates the results of applying the model for pore diffusion with non-linear adsorption. The same curvature as noted for the DNOSBP data in Figure 5-21 was obtained and reflected a rate limiting process involving film diffusion in series with pore diffusion.

A comparison of adsorption rate behavior of thethree sorbates, DNOCHP, DNOSBP and DNP (A) is shown in Figure 5-24. All these experiments were designed such that C_{F_o} was 1.0 x 10^{-4} $\underline{M}$ and ϕ_e was 0.2. The adsorption equilibrium for each as shown in Table 4-4, were found to be quite similar; thus, the observed differences in adsorption rates appear due to differences in molecular diffusivity.

Addition of 10^{-2} $\underline{M}$ phosphate buffer (10^{-2} $\underline{M}$ K_2HPO_4 - 10^{-2} $\underline{M}$ KH_2PO_4) has been shown to almost double the adsorption capacity for DNP (A). Figures 5-25 and 5-26 graphically illustrate the corresponding increase in adsorption rate when the phosphate buffer was added. Both experiments were identical in all other respects, having a C_{F_o} of 1.0 x 10^{-4} $\underline{M}$, carbon dosage of 0.16 gm/l, particle radius of 0.0136 cm, pH of 7.2 and stirring speed of 1250 rpm. As seen in Figure 5-26, rate data for the unbuffered system conformed quite closely to the film and pore diffusion model, producing values of D

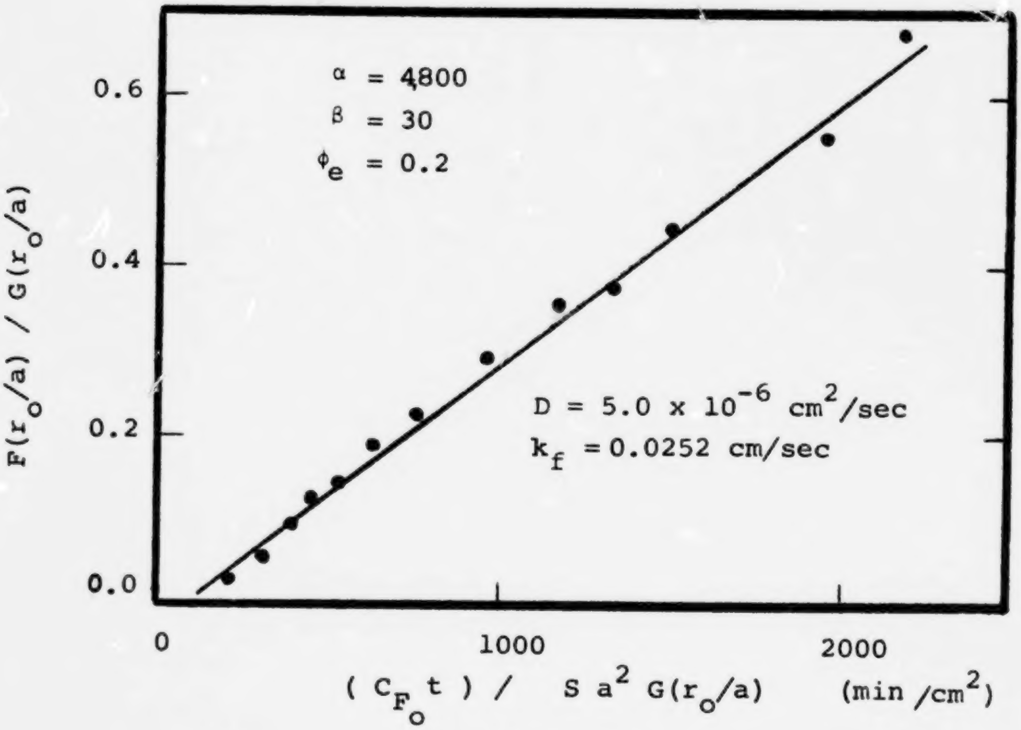

FIGURE 5-22. LINEARIZED FORM OF FILM AND PORE MODEL. DATA FOR DNP(A). (C_{F_o} = 1.0 x 10^{-4} M , ϕ_e= 0.2, a= 0.0105 cm, 1250 rpm)

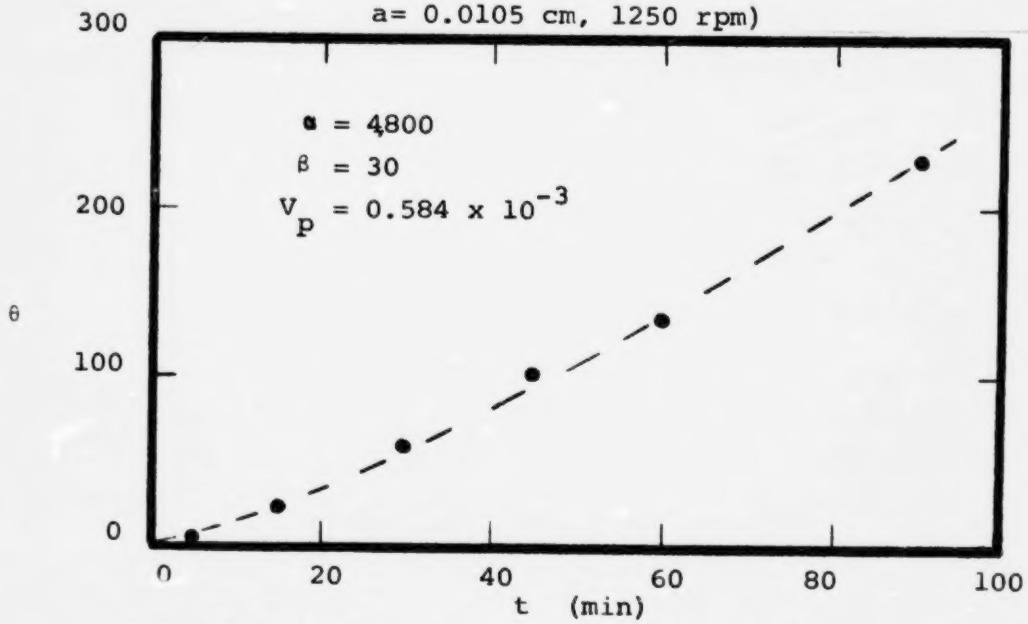

FIGURE 5-23. MODEL FOR PORE DIFFUSION WITH SIMULTANEOUS NON-LINEAR ADSORPTION. DATA FOR DNP (A) .

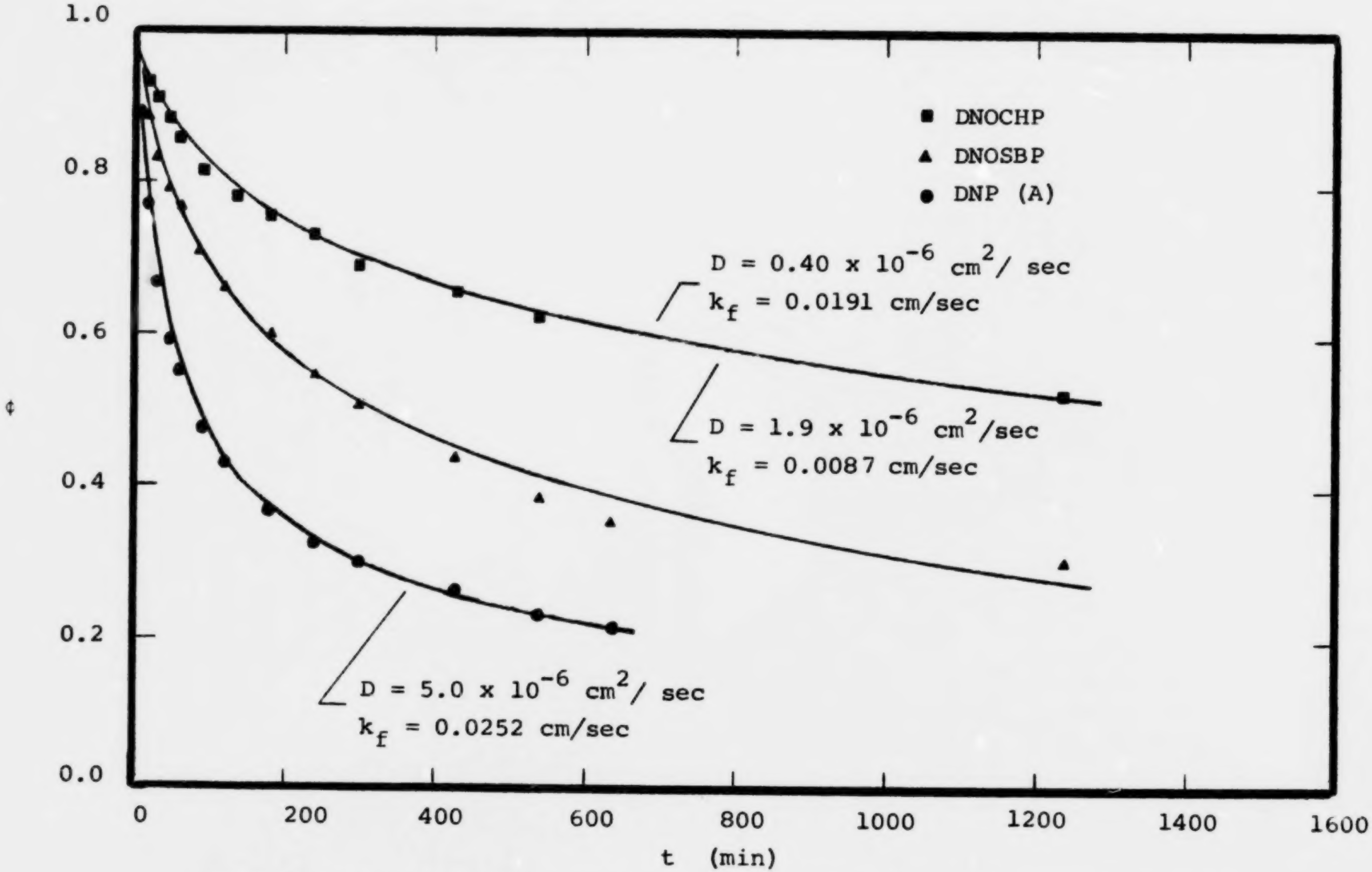

FIGURE 5-24. CALCULATED RATE CURVES FOR FILM AND PORE DIFFUSION MODEL. DATA FOR DNOCHP, DNOSBP AND DNP (A).

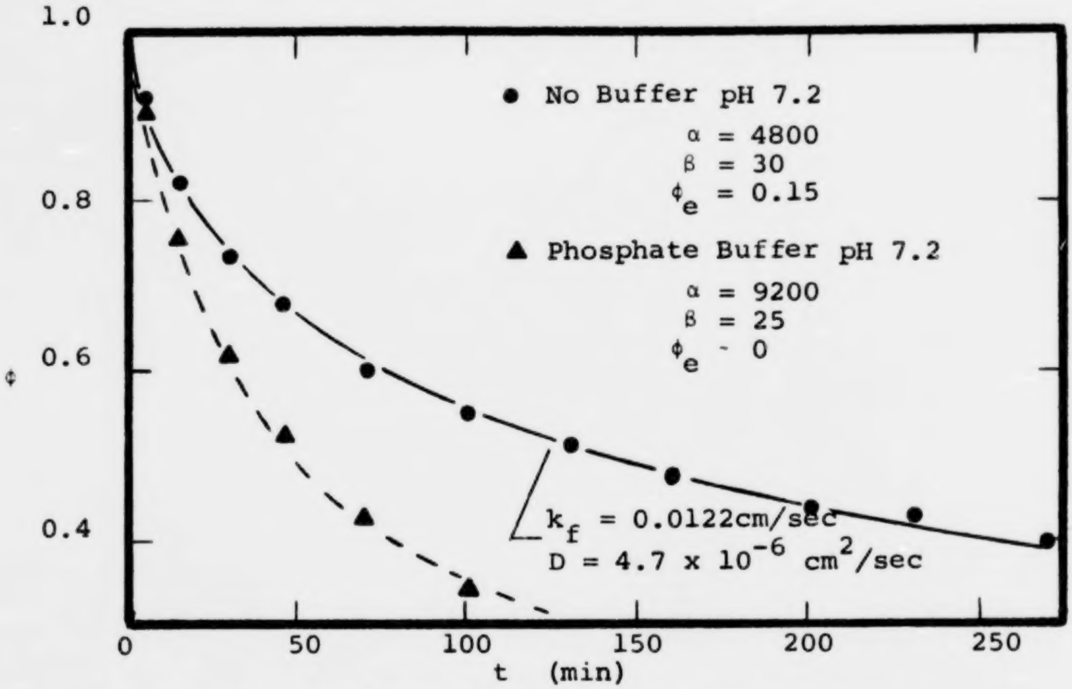

FIGURE 5-25. EFFECT OF PHOSPHATE BUFFER SYSTEM ON THE RATE OF ADSORPTION FOR DNP (A). ($C_{F_o} = 1.0 \times 10^{-4}$ M W = .16 gm/l., a = 0.0136 cm, 1250 rpm)

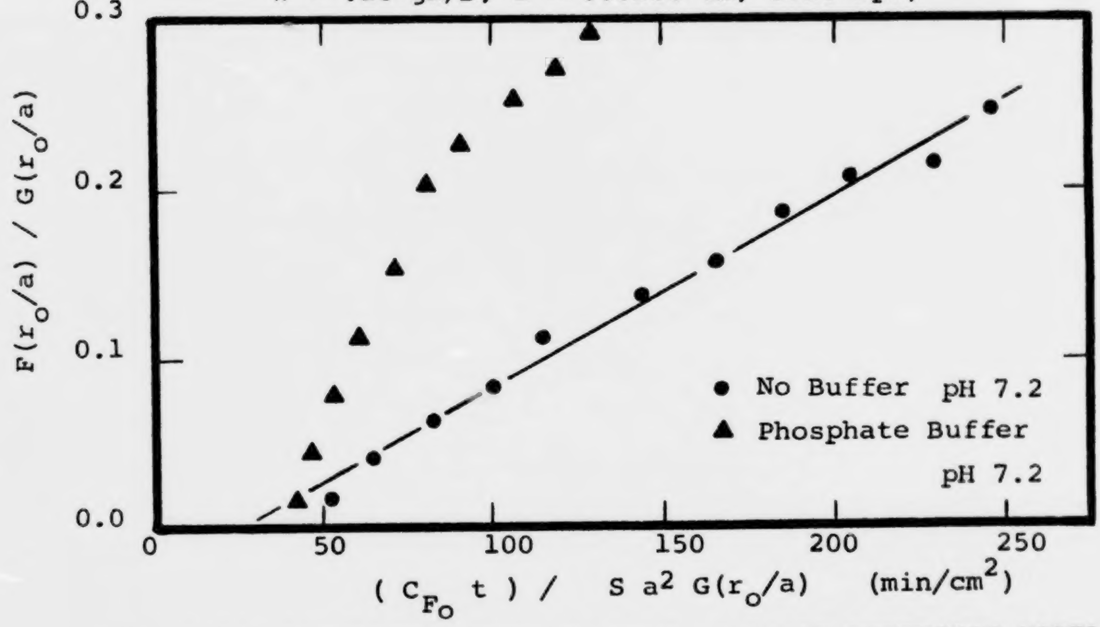

FIGURE 5-26. LINEARIZED FORM OF FILM AND PORE DIFFUSION MODEL. DATA FOR BUFFERED AND UNBUFFERED DNP (A) SYSTEMS .

and k_f of 4.7×10^{-6} cm^2/sec and 0.0122 cm/sec respectively. Data for the buffered system resulted in a convex curve primarily because ϕ_e was much lower and α had doubled while β remained the same.

Other rate experiments in buffered systems repeatedly supported the observed higher adsorption capacity. Addition of a comparable ionic strength solution of NaCl (4×10^{-3} M) also increased the rate of adsorption. This question will be further discussed in Chapter 6, in which infinite-bath studies are examined and discussed.

The rates of adsorption for the neutral species of DNP are shown in Figure 5-27 for a C_{F_0} of 1.0×10^{-4} M and final equilibrium values of 0.2 and 0.5×10^{-4} M. It may be recalled that the adsorption isotherm for DNP (N) was characterized in Chapter 4 by Q and b values of 2.5 mmol/gm and 0.40×10^6 l/mol respectively. Thus the dimensionless parameters α and β for these experiments were 8,750 and 40 respectively. For the given ϕ_e values of 0.2 and 0.5, the irreversible immobilization assumption should be adequate, based on previous investigations of a similar hypothetical isotherm. However, as seen from Figure 5-28, the combined film and pore diffusion model failed to describe the experimental data for the lower ϕ_e value of 0.2 but did appear adequate for the higher ϕ_e value of 0.5. The resulting values of D and k_f were 4.3×10^{-5} cm^2/sec and 0.013 cm/sec respectively. It may be noted that the diffusion coefficient calculated for the anion species was smaller by about an order of magnitude. This effect could possibly be related to molecular charge differences, since the anion species carries a negative charge and may be repelled by the negative carbon surface, while the neutral species predominates at pH 2; this pH is also near the isolectric point of the activated carbon (27). Therefore

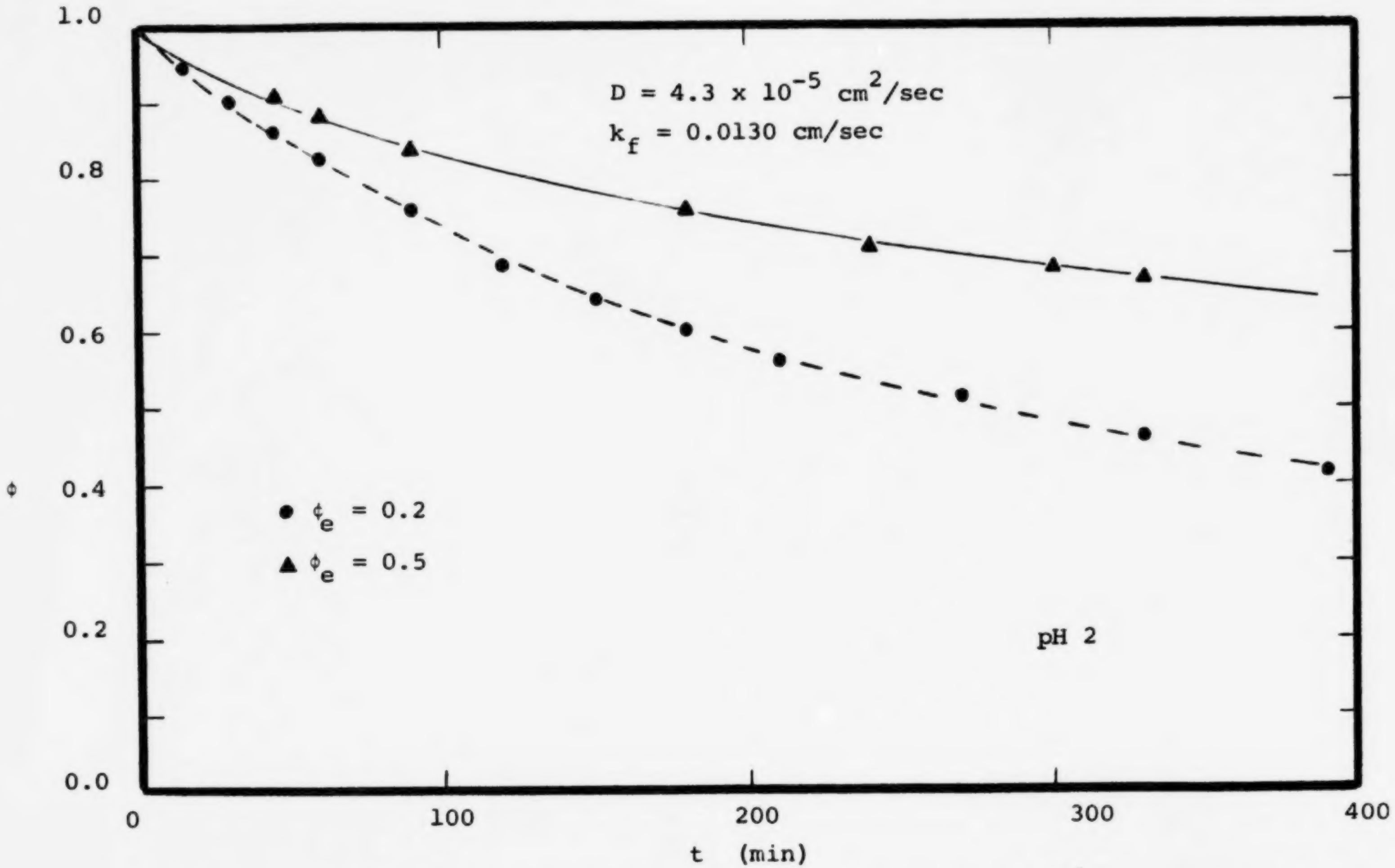

FIGURE 5-27 . RATES OF ADSORPTION FOR DNP (N). ($C_{F_o} = 1.0 \times 10^{-4}$ M , a = 0.025 cm, 1250 rpm)

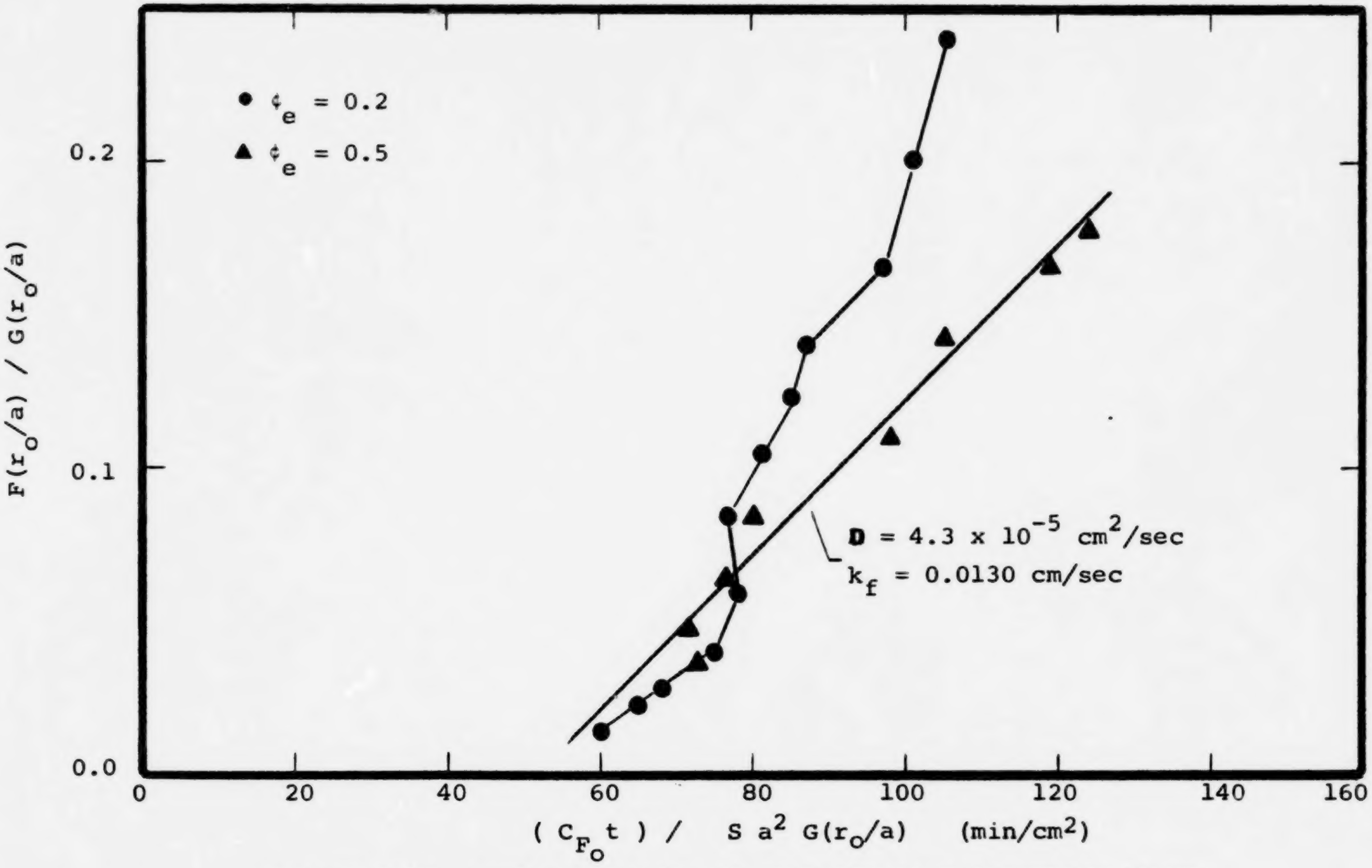

FIGURE 5-28. LINEARIZED FORM OF FILM AND PORE DIFFUSION MODEL. DATA FOR DNP (N) WITH ϕ_e OF 0.5 AND 0.2 .

at this pH charge effects become insignificant for both sorbate and sorbent.

The most striking difference in adsorption rate behavior between the anion and neutral species of DNP occurred in the initial kinetic data. A finite initial slope is quite apparent in the case of DNP (N), indicative of a film diffusion controlled process. This is also apparent from the negative intercept obtained using the film-pore diffusion model shown in Figure 5-28. Examination of the film diffusion parameter $(D/k_f a)$ $(G(r_o/a))$ showed it to be four times larger than the pore diffusion parameter $F(r_o/a)$ after 45 minutes and about equal to $F(r_o/a)$ after 240 minutes. This very significant shift in rate limiting step is related to the ten fold increase in D noted for the neutral species. In other words, pore diffusion appears to be a much faster process for DNP (N) than for DNP (A).

A summary of findings for DNP rate experiments is shown in Table 5-5. Free-liquid diffusivity for DNP was calculated to be 9×10^{-6} cm^2/sec and again, for the anion species, the experimental D value was found to be lower. In contrast, the value experimentally obtained for the neutral species was higher.

EXPERIMENTAL RESULTS - PHENOL AND PNP

The rate of adsorption for the anion species of phenol is shown in Figure 5-29. Data was obtained in an experiment conducted at pH 12 with a stirring speed of 1250 rpm, particle radius of 0.025 cm, C_{F_o} of 1.0×10^{-4} M and calculated equilibrium, ϕ_e, of 0.3×10^{-4} M . The resulting values of α and β were 2800 and 2.2 respectively, and once again, convex curvature of data plotting points was observed upon

TABLE 5-5

RESULTS OF DNP INVESTIGATIONS

					Film-Pore Diffusion Model		
C_{F_o} $\times 10^4$ M/L	a cm	α	β	ϕ_e	D$\pm$ $\times 10^6$ cm /sec	$D/k_f a \pm$ $-\times 10^3$	$^* k_f$ $\times 10^3$ cm/sec
				ANION			
0.5	0.0105	2400	15	0.10	5.4±.3	76±12	6.8
1.0	0.0105	4800	30	0.20	5.0±.4	20±29	25.2
1.0	0.0136	4800	30	0.15	4.7±.4	28±14	12.2
				NEUTRAL			
1.0	0.025	18750	40	0.50	42.6±7	132±40	13.0

---

* See Appendix C for correlation of transfer coefficient, k_f , with hydrodynamics fluid properties and free-liquid diffusivities.

application of the simplified film and pore diffusion model. However, as shown in Figure 5-30, the data conformed quite closely to the model for pore diffusion with simultaneous non-linear adsorption. The resulting value of D was 2.8 x 10^{-6} cm^2/sec, which was somewhat smaller than anticipated.

A similar experiment was conducted using PNP (A). All conditions were the same with the exception of pH, which was adjusted to 10. The values of α and β were calculated to be 3,400 and 13 respectively. As expected, the simple film and pore diffusion model was not applicable. It is readily apparent from inspection of the initial rate of adsorption, shown in Figure 5-31, that film diffusion is significantly affecting the mass transfer process, since the initial slope is finite. Other systems using the anion species of PNP produced similar results.

The rates of adsorption exhibited by the neutral species of phenol and PNP are shown in Figure 5-32 for C_{F_o} and C_{F_e} values of 1.0 x 10^{-4} and 0.2 x 10^{-4} $\underline{M}$ respectively. In both cases, the initial rate of adsorption is obviously finite and indicative of a film diffusion controlled process. Since the adsorption isotherm for PNP (N) is more favorable than that for phenol (N), less carbon is required to reach the same C_{F_e} and thus the rate of adsorption for PNP is slower than that of phenol (N).

The adsorption isotherm for phenol (N), as given in Figure 4-2, is similar in shape to that of Phenol (A) but reaches a higher ultimate capacity. Hence, it was anticipated and confirmed that the combined film and pore diffusion model would not describe the data. A similar result was obtained for the PNP (N) data. Investigation of other systems with different values of C_{F_o} and C_{F_e} also led to the same conclusion.

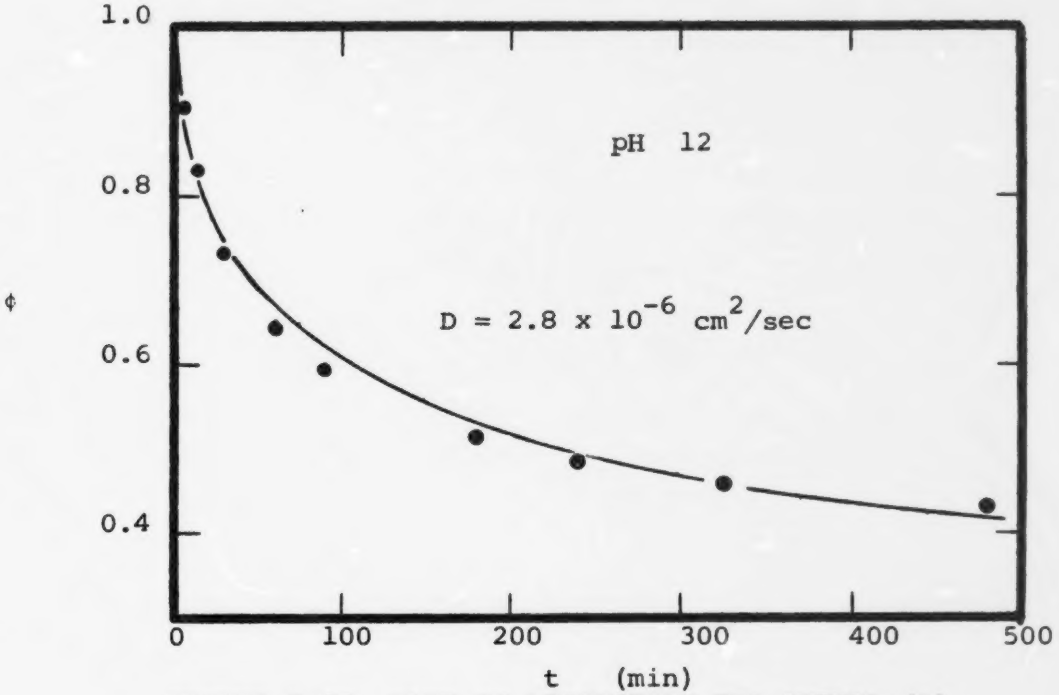

FIGURE 5-29. RATE OF ADSORPTION FOR PHENOL (A).
(C_{F_0} = 1.0 x 10^{-4} M., ϕ_e = 0.3, a = 0.025 cm, 1250 rpm)

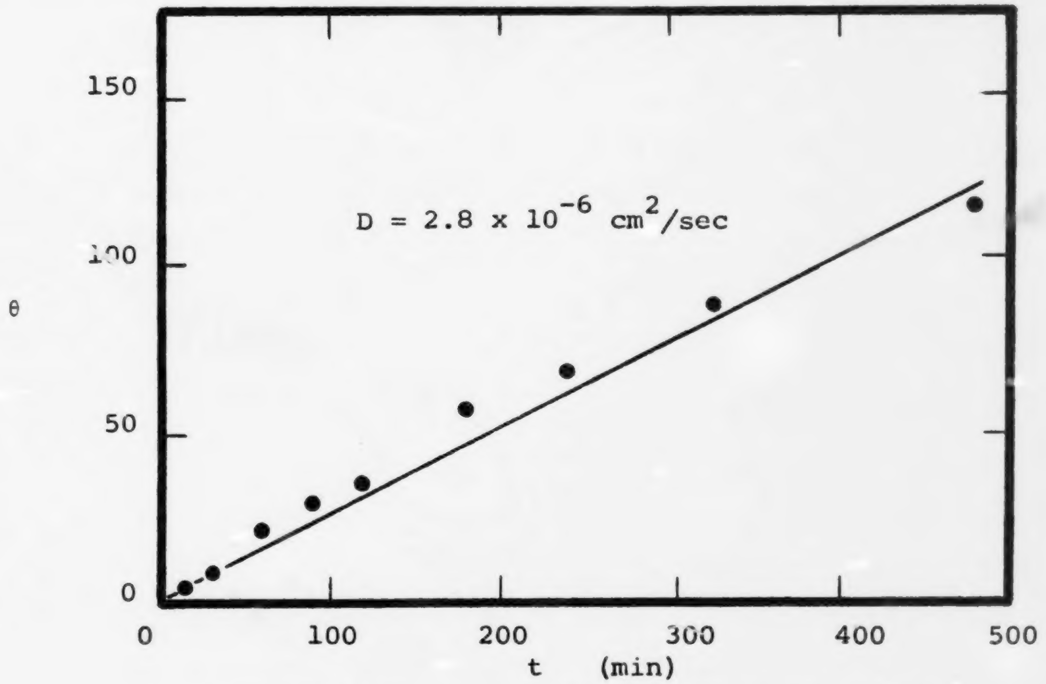

FIGURE 5-30. MODEL FOR PORE DIFFUSION WITH SIMULTANEOUS NON-LINEAR ADSORPTION. DATA FOR PHENOL (A).

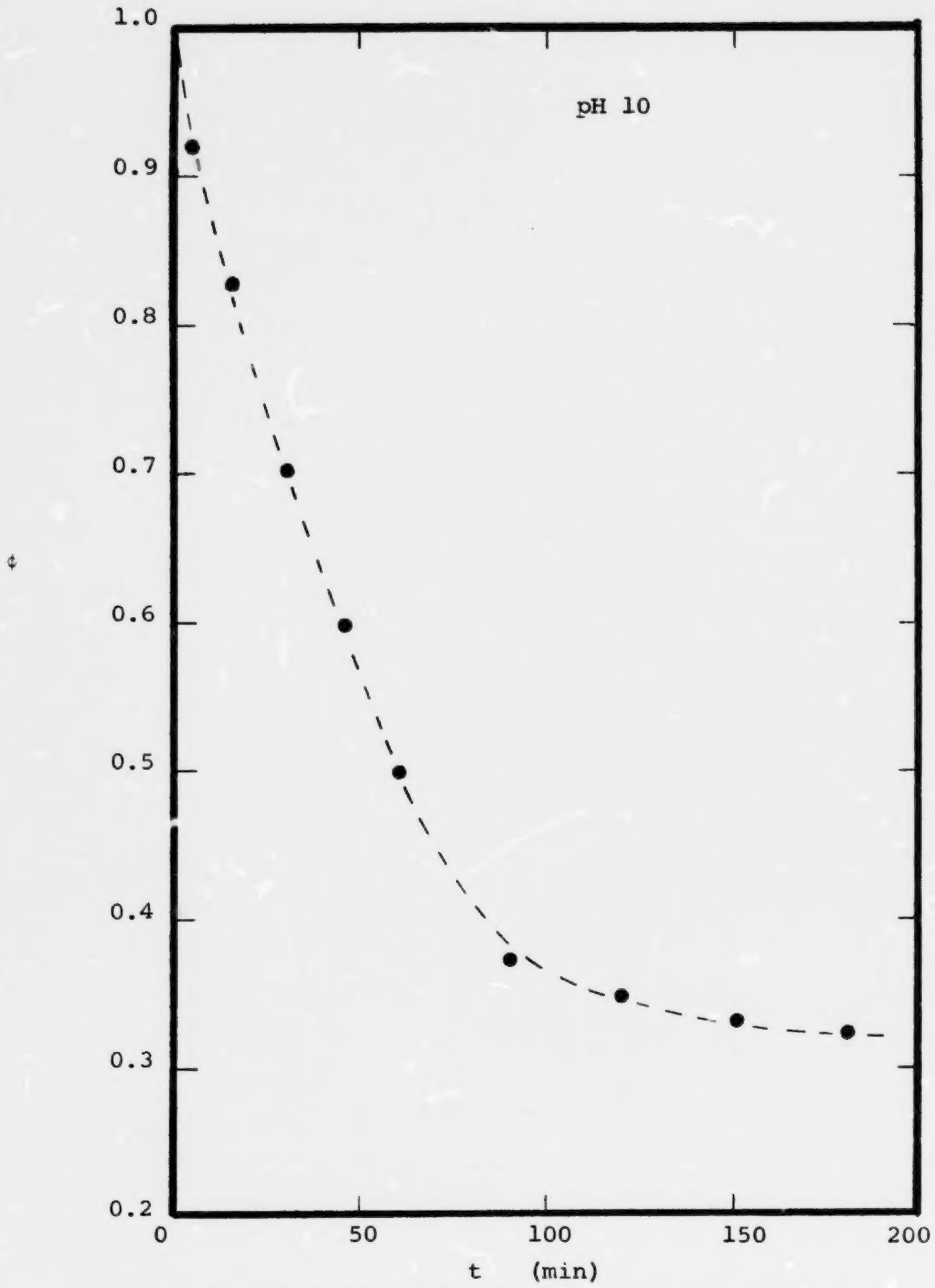

FIGURE 5-31. RATE OF ADSORPTION FOR PNP (A).
($C_{F_0} = 1.0 \times 10^{-4}$ M, $\phi_e = 0.3$, a = 0.025 cm, 1250 rpm)

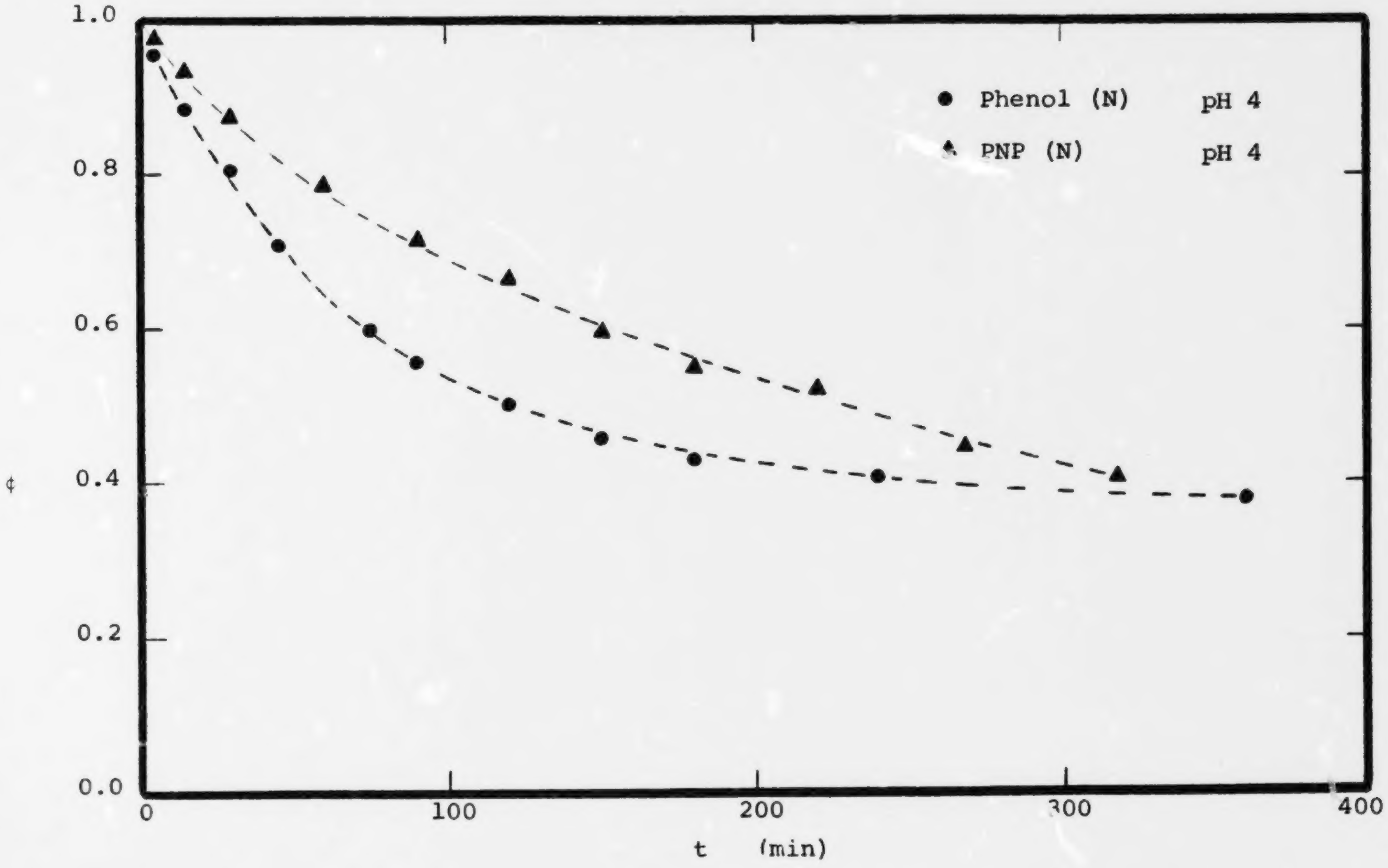

FIGURE 5-32. RATES OF ADSORPTION FOR PHENOL (N) AND PNP (N).
($C_{F_o} = 1.0 \times 10^{-4}$ $\underline{M}$, $\phi_e = 0.2$, a = 0.025 cm, 1250 rpm)

INITIAL CARBON-SOLUTE INTERACTION AND STIRRING SPEED STUDIES

It was postulated that perhaps initial interaction between carbon surfaces and solution could account for the observed behavior and that film resistance was actually not important. To determine the effect of initial carbon-solution interaction, experiments were conducted in which the carbon was shaken for one hour with 100 ml of test solution prior to addition to the remaining 2900 ml of solution to begin the actual kinetic study. No appreciable difference in the rate of adsorption was observed, indicating that initial induction period has no effect on the rate controlling processes. This was also concluded by Dedrick and Beckmann (15) without experimentation, in their work with adsorption of 2,4 dichlorophenoxyacetic acid (2,4-D) on Columbia carbon.

Although film resistance appeared to be part of the rate controlling mechanism, no reproducible difference in the rates of adsorption was noted for the anion species investigated when stirring speed was varied between 700 and 1250 rpm. However, as discussed previously, it is difficult to establish the velocity change required to significantly affect film thickness. It will be shown in the next section, however, that effects of film transfer for the neutral species of phenol, PNP and DNP were much more pronounced.

SIMPLE FILM DIFFUSION MODEL

From the preceeding discussion of phenol and PNP adsorption behavior, it may be concluded that the simplified film and pore diffusion model does not adequately describe the mass transfer process. Evidence was presented which indicates film diffusion to be important. If pore diffusion is ignored, a simple film transport model may be used to describe initial rate data.

$$V \frac{d\, C_F}{dt} = - k_f\, A_o\, [C_F - C_{F_i}] \tag{5-38}$$

The interfacial concentration, C_{F_i} may be assumed to be the local equilibrium concentration on the inside of the film. If the amount adsorbed at any time is uniformly distributed within the particle, then C_{F_i} can be calculated from the adsorption equilibrium relationship. Dividing both sides of Equation 5-38 by C_{F_o} and integrating yields Equation 5-39.

$$\int_1^{\phi} \frac{d\,\phi}{\phi - \frac{C_{F_i}}{C_{F_o}}} = - \frac{k_f A_o}{V}\, t \Big|_o^t \tag{5-39}$$

If C_{F_i} is negligible for initial adsorption, then Equation 5-39 reduces to Equation 5-40.

$$\ln \phi = - \frac{k_f\, A_o}{V}\, t \tag{5-40}$$

This assumption becomes more valid as the distribution ratio of solid to liquid phase concentrations increases, since C_{F_i} correspondingly decreases for any given amount, C_S, adsorbed.

The rate data for the neutral species of phenol, PNP, and DNP, which was presented in Figures 5-27 and 5-32 for the same C_{F_o} and ϕ_e, are shown on a semi-logarithmic plot in Figure 5-33. Mass transfer coefficients, k_f of .82, .88 and .76 x 10^{-2} cm/sec were calculated for phenol, PNP and DNP respectively. These values are obtained by dividing the initial slope by external carbon surface area per cm^3 of solution. Accordingly, phenol exhibited

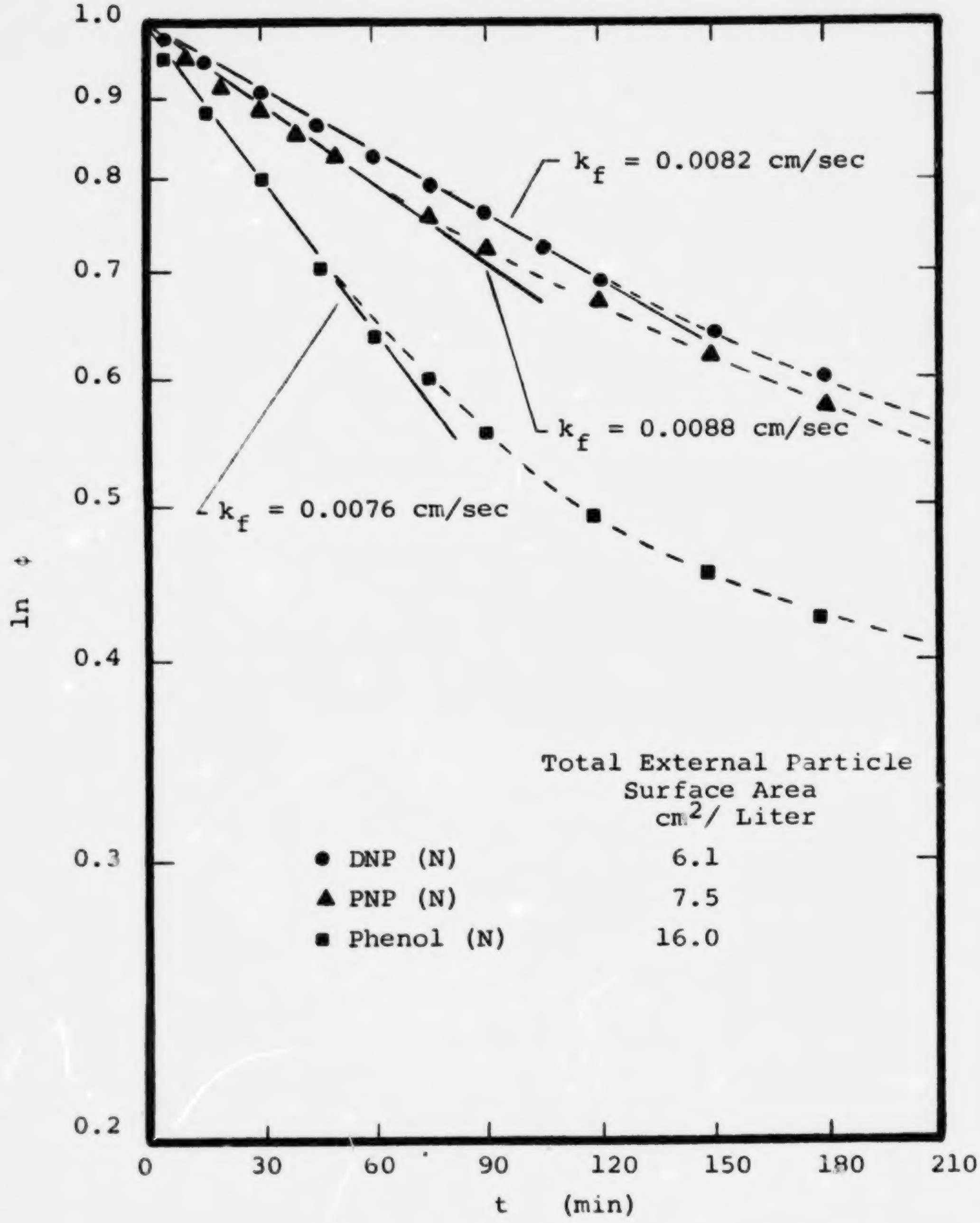

FIGURE 5-33. SIMPLE FILM DIFFUSION MODEL. DATA FOR DNP (N), PNP (N)AND PHENOL (N) . (C_{F_o} = 1.0×10^{-4} M , $\phi_e = 0.2$, a = 0.025 cm, 1250 rpm)

the fastest rate of adsorption since it has the lowest distribution ratio and consequently required the largest carbon dosage to reach the same value of Φ_e. However, approximately the same value of k_f was obtained.

Obviously, the simple film diffusion model cannot describe the entire approach to equilibrium since the increase in C_{F_i} is ignored. An attempt was made to include the term C_{F_i}/C_{F_o} based on values of C_{F_i} obtained from the adsorption isotherm. However, this model proved to be no more adequate than the simple film model. Therefore, either a series mechanism of film and pore diffusion may be postulated or film diffusion alone controls and the method of calculating local equilibrium concentration C_{F_i} is incorrect.

From investigations of alkylbenzenesulfonates, DNOCHP, DNOSBP, and DNP rates of adsorption, a series mechanism appears to be the more plausible reason for the failure of a film diffusion model. The interruption test as given by Helfrich (18) was tried so that the importance of pore transport could be ascertained. The procedure consisted of stopping the experiment at various times, separating the solution from the carbon by settling and draining and then beginning the experiment once again after 1 1/2 hours. Presumably, if intraparticle transport affected the rate of adsorption, the concentration gradient would level out during the interruption period and an increased rate of adsorption would be observed when the test was resumed. In this series of experiments, PNP (N) was used with a C_{F_o} of 0.35×10^{-4} M and a carbon dosage of 0.025 gm/l. Duplicate experiments were carried out with one being interrupted at 80, 180 and 270 minutes. No difference in the rate of adsorption compared to the uninterrupted test was noted when the experiments were resumed. Another experiment was conducted in which the length of interruption was 11 hours rather than 1 1/2 hours and again, no difference in the rate of adsorption was observed. Although the simple film model could only be used for about the first 150 minutes of the experiment, it appeared that external film resistance was still very important for at least an additional 120 minutes. Smith, et al., (32) using dichlorophenol concluded from a similar interruption test, that pore diffusion either in series with film diffusion or by itself, was rate controlling. They had great difficulty, however, in applying a pore diffusion model, perhaps because film diffusion was significant. Conversely, Weber and Morris (38) found significant differences in the rate of adsorption of sulfonated alkylbenzenes when the carbon was reintroduced to the system which supported the pore diffusion model proposed by Weber and Rumer (41) for these same sorbates.

Tables 5-6 and 5-7 show the results of experiments in which stirring speed and particle size were investigated. From Table 5-6 it can be seen that k_f increased from $.45 \times 10^{-2}$ to $.84 \times 10^{-2}$ cm/sec for phenol and $.50 \times 10^{-2}$ to 1.12×10^{-2} cm/sec for PNP as stirring speed was varied from 275 to 1550 rpm. For each sorbate, the time, t^*, at which the film model could no longer be applied, lengthened as stirring speed decreased. The corresponding fractional approach to equilibrium $(1 - C^*/C_{F_O})/(1 - \phi_e)$, however, remained almost constant. This seems to indicate that there was some critical concentration C_{F_i}, at which the simple film model no longer applied and, as the boundary layer increased by decreasing stirring speed, the time necessary to reach that concentration increased. From Table 5-7 it may be concluded that k_f is independent of particle size. Similar results have been obtained by others investigating mass transfer in agitated vessels. Correlation of k_f with hydrodynamics

TABLE 5-6

THE EFFECT OF STIRRING SPEED ON THE TRANSFER COEFFICIENT, k_f, AND FRACTIONAL APPROACH TO EQUILIBRIUM

Stirring Speed	* k_f x10^2 cm/sec	t* min	$\frac{1 - C^*/C_{F_o}}{1 - \Phi_e}$
	Phenol (N)		
275	.45	110	.425
750	.58	90	.450
1250	.76	60	.475
1550	.84	50	.475
	PNP (N)		
275	.5	300	.350
500	.65	180	.303
750	.82	110	.236
1250	1.06	90	.313
1550	1.12	60	.236

*See Appendix C for correlation of k_f with hydrodynamics, fluid properties and free-liquid diffusivities.

TABLE 5-7

THE EFFECT OF EXTERNAL PARTICLE SURFACE AREA ON THE TRANSFER COEFFICIENT, k_f, FOR PNP (N)

Particle Diameter cm	Total External Surface Area cm^2	k_f x10^2 cm/sec
.100	2.00	.99
.0710	2.82	1.08
.0500	4.00	1.06
.0350	5.70	1.24
.0273	7.33	1.10

and free-liquid diffusivity, as presented in Appendix C, indicates these values to be consistent with the findings of other workers[1].

A comparison of phenol (N) and DNP (N) systems, having the same C_{F_o} and C_{F_e} are shown in Table 5-8. The value of C_{F_o} was 1.0×10^{-4} $\underline{M}$ in each experiment while two positions of equilibrium were chosen to be 0.2 and 0.5×10^{-4} $\underline{M}$. It may be noted that the simple film model could only be applied for 60 minutes in the phenol (N) experiments as opposed to 120 minutes in the DNP (N) experiments. However, the calculated transfer coefficients were quite comparable. The result may be explained on the basis of adsorption isotherm differences. As shown in Figure 4-2, DNP (N) adsorption is more favorable than that of phenol (N). Therefore, a higher concentration gradient can be maintained across the liquid film and thus Equation 5-40, the simple film diffusion model, may be applied for a longer time.

TABLE 5-8

APPLICATION OF SIMPLE FILM DIFFUSION MODEL TO PHENOL (N) AND DNP (N) RATES OF ADSORPTION

C_{F_o} $\times 10^4$ $\underline{M}$	C_{F_e} $\times 10^4$ $\underline{M}$	t^* min	k_f cm/sec $\times 10^2$
		Phenol	
1.0	0.2	60	.76
1.0	0.5	60	.77
		DNP	
1.0	0.2	120	.82
1.0	0.5	120	.81

---

[1] Calderbank, P. H. and Moo-Young, M. B., "The Continuous Phase Heat and Mass-Transfer Properties of Dispersions", Chem. Eng. Sci. 16, 39 (1961).

The anion species of PNP was similarly investigated. A semilogarithmic plot of the data given in Figure 5-31 is shown in Figure 5-34. A transfer coefficient, k_f, of 0.593×10^{-2} cm/sec was calculated from the initial slope. This is somewhat lower than the value of 0.88×10^{-2} cm/sec which was obtained for the neutral species of PNP and may be the result of molecular and surface charge characteristics.

SUMMARY OF FINITE-BATH KINETICS

Investigations have shown that a complex mass transfer process, involving film and pore diffusion with simultaneous non-linear adsorption, can be described by a simplified model incorporating the assumptions of irreversible immobilization and quasi-steady state. However, the model is subject to limitations imposed by the shape of the adsorption isotherm and the choice of C_{F_o} and ϕ_e for the rate experiment.

Hypothetical isotherms, characterized by the dimensionless Langmuir parameters α and β were used to test the assumptions of irreversible immobilization and quasi-steady state. Dimensionless solution concentration-time profiles were calculated using the hypothetical isotherms and pore diffusion models with simultaneous non-linear and simultaneous irreversible adsorption. Two positions of dimensionless equilibrium concentration, ϕ_e, were chosen as 0.1 and 0.2. It was shown that the irreversible immobilization model more closely approximated the non-linear adsorption model as β and ϕ_e increased.

Because β, the dimensionless adsorption energy term, is the product of b times C_{F_o}, increasing C_{F_o} improves the assumption of irreversible immobilization. Although increasing ϕ_e also improves the approximation, experimental observation time lengthens as the volume served per particle, V,

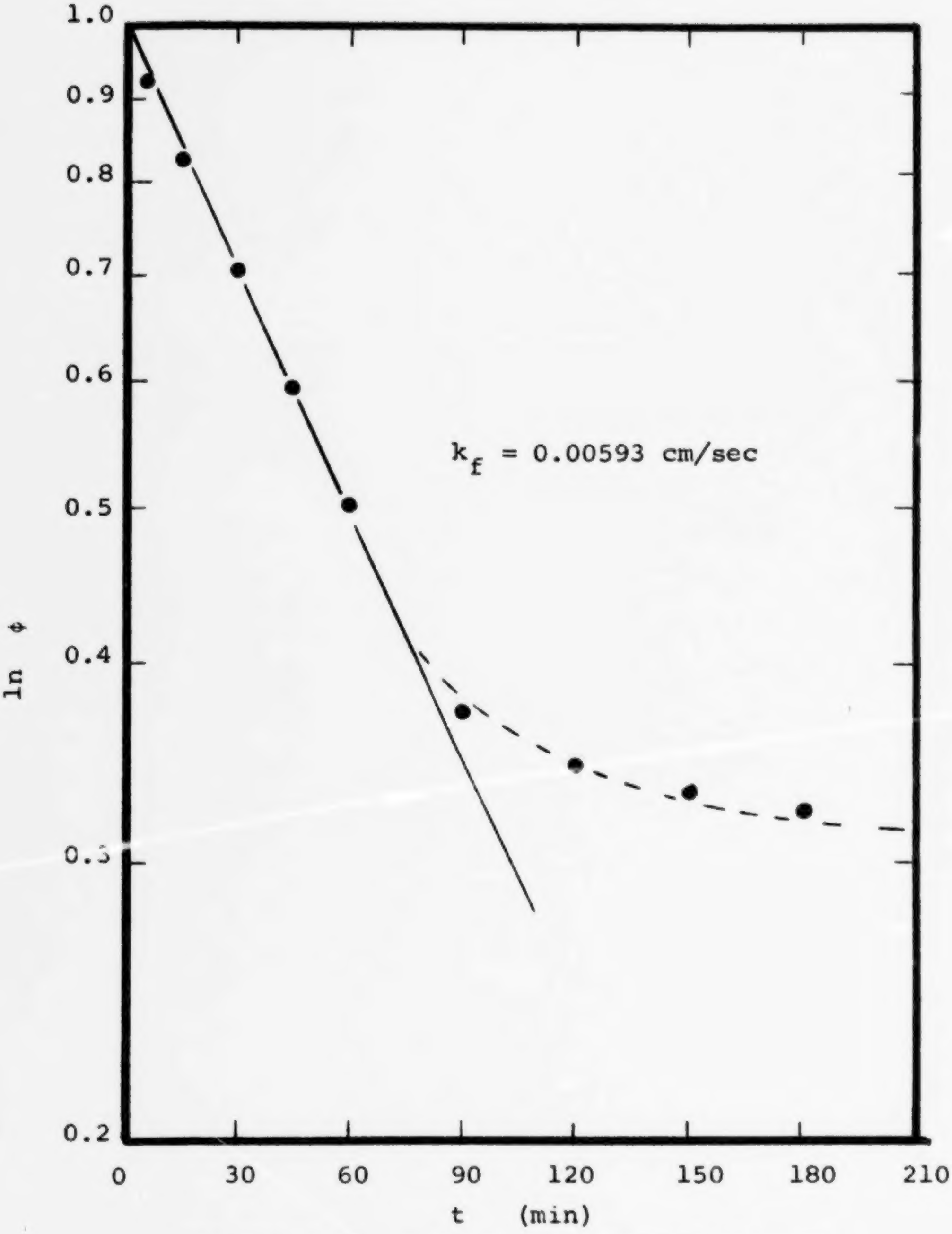

FIGURE 5-34. SIMPLE FILM DIFFUSION MODEL.
DATA FOR PNP (A). (C_{Fo} = 1.0 x 10^{-4} $\underline{M}$, ϕ_e = 0.3, a = 0.025 cm, 1250 rpm)

increases in proportion to the fewer particles needed.

The linearized form of the combined film and pore diffusion model (Equation 5-37) was tested using calculated curves from the model of pore diffusion with non-linear adsorption as data input. It was shown that as β decreased from 50 to 30 to 5, convex curvature of model test points increased, which was consistent with the comparison of calculated concentration-time profiles discussed above. It was also noted that if convex curvature was mistakenly ignored, diffusion coefficients calculated from the slope of the plot could be about double the actual value.

Adsorption rate data for 2-hexyl-, 2-octyl-, 2-decylbenzenesulfonate, DNOCHP, DNOSBP and DNP (A) were adequately described by the film and pore diffusion model using the assumptions of irreversible immobilization and quasi-steady state. However, experimental design was quite critical. In experiments in which β was less than about 30, and ϕ_e close to zero, convex curvature of data plotted according to the linearized model form indicated that improvement in the irreversible adsorption assumption was needed. Moreover, convex curvature was not apparent until fractional solution concentration had reached about 0.5 . Therefore, experimental design should also emphasize the use of the smallest particle size within the range of interest. This increases the rate of adsorption and approach to equilibrium since carbon dosage to attain a given ϕ_e is almost independent of particle size, while the volume served per particle decreases with increasing particle numbers.

The combined film and pore diffusion model graphically illustrated the importance of both transport mechanisms on the overall rate of adsorption. Pore diffusion almost entirely controlled the rate of adsorption for the larger more bulky molecules, exemplified by the alkylbenzenesulfonates and DNOCHP. This was also shown by neglecting film diffusion and applying the model for pore diffusion with non-linear adsorption. Conversely, film diffusion became a significant part of the rate controlling mechanism in rate studies of DNOSBP and DNP, which exemplify the smaller, more compact molecules. A test of the model for pore diffusion with non-linear adsorption further showed that film diffusion could not be neglected because the initial rate of adsorption was noticeably retarded.

The values obtained for diffusion coefficients varied from about 1×10^{-6} cm^2/sec for 2-decylbenzenesulfonate to about 5×10^{-6} cm^2/sec for DNP (A). Using superficial flux reduces the value of apparent diffusivity by a factor relating to porosity. This, together with neglecting tortuousity effects may explain the discrepancy between observed pore diffusivities and free-liquid diffusivities. Complex pore structures and sorbate-sorbent interactions which defy simple mathematical description may also be factors of import. However, these do not detract from the capability of the model to closely represent the rate controlling mechanisms.

Some difficulty was encountered in fitting the experimental data for the neutral species of DNP to the simplified model. However, the results seem to indicate that diffusion of the neutral form was about ten times faster than that of the anion. Thus, it was postulated that molecular charge influences the ability of the molecule to diffuse through the internal carbon pore structure.

The weaker adsorbers, phenol and PNP, made application of the irreversible adsorption and quasi-steady state approximations more difficult since the adsorption energy term, b, was quite small. Initial concentrations, C_{F_o}, would thus have to be increased to values beyond the range of interest. Moreover, increasing C_{F_O} correspondingly decreases α , the dimensionless adsorption capacity term, which might affect the assumption of quasi-steady state.

Finally, a simple film diffusion model was found adequate for description of initial rate data for phenol (N), PNP (N), DNP (N) and PNP (A). The build-up of fluid phase concentration, C_{F_i}, on the inside of the boundary layer surrounding the particle was ignored; thus, a simple first order equation related solution concentration and time. This was a reasonable assumption since equilibrium adsorption studies have shown the distribution ratio of solid to liquid phase concentrations to be quite large. The simple film model was shown to be applicable for about the first one to two hours of adsorption. Two explanations for the failure of the model after this time were postulated: 1) concentration build-up on the inside of the boundary layer could no longer be ignored or 2) pore diffusion began to significantly control the rate of adsorption. The latter explanation seemed more plausible, based on previous studies in which a combined film and pore transport mechanism was indicated.

Furthermore, transfer coefficients of about 0.01 cm/sec were obtained from the simple film model and remained consistent with the values calculated from the combined film and pore diffusion model. As stirring speed increased from 275 to 1550 rpm, the transfer coefficient, k_f, was noted to approximately double. The transfer coefficient was also shown to be independent of particle size. Finally, correlation of k_f with hydrodynamics and free-liquid diffusivity given in Appendix C, indicates the obtained values of k_f to be reasonable for the system employed.

CHAPTER 6

INFINITE-BATH KINETICS

As outlined in Chapter 3, the mathematics of infinite-bath kinetics are much simpler to deal with than those of a finite-bath. However, experimental design is often a difficulty with systems of the former type. Snoeyink and Weber (31), in their investigation of hydrogen ion adsorption on activated carbon, used a convenient infinite-bath system consisting of a Sargent recording pH Stat, which held pH constant and recorded acid addition with time. Dedrick and Beckman (15) approximated an infinite-bath for adsorption rate studies of 2,4 dichlorophenoxyacetic acid (2,4-D) on activated carbon. Their method was to use a very small quantity of adsorbent in a sufficiently large solution volume to prevent a significant decrease in bulk phase concentration. The carbon pellets, having a diameter of 0.2 cm, were large enough to be removed from solution at various times and analyzed for 2,4-D. Such a method would appear not only tedious, but also inaccurate, since results are dependent upon a somewhat involved analytical technique for 2,4-D in amounts of less than 1 x 10^{-5} moles per pellet.

EXPERIMENTAL APPARATUS

An automatically controlled, photometric titrating device was constructed to obtain an infinite-bath system. This method was more accurate and convenient than that employed by Dedrick and Beckman (15), especially since small adsorbent particles were to be studied. A schematic diagram of the apparatus is shown in Figure 6-1. The baffles, stirring device and control, and reaction vessel have been

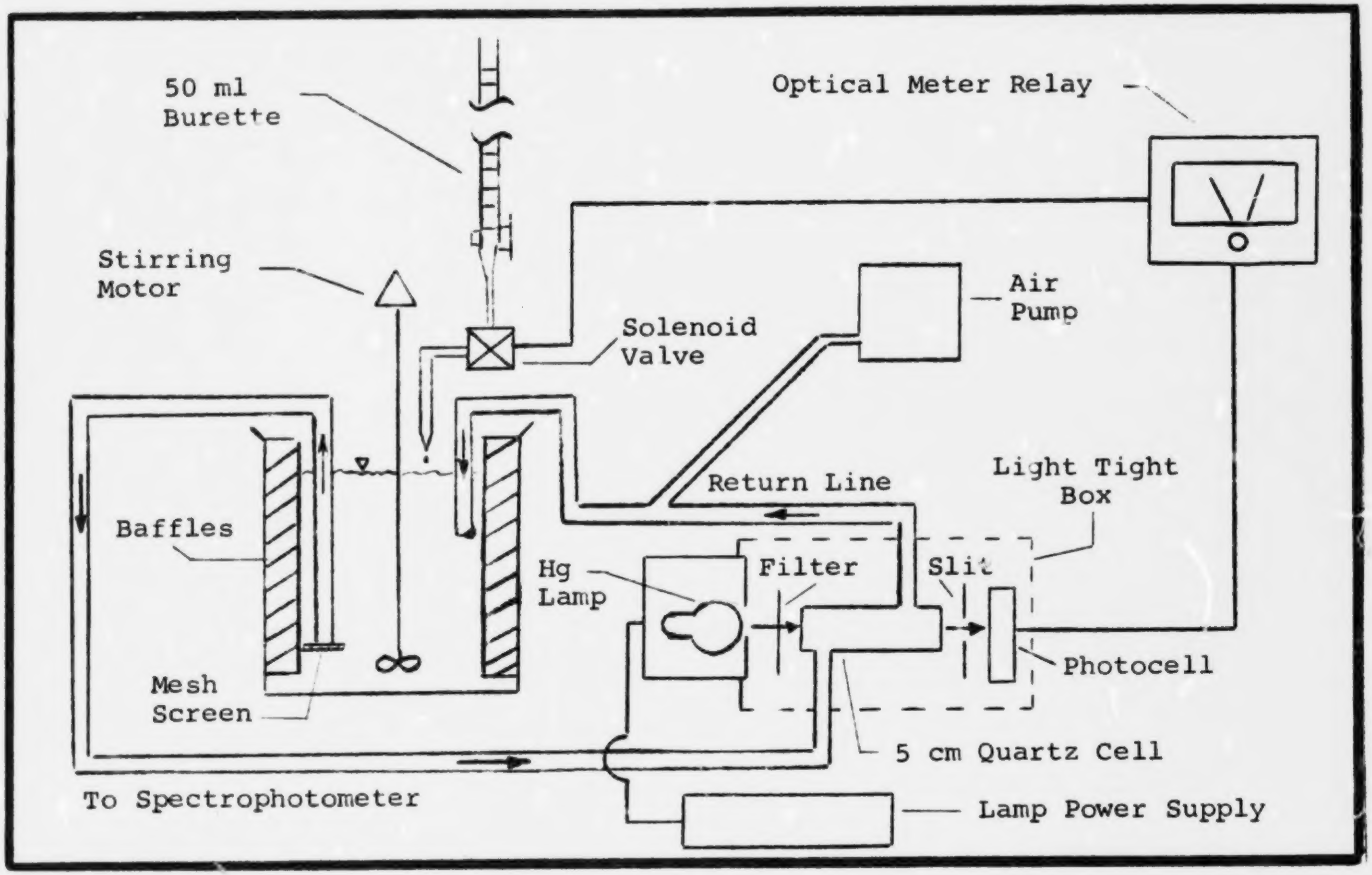
50 ml
Burette
Optical Meter Relay
Stirring
Motor
Air
Pump
Solenoid
Valve
Return Line
Light Tight
Box
Baffles
Hg
Lamp
Filter
Slit
Photocell
Mesh
Screen
5 cm Quartz Cell
To Spectrophotometer
Lamp Power Supply

FIGURE 6-1. SCHEMATIC DIAGRAM OF INFINITE-BATH APPARATUS.

described in Chapter 5. Solution was continuously siphoned from the reaction vessel, passed through a spectrophotometer, and returned to the vessel with the aid of a small aquarium air pump. Flow rate was such that residence or detention time in the absorbance cell was less than 15 seconds. An 80 mesh plastic screen was inserted at the intake end of the tygon tubing to prevent carbon particles being withdrawn from the reaction vessel.

A Coleman Ultraviolet Illuminator unit, housing a mercury vapor lamp, provided the light source for the spectrophotometer. To prevent the higher bands of light energy from passing through the absorbance cell, a blue filter was placed in front of the lamp. A flow-thru cell was custom-made by a glassblower, who simply fitted another outlet, diametrically opposed to the original filler hole of a Beckman 5 cm quartz end cell. Stray light was prevented from impinging on the photocell by placing a thin metal plate, with a hole of slightly smaller diameter than the cell, between the photocell and absorbance cell. A Weston model 856, type GG, barrier layer photronic cell was used to convert light energy to electrical energy. The entire assembly consisting of filter, absorbance cell, slit and photocell was enclosed in a light tight black box which was attached to the face of the Coleman Ultraviolet Illuminator. Electrical output from the photocell then passed to an API optical meter relay, having a full scale current reading of 10 μ amps DC. The load relay to be energized was a solenoid valve controlling the flow of solute from the burette to the reaction vessel.

EXPERIMENTAL PROCEDURE

Prior to addition of activated carbon to the reaction vessel, the flow cycle was activated and bath solute described in Chapter 5. Solution was continuously siphoned from the reaction vessel, passed through a spectrophotometer, and returned to the vessel with the aid of a small aquarium air pump. Flow rate was such that residence or detention time in the absorbance cell was less than 15 seconds. An 80 mesh plastic screen was inserted at the intake end of the tygon tubing to prevent carbon particles being withdrawn from the reaction vessel.

A Coleman Ultraviolet Illuminator unit, housing a mercury vapor lamp, provided the light source for the spectrophotometer. To prevent the higher bands of light energy from passing through the absorbance cell, a blue filter was placed in front of the lamp. A flow-thru cell was custom-made by a glassblower, who simply fitted another outlet, diametrically opposed to the original filler hole of a Beckman 5 cm quartz end cell. Stray light was prevented from impinging on the photocell by placing a thin metal plate, with a hole of slightly smaller diameter than the cell, between the photocell and absorbance cell. A Weston model 856, type GG, barrier layer photronic cell was used to convert light energy to electrical energy. The entire assembly consisting of filter, absorbance cell, slit and photocell was enclosed in a light tight black box which was attached to the face of the Coleman Ultraviolet Illuminator. Electrical output from the photocell then passed to an API optical meter relay, having a full scale current reading of 10 μ amps DC. The load relay to be energized was a solenoid valve controlling the flow of solute from the burette to the reaction vessel.

EXPERIMENTAL PROCEDURE

Prior to addition of activated carbon to the reaction vessel, the flow cycle was activated and bath solute concentration measured by the optical meter. A variable resistor was used to adjust the photocell output current to an arbitrary scale reading of 5 μ amps. The set point needle was then adjusted to as close to 5 μ amps as possible without activating the solenoid valve. Electrical circuitry was such that when the output from the photocell increased above the set point, the solenoid valve would be energized and solute added to the reaction vessel until the current again returned to the set point. This would occur upon addition of the activated carbon to the reaction vessel to begin the adsorption process. The flow rate of the burette was manually adjusted to allow sufficient response time, thus preventing "overshoot", while delivering enough solute to "keep up" with the reaction. Addition of solute therefore occurred in a step wise fashion which depended on the sensitivity of the spectrophotometer to the particular solute under investigation.

SOLUTES

In Chapter 5, it was noted that the rates of adsorption of phenol, PNP and DNP were not adequately described by the proposed simplified film and pore resistance model. Hence, the intent was to study these solutes using the infinite bath technique which would allow consideration of the actual non-linear isotherm together with film and pore resistance. As shown in Table 4-2, the neutral and anionic forms of phenol do not absorb light energy in the high UV range and consequently could not be investigated using a mercury lamp as a light source. However, addition of the nitro group to the phenolic structure enhances the absorbance of light energy between 300 and 400 mμ as also indicated in Table 4-2. It may be noted that although the absorbance peak for DNP (N) is at 260 $m\mu$, an absorbance shoulder exists at 292 $m\mu$ and continues to "tail off" to 400 $m\mu$. Thus both species of PNP and DNP were amenable to analysis. The intent of investigating DNP (A) was to compare results with those previously obtained using the finite-bath and simplified model.

SENSITIVITY OF APPARATUS

The relative sensitivity of the photocell, as given by the manufacturer, is 50 per cent at 400 $m\mu$ and 10 per cent at 300 $m\mu$. A movement of approximately 0.1 μ amps on the optical meter relay scale was enough to energize the solenoid valve. This corresponded to a change in solution concentration of about 5 $\mu\underline{M}$ for the neutral species of PNP and DNP and about 0.5 $\mu\underline{M}$ for anions. An increase in sensitivity was expected for the anion forms since they possess higher molar absorptivities than the neutral forms as indicated in Table 4-2. A 50 ml burette, graduated in 0.1 ml units, was filled with 10^{-2} $\underline{M}$ solution of solute. A change of 0.1 ml therefore constituted an addition of 0.333 μ moles of solute per liter of solution. The adsorption capacities of the systems investigated were such that less than 100 ml of titrant were added during the rate studies, thus giving a volume increase of less than three per cent.

FILM AND PORE RESISTANCES IN SERIES WITH SIMULTANEOUS NON-LINEAR ADSORPTION

The following is a mathematical description of the model to be considered:

Transient Radial Diffusion Mass Balance

$$D \left[\frac{\partial^2 C_F}{\partial r^2} + \frac{2}{r} \frac{\partial C_F}{\partial r} \right] = \frac{\partial}{\partial t} (\varepsilon C_F + (1 - \varepsilon) C_S) \quad (6\text{-}1)$$

Langmuir Adsorption Isotherm

$$C_S = \frac{Q \; b \; C_F}{1 + b \; C_F} \cdot \rho_{solid} \quad (6\text{-}2)$$

Boundary Conditions

$$C_F = C_{F_o}, \qquad r \geq a, \; t \geq 0 \quad (6\text{-}3)$$

$$D \frac{\partial C_{F_i}}{\partial r} = k_f (C_{F_o} - C_{F_i}) \qquad r = a, \; t \geq 0 \quad (6\text{-}4)$$

Using the same dimensionless parameters for radius, r, and concentration C_{F_i}, as given in Appendix A, Equation 6-4 becomes:

$$\left. \frac{\partial \phi}{\partial \xi} \right|_{\xi = 1} = \gamma (1 - \phi) \quad (6\text{-}5)$$

where

$$\gamma = \frac{k_f a}{D} \quad (6\text{-}6)$$

A finite difference form for Equation 6-5 is given by

$$\frac{\phi_{m+1} - \phi_{m-1}}{2 \; \Delta \xi} = \gamma (1 - \phi_m) \quad (6\text{-}7)$$

As developed in Appendix A, the left hand side of Equation 6-1, written in dimensionless parameters, may also be transformed to a finite difference expression.

$$\frac{\partial^2 \phi_m}{\partial^2 \xi} + \frac{2}{\xi} \frac{\partial \phi_m}{\partial \xi} = \frac{(m+1) \; \phi_{m+1} - 2 \; m \; \phi_m + (m-1) \; \phi_{m-1}}{m (\Delta \xi)^2} \quad (6\text{-}8)$$

Transient Radial Diffusion Mass Balance

$$D\left[\frac{\partial^2 C_F}{\partial r^2}+\frac{2}{r}\frac{\partial C_F}{\partial r}\right]=\frac{\partial}{\partial t}(\epsilon C_F+(1-\epsilon)C_S) \qquad (6\text{-}1)$$

Langmuir Adsorption Isotherm

$$C_S=\frac{Q\ b\ C_F}{1+b\ C_F}\cdot\rho_{solid} \qquad (6\text{-}2)$$

Boundary Conditions

$$C_F=C_{F_o},\qquad r\geq a,\ t\geq 0 \qquad (6\text{-}3)$$

$$D\frac{\partial C_{F_i}}{\partial r}=k_f(C_{F_o}-C_{F_i})\qquad r=a,\ t\geq 0 \qquad (6\text{-}4)$$

Using the same dimensionless parameters for radius, r, and concentration C_{F_i}, as given in Appendix A, Equation 6-4 becomes:

$$\left.\frac{\partial\phi}{\partial\xi}\right|_{\xi=1}=\gamma(1-\phi) \qquad (6\text{-}5)$$

where

$$\gamma=\frac{k_f a}{D} \qquad (6\text{-}6)$$

A finite difference form for Equation 6-5 is given by

$$\frac{\phi_{m+1}-\phi_{m-1}}{2\,\Delta\xi}=\gamma(1-\phi_m) \qquad (6\text{-}7)$$

As developed in Appendix A, the left hand side of Equation 6-1, written in dimensionless parameters, may also be transformed to a finite difference expression.

$$\frac{\partial^2\phi_m}{\partial^2\xi}+\frac{2}{\xi}\frac{\partial\phi_m}{\partial\xi}=\frac{(m+1)\ \phi_{m+1}-2\,m\ \phi_m+(m-1)\ \phi_{m-1}}{m(\Delta\xi)^2} \qquad (6\text{-}8)$$

To begin a numerical solution of the diffusion gradient within the sphere, the solution concentration, ϕ_{m+1} is specified by the surface boundary condition, or after rearranging Equation 6-7.

$$\phi_{m+1} = 2\gamma\,\Delta\xi\,(1 - \phi_m) + \phi_{m-1} \qquad (6\text{-}9)$$

Therefore, ϕ_{m+1} in Equation 6-8 may be replaced by Equation 6-9 to yield

$$\left.\frac{\partial^2 \phi_m}{\partial^2 \xi} + \frac{2}{\xi}\,\frac{\partial \phi_m}{\partial \xi}\right|_{\xi=1} = \frac{(m+1)\left[2\gamma\,\Delta\xi\,(1 - \phi_m) + \phi_{m-1}\right] - 2m\,\phi_m + (m-1)\,\phi_{m-1}}{m(\Delta\xi)^2} \qquad (6\text{-}10)$$

which may be rearranged to give Equation 6-11.

$$\left.\frac{\partial^2 \phi_m}{\partial^2 \xi} + \frac{2}{\xi}\,\frac{\partial \phi_m}{\partial \xi}\right|_{\xi=1} = \frac{2\left[(m+1)\gamma\,\Delta\xi - (m\gamma\Delta\xi + \gamma\Delta\xi + m)\,\phi_m + m\,\phi_{m-1}\right]}{m(\Delta\xi)^2} \qquad (6\text{-}11)$$

The right hand side of Equation 6-1, after conversion to dimensionless parameters given in Appendix A,[1] may be written as

$$\frac{\partial}{\partial t}\left(\varepsilon C_F + (1-\varepsilon)C_S\right) = \frac{\varepsilon\phi'_m - \varepsilon\phi_m + \sigma'_m - \sigma_m}{\Delta\theta} \qquad (6\text{-}12)$$

where ϕ'_m and σ'_m are the new dimensionless concentrations in the liquid and solid phase respectively after a dimensionless time increment of $\Delta\theta$.

---

[1] The term σ_m includes $(1 - \varepsilon)$ since α, which is used to obtain σ in Equation 5-30, is calculated on the basis of $(1 - \varepsilon)\rho_{solid}$ (see page 63)

Considering first the case of linear adsorption equilibria, the solid phase is related to the liquid phase concentration by

$$\sigma_m = R \ \phi_m \tag{6-13}$$

where R is the dimensionless slope of the adsorption isotherm. Substituting for σ_m and σ'_m in Equation 6-12 gives Equation 6-14.

$$\frac{\sigma'_m - \sigma_m + \varepsilon \phi'_m - \varepsilon \phi_m}{\Delta \theta} = \frac{(\varepsilon + R)(\phi'_m - \phi_m)}{\Delta \theta} \tag{6-14}$$

Thus recombining both sides of Equation 6-1, written in dimensionless finite difference form, and solving for ϕ'_m yields

$$\phi'_m = \frac{2 \Delta \theta \ [(m+1) \ \gamma \Delta \xi \ - (m \gamma \Delta \xi + \gamma \Delta \xi + m) \ \phi_m + m \ \phi_{m-1}]}{(\varepsilon + R) \ m \ (\Delta \xi)^2} + \phi_m \tag{6-15}$$

for $\xi = 1$, and

$$\phi'_m = \frac{\Delta \theta \ [(m+1) \ \phi_{m+1} - 2m \ \phi_m + (m-1) \ \phi_{m-1}]}{(\varepsilon + R) \ m (\Delta \xi)^2} + \phi_m \tag{6-16}$$

for $0 < \xi < 1$.

A numerical solution is then obtained explicitly, starting with all values of ϕ_m equal to zero at θ equal zero, and calculating ϕ'_m by Equation 6-15 for the first distance step $\Delta \xi$. Equation 6-16 is used for each step thereafter, except of course at ξ equal zero, where ϕ_{m-1} does not exist. Another finite difference equation could be written for this special case; however, ϕ_m values were only needed for a fraction of the total radius.

The concentration gradient may be calculated in a similar fashion if non-linear rather than linear adsorption is considered. That is, R may be assumed to be the instantaneous slope of the isotherm at the current value of ϕ_m or R is given by the derivative of the Langmuir isotherm model.

$$R = \frac{\alpha \beta}{(1 + \beta \phi_m)^2} \qquad (6\text{-}17)$$

The dimensionless Langmuir constants α and β are as defined in Chapter 5 and Appendix A. An explicit technique is again suitable with one minor change: Prior to calculating ϕ'_m by either Equation 6-15 or 6-16, it is first necessary to calculate R from equation 6-17 for the current value of ϕ_m.

For application of the model to experimental data, the desired output from the numerical solution is dimensionless surface flux as a function of dimensionless time. Surface flux is obtained from Equation 6-5, where ϕ is calculated from Equation 6-15. Since all values of ϕ_m are initially zero, surface flux has a maximum value of γ at θ equal zero.

SELECTION OF GRID SIZE

The analytical solution for the given boundary conditions assuming a linear isotherm is given by Equation 6-18 (8,12).

$$\left.\frac{\partial \phi}{\partial \xi}\right|_{\xi=1} = \frac{2\gamma^2}{\xi} \sum_{n=1}^{\infty} \frac{e^{\frac{-\psi_n^2 \theta}{1+R}} \sin \psi_n \xi}{\psi_n^2 + \gamma[\gamma - 1] \sin \psi_n} \qquad (6\text{-}18)$$

The terms of the infinite series, ψ_n, are given by the triginometric function shown in Equation 6-19.

$$\psi_n \cot \psi_n + \gamma - 1 = 0 \qquad (6\text{-}19)$$

To select the proper grid size, the finite difference solution presented for the linear isotherm case, was compared with the analytical solution. The values of R chosen were 10^4 and 10^5 since these represent the general range of R calculated from Equation 6-17 for the non-linear case, assuming α and β values as discussed in Chapter 5. The value of γ was selected to be 25 based on estimates of D and k_f of 1×10^{-5} cm^2/sec and 0.01 cm/sec respectively and a radius, a, of 0.025 cm. A small table of triginometric roots for Equation 6-19 is available (12); however, the first fifteen roots, or terms of the infinite series, were required for convergence of Equation 6-18 when the value of R was 10^4.

The University of Michigan IBM 360 computer was used for numerical solutions to the finite difference equation. The computer program, written in Fortran IV, is listed in Appendix B for the non-linear isotherm case. To obtain the program used for the linear isotherm case, it is only necessary to delete the statement following Statement Number 45, in which R is calculated by Equation 6-17.

Figure 6-2 illustrates the results of comparing the finite difference to the analytical solution. After some experimenting, the distance step, $\Delta\xi$, was chosen to be 0.02 and the time step, $\Delta\theta$, to be 1.0 for an R value of 10^5. However, $\Delta\theta$ was reduced to 0.5 when the distribution ratio was lowered to 10^4. As can be seen, the surface flux decreases faster for the smaller R value since the fluid phase concentration within the sphere builds up more rapidly.

A small distance step was required since such high distribution ratios imply that movement of the fluid phase

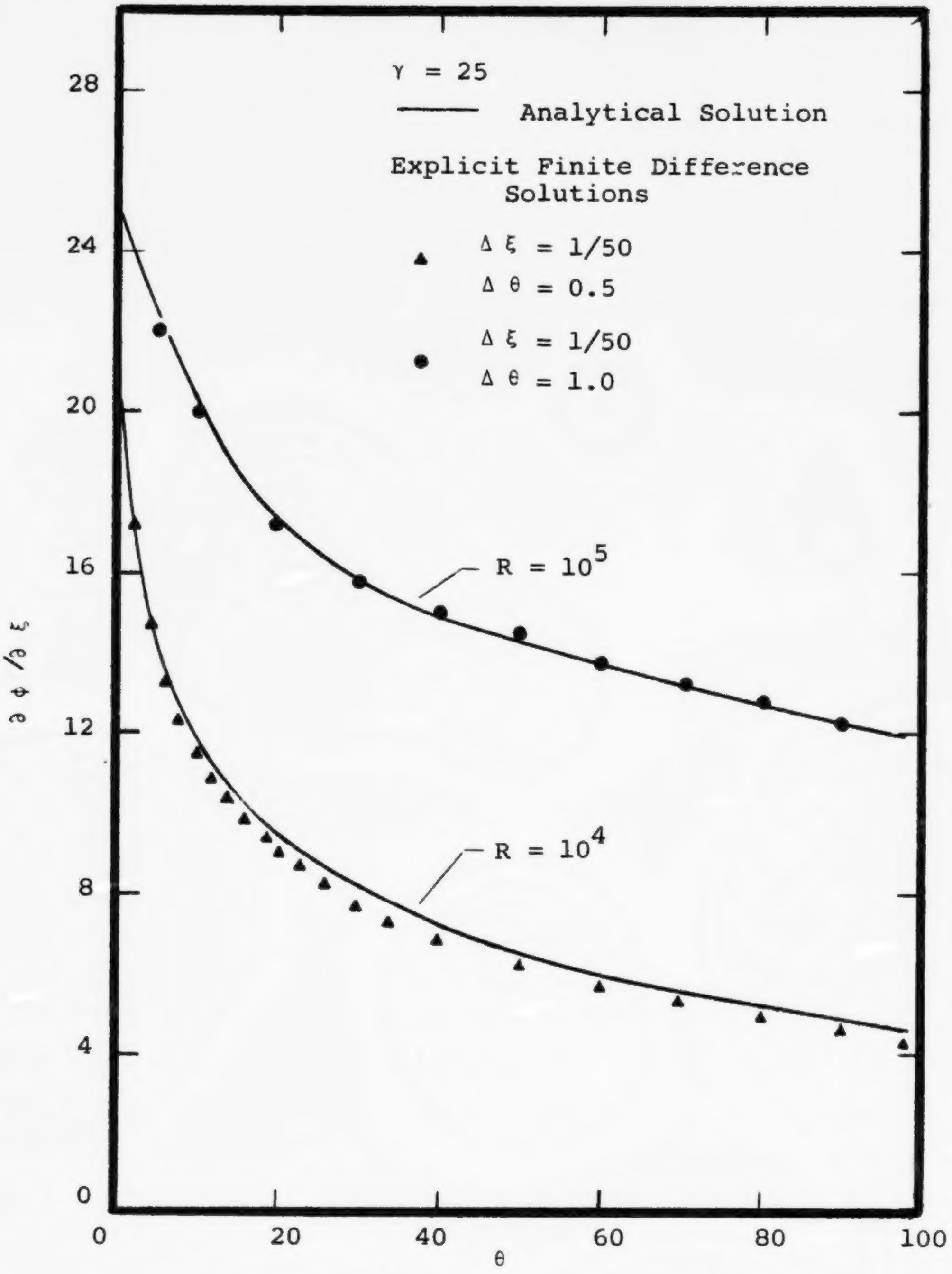

FIGURE 6-2. COMPARISON OF FINITE DIFFERENCE AND ANALYTICAL SOLUTIONS FOR $R = 10^4$ AND $R = 10^5$.

"front" is slow and thus significant changes in fluid phase concentration occur in the first fraction of the sphere. It was found necessary then, to calculate only the first 8 to 10 distance steps before fluid phase concentration became neglible. A counter called "L" in the program given in Appendix B, indicated the distance step at which calculation was stopped and the value of ϕ_L was printed out to insure that enough steps had been considered.

EXPERIMENTAL RESULTS - PNP (N)

The bath concentration of all PNP (N) experiments was chosen to be 1×10^4 M . As previously described, a 5 μM change in solution concentration was required to activate the solenoid and thus bath concentration remained within ±5 per cent of the initial value. The resulting values of α and β were 15,800 and 24 respectively.

From Figure 6-3, the effect of γ on surface flux, $\partial \phi / \partial \xi$, as a function of θ can be observed. The curves were calculated using the computer program of Appendix B with a distance step, $\Delta \xi$, of 0.02 and time step, $\Delta \theta$, of 0.25. It may be noted that as γ increases from 2.5 to 10, the ratio of k_f to D increases and thus internal pore diffusion becomes more rate controlling, yielding a sharper initial decrease in surface flux. This behavior is similar to that shown in Figure 5-5 for finite-bath kinetics using a combined film and pore diffusion model.

Integrating surface flux over time, dimensionless uptake, M_θ, is given by

$$M_\theta = \int_1^\theta \left. \frac{d\phi}{d\xi} \right|_{\xi=1} d\theta \qquad (6\text{-}20)$$

Numerical integration of the curves shown in Figure 6-3

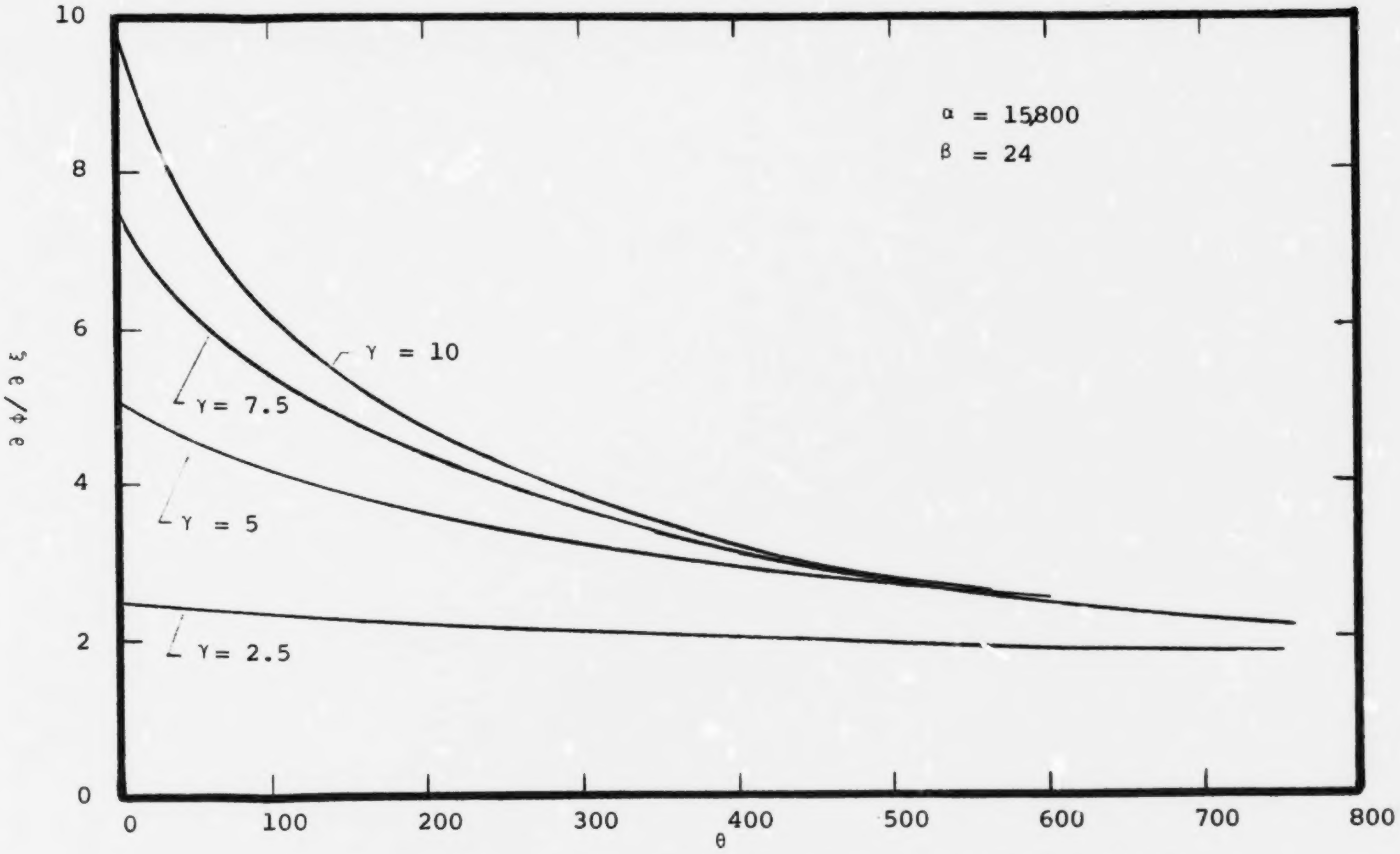

FIGURE 6-3. DIMENSIONLESS SURFACE FLUX - DIMENSIONLESS TIME PROFILES FOR PNP (N) AND γ VALUES OF 2.5, 5, 7.5 AND 10 .

yields the corresponding M_θ versus θ functions illustrated in Figure 6-4. It can be seen that uptake increases for a given θ as pore diffusion becomes more rate controlling. However, all uptake curves must reach the same equilibrium uptake value, M_∞ . Similarly, the surface flux functions of Figure 6-3 must eventually cross one another so that the total area beneath each curve is the same.

The data obtained from the infinite-bath experiments consisted of volume of titrant added versus time. Converting volume of titrant to μM added per liter of solution and dividing by carbon external surface area per liter of solution yields solute uptake per unit surface area, M_t, in $\mu M/cm^2$. Dimensionless uptake, given by Equation 6-20, is obtained by expressing M_t as

$$M_t = \int_0^t D \left.\frac{dC_F}{dr}\right|_{r=a} dt = \int_0^\theta \frac{D\,C_{F_o}}{a} \frac{d\phi}{d\xi}\, d\left(\frac{a^2\theta}{D}\right) \qquad (6\text{-}21)$$

or,

$$M_\theta = \frac{M_t}{a\,C_{F_o}} \qquad (6\text{-}22)$$

where C_{F_o} is the bath concentration in $\mu M/cm^3$.

A trial and error procedure was required to find the correct value of γ . After selecting a trial γ , values of θ were graphically determined from Figure 6-4 for each M_θ calculated according to Equation 6-22. The resulting values of θ were then plotted versus the corresponding experimental time, t, as shown in Figure 6-5 for data obtained from Experiment A. If the selected value of γ is too large, then initial values of θ will be too small, while the opposite holds if γ is too small. The correct value of γ will yield a linear function since real and

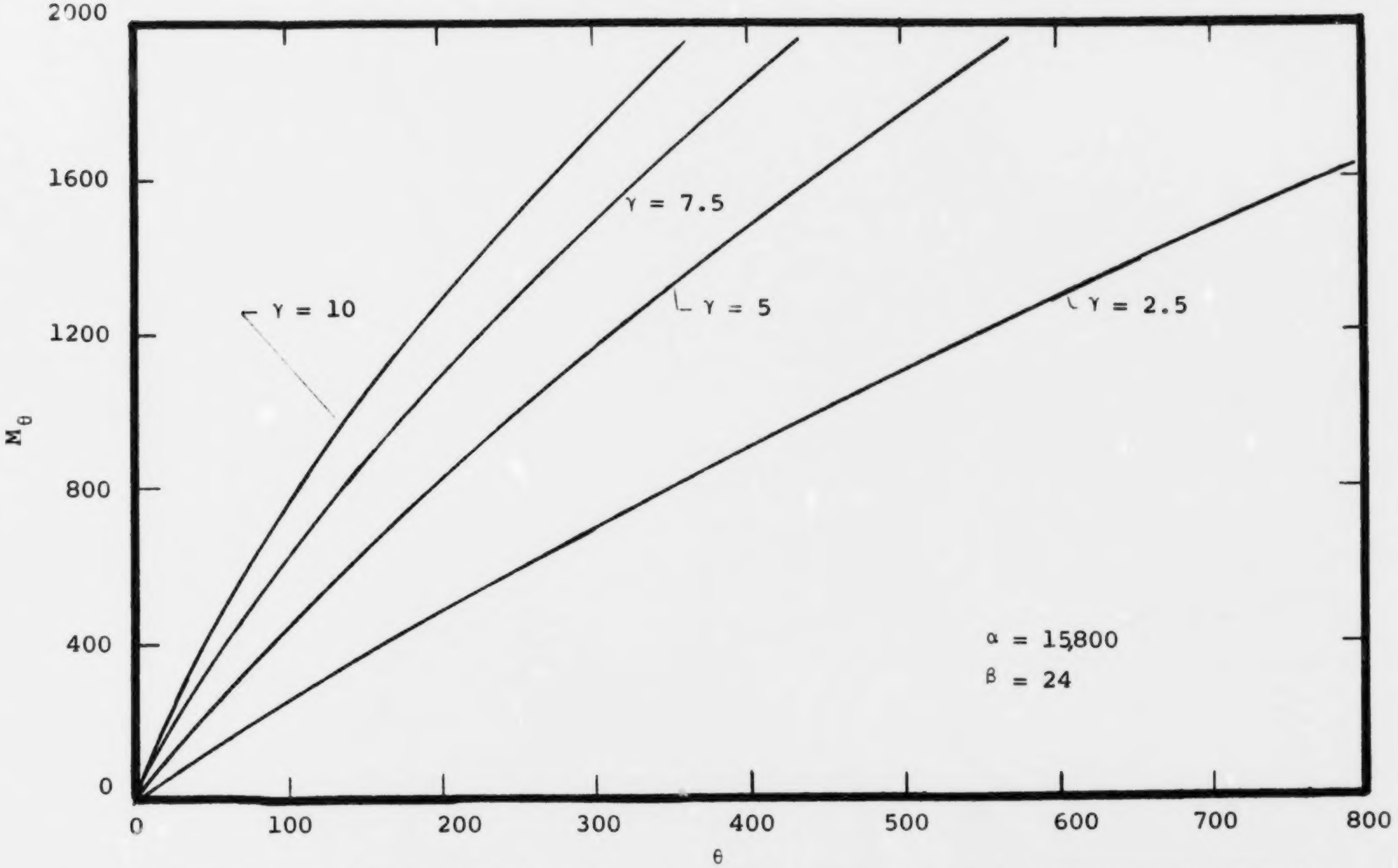

FIGURE 6-4. DIMENSIONLESS UPTAKE, M_θ , AS A FUNCTION OF DIMENSIONLESS TIME, θ , FOR PNP (N) AND γ VALUES OF 2.5, 5, 7.5 AND 10 .

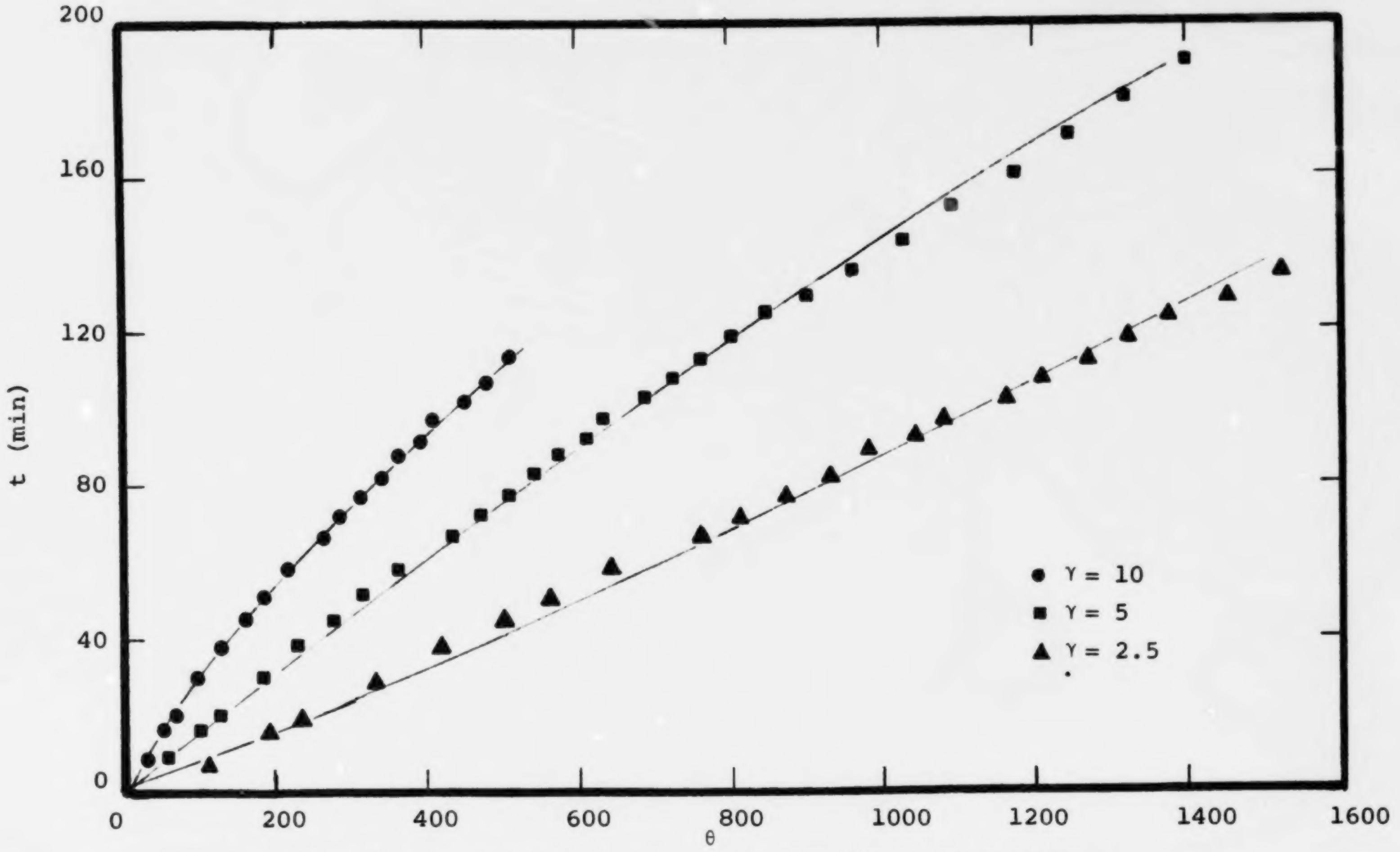

FIGURE 6-5. SELECTION OF γ FOR PNP (N) - EXPERIMENT A
(C_{F_o} = 1.0 x 10^{-4} $\underline{M}$, W = 0.15 gm/l, a = 0.025 cm, 1250 rpm)

dimensionless time are related by a constant. Therefore, the procedure was to decrease γ until the convex curve became either linear or concave. Although, for Experiment A, a γ value of 10 was too large, it was difficult to distinguish between a γ of 5 and 2.5.

The above method of selecting γ, termed the "integral method", was found to be less sensitive than the "differential method". Reexamination of the surface flux versus θ curves in Figure 6-3 reveals that the initial shape of the curve for a γ value of 5 is quite different from that of γ equal 2.5. Experimental surface flux data may be obtained by dividing the incremental uptake, ΔM_t, by the incremental time, Δt as shown in Figure 6-6 for experiment A. A certain amount of experimental error is apparent from the up and down variations in surface flux which were observed. The differential method consists of obtaining the initial surface flux, from which k_f can be calculated as follows:

$$D \frac{dc}{dr} \Bigg|_{t=0,\ r=a} = \frac{D\, C_{F_o}}{a} \frac{d\phi}{d\xi} \Bigg|_{\theta=0} \qquad (6\text{-}23)$$

$$\frac{d\phi}{d\xi} \Bigg|_{\theta=0} = \gamma = \frac{k_f\, a}{D} \qquad (6\text{-}24)$$

$$D \frac{dC}{dr} \Bigg|_{t=0,\ r=a} = \frac{D\, C_{F_o}}{a} \cdot \gamma \qquad (6\text{-}25)$$

$$k_f = \frac{D \frac{dc}{dr}}{C_{F_o}} \Bigg|_{t=0,\ r=a} \qquad (6\text{-}26)$$

Surface flux curves can then be plotted for various values of γ to determine the best fit to the experimental data.

Both the integral and differential method have certain disadvantages. The former is certainly less sensitive than the latter; but, on the other hand, the differential method

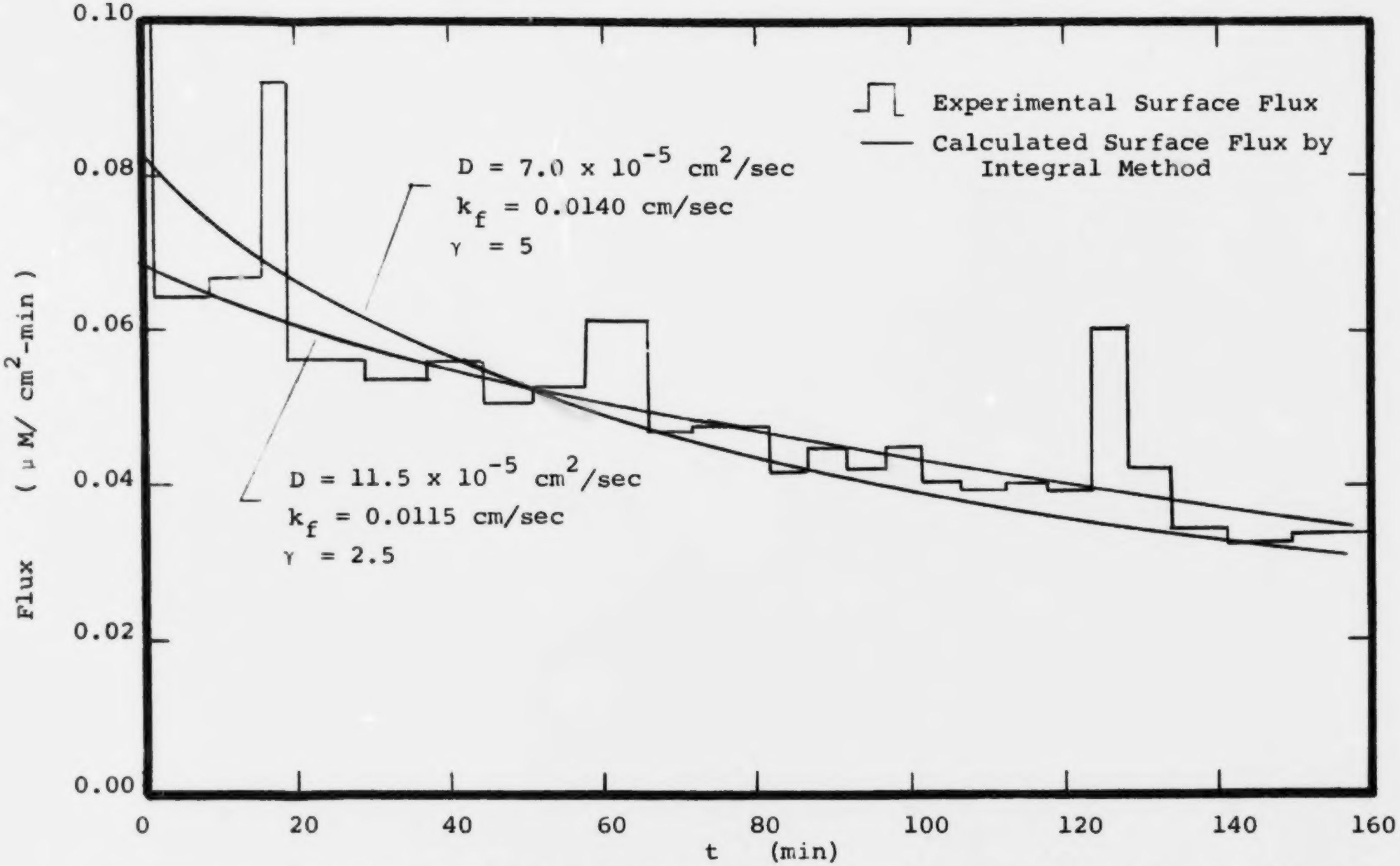

FIGURE 6-6. CALCULATED AND EXPERIMENTAL SURFACE FLUX VERSUS TIME. DATA FOR PNP (N) EXPERIMENT A AND γ VALUES OF 5 AND 2.5 .

requires accurate initial surface flux data. A combination of the two was therefore chosen. Data was first plotted according to the integral method. Values of γ which appeared to give a good fit were then used to plot a calculated surface flux curve and superimposed on the experimental surface flux data as shown in Figure 6-6. The results of applying the integral method to experiment A indicated that a γ of 5 or 2.5 seemed suitable (see Figure 6-5); however, initial surface flux data, although somewhat inaccurate, appears to favor a γ of 5. It may be pointed out that only certain values of γ were initially chosen for investigation since computer solution was required.

The results of three experiments with PNP (N), using a particle radius of 0.025 cm and a stirring speed of 1250 rpm, are shown in Figure 6-7. Experimental values of M_t in $\mu M/cm^2$, were converted to fractional uptakes, M_t/M_∞ . The equilibrium uptake, M_∞ , was calculated according to Equation 6-27.

$$M_\infty = \frac{Q\ b\ C_{F_O}}{1+b\ C_{F_O}} \cdot \rho \cdot \frac{a}{3} \qquad (6\text{-}27)$$

Carbon dosage was 0.15 gm/l in Experiment A and 0.30 gm/l in Experiments B and C. These three experiments were included to indicate the maximum experimental error observed. Theoretically, all three should coincide, since uptake has been expressed per unit surface area. Experiments A and C agreed quite closely and are shown with one calculated curve which was obtained from Figure 6-5. The diffusion coefficients of 7.0×10^{-5} and 5.9×10^{-5} cm^2/sec calculated for Experiments A and B respectively, are in reasonable agreement. The corresponding transfer coefficients of 0.0140 and 0.0117 cm/sec are within the range of values obtained in Chapter 5 using the simplified film and pore model (see Tables 5-2, 5-3 and 5-5).

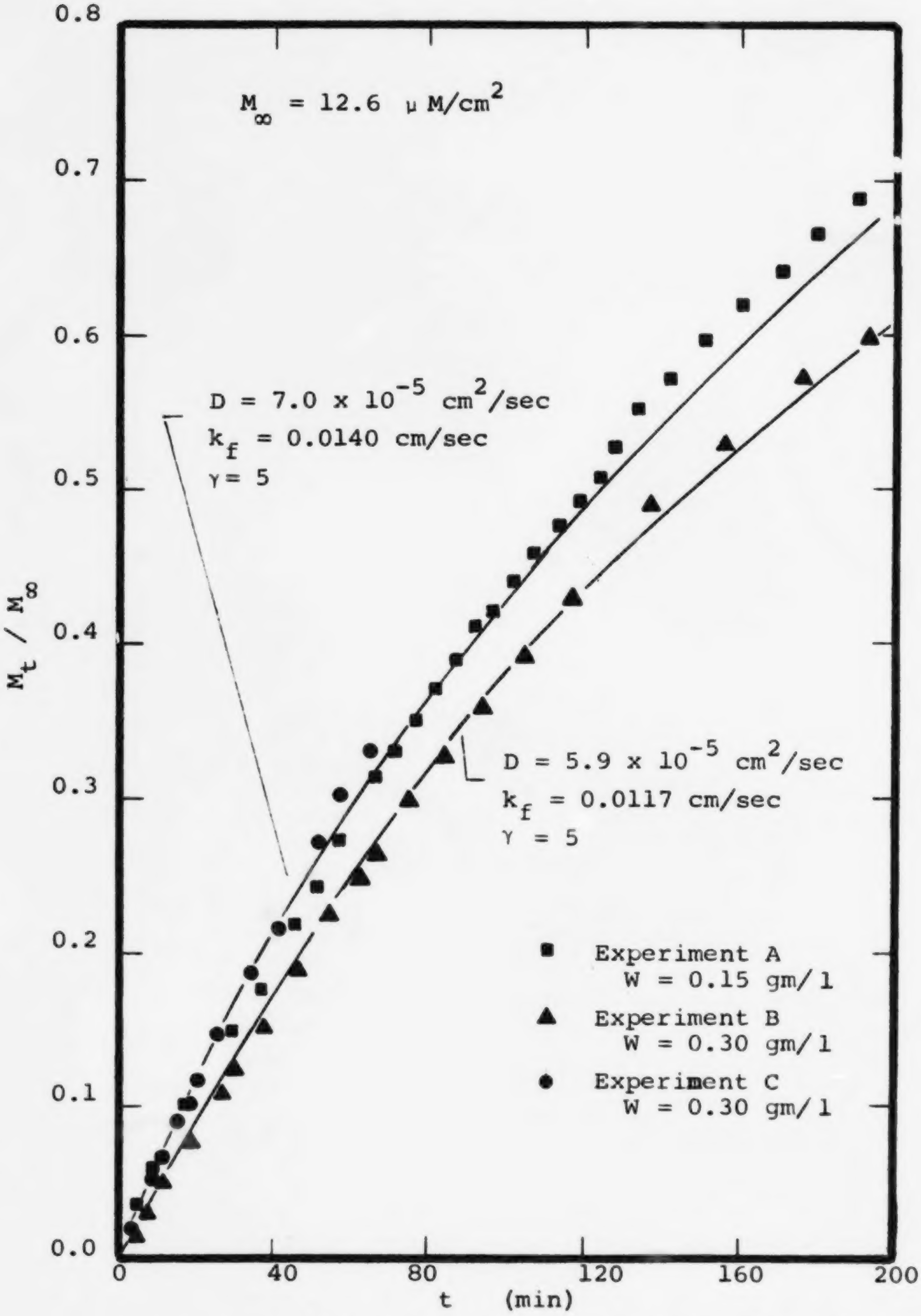

FIGURE 6-7. CALCULATED AND EXPERIMENTAL FRACTIONAL UPTAKES OF PNP (N) - EXPERIMENTS A,B AND C .

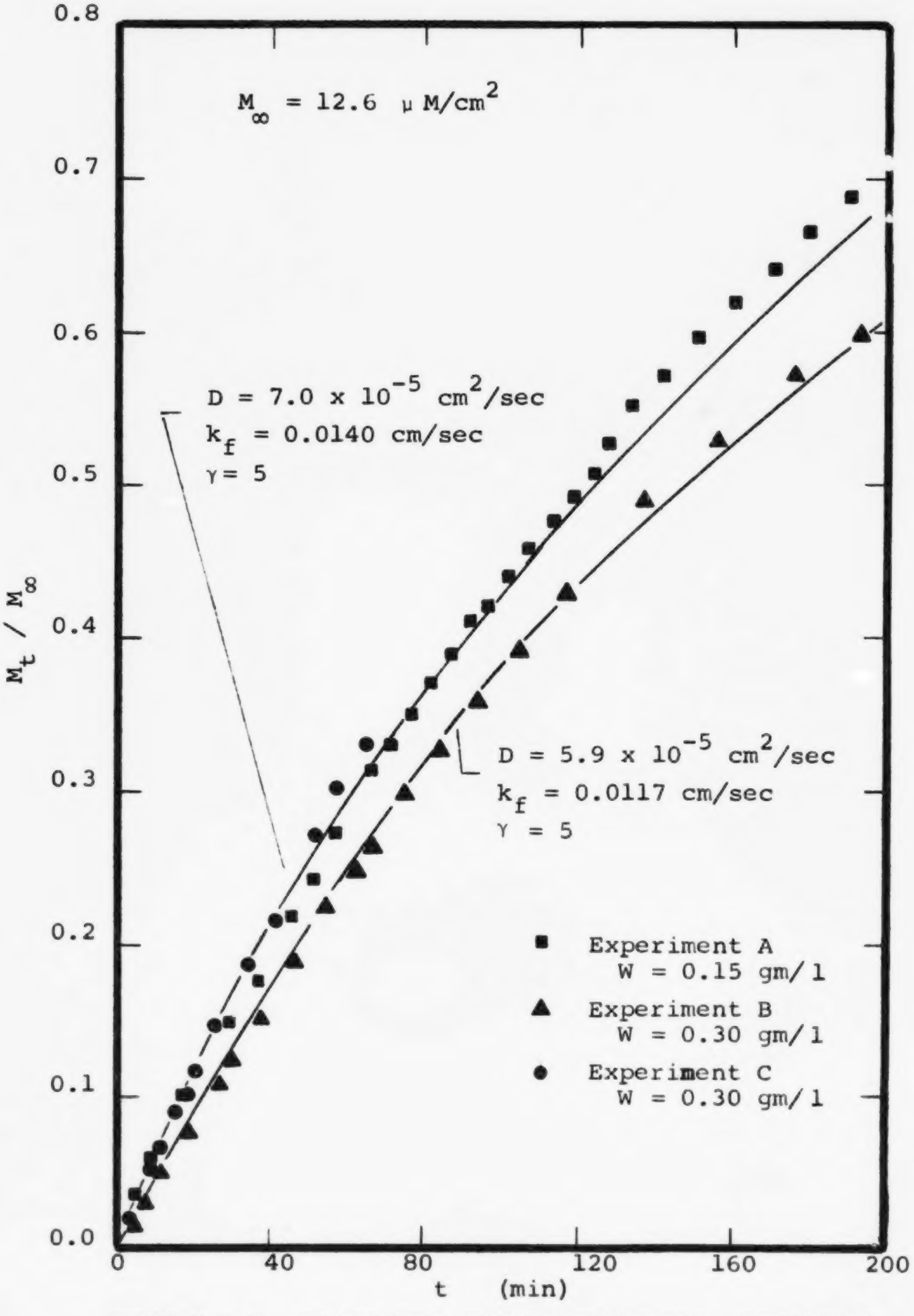

FIGURE 6-7. CALCULATED AND EXPERIMENTAL FRACTIONAL UPTAKES OF PNP (N) - EXPERIMENTS A,B AND C .

Fractional uptake data for duplicate experiments using a particle radius of 0.0136 cm are shown in Figure 6-8 together with the calculated curve. The value of γ was chosen to be 2.5 based on a value of 5 applied to Experiments A, B, and C and the fact that particle radius had been reduced by approximately 50 per cent. Thus, D and k_f were assumed to remain constant as predicted by the model. The resulting values of D and k_f were 8.4×10^{-5} cm^2/sec and 0.0154 cm/sec which agreed with previous values obtained in Figure 6-7 for a particle radius of 0.025 cm. Calculated and experimental surface flux are shown in Figure 6-9. It may be observed that the fractional uptake data did not reflect the differences in surface flux which are apparent from Figure 6-9.

The importance of film diffusion is illustrated in Figure 6-10. Duplicate experiments conducted with a stirring speed of 600 rpm showed a marked decrease in uptake rate when compared to uptake rate at 1250 rpm. An average calculated curve, with D and k_f values of 6.8×10^{-5} cm^2/sec and 0.0068 cm/sec respectively, is shown for a γ value of 2.5. The diffusion coefficient remain consistent with previously calculated values, while the transfer coefficient decreased by approximately 50 per cent, confirming similar findings of Chapter 5.

EXPERIMENTAL RESULTS - PNP (A)

The numerical solutions for surface flux and uptake curves are shown in Figures 6-11 and 6-12 respectively. A bath concentration of 0.5×10^{-4} $\underline{M}$ was used, thus giving an α value of 6,800 and a β value of 6.5. As previously noted, a change of about 0.5 $\underline{\mu M}$ was sufficient to actuate the solenoid. The γ values of 12, 25 and 40, used in Figures 6-11 and 6-12, are typical of the range of

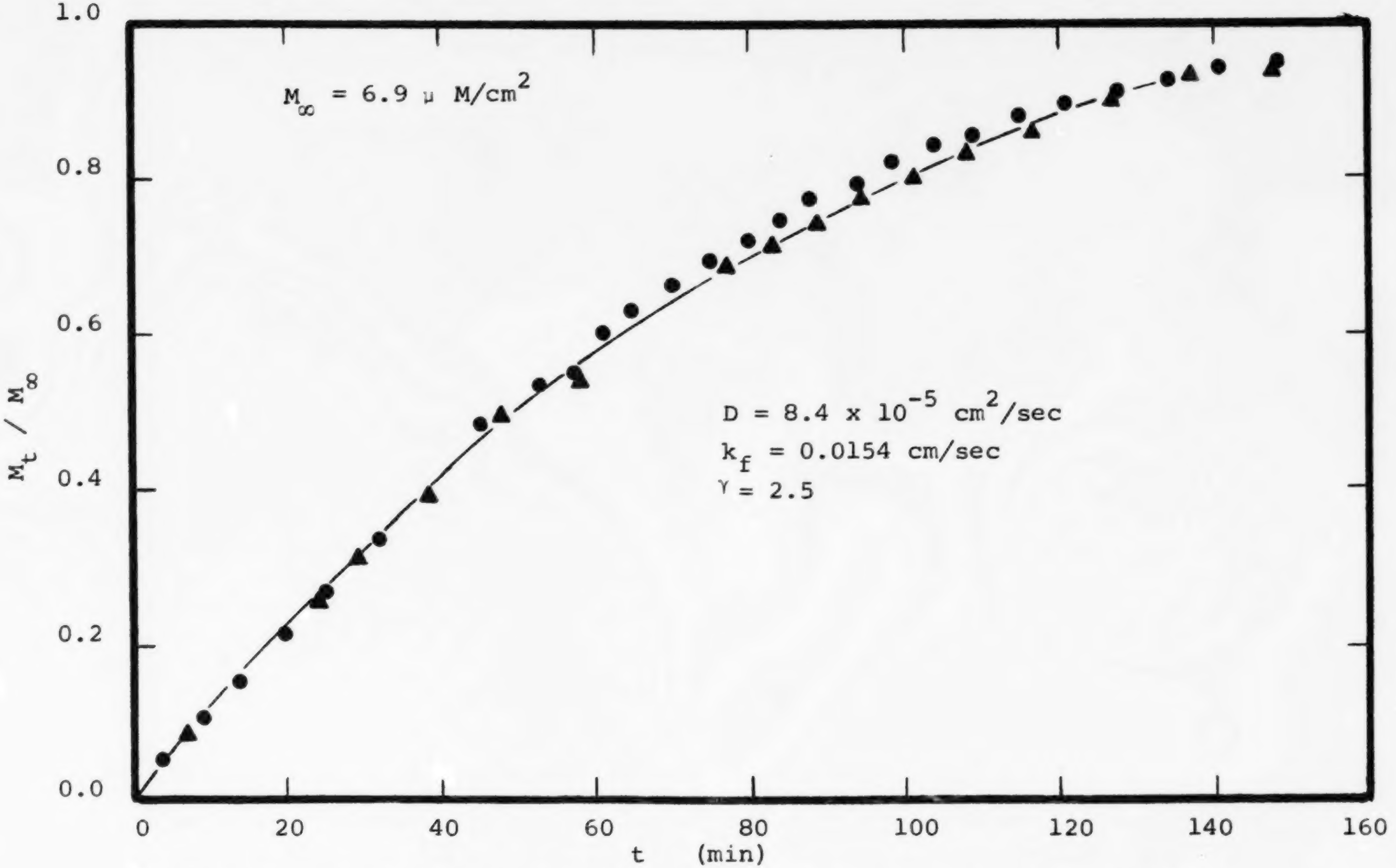

FIGURE 6-8. CALCULATED AND EXPERIMENTAL FRACTIONAL UPTAKES OF PNP (N) .
(C_{F_o} = 1.0 x 10^{-4} M , W = 0.15 gm/l, a = 0.0136 cm, 1250 rpm)

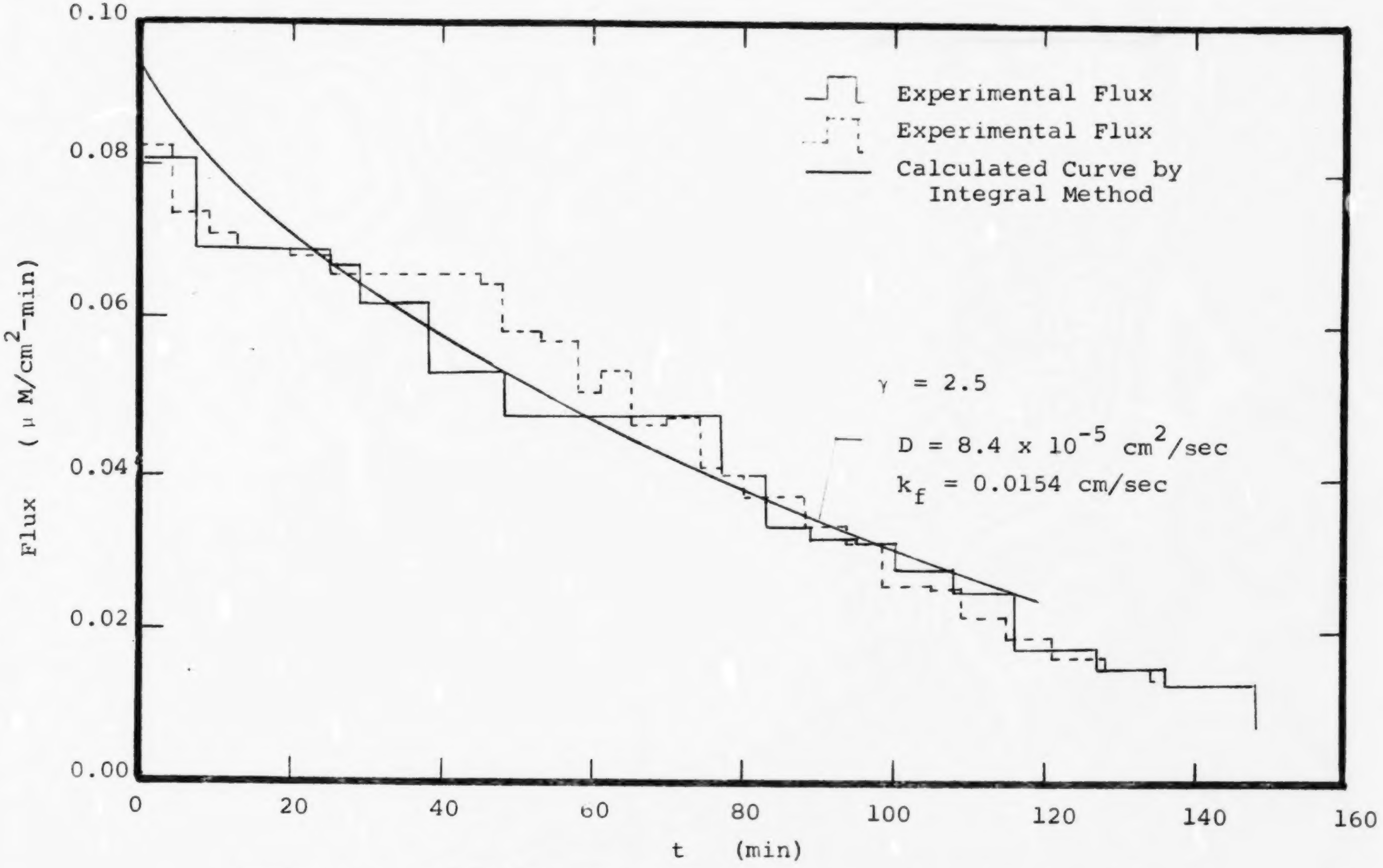

FIGURE 6-9. CALCULATED AND EXPERIMENTAL SURFACE FLUX VERSUS TIME. DATA FOR PNP (N). (C_{F_o} = 1.0 x 10^{-4} $\underline{M}$, W = 0.15 gm/l, a = 0.0136 cm, 1250 rpm)

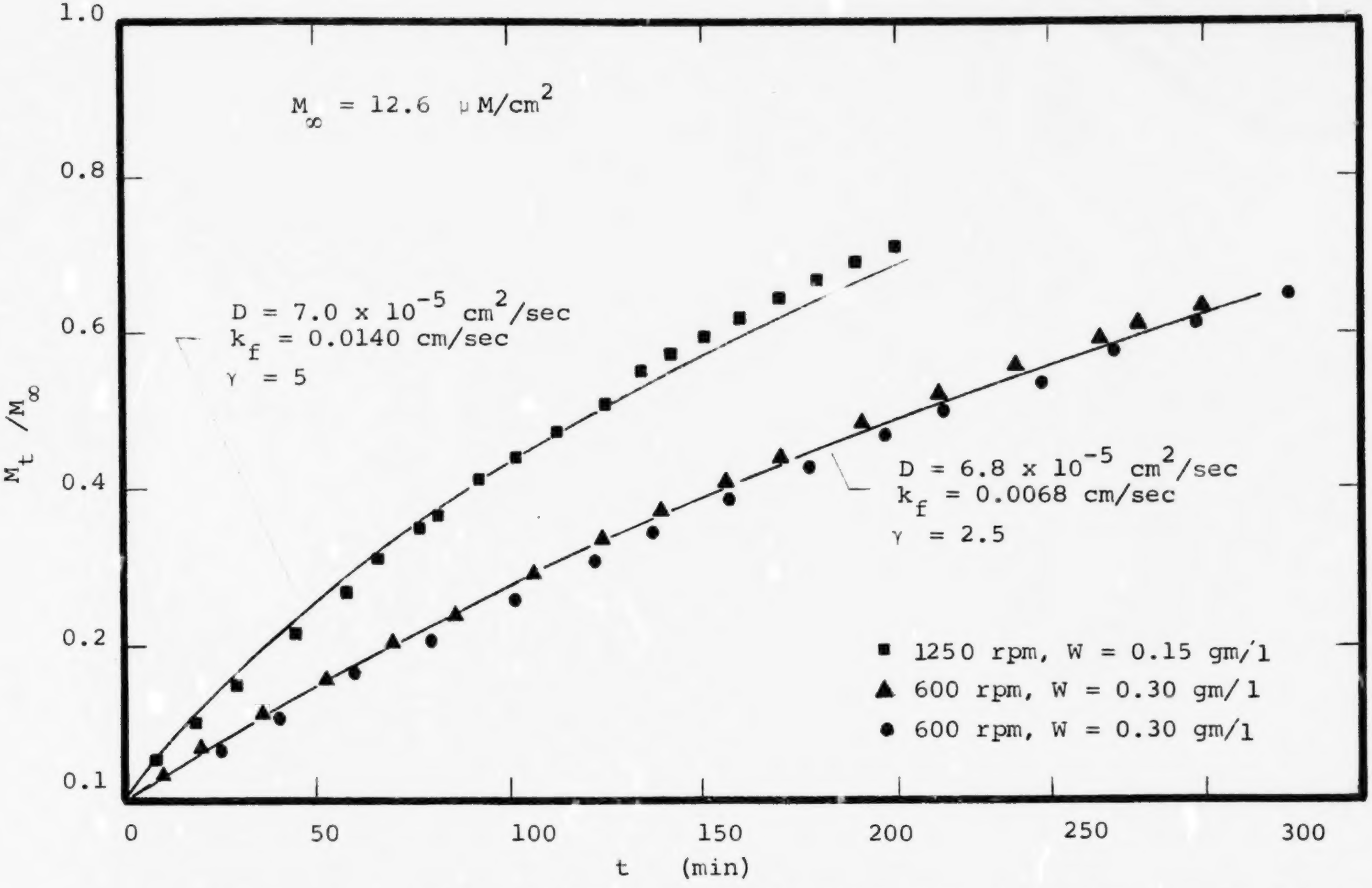

FIGURE 6-10. EFFECT OF STIRRING SPEED ON THE RATE OF UPTAKE OF PNP (N).
($C_{F_o} = 1.0 \times 10^{-4}$ M , a= 0.025 cm) .

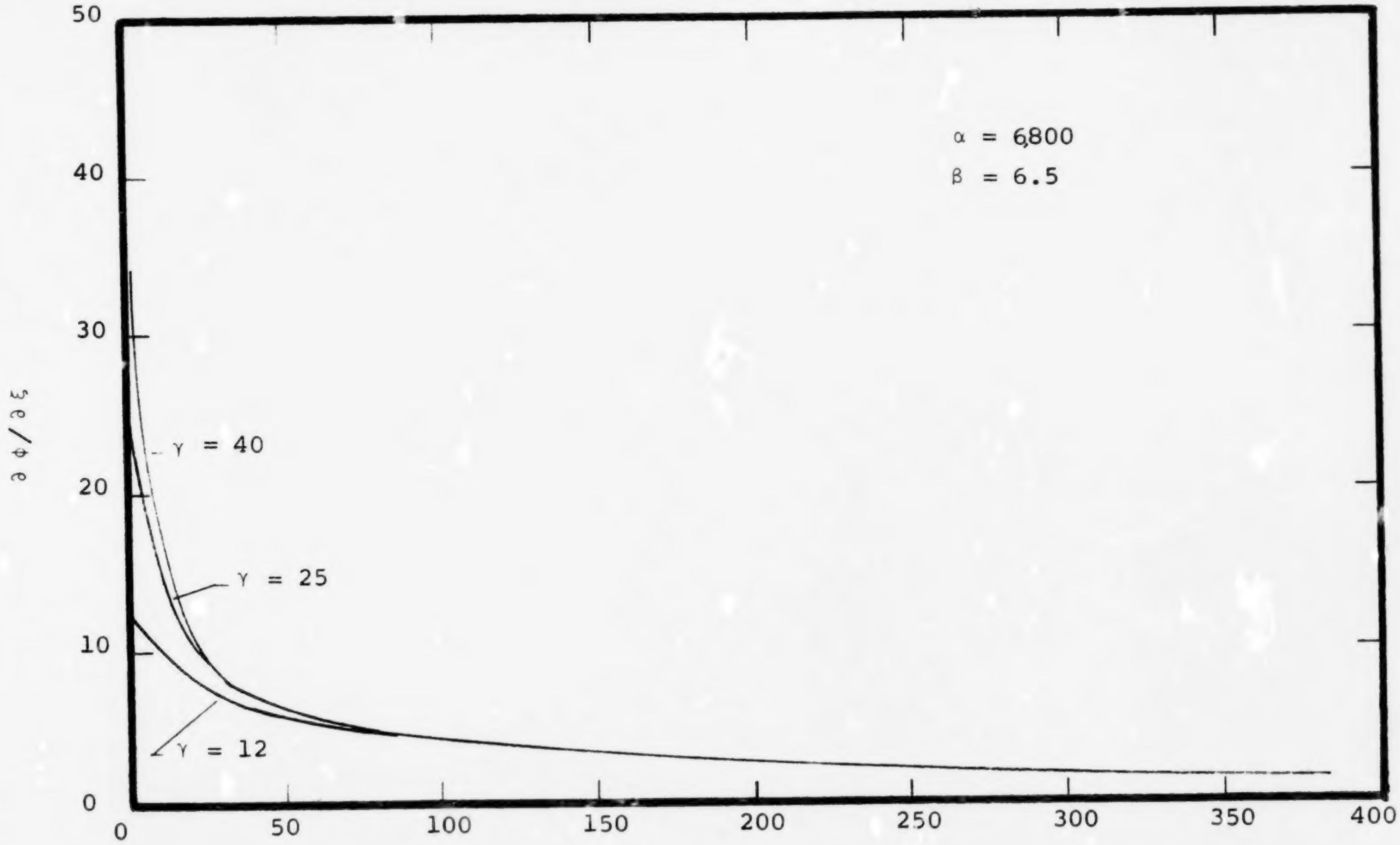

FIGURE 6-11. DIMENSIONLESS SURFACE FLUX-DIMENSIONLESS TIME PROFILES FOR PNP (A) AND γ VALUES OF 12, 35 AND 40 .

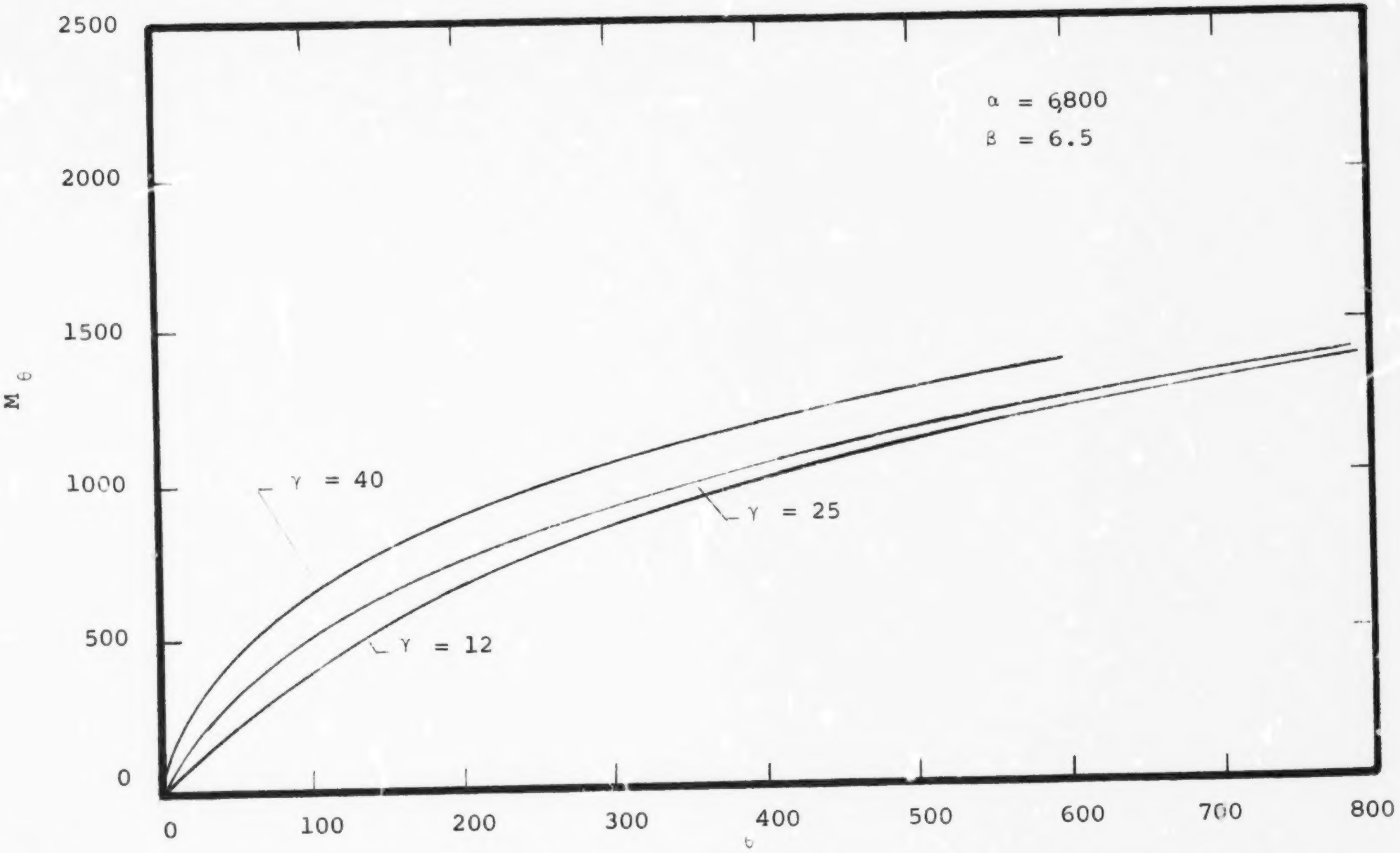

FIGURE 6-12. DIMENSIONLESS UPTAKE, M_θ, AS A FUNCTION OF DIMENSIONLESS TIME, θ, FOR PNP (A) AND γ VALUES OF 12, 25 AND 40 .

interest. Comparitive surface flux curves for PNP (N) and PNP (A) with a γ value of 25 are shown in Figure 6-13 to illustrate the effect of reducing the values of α and β. As expected, the weaker adsorption equilibrium for PNP (A) gives a faster reduction in surface flux since fluid phase concentration builds up more quickly.

The experimental surface flux - time relationship found for a stirring speed of 1250 rpm and particle radius of 0.0136 cm, is shown in Figure 6-14. Generally, experimental results were much better for the anion than for the neutral species, since spectrophotometric sensitivity was greater for the anion. Two calculated curves for γ values of 17 and 25 are also illustrated in Figure 6-14. Although both were found satisfactory by the integral method, it is apparent that a γ value of 25 provided a better fit to the initial surface flux data.

The fractional approach to equilibrium for duplicate experiments are given in Figure 6-15 along with the calculated curves which correspond to those given in Figure 6-14. Only a slight difference in the two curves is noticeable in the initial region of uptake. Diffusion coefficients were almost the same for each, but the value of k_f increased from 0.00982 to 0.0142 cm/sec when γ was increased.

The most striking result to be noted is that the diffusion coefficient calculated from the model was 0.77 $\times 10^{-5}$ cm^2/sec, or about one tenth the value found for the neutral species of PNP. Some indication was also given in Chapter 5 that surface and molecular charge may have an influence on the ability of the molecule to diffuse within carbon structure.

Another example of applying the integral method to selection of γ is shown in Figure 6-16 for a PNP (A)

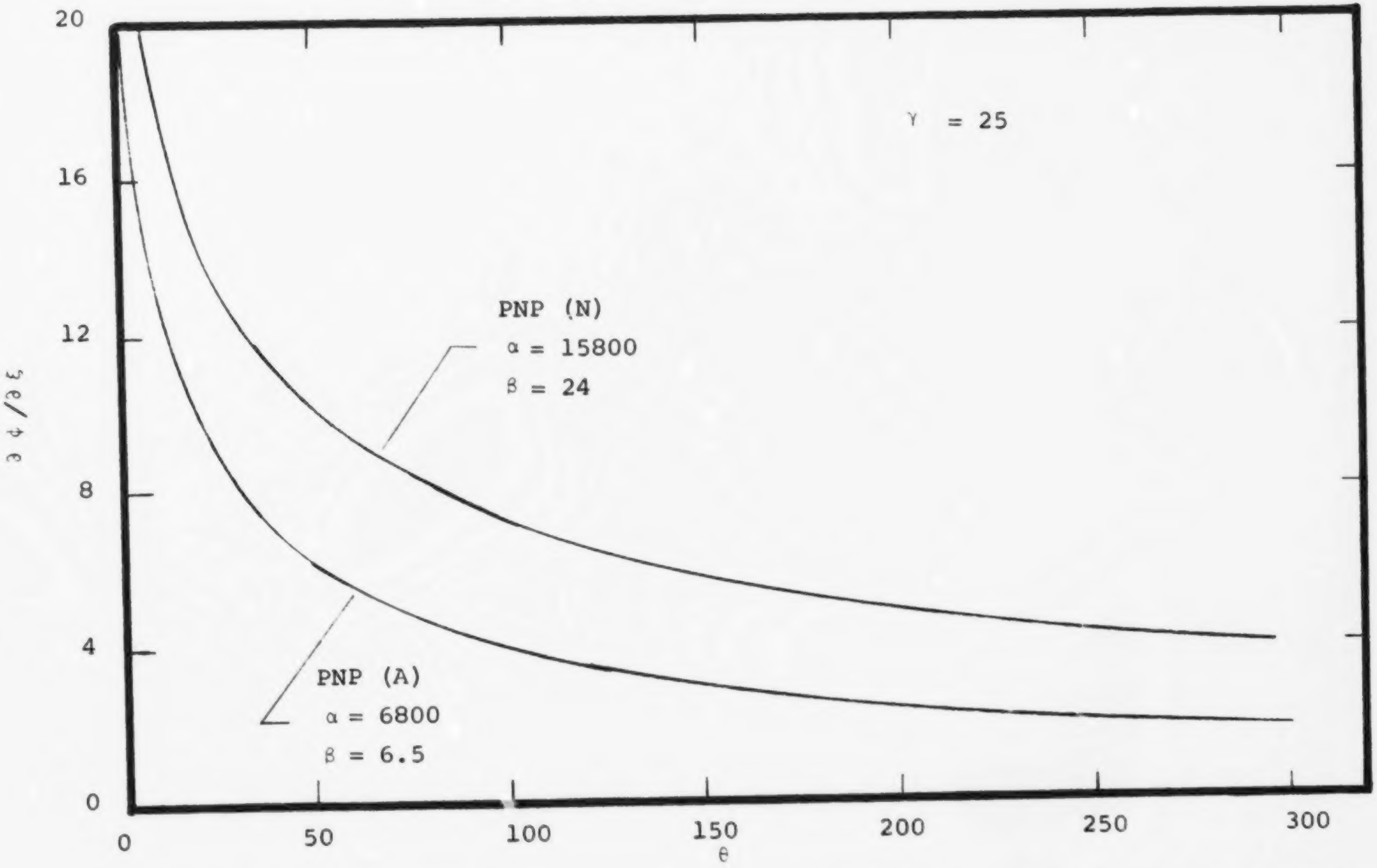

FIGURE 6-13. COMPARISON OF DIMENSIONLESS SURFACE FLUX- DIMENSIONLESS TIME PROFILES FOR PNP (N) AND PNP (A) .

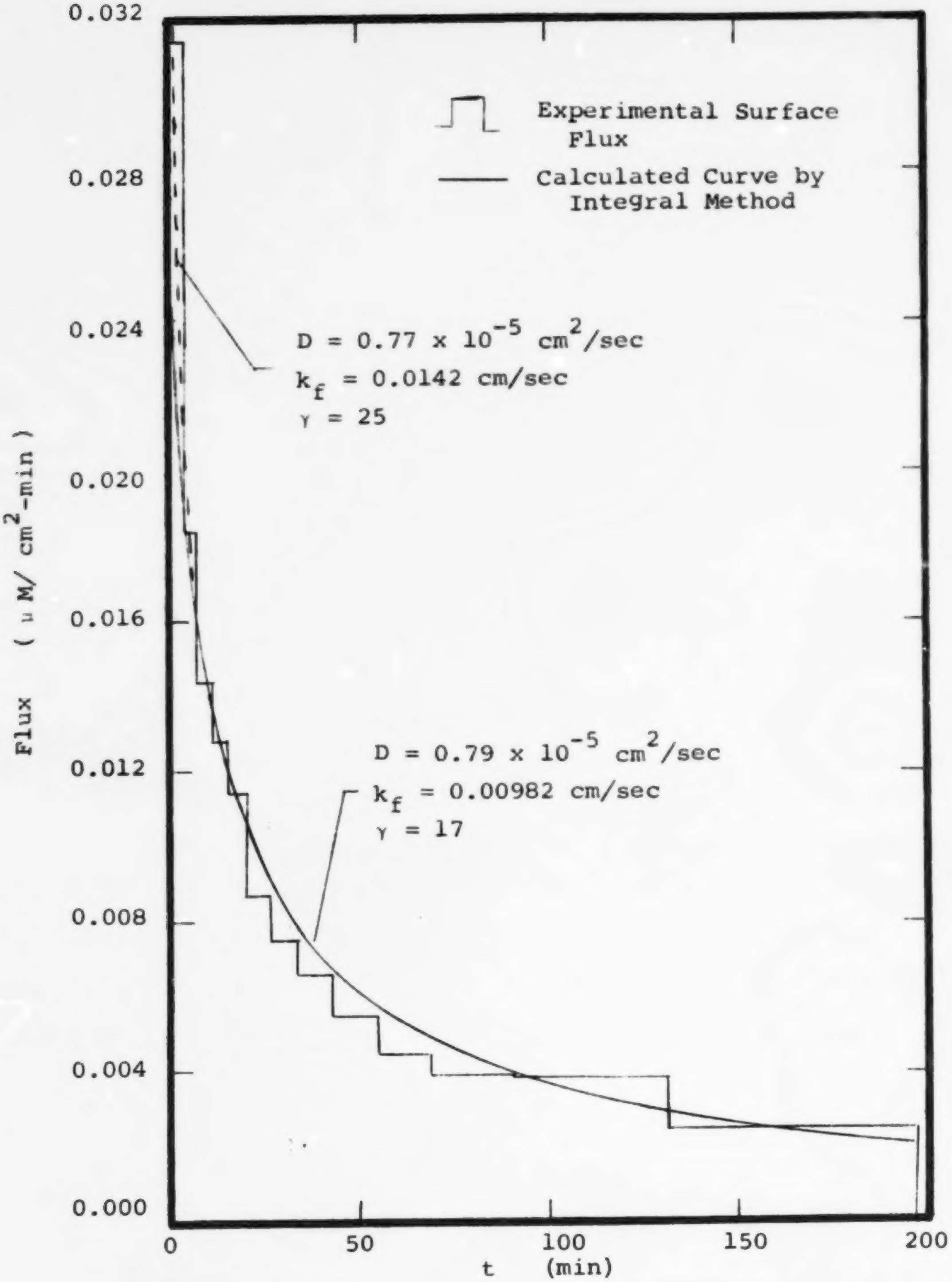

FIGURE 6- 14. CALCULATED AND EXPERIMENTAL SURFACE FLUX VERSUS TIME. DATA FOR PNP (A). (C_{F_o} = 0.5 x 10^{-4} $\underline{M}$, W = 0.25 gm/l, a = 0.0136 cm, 1250 rpm)

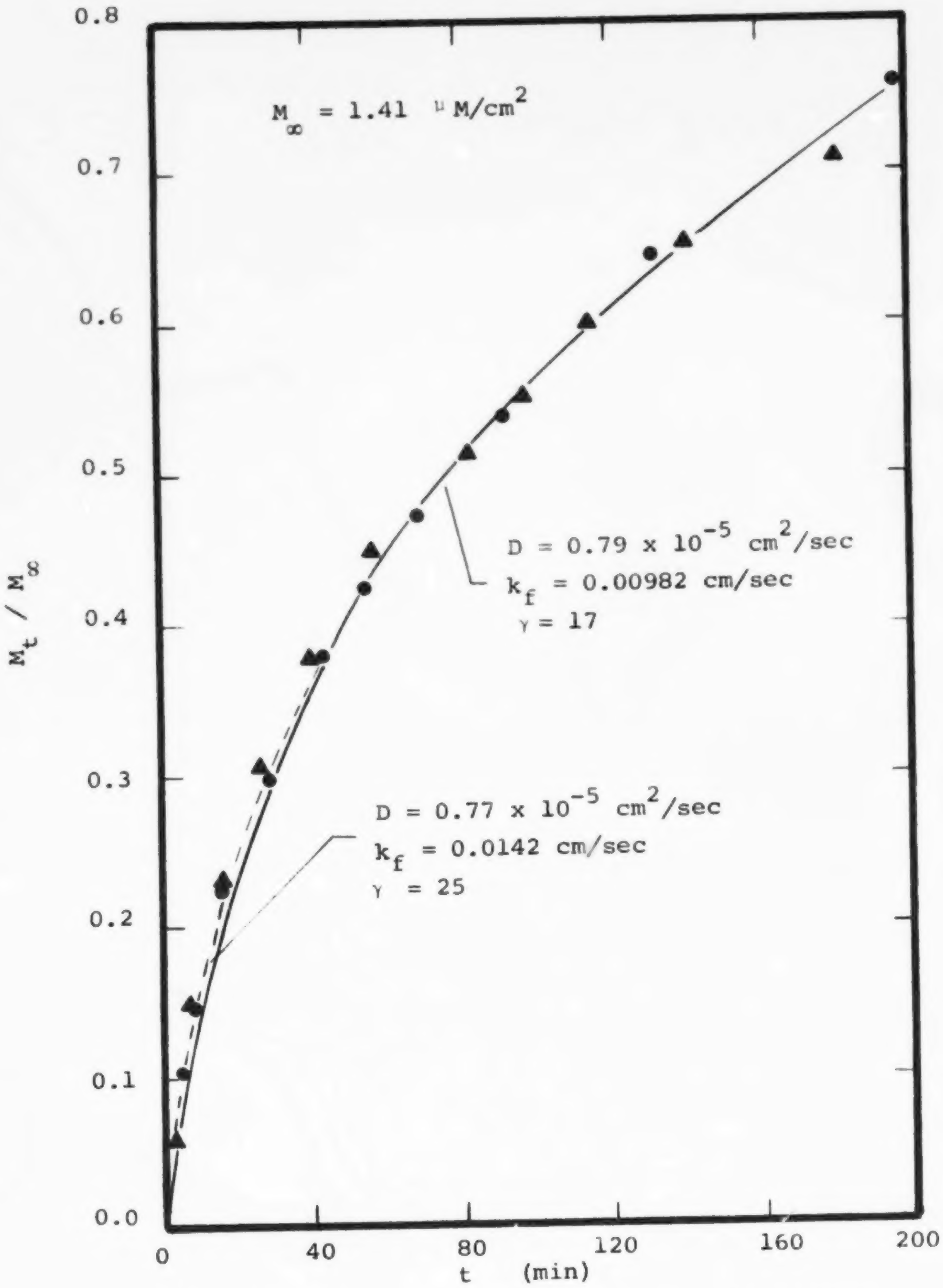

FIGURE 6-15. CALCULATED AND EXPERIMENTAL FRACTIONAL UPTAKES OF PNP (A). COMPARISON OF $\gamma = 17$ AND $\gamma = 25$.

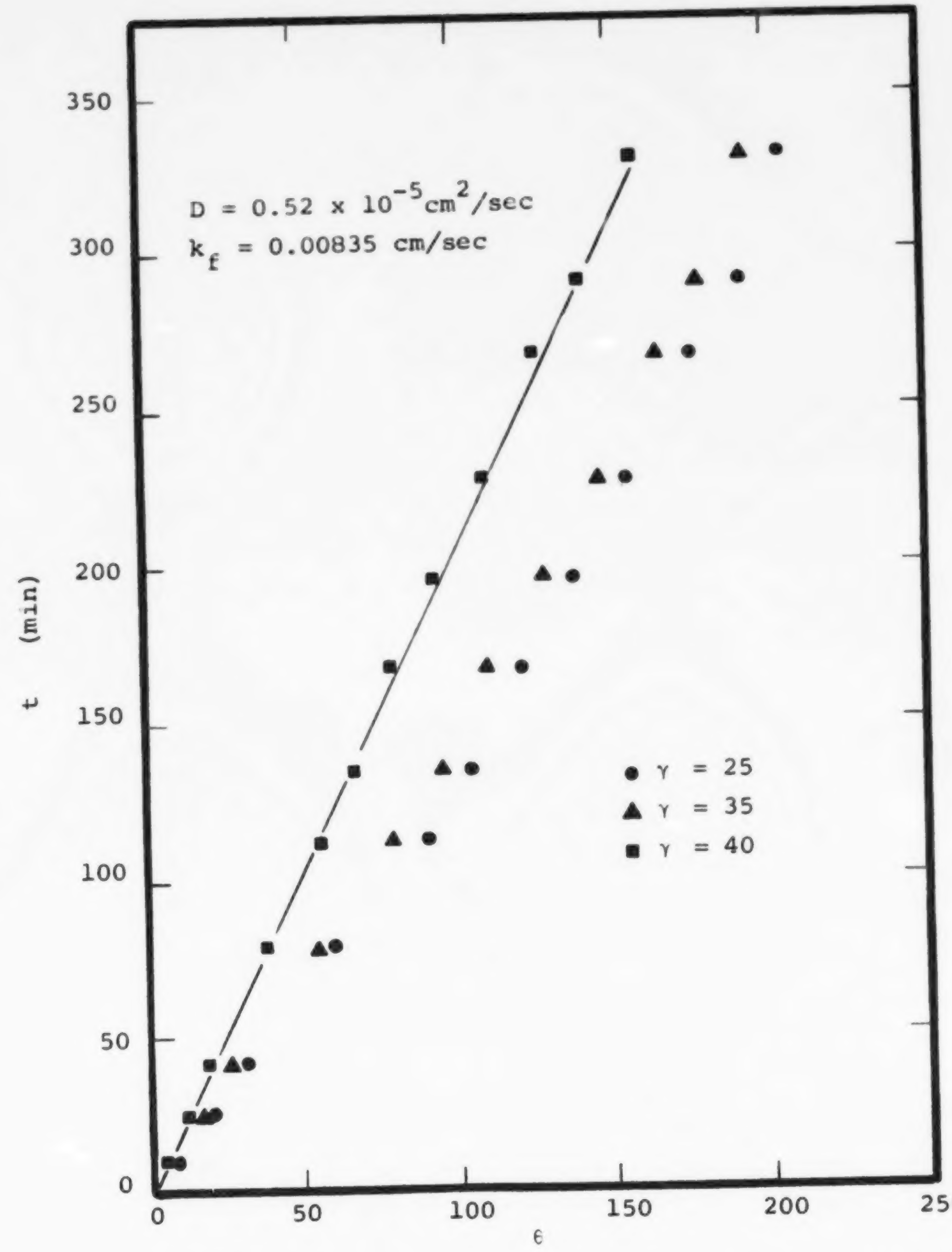

FIGURE 6-16. SELECTION OF γ . DATA FOR PNP (A) .
(C_{F_o} = 0.5 x 10^{-4} $\underline{M}$, W = 0.25 gm/ℓ, a = 0.025 cm, 1250 rpm)

experiment using a particle of radius 0.025 cm. As seen, values of 25 and 35 produced concave functions, while a value of 40 gave a linear function.

The effect of film diffusion on the fractional approach to equilibrium is illustrated in Figure 6-17. As shown from Figure 6-16, a value of 40 was used to obtain the calculated curve for experiments with a stirring speed of 1250 rpm, which gave D and k_f values of 0.520×10^{-5} cm^2/sec and 0.00835 cm/sec respectively. In contrast, the calculated curve for the experiment at 600 rpm produced D and k_f values of 0.47×10^{-5} cm^2/sec and 0.00467 cm/sec respectively. Experimental surface flux, together with the corresponding calculated curve from above are given in Figure 6-18 and show good agreement.

Somewhat lower values of transfer coefficient were calculated for the anion than for the neutral species of PNP. This may in part be in support of evidence given in Chapter 5 for the simple film model as applied to PNP, in which k_f was smaller for the anion than for the neutral species. However, it is also more difficult to establish an accurate estimate of the transfer coefficient in anion experiments since the diffusion coefficient has been reduced by an order of magnitude. This has shifted the controlling rate mechanism towards pore diffusion and thus k_f has less effect on the rate of uptake, as was shown in Figure 6-15.

EXPERIMENTAL RESULTS - DNP (N)

Numerical solutions for surface flux and dimensionless uptake as a function of θ are shown in Figure 6-19 and 6-20 respectively. The γ values of 4, 8, and 12 are within the range of interest for this series of experiments. A bath concentration of 1×10^{-4} M produced α and β

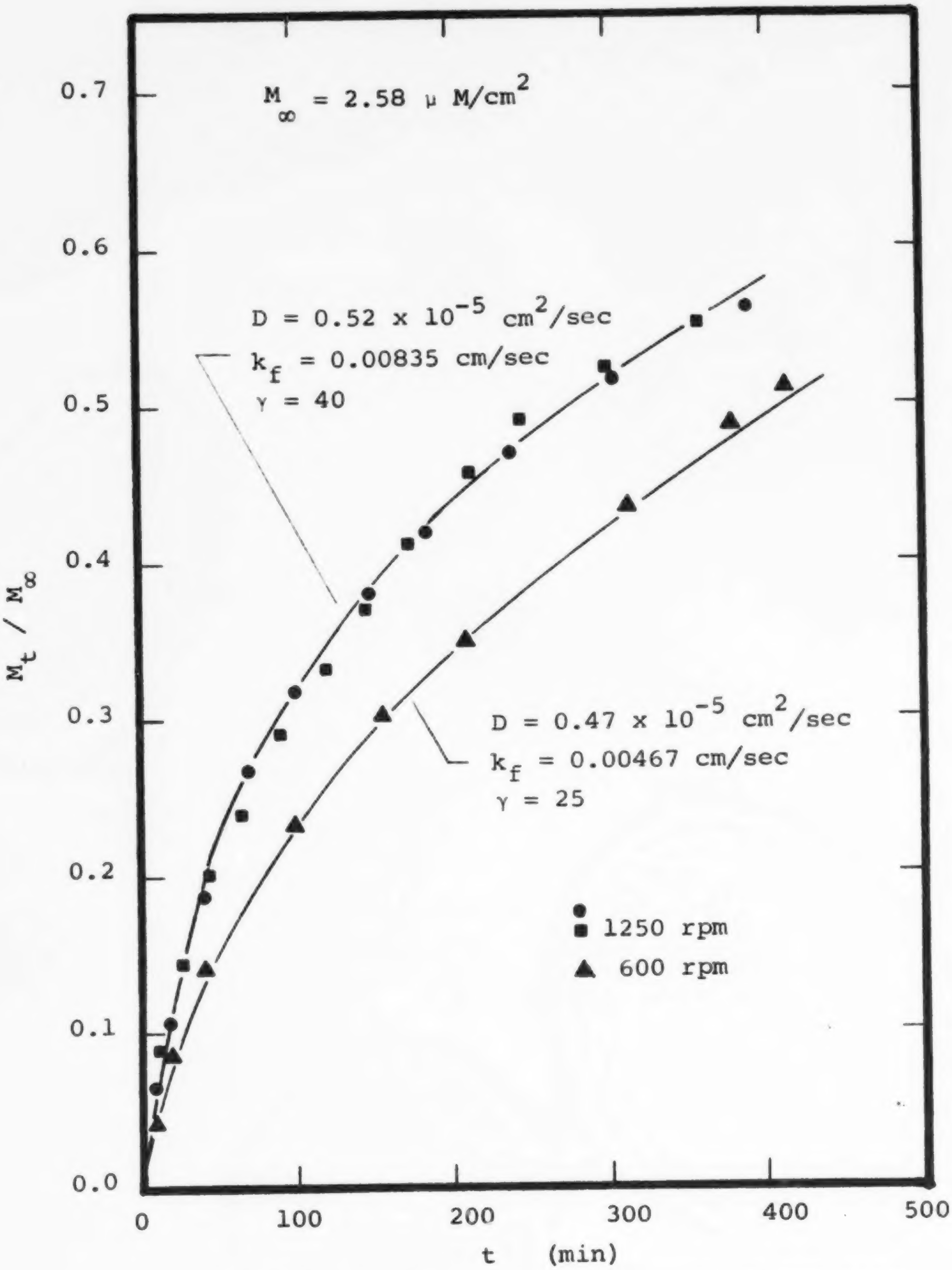

FIGURE 6-17. EFFECT OF STIRRING SPEED ON THE RATE OF UPTAKE OF PNP (A). ($C_{F_0} = 0.5 \times 10^{-4}$ M, W = 0.25 gm/l, a = 0.025 cm, 1250 rpm)

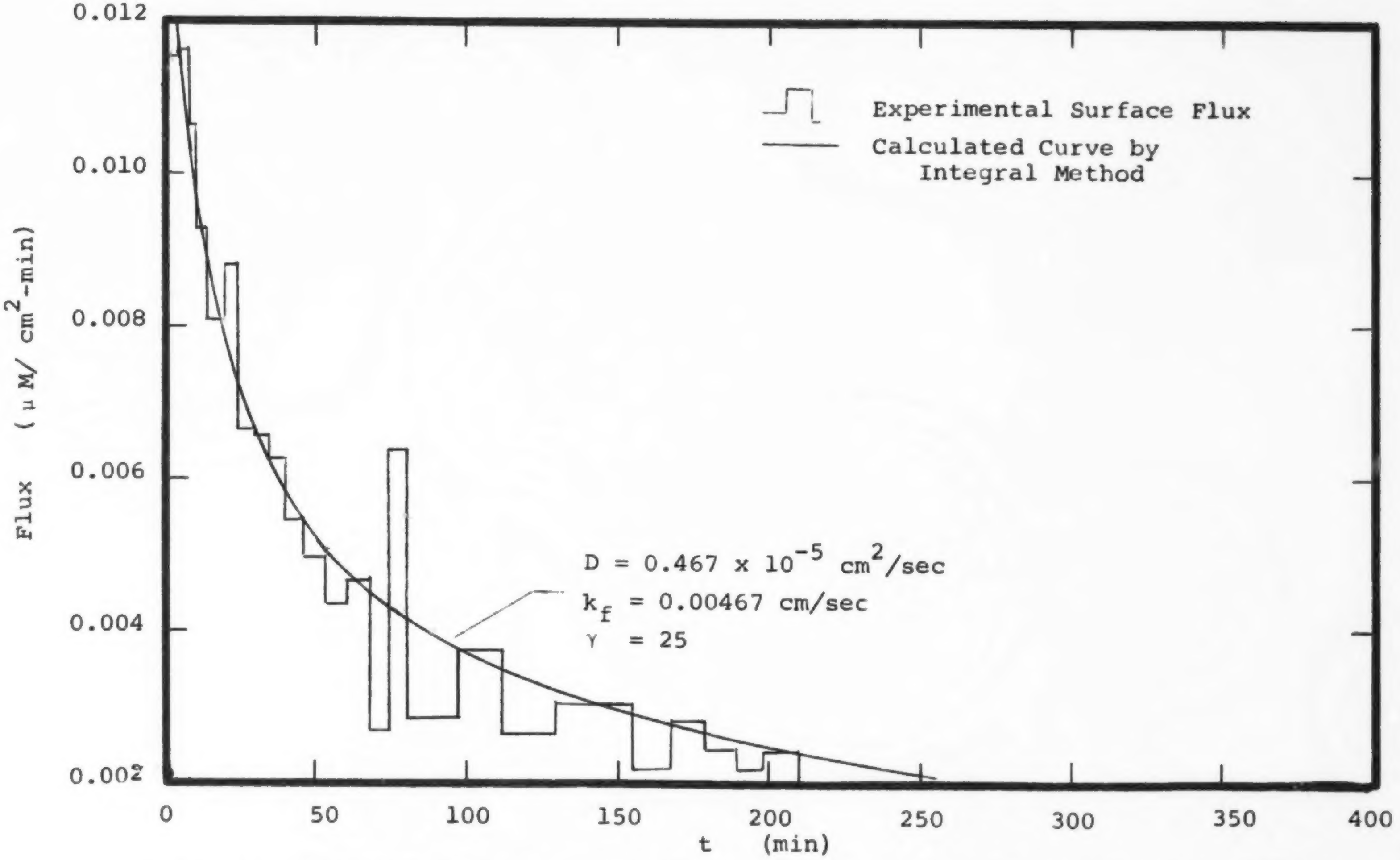

FIGURE 6-18. CALCULATED AND EXPERIMENTAL SURFACE FLUX VERSUS TIME. DATA FOR PNP (A) ($C_{F_O} = 0.5 \times 10^{-4}$ M , W = 0.25 gm/1, a = 0.025 cm, 600 rpm)

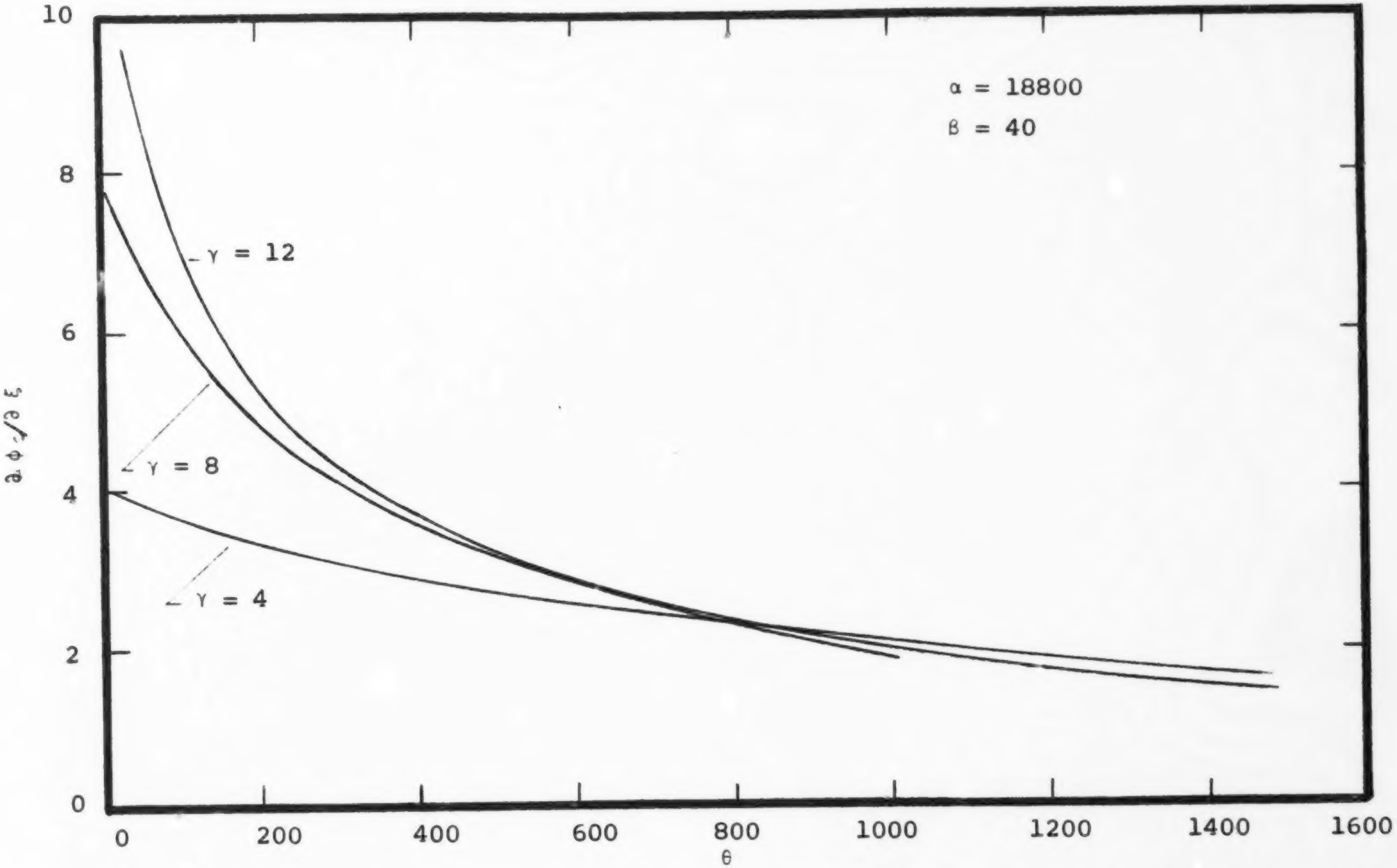

FIGURE 6-19. DIMENSIONLESS SURFACE FLUX - DIMENSIONLESS TIME PROFILES FOR DNP (N) AND γ VALUES OF 4, 8 AND 12 .

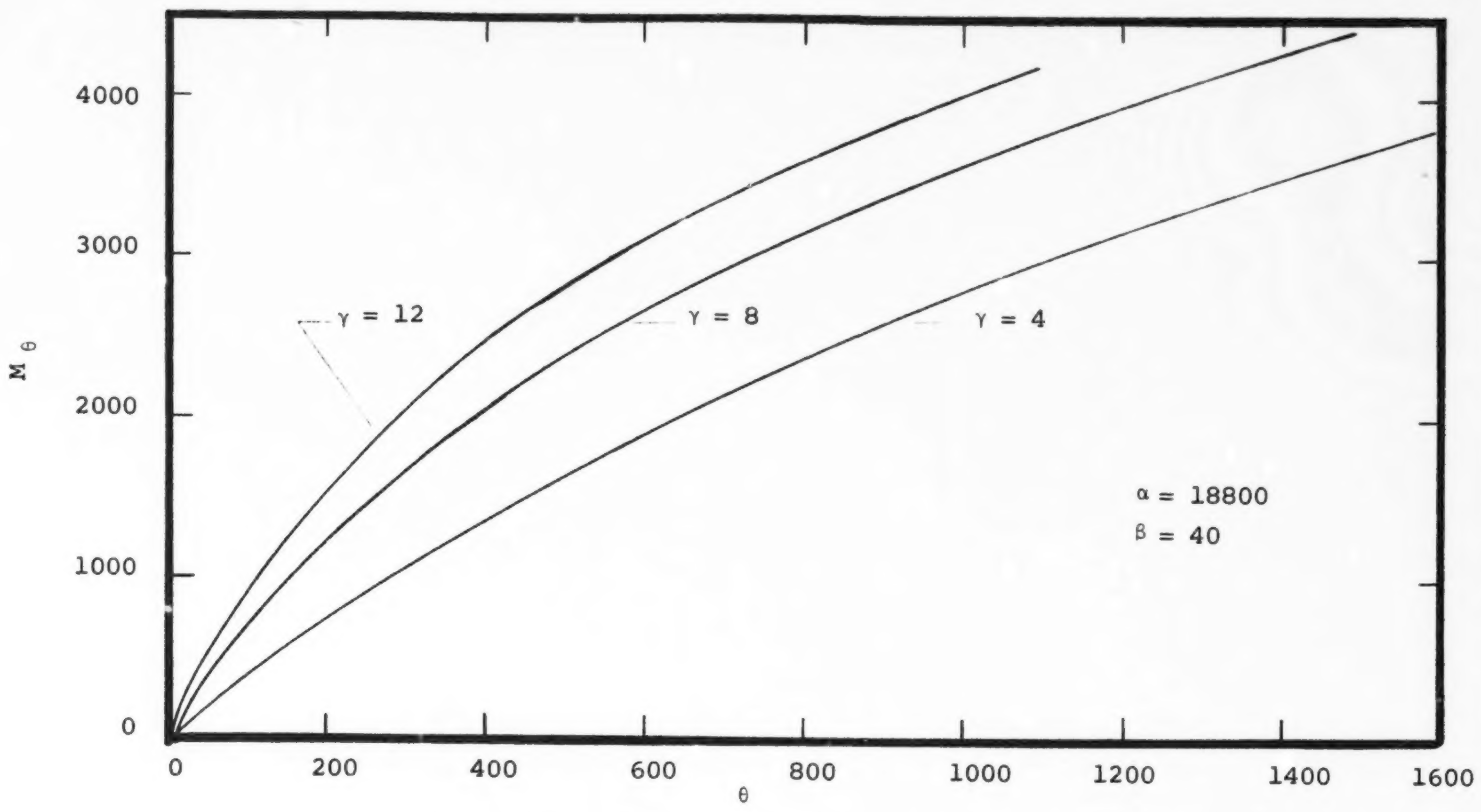

FIGURE 6-20. DIMENSIONLESS UPTAKE, M_θ, AS A FUNCTION OF DIMENSIONLESS TIME, θ, FOR DNP (N) AND γ VALUES OF 4, 8 AND 12 .

values of 18,800 and 40 respectively.

Fractional approaches to equilibrium for duplicate experiments, are illustrated in Figure 6-21. The calculated D value of 4.5×10^{-5} cm^2/sec is about one third smaller than that generally found for PNP (N). According to the Wilke-Chang formulation for free-liquid diffusivities (44), values of 1.10×10^{-5} and 0.90×10^{-5} cm^2/sec were calculated for PNP and DNP respectively. Thus, there appears to be a much stronger dependence on molal volume than predicted by free-liquid diffusivity calculations. It may also be noted that similar values of D and k_f were obtained for DNP (N) in a finite-bath experiment presented in Figure 5-27.

A decrease in stirring speed resulted in a retarded rate of uptake of DNP (N) as illustrated in Figure 6-22. It can also be seen that a stirring speed of 1250 rpm and particle radius of 0.025 cm, gave D and k_f values of 3.64×10^{-5} cm^2/sec and 0.0116 cm/sec respectively which agreed quite well with those found for the smaller particle radius of 0.0136 cm. As shown the duplicate experiments at 600 rpm were in good agreement and produced consistent values of D and k_f when fitted to the model. Thus, a reduction in stirring speed from 1250 to 600 rpm decreased k_f from 0.0116 cm/sec to 0.0071 cm/sec.

EXPERIMENTAL RESULTS - DNP (A)

Lastly, the infinite-bath technique was applied to the study of DNP (A) adsorption rates in order to further examine the effect of phosphate buffer and to compare experimental results with those from finite-bath studies. As in the PNP (A) studies, a bath concentration of 0.5×10^{-4} M and carbon dosage of 0.250 gm/l were used. The resulting values of α and β for the phosphate buffered system were 18,400 and

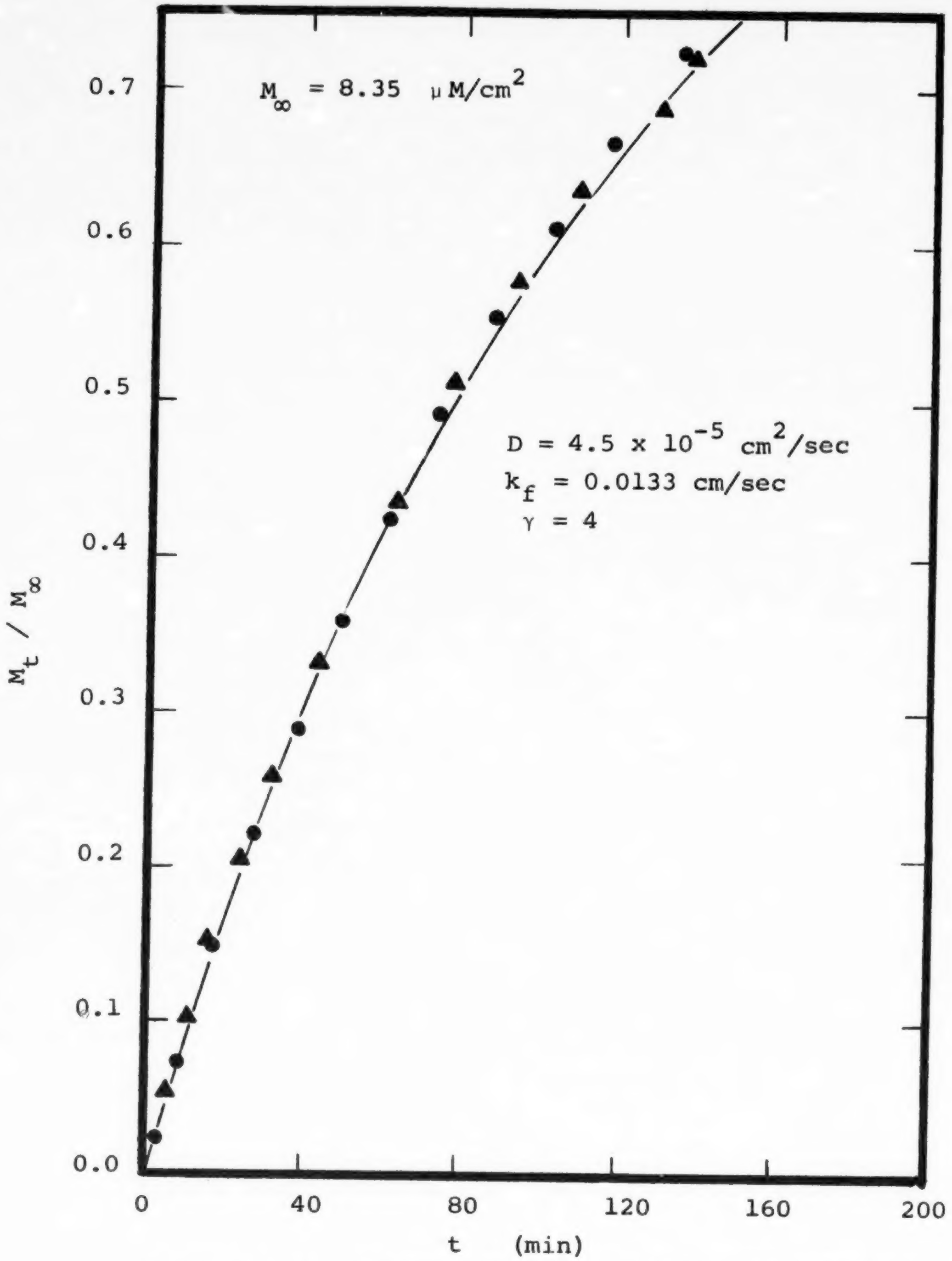

FIGURE 6-21. CALCULATED AND EXPERIMENTAL FRACTIONAL UPTAKES OF DNP (N). (C_{F_O} = 1.0 x 10^{-4} M, W = 0.06 gm/l, a = 0.0136 cm, 1250 rpm)

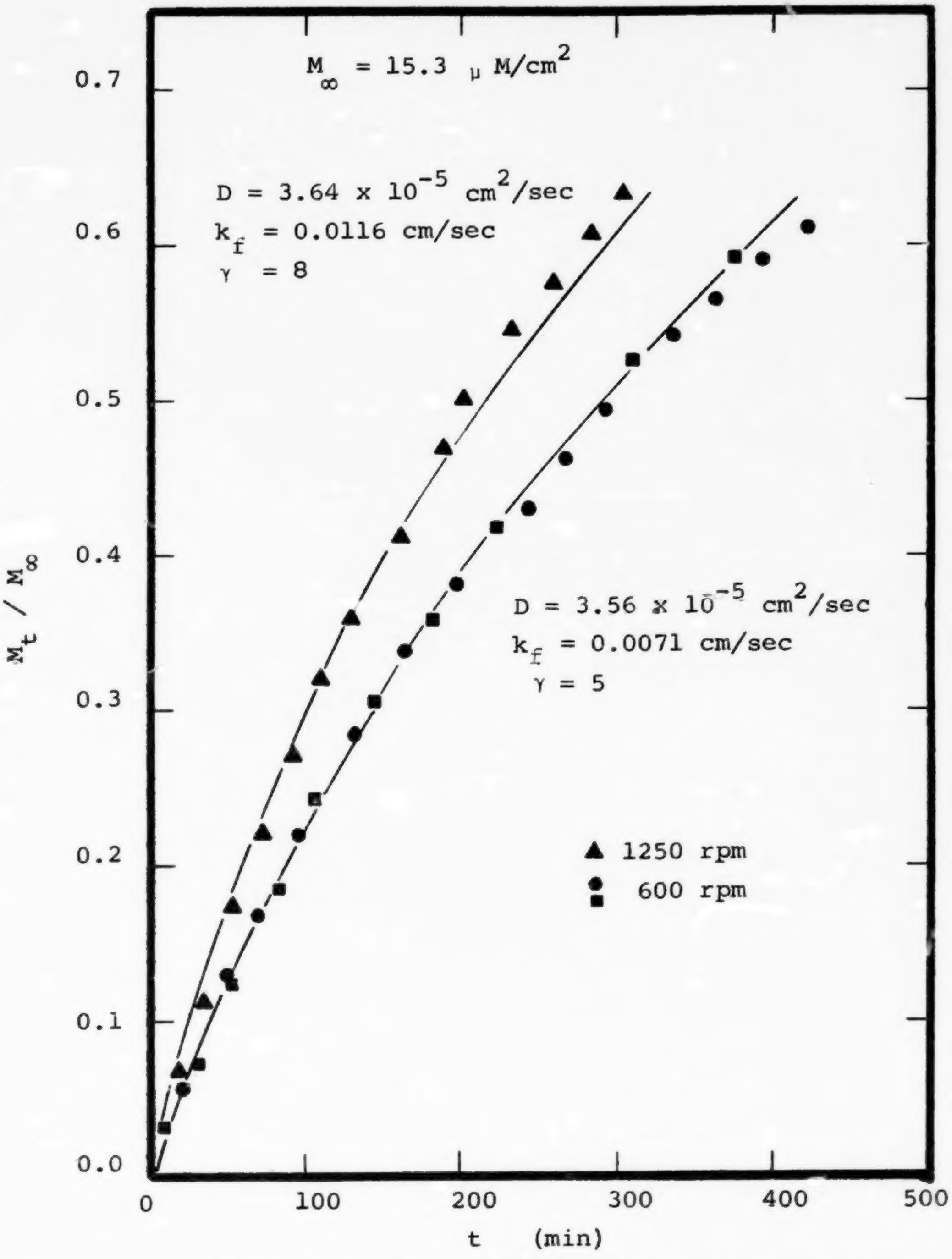

FIGURE 6-22. EFFECT OF STIRRING SPEED ON THE RATE OF UPTAKE OF DNP (N). ($C_{F_0} = 1.0 \times 10^{-4}$ $\underline{M}$, W = 0.15 gm/l, a = 0.025 cm)

12.5 respectively, while those calculated for the unbuffered system were 9,600 and 15 respectively.

In Figure 6-23, experimental uptake, in $\mu M/cm^2$ has been plotted versus time for the 10^{-2} M phosphate buffered and unbuffered systems. These two experiments were carried out at pH 7.2 with a stirring speed of 1250 rpm and particle radius of 0.0136 cm. Superimposed on the experimental data are the calculated curves obtained by applying the infinite-bath model with the appropriate α and β input values. As seen, the uptake rate of the buffered system is expectedly greater since the adsorption capacity has almost doubled. The D value of 1.10×10^{-5} cm^2/sec obtained in the buffered system was somewhat larger than that of 0.79×10^{-5} cm^2/sec obtained in the unbuffered system. However, this should not be construed as evidence that molecular diffusion is enhanced by the presence of the buffer system. Since the optimum value of γ was found to be 25 in both systems, transfer coefficients, k_f, were correspondingly different, having values of 0.0202 and 0.0145 cm/sec in the buffered and unbuffered systems respectively. Finite-bath studies of DNP (A), with no buffer added, produced diffusion coefficients of about 0.5×10^{-5} cm^2/sec, which were lower than that of 0.79×10^{-5} cm^2/sec obtained in this study. However, the latter value is closer to the free-liquid diffusivity of 0.9×10^{-5} cm^2/sec.

Comparison of diffusion coefficients calculated for the neutral and anion species of DNP reveals a marked decrease (from 4.50×10^{-5} cm^2/sec to 0.79×10^{-5} cm^2/sec) and supports postulations concerning charge effects previously noted.

SUMMARY OF INFINITE-BATH KINETICS

Values of D and k_f experimentally found by applying the non-linear film and pore diffusion model, with an infinite-

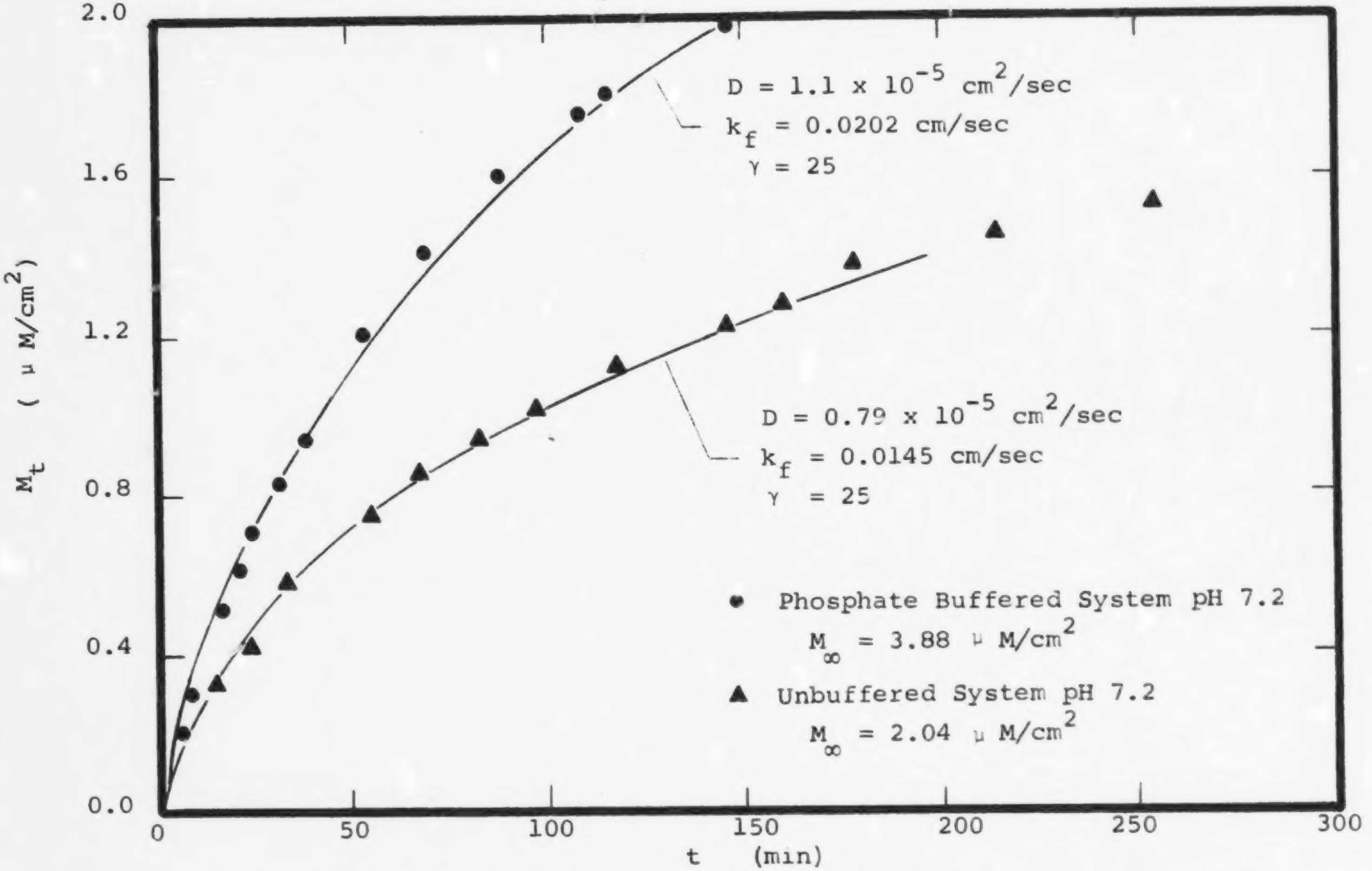

FIGURE 6-23. CALCULATED AND EXPERIMENTAL UPTAKES OF DNP (A), BUFFERED AND UNBUFFERED SYSTEMS. (C_{F_o} = 0.5 x 10^{-4} $\underline{M}$, W = 0.25 gm/1, a = 0.0136 cm, 1250 rpm)

bath boundary condition, are shown in Table 6-1 for each sorbate.

In most experiments, the data conformed quite closely to the model. Decreases in particle size and stirring speed gave corresponding decreases in γ . This is expected, since k_f is independent of particle size; and decreasing stirring speed should decrease k_f. The model also seemed to support the results of finite-bath kinetic experiments with DNP (N) and DNP (A).

Perhaps the most noteworthy finding was the approximate ten-fold decrease in diffusion coefficient observed in comparing PNP (N) with PNP (A). Although less marked, there was also a considerable decrease in D comparing DNP (N) with DNP (A). This difference, as pointed out in Chapter 5, has a pronounced effect on the nature of the rate limiting mechanism. In this regard, it may be recalled, that γ is actually the ratio of film to pore diffusion parameters. As shown in Figure 6-3, for example, the smaller the value of γ, the greater the influence of film diffusion on the overall transfer process. Perusal of Table 6-1 illustrates that γ values obtained for the neutral species were five to ten times smaller than those for the anion species.

Furthermore, free-liquid diffusivities for PNP and DNP were found to be 1.00 and 0.90 x 10^{-5} cm^2/sec respectively. Experimental diffusion coefficients for the neutral species were five to seven times larger, while the anions exhibited values somewhat lower than the free-liquid values. These discrepancies could be due to many factors. For example, variations of carbon surface charge with pH could influence the aqueous system constant which is applied in the Wilke-Chang equation. Moreover, anions do not exist in the same resonance bath boundary condition, are shown in Table 6-1 for each sorbate.

In most experiments, the data conformed quite closely to the model. Decreases in particle size and stirring speed gave corresponding decreases in γ . This is expected, since k_f is independent of particle size; and decreasing stirring speed should decrease k_f. The model also seemed to support the results of finite-bath kinetic experiments with DNP (N) and DNP (A).

Perhaps the most noteworthy finding was the approximate ten-fold decrease in diffusion coefficient observed in comparing PNP (N) with PNP (A). Although less marked, there was also a considerable decrease in D comparing DNP (N) with DNP (A). This difference, as pointed out in Chapter 5, has a pronounced effect on the nature of the rate limiting mechanism. In this regard, it may be recalled, that γ is actually the ratio of film to pore diffusion parameters. As shown in Figure 6-3, for example, the smaller the value of γ, the greater the influence of film diffusion on the overall transfer process. Perusal of Table 6-1 illustrates that γ values obtained for the neutral species were five to ten times smaller than those for the anion species.

Furthermore, free-liquid diffusivities for PNP and DNP were found to be 1.00 and 0.90 x 10^{-5} cm^2/sec respectively. Experimental diffusion coefficients for the neutral species were five to seven times larger, while the anions exhibited values somewhat lower than the free-liquid values. These discrepancies could be due to many factors. For example, variations of carbon surface charge with pH could influence the aqueous system constant which is applied in the Wilke-Chang equation. Moreover, anions do not exist in the same resonance

TABLE 6-1

RESULTS OF INFINITE-BATH INVESTIGATIONS

Sorbate	a cm	W gm/ 1	γ	D $\times 10^5$ cm^2/sec	$^{**}k_f$ $\times 10^3$ cm/sec	Stirring Speed rpm
PNP (N)	0.0250	0.15	5	7.0	14.0	1250
" "	0.0250	0.30	5	5.9	11.7	1250
" "	0.0250	0.30	2.5	6.8	6.8	600
" "	0.0136	0.15	2.5	8.4	15.4	1250
PNP (A)	0.0136	0.25	25	0.77	14.2	1250
" "	0.0250	0.25	40	0.52	8.35	1250
" "	0.0250	0.25	25	0.47	4.67	600
DNP (N)	0.0136	0.06	4	4.50	13.2	1250
" "	0.0250	0.15	8	3.64	11.6	1250
" "	0.0250	0.15	5	3.56	7.1	600
DNP (A)	0.0136	0.25	25	0.79	14.5	1250
" "	*0.0136	0.25	25	1.10	20.2	1250

*10^{-2} M Phosphate Buffer System

**See Appendix C for correlation of transfer coefficient, k_f, with hydrodynamics, fluid properties and free-liquid diffusivities.

forms as the neutral species; thus variations in molecular charge distribution and bond energies could effect molal volume.

Finally, the addition of 10^{-2} $\underline{M}$ phosphate buffer has been shown to greatly increase uptake rates, which was expected from the observed increase in adsorption capacity. As shown in Table 6-1, the diffusion coefficient in this system was slightly larger than that obtained in the absence of the buffer. Although uptake rates were quite reproducible, it would be premature to postulate any effect of system additives on intraparticle diffusion until further evidence is provided.

Thus, the infinite-bath method of studying adsorption kinetics has been shown to give reproducible results and to be amenable to mathematical analysis when non-linear adsorption and film diffusion must be considered. Obviously, certain refinements of the experimental apparatus, such as the use of a hydrogen lamp, could permit adsorption rate studies for any organic compound which absorbs sufficient light energy.

Although the model for film and pore diffusion, with simultaneous non-linear adsorption, requires a numerical methods solution, the technique is rather straightforward. As in Chapter 5, the assumptions of irreversible immobilization and quasi-steady state may also be used to simplify mathematical solution. Basically, it is only necessary to replace solution concentration, C_{F_1}, by a constant, C_{F_O}, in Equation 5-18 and equate the surface fluxes given by Equations 5-18 and 5-8 to obtain internal film concentration, C_{F_i}, as a function of frontal position, r_o, as shown in Equation 6-28.

$$C_{F_i} = \frac{\gamma\, C_{F_o}\,(a - r_o)}{\gamma\,(a - r_o) + r_o} \qquad (6\text{-}28)$$

Surface flux may then be related to flux at the frontal boundary, given by Equation 5-4, which then yields

$$\frac{a\,D}{r_o\,(a - r_o)} \left[\frac{\gamma\, C_{F_o}\,(a - r_o)}{\gamma\,(a - r_o) + r_o} \right] = S\,\frac{dr_o}{dt} \qquad (6\text{-}29)$$

After rearrangement and integration, dimensionless time, T, as a function of (r_o/a) is given by

$$T = \frac{1}{2}\left[\left(\frac{r_o}{a}\right)^2 - 1 \right] + \frac{1}{3}\left[\frac{1-\gamma}{\gamma} \right] \left[\left(\frac{r_o}{a}\right)^3 - 1 \right] \qquad (6\text{-}30)$$

Surface flux may be expressed in terms of frontal position by substituting Equation 6-28 into the surface boundary condition to yield

$$N_o = \frac{k_f C_{F_o}}{1 - \gamma + \dfrac{\gamma}{\left(\frac{r_o}{a}\right)}} \qquad (6\text{-}31)$$

Thus, at t equals zero, (r_o/a) equals one and

$$N_o = k_f C_{F_o} \qquad (6\text{-}32)$$

Surface flux-dimensionless time profiles may be calculated for values of γ by using Equations 6-30 and 6-31 together. Plotting T versus experimental time, t, for values of N_o would then determine the validity of the model, since a linear function should result. Of course, the limitations of the irreversible immobilization assumption would, as in Chapter 5, have to be investigated.

CHAPTER 7

CONCLUSIONS AND FURTHER RESEARCH

A principal conclusion deriving from this research is that pore diffusion does not automatically become the rate limiting step for mass transport in the adsorption of organic molecules from solution by porous active carbon in rapidly agitated batch reactors. If this assumption is made *a priori*, the interpretation of experimental results may, for such systems, be misleading. A more logical approach is to consider film diffusion in series with pore diffusion. It has been shown in the present work that such a model may be applied with minor additional mathematical complications. For sorbate systems which are not controlled even in part by film diffusion, the model merely reduces to that for the pore diffusion case. On the other hand, when film diffusion is significant, the importance of each transport mechanism can be ascertained. In addition, calculation of a meaningful value for the pore diffusion coefficient in the two-resistance case requires that the film diffusion step be accounted for in the model.

The two most significant mathematical limitations in studying batch reactor kinetics are: 1) the boundary condition imposed by a finite-bath system; and, 2) the non-linearity of most adsorption equilibria, including those for all of the sorbates investigated in the present study.

A simplified model was developed for the finite-bath boundary condition, in which the conditions of transient diffusion and non-linear adsorption were approximated by the assumptions of quasi-steady state and irreversible immobilization respectively. A surface boundary condition of film diffusion in series with pore diffusion was also included. This model was found adequate for the stronger adsorbers, including: the sulfonated alkylbenzenes, 2,4-dinitro-o-cyclohexylphenol (DNOCHP), 2,4-dinitro-o-sec-butylphenol (DNOSBP) and 2,4-dinitrophenol (DNP).

The success of the model in fitting the experimental data was shown to strongly depend on the initial and final equilibrium concentrations selected for a rate study, since these two system parameters defined the model limitations. Moreover, it was necessary to follow adsorption rates almost to equilibrium to insure model conformity. Thus, using smaller sorbent particles shortened the required experimental observation time.

Identification and characterization of the rate controlling process was of more interest in the present work than was evaluation of diffusion coefficients. A straightforward mathematical inspection of the model which evolved showed that film diffusion is much more significant for adsorption of smaller sorbates such as DNP than for larger, more bulky sorbates such as the sulfonated alkylbenzenes.

Molecular charge was also shown to influence the controlling mass transport mechanism. Investigations of the neutral species of DNP revealed a ten-fold increase in pore diffusivity over that of the anion. This actually meant that pore resistance had decreased, effectively shifting the rate control toward film diffusion. Moreover, the pore diffusivity calculated for the anionic species of DNP was about one half the free-liquid value while the diffusion coefficient for the neutral species was about four times larger than the free-liquid value.

A simple film diffusion model indicated the importance of film transport for initial rates of adsorption of the weaker adsorbers; i.e., the neutral species of phenol, p-nitrophenol (PNP). The assumption of irreversible immobilization was found inadequate for phenol and PNP and it was noted that the weakest adsorbers, corresponding to the smallest molecules, showed the strongest dependence on film transport.

Replacement of the decreasing solution concentration boundary condition by one of constant concentration greatly simplified mathematical description of a combined film and pore diffusion model and allowed consideration of non-linear isotherms. Reproducible experimental results were obtained for the uptake rates of PNP and DNP, neutral and anionic species, using the laboratory built infinite-bath device. Postulations concerning the relative importance of film and pore diffusion were further delineated. The model parameter, λ, representing the ratio of film to pore resistance, illustrated the shift toward film diffusion controlling when the neutral molecules were investigated.

No conclusions could be reached regarding the equilibrium behavior of adsorption systems containing a 10^{-2} $\underline{M}$ phosphate buffer or 10^{-2} $\underline{M}$ $NaHCO_3$ because the evidence indicated both pH and ionic strength to be interacting factors. Although adsorption rate studies revealed a somewhat larger pore diffusivity for DNP (A) in a system containing a 10^{-2} $\underline{M}$ phosphate buffer, no interpretation of phosphate buffer effects on pore transport could be ascertained. However, rate studies consistently confirmed an increase in the adsorption capacity upon addition of the buffer.

FURTHER RESEARCH

Keinath and Weber (22), in investigations of expanded-bed operation of an activated carbon adsorber, have indicated that film diffusion almost entirely controls the effluent concentration profile for DNOSBP; however, for larger sorbate molecules, the results of batch reactor studies in this research suggest that pore diffusion will be more rate controlling. If this postulation can be extended to a flow-through system then pore diffusivity, for larger sorbates, will be a critical input to the model used to describe adsorber performance. Moreover, in the practical application of the adsorption process, large protein, carbohydrate and lipid molecules in addition to complex organic pesticides, e.g., DDT, Dieldrin and Parathion, will be encountered in wastewaters. Future investigations, therefore, of fixed- or expanded-bed operation should focus on the removal of the above classes of sorbates. Batch reactor studies, as described in this research, compliment flow-through system studies by supplying the value of pore diffusivity needed in models, such as discussed in Chapter 2, for predicting effluent concentration profiles.

As indicated at the end of Chapter 6, the assumptions of irreversible immobilization and quasi-steady state can be used to simplify adsorption kinetics in an infinite-bath system as well as a finite-bath system. Thus, future investigations of relatively strong adsorbers, could be readily accomplished by this means. Pore diffusion coefficients could thus be obtained for a spectrum of sorbates found in wastewaters. Hopefully, pore diffusivities, calculated in this manner, could be empirically related to free-liquid diffusivities such that batch studies may be ultimately unnecessary.

An area of research which unexpectedly became of interest in this study was that concerning the effect of inorganic additives in sorbate-sorbent systems. For example, the phosphate and carbonate buffer systems were shown to markedly increase the adsorption capacities of DNP and DNOSBP. Furthermore, in response to the higher adsorption capacity, rate studies in which a phosphate buffer system was added, showed an increased rate of adsorption as did studies in which a comparable ionic strength of NaCl was added. Therefore, further research should be directed towards characterizing the effects of pH and ionic strength on equilibrium adsorption of various sorbates. Following this, rate studies could delineate the effect of inorganic additives on the mobility of the diffusing sorbate molecule.

One of the ultimate objectives of batch studies, as discussed in Chapter 1, is to examine the nature of competitive adsorption. Before formulating a kinetic model, a thorough investigation of competitive adsorption equilibria must be undertaken. Weber and Morris (39) have already examined some simple two component systems. Once mathematical description of competitive adsorption equilibria has been established, the kinetic models used in this study may be expanded to include simultaneous transport of sorbates. Observed differences in competitive kinetic behavior may then be interpreted in terms of "hindered" diffusion or merely competitive surface adsorption.

A competitive adsorption study could also be directed towards uncharged sorbates, which exhibit rates of adsorption in non-competitive systems that are controlled by film diffusion for a considerable time. Application of the simple film model given in Chapter 5 should yield information concerning the influence of competitive adsorption. That is, the value of the transfer coefficient should remain the same in a competitive system; however, the time, t^*, of applicability of the simple film model should be reduced because of the more rapid "build up" of fluid-phase concentration on the inside of the film as a result of competitive adsorption.

Kinetic modeling may also be extended to measurements of total organic carbon (TOC) uptake in a heterogeneous system. Adsorption equilibria, expressed in terms of TOC could be used in conjunction with a kinetic model from which approximate, or overall average, transfer coefficients may be obtained. These results could then be directly applied to continuous flow transport models as discussed in Chapter 2.

Finally, mathematical formulations, presented in this study, can obviously be applied to mass transport in similar systems of interest. In particular, sorbents such as activated alumina and fly ash (28) may have potential for waste treatment and could be evaluated in this manner.

APPENDIX A

IMPLICIT FINITE DIFFERENCE SOLUTION TO TRANSIENT DIFFUSION WITH NON-LINEAR ADSORPTION

Given Equation 3-3

$$D\left[\frac{\partial^2 C_F}{\partial r^2} + \frac{2}{r}\frac{\partial C_F}{\partial r}\right] = \frac{\partial}{\partial t}(\varepsilon C_F + (1-\varepsilon)\, C_S) \qquad \text{(A-1)}$$

Let

$$\xi = \frac{r}{a}, \quad \theta = \frac{Dt}{a^2}, \quad \phi = \frac{C_F}{C_{F_o}}, \quad \alpha = Q\cdot\frac{\rho}{C_{F_o}}, \quad \beta = b\, C_{F_o}$$

and $\sigma = \dfrac{\alpha\beta\phi}{1+\beta\phi}$

The dimensionless form[1] of Equation A-1 is then

$$\frac{\partial^2 \phi}{\partial \xi^2} + \frac{2}{\xi}\frac{\partial \phi}{\partial \xi} = \frac{\partial}{\partial \theta}(\varepsilon\,\phi + \sigma) \qquad \text{(A-2)}$$

The finite difference equation for the second derivative at the m^{th} distance step or shell is

$$\left.\frac{\partial^2 \phi}{\partial \xi^2}\right|_m = \frac{\phi_{m+1} - 2\,\phi_m + \phi_{m-1}}{(\Delta\xi)^2} \qquad \text{(A-3)}$$

where $(\Delta\xi)$ is the distance step.

The finite difference equations for the first derivative with respect to ξ and θ at the m^{th} step are

$$\left.\frac{\partial \phi}{\partial \xi}\right|_m = \frac{\phi_{m+1} - \phi_{m-1}}{2(\Delta\xi)} \qquad \text{(A-4)}$$

---

[1] The term σ includes $(1-\varepsilon)$ since α, which is used to obtain σ in Equation 5-30, is calculated on the basis of $(1-\varepsilon)\rho_{solid}$ (see page 63)

$$\left.\frac{\partial \phi}{\partial \theta}\right|_m = \frac{\varepsilon \phi'_m - \varepsilon \phi_m}{\Delta \theta} \qquad \text{(A-5)}$$

$$\left.\frac{\partial \sigma}{\partial \theta}\right|_m = \frac{\sigma'_m - \sigma_m}{\Delta \theta} \qquad \text{(A-6)}$$

where ϕ'_m is the new value after a time step of $\Delta \theta$.

The value of ξ at the m^{th} step is $m(\Delta \xi)$

Therefore, Equation A-2 becomes

$$\frac{\phi_{m+1} - 2\phi_m + \phi_{m-1}}{(\Delta \xi)^2} + \frac{\phi_{m+1} + \phi_{m-1}}{m(\Delta \xi)(\Delta \xi)} =$$

$$\frac{\varepsilon \phi'_m - \varepsilon \phi_m}{\Delta \theta} + \frac{\sigma'_m - \sigma_m}{\Delta \theta} \qquad \text{(A-7)}$$

or,

$$\varepsilon \phi'_m = \frac{\Delta \theta}{m(\Delta \xi)^2} \left[(m+1)\, \phi_{m+1} - 2m\phi_m + (m-1)\, \phi_{m-1} \right]$$

$$+ \varepsilon \phi_m + \sigma_m + \sigma'_m \qquad \text{(A-8)}$$

The boundary conditon at $r = a$, $t \geq 0$ is

$$V(C_{F_o} - C_F) = 4\pi \int_o^a (\varepsilon C_F + (1-\varepsilon) C_S) r^2 dr \qquad \text{(A-9)}$$

or, in dimensionless form at $\xi = 1$, $\theta \geq 0$

$$\phi = 1 - \frac{4\pi a^3}{V} \int_o^1 (\varepsilon \phi + \sigma)\, \xi^2\, d\xi \qquad \text{(A-10)}$$

$$= 1 - V_p \int_o^1 (\varepsilon \phi + \sigma)\, \xi^2\, d\xi \qquad \text{(A-11)}$$

The integral in Equation A-11 is given by Simpson's Rule to be

$$\frac{1}{3}(\Delta \xi)^3 \Big[m^2(\varepsilon \phi'_m + \sigma'_m) + 4\,(m-1)^2\,(\varepsilon\phi'_{m+1} + \sigma'_{m-1}) + 2(m-2)^2\,(\varepsilon\phi'_{m-2} + \sigma'_{m-2}) + \cdots + 4(\varepsilon\phi'_1 + \sigma'_1)\Big] \qquad \text{(A-12)}$$

Computational Procedure

1) Input

ARR = V_p

A = α

B = β

P = Number of distance steps m

DELT = $\Delta \theta$

L = Distance Step Counter

2) Set all values of ϕ_m, ϕ'_m, σ_m and σ'_m to zero

C(J) = ϕ_m

CC(J) = temporary location of ϕ'_m

CNEW(J) = ϕ'_m

S(J) = σ_m

SNEW(J) = σ'_m

3) Calculate new value of ϕ'_m at first distance step according to Equation A-8.

Note: values of ϕ_{m+1}, ϕ_m, and ϕ_{m-1} are given as time step average values in the program.

4) Compare new value of ϕ'_m given by CC(J) with current value given by CNEW(J).

5) If tolerance is not met in step 4), switch counter called INDEX to one.

6) Calculate Corresponding value of σ'_m

7) Repeat procedure for the number of distance steps to be calculated as set by counter called L.

8) Calculate new solution concentration $\phi_{\xi=1}$ using Equation A-12.

9) Compare new value of $\phi_{\xi=1}$ with current value.

10) If tolerance is not met in step 9) switch INDEX to one.

11) If all tolerances have been met in steps 5) and 10), replace current values of ϕ_m and σ_m with current values of ϕ'_m and σ'_m, project new values of ϕ'_m and σ'_m, increment $\Delta\theta$ and repeat entire procedure.

12) If all tolerances have not been met in steps 5) and 10), reset INDEX to zero and recalculate the concentration profile starting with step 3).

COMPUTER PROGRAM

IMPLICIT FINITE DIFFERENCE SOLUTION TO TRANSIENT DIFFUSION WITH NON-LINEAR ADSORPTION

```
      DIMENSION C(50),S(50),CNEW(50),CC(50),CTEMP(50),STEMP(50),
     1 SNEW(50)
      REAL NEXT,NEXT1,NEXT2,NEXT3
       NAMELIST /INPUT/ ARR,A,B,P,DELT,TEND,L,SUB,SUB1,SUB2,SUB3,
     1  NEXT,NEXT1,NEXT2,NEXT3,KOUNT,KANG,PROF,ERR,EPS
    1 READ(5,INPUT)
      WRITE (6,INPUT)
      KO=0
      KP=P
      DELR=1./P
      IP=KP+1
      LL=L-2
      DO 50 J=LL,IP
      CC(J)=0
      C(J)=0
      CNEW(J)=0
      S(J)=0
   50 SNEW(J)=0
      I=0
   70 INDEX=0
      M=P
   60 FM=M-1
      COEF=DELT/(2.*FM*DELR**2)
      TERM=(FM-1.)*(C(M-1)+CNEW(M-1))
      TERMS=(FM+1.)*(C(M+1)+CNEW(M+1))-2.*FM*(C(M)+CNEW(M))+TERM
      IF (SNEW(M)-CNEW(M))  41,42,42
   41 CONTINUE
       CC(M)=( EPS*C(M) +COEF*TERMS-(SNEW(M)-S(M)))/EPS
      CC(M)=ABS(CC(M))
      IF (ABS(CC(M)-CNEW(M)).GT.ERR*CNEW(M))     INDEX=1
      CNEW(M)=CC(M)
      SNEW(M)=A*B*CNEW(M)/(1.+B*CNEW(M))
      GO TO 43
   42 CONTINUE
      SS=S(M)+COEF*TERMS-(CNEW(M)-C(M))*EPS
      CC(M)=ABS(SS/(A*B-SS*B))
       IF (CC(M) .LE. 1.E-10)  CC(M)=0.
      SNEW(M)=ABS(SS)
      IF(ABS(CC(M)-CNEW(M)).GT.ERR*CNEW(M))  INDEX=1
      CNEW(M)=CC(M)
   43 M=M-1
       IF (M .GE. L) GO TO 60
      I=KP
      SUM2=0
      SUM1=0
   31 SUM1=SUM1 + (I-1)**2*(EPS*CNEW(I) +SNEW(I))
      SUM2 = SUM2 + (I-2)**2*(EPS*CNEW(I-1) + SNEW(I-1))
       IF ( I-L) 33,33,32
   32 I=I-2
```

COMPUTER PROGRAM (CONTINUED)

```
      GO TO 31
   33 CONTINUE
      PROD1=4.*SUM1
      PROD2=2.*SUM2
      COE=DELP**3/3.
      GRAL=COE*(P*P*(EPS*CNEW(IP) + SNEW(IP)) + PROD1 +PROD2)
      CC(IP)=ABS(1.-GRAL*ARR)
      IF (ABS(CC(IP)-CNEW(IP)).GT.ERR*CNEW(IP))  INDEX=1
      CNEW(IP)=CC(IP)
      SNEW(IP)=A*B*CNEW(IP)/(1.+B*CNEW(IP))
      IF (INDEX.EQ.1)  GO TO 70
      T=T+DELT
      KO=KO+1
       IF (KO .LT. KOUNT) GO TO 80
       WRITE (6,300) T,CNEW(IP),CNEW(L)
      KO=0
   80 CONTINUE
       IF ( T .GT. (TEND-PROF)) GO TO 1
      IF (T.LE.SUB) GO TO  91
      DELT=NEXT
      KOUNT=KANG
      SUB=SUB1
      SUB1=SUB2
      SUB2=SUB3
      NEXT=NEXT1
      NEXT1=NEXT2
      NEXT2=NEXT3
   91 CONTINUE
      DO 10 I=LL,IP
      CTEMP(I)=C(I)
      STEMP(I)=S(I)
      C(I)=CNEW(I)
      S(I)=SNEW(I)
      SNEW(I)=SNEW(I)+(SNEW(I)-STEMP(I))
   10 CNEW(I)=CNEW(I)+(CNEW(I)-CTEMP(I))
      GO TO 70
  300 FORMAT (// 3E14.6)
      END
```

APPENDIX B

COMPUTER PROGRAM FOR EXPLICIT FINITE DIFFERENCE SOLUTION TO FILM AND PORE DIFFUSION WITH NON-LINEAR ADSORPTION - INFINITE-BATH

```
      DIMENSION C(100)
      NAMELIST /INPUT/ P,DELT,TEND,PROF,KOUNT,GAM,F1,F2, L, EPS
    1 READ (5,INPUT)
      WRITE (6,INPUT)
      KP=P+ .1
      DELR= 1./P
      NO=0
      DO 50  J=1,KP
   50 C(J)=0
      T=0.
   70 M=KP
   60 EM=M-1
      COEF= DELT/DELR**2.
      IF(M-1) 42,42,43
   43 IF(M .EQ. KP) GO TO 48
      CALL TERMS (EM, C(M+1), C(M), C(M-1), VAR)
      GO TO 45
   42 CALL TONE (C(2), C(1), VAR)
      GO TO 45
   48 CALL TERM (EM, C(M), C(M-1), GAM, DELR, VAR)
   45 DIFF= COEF*VAR
      R= F1*F2/ (( 1. + F2*C(M))**2.)
      CC=DIFF/ (EPS + R)
      C(M)= CC+ C(M)
      M=M-1
      IF (M-1) 51,60,60
   51 CONTINUE
      NO=NO+1
      T=T+DELT
      IF (NO .LT. KOUNT)  GO TO 89
      NO=0
      GRAD=GAM*(1.- C(KP))
      WRITE (6,301) T,GRAD,C(L)
   89 IF (T-(TEND-PROF)) 70,70,1
  301 FORMAT (3F20.4)
      END
      SUBROUTINE TERM (X,Y,YY,G,D,Z)
          Z=2.* ((X+1.)*G*D-(X*G*D+ G*D +X)*Y+ X*YY)/X
           RETURN
      END
      SUBROUTINE TERMS (X, YF, Y,YY,Z)
          Z=((X+1.)*YF-2.*X*Y+ (X-1.)*YY)/X
           RETURN
      END
      SUBROUTINE TONE (Y, YY, Z)
          Z=6.*(Y-YY)
           RETURN
      END
```

PRINCIPLE SYMBOLS USED IN COMPUTER PROGRAM

P = NUMBER OF DIMENSIONLESS DISTANCE STEPS

DELT = LENGTH OF DIMENSIONLESS TIME STEP

EPS = POROSITY

TEND = TOTAL DIMENSIONLESS TIME

KOUNT = COUNTER FOR PRINT OUT

GAM = DIMENSIONLESS RATIO $k_f\ a/D$

E1 = DIMENSIONLESS LANGMUIR MONOLAYER COVERAGE, Q

E2 = DIMENSIONLESS LANGMUIR ENERGY OF ADSORPTION, B

I = TERMINAL DISTANCE STEP FOR CALCULATION OF CONCENTRATION PROFILE

DELR = LENGTH OF DISTANCE STEP

C(J) = DIMENSIONLESS CONCENTRATION AT DISTANCE STEP J

TERMS(EM,C(M+1),C(M),C(M-1),VAR) = SUBROUTINE TO CALCULATE C(J) WITHIN PARTICLE (SEE EQN 6-16)

TONE (C(2),C(1),VAR) = SUBROUTINE TO CALCULATE C(J) AT CENTER OF PARTICLE

TERM (EM,C(M),C(M-1),GAM,DELR,VAR) = SUBROUTINE TO CALCULATE SURFACE CONCENTRATION C(KP) (SEE EQN 6-15)

T = CURRENT VALUE OF DIMENSIONLESS TIME

GRAD = DIMENSIONLESS SURFACE FLUX (SEE EQN 6-5)

APPENDIX C

CORRELATION OF MASS TRANSFER COEFFICIENTS

For dilute mass transfer in an agitated mixing vessel, the average mass transfer coefficient, $k_{f,local}$, for any given location on the surface at which transfer occurs can be described by

$$k_{f,local} = f(\, P/v,\ \vec{L},\ \rho_f,\ \mu_f,\ D_{AB}\,) \qquad \text{(C-1)}$$

where P/v is the power input per unit volume produced by the stirring blade; $\vec{L}$, the length vectors describing the shape of the system; ρ_f, the density of the fluid; μ_f, the viscosity of the fluid; and D_{AB}, the free-liquid diffusivity of the component being transferred. Interestingly enough, investigators[1,2] have found the transfer coefficient to be independent of particle size in agitated vaessels; the same conclusion was reached in this study (see Table 5-7). All other length vectors, $\vec{L}$, may be neglected in Equation C-1 since these remained constant in the system investigated and thus Equation C-1 may be rewritten as

$$k_{f,local} = f(\, P/v,\ \rho_f,\ \mu_f,\ D_{AB}\,) \qquad \text{(C-2)}$$

The equations for dimensional analysis are as follows:

$$\frac{L}{T} = \left[\frac{M}{LT^3}\right]^a \left[\frac{M}{L^3}\right]^b \left[\frac{M}{LT}\right]^c \left[\frac{L^2}{T}\right]^d \qquad \text{(C-3)}$$

---

[1] Miller, D. N., "Liquid Film Controlled Mass Transfer in Agitated Vessels", Ind. and Eng. Chem., 56 18 (1964).

[2] Calderbank, P.H. and Moo-Young, M. B., "The Continuous Phase Heat and Mass-Transfer Properties of Dispersions", Chem. Eng. Sci., 16 39 (1961).

$$\sum M \qquad 0 = a + b + c \tag{C-4}$$

$$\sum L \qquad 1 = -a - 3b - c + 2d \tag{C-5}$$

$$\sum T \qquad -1 = -3a - c - d \tag{C-6}$$

Since there are four variables and only three dimensions, dimensional analysis leaves one exponent undetermined. Solving Equation C-4 for c, substituting for c in Equations C-5 and C-6 and solving the resulting two equations simultaneously gives

$$a = 1/4 \tag{C-7}$$

The exponents b and c may then be obtained in terms of d by solving Equations C-5 and C-6 for b and c respectively. Thus,

$$k_{f,\mathrm{local}} = f\left[(P/v)^{1/4},\ (\rho_f)^{d-1/2},\ (\mu_f)^{1/4-d},\ (D_{AB})^{d}\right] \tag{C-8}$$

Regrouping yields

$$k_{f,\mathrm{local}} = f\left[\left[\frac{\frac{P}{\overline{V}}\mu_f}{\rho_f^{2}}\right]^{1/4},\ \left[\frac{\rho_f D_{AB}}{\mu_f}\right]^{d}\right] \tag{C-9}$$

The concentration gradient is the same everywhere on the surface (a model assumption) and therefore

$$k_{f,\mathrm{local}} = k_f \tag{C-10}$$

From boundary layer theory[1], it may be shown that

---

[1] Miller, D. N., "Liquid Film Controlled Mass Transfer in Agitated Vessels", Ind. and Eng. Chem., 56 18 (1964).

$$k_f \propto (D_{AB})^{2/3} \qquad \text{(C-11)}$$

This has also been experimentally established[1]. Allowing the exponent d to therefore be two-thirds in Equation C-9 and recognizing this group as the inverse of N_{Sc} gives

$$k_f = C \left[\frac{\frac{P}{V} \mu_f}{\rho_f^{\,2}} \right]^{1/4} \Big/ (N_{Sc})^{2/3} \qquad \text{(C-12)}$$

Calderbank and Moo-Young[2] applied equations of local isotropic turbulence to estimate velocity in calculating a Reynolds number for use in the functional relationship between the Sherwood, Schmidt and Reynolds number for mass transfer given by

$$N_{Sh} \propto \left[N_{Re} \right] \cdot \left[N_{Sc} \right] \qquad \text{(C-13)}$$

where

$$N_{Sh} = \frac{k_f \, d}{D_{AB}} = \text{Sherwood Number} \qquad \text{(C-14)}$$

$$N_{Re} = \frac{\rho_f^{\,1/3} \, (P/v)^{1/6} \, d^{\,2/3}}{\mu_f^{\,1/2}} = \text{Reynolds Number} \qquad \text{(C-15)}$$

and d represents the particle diameter. After assuming

$$k_f \propto (D_{AB})^{2/3}$$

and k_f independent of particle size, Equation C-12 was obtained.

[1] Miller, D.N., "Liquid Film Controlled Mass Transfer in Agitated Vessels", Ind. and Eng. Chem., 56 18 (1964).

[2] Calderbank, P. H. and Moo-young, M. B., "The Continuous Phase Heat and Mass-Transfer Properties of Dispersions", Chem. Eng. Sci., 16 39 (1961).

CALCULATION OF POWER

A modified Reynolds number, which is based on impeller diameter and stirring speed, has been related to power dissipation for standard baffling arrangements and propellers. Because the experimental system used in this study was not of standard design, it was desirable to experimentally obtain power as a function of stirring speed. This was accomplished by measuring the angle of rotation of a disk on which the mixing vessel had been placed and calculating the corresponding torque and power. The assembly was suspended by three piano wires while the stirring motor was independently supported. The components of force on each wire are shown as follows:

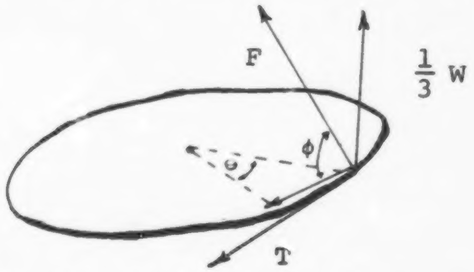

The force of interest is T acting tangentially to the disk. Rotation in the plane of the disk is represented by the angle designated as θ while ϕ is the angle formed by the piano wire and the plane of the disk. The vertical component of force in each wire is equal to one-third the weight of the disk, vessel and water. Upon a simple force analysis, torque may be expressed in terms of angular deflection according to Equation C-16.

$$\text{Torque} = \frac{R \cdot W \cdot \cos(\theta/2) \cdot \frac{2R}{L} \sin(\theta/2)}{\sqrt{1 - \left[\frac{2R}{L} \cdot \sin(\theta/2)\right]^2}} \tag{C-16}$$

CALCULATION OF POWER

A modified Reynolds number, which is based on impeller diameter and stirring speed, has been related to power dissipation for standard baffling arrangements and propellers. Because the experimental system used in this study was not of standard design, it was desirable to experimentally obtain power as a function of stirring speed. This was accomplished by measuring the angle of rotation of a disk on which the mixing vessel had been placed and calculating the corresponding torque and power. The assembly was suspended by three piano wires while the stirring motor was independently supported. The components of force on each wire are shown as follows:

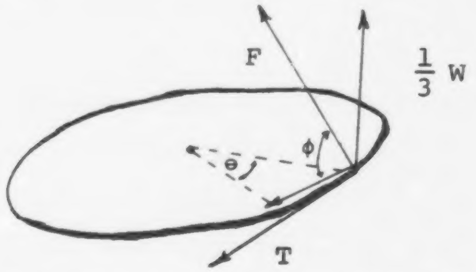

The force of interest is T acting tangentially to the disk. Rotation in the plane of the disk is represented by the angle designated as θ while ϕ is the angle formed by the piano wire and the plane of the disk. The vertical component of force in each wire is equal to one-third the weight of the disk, vessel and water. Upon a simple force analysis, torque may be expressed in terms of angular deflection according to Equation C-16.

$$\text{Torque} = \frac{R \cdot W \cdot \cos(\theta/2) \cdot \frac{2R}{L} \sin(\theta/2)}{\sqrt{1 - \left[\frac{2R}{L} \cdot \sin(\theta/2)\right]^2}} \qquad \text{(C-16)}$$

The values of radius R, force W, and length L, were 10 cm, 4.8×10^6 dynes and 288 cm respectively. Lateral movement of the disk was damped by means of a nail protruding from below the disk into an oil bath. A circular fin was attatched above the tip of the nail, which loosely fit into a hole in an inverted can submerged in the oil bath. Angular deflection θ was measured for motor speeds of 450, 600, 650, 950, 1200, 1400, 1600 and 1700 rpm and ranged from 0.76° to 13°. The product of torque and angular velocity is power as given by Equation C-17.

$$\text{Power} = \text{Torque} \cdot \frac{\text{rpm}}{60} \cdot 2\pi \qquad \text{(C-17)}$$

RESULTS

The power dissipation-stirring speed relationship from these experiments is shown in Figure C-1 along with that calculated by Rushton[1] for a propeller with pitch equal to twice the diameter and four baffles, each 0.1 the tank diameter in width. In contrast, the experimental system employed in this study consisted of two baffles, each 0.2 the tank diameter in width and a polyethylene propeller, which, although easily deformed, was of pitch close to that given by Rushton[1]. It may be noted that the experimental data agrees quite closely with that obtained by Rushton despite differences in baffling and propeller shape.

In Figure C-2, all values of k_f obtained from the finite and infinite-bath experiments have been plotted versus

$$\left[\frac{\frac{P}{V} \cdot \mu_f}{\rho_f^2}\right]^{1/4} \Bigg/ (N_{Sc})^{2/3}$$

on logarithmic scale. Included are the k_f values calculated

---

[1] Rushton, J. H., Costich, E. W. and Everett, H. J., "Power Characteristics of Mixing Impellers", Chem. Eng. Prog. Part II, 46 467 (1950).

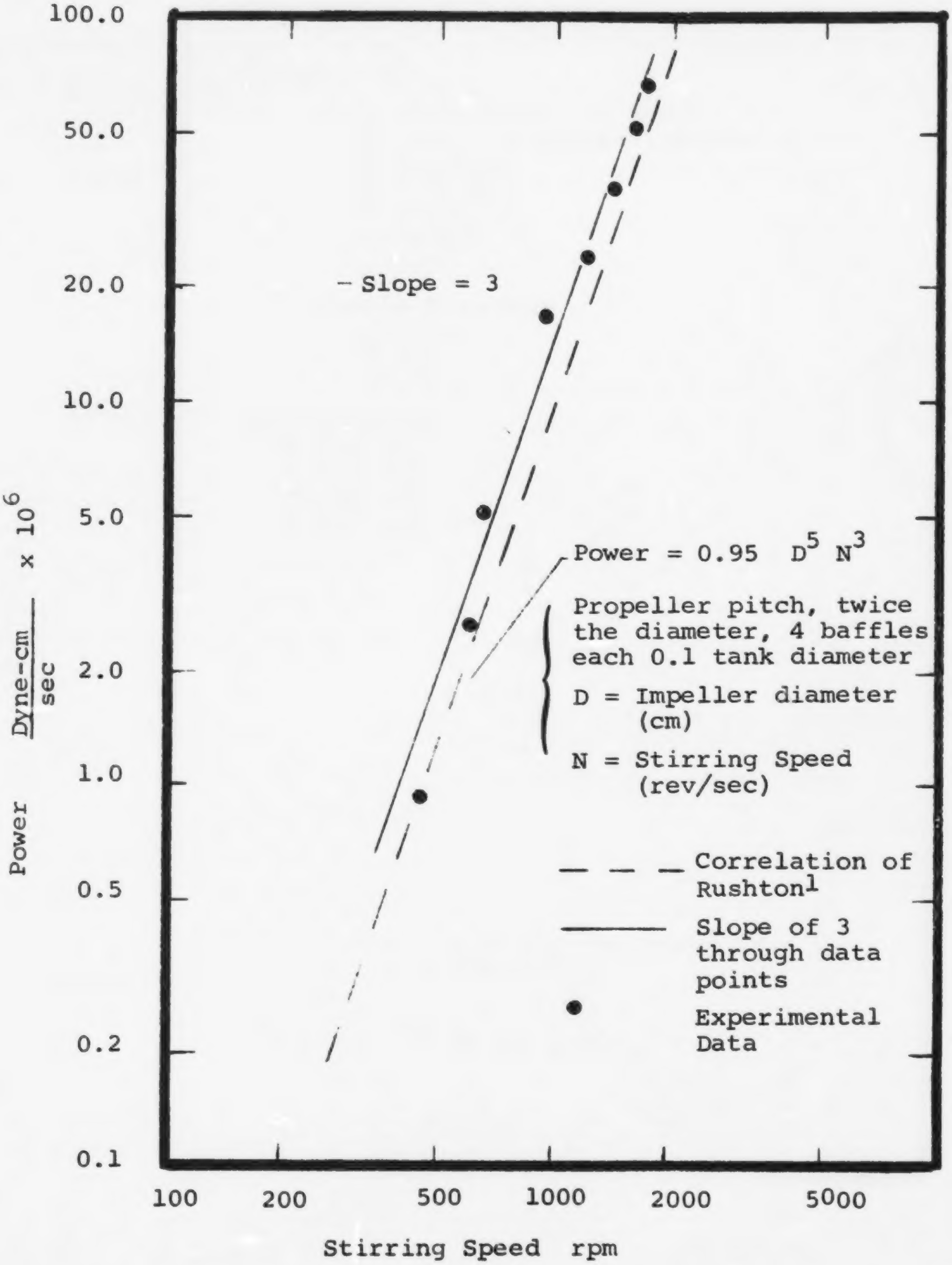

FIGURE C-1. CORRELATION OF POWER WITH STIRRING SPEED

---

[1] Rushton, J. H., Costich, E. W. and Everett, H. J., " Power Characteristics of Mixing Impellers", _Chem. Eng. Prog. Part II_, _46_ 467 (1950).

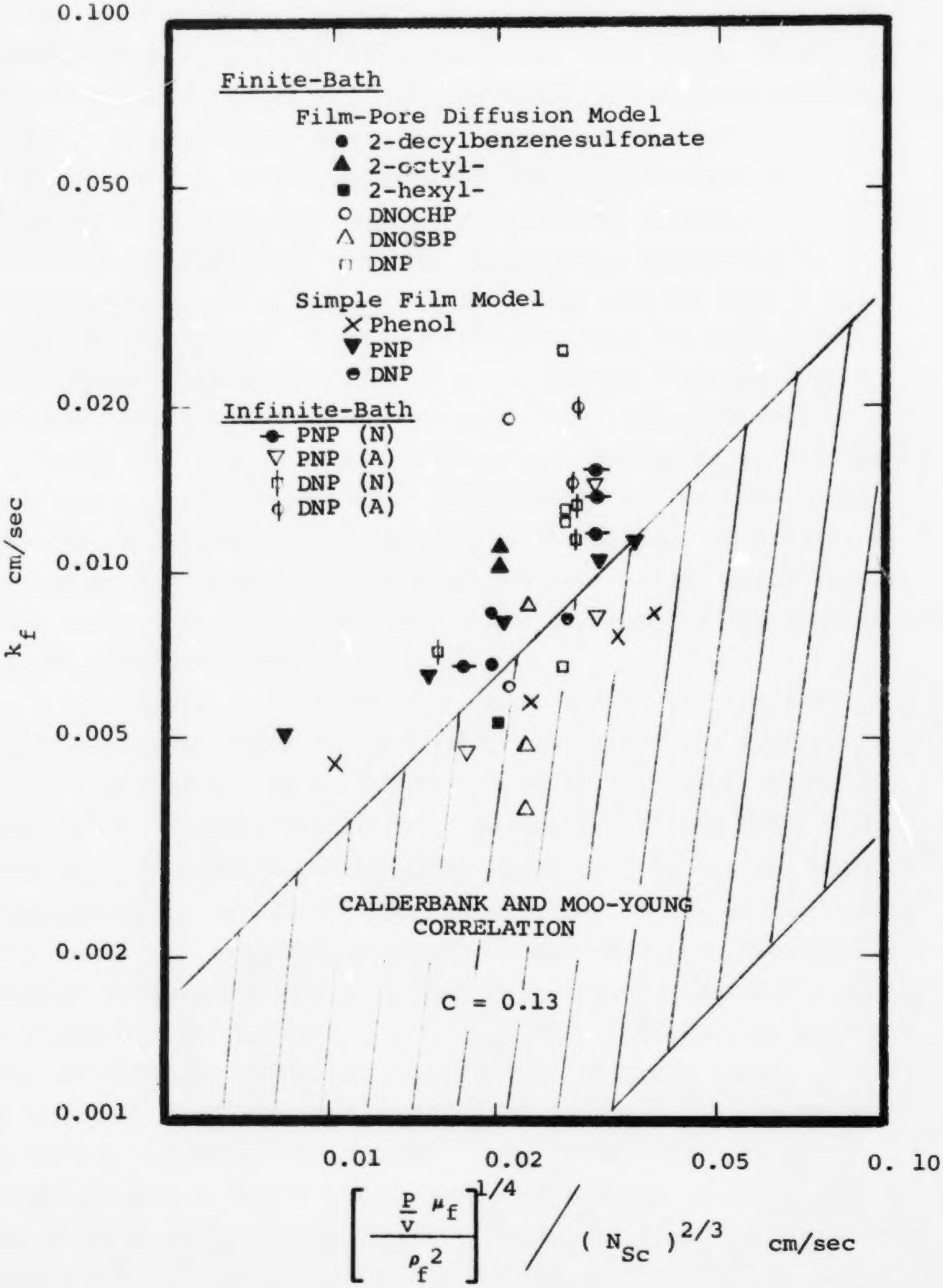

FIGURE C-2 . CORRELATION OF TRANSFER COEFFICIENTS using the combined film and pore diffusion model with irreversible adsorption (Equation 5-36), the simple film model (Equation 5-40) and the combined film and pore diffusion model with non-linear adsorption (Equations 6-1 to 6-4). According to the correlation developed and presented in Equation C-12, the slope of the plot should be equal to one. The envelope enclosing the data compiled by Calderbank and Moo-Young[1] for various mass and heat transfer systems is also shown in Figure C-2. They calculated a value of 0.13 for C, the constant appearing in Equation C-12,with transfer coefficients ranging over seven orders of magnitude. As shown in Figure C-2, the scatter of their data is rather substantial over one order of magnitude. Furthermore, the authors state that variations in the abscissa were largely due to variations in the Schmidt number rather than the power dissipation factor. Thus the correlation is largely a confirmation of the coefficient of the Schmidt number.

From Figure C-2 it may be concluded that the transfer coefficients obtained in this study are within the range to be expected for mass transfer in agitated vessels based on comparison of results with those of Calderbank and Moo-Young[1]. However, the correlation given by Equation C-12 has not been experimentally verified to the extent that it may be used to calculate k_f. It is interesting to note that mass transfer in aqueous systems for a wide range of molecular size will yield a relatively constant value of $(N_{Sc})^{2/3}$. Power dissipation may increase two orders of magnitude as stirring speed increases from 450 to 1700 rpm, but $(P/v)^{1/4}$ of Equation C-12 increases by only a factor of about three. The correlation therefore suggests that a rather narrow range of transfer coefficients can be expected in such systems. Moreover, increasing stirring increases turbulence and power dissipation while affecting the hydrodynamics of the boundary layer surrounding the particles to a much lesser extent. This is evidenced by the results given in Table 5-6, in which k_f was noted to approximately double upon increasing stirring speed from 275 to 1550 rpm.

---

[1] Calderbank, P. H. and Moo-Young, M. B., " The Continuous Phase Heat and Mass-Transfer Properties of Dispersions", Chem. Eng. Sci., 16 39 (1961).

LIST OF REFERENCES

1. Adamson, A. W., Physical Chemistry of Surfaces, p. 568; Interscience Publishers, New York, London, (1967).

2. Allen, J. B., and Joyce, R. S., "Column Calculations for Intraparticle Diffusion Controlled Adsorption", Chem. Eng. Progr. Symp. Ser. 74, 63 (1967).

3. Anon., "Advanced Waste Treatment Plant Running Well", Environ. Sci. and Tech., 2, 750 (1968).

4. Brecher, L. E., Kostecki, J. A., Camp, D. T., "Combined Diffusion in Batch Adsorption Systems Displaying B.E.T. Isotherms: Part I", Chem. Eng. Progr. Symp. Ser. 74, 63 (1967).

5. Burleson, N. K., Eckenfelder, W. W., Jr., and Malina, J. F., "Tertiary Treatment of Secondary Industrial Effluents by Activated Carbon", paper presented at the 23rd Industrial Waste Conference, Purdue University, Lafayette, Ind. (May 1968).

6. Buzzell, J. C., Jr., Adsorption of Phenols on Activated Carbon", Ph.D. Thesis, Dissertation Abstracts 27 No. 2, p. 453 B (Aug. 1966).

7. "Calgon Activated Carbon Product Bulletin", #AC7-556, Calgon Corporation, Pittsburgh, Pa.

8. Carslaw, H. S., and Jaeger, J. C., Conduction of Heat in Solids, p. 237; Clarendon Press (1959).

9. "Columbia Activated Carbon Product Bulletin", Supplement to Catalog Section S-6450 Data Sheet No. 12, National Carbon Company Div. of Union Carbide Corporation, New York, N. Y.

10. Coughlin, R. W., and Ezra, F. S., "Role of Surface Acidity in the Adsorption of Organic Pollutants on the Surface of Carbon", Environ. Sci. and Tech. 2, 291 (1968).

11. Crank, J., "A diffusion Problem in which the Amount of Diffusing Substance is Finite. - II. Diffusion with Non Linear Adsorption." Phil. Mag., 39 140 (1948).

12. Crank, J., Mathematics of Diffusion, Clarendon Press, London (1965).

13. Crank, J., "Diffusion with Rapid Irreversible Immobilization", Faraday Society Transactions, 53, 1083 (1957).

14. Culp, R. L., "Wastewater Reclamation at South Tahoe Public Utilities District", J. AWWA, 60, 84 (1968).

15. Dedrick, R. L., and Beckman, R. B., "Kinetics of Adsorption by Activated Carbon from Dilute Aqueous Solution", Chem. Eng. Prog., Symp. Ser. 74, 63 (1967).

16. Edeskuty, F. J., and Amundson, N. R., "Mathematics of Adsorption. IV. Effect of Intraparticle Diffusion in Agitated Static Systems", J. Phys. Chem., 56, 148 (1952).

17. Edeskuty, F. J. and Amundson, N. R., "Effect of Intraparticle Diffusion - Agitated Nonflow Adsorption Systems", Ind. and Eng. Chem. 44, 1698 (1952).

18. Helfrich, F., Ion Exchange, p. 256; McGraw-Hill Book Company, Inc. (1962).

19. Hougen, O. A., and Watson, K. M., Chemical Process Principles - Part Three Kinetics and Catalysis pp. 982-987; Wiley, New York 1964.

20. Hougen, O. A., Watson, K. M., Ragatz, R. A., Chemical Process Principles Charts 2 ed., Wiley, New York 1960.

21. Joyce, R. S., and Sukenik, V. S., Feasibility of Granular Activated-Carbon Adsorption for Waste-Water Renovation, AWTR-10, Environmental Health Series, Water Supply and Pollution Control, U. S. Dept. of Health, Education and Welfare (May 1964).

22. Keinath, T M., and Weber, W. J., Jr., "A Predictive Model for the Design of Fluid-Bed Adsorbers", J. Water Poll. Control Fed. 40, 743 (1968).

23. Keinath, T. M., Research Associate in Water Resources Engineering, The University of Michigan, personal communication.

24. Kipling, J. J., Adsorption from Solutions of Non-Electrolytes p. 263; Academic Press, London, New York (1965).

25. Levich, V. G., Physiochemical Hydrodynamics, p. 87; Translated by Scripta Technica, Inc., Englewood Cliffs, N. J., Prentice-Hall, (1962).

26. Lightfoot, E N., Sanchez-Palma, R. J., and Edwards, D. O., "Chromatography and Allied Fixed-Bed Separations Processes", New Chemical Engineering Separation Techniques by Schoen, H. M., Interscience Pub. (1962).

27. Mattson, J. S., Mark, H. B., Malbin, M. D., Weber, W. J., Jr., and Crittenden, J. C., "Surface Chemistry of Active Carbon: Specific Adsorption of Phenols", Adsorption from Solution Symposium at Case Western Reserve University, Cleveland, Ohio, June 23-25 (1969).

28. Morris, J. C., and Weber, W. J., Jr., Adsorption of Biochemically Resistant Materials from Solution .1., AWTR-9, Environmental Health Series, Water Supply and Pollution Control, U. S. Dept. of Health, Education and Welfare (May 1964).

29. Schwartz, H. G., Jr., "Adsorption of Selected Pesticides on Activated Carbon and Mineral Surfaces", Environ. Sci. and Tech. 1, 333 (1967).

30. Snoeyink, V. L., and Weber, W. J., Jr., Adsorption of Strong Acids, Phenol and 4-Nitrophenol by Active Carbon in Agitated Non-Flow Systems, Ph.D. Thesis, University of Michigan, Ann Arbor, Mich. (1968).

31. Snoeyink, V. L., and Weber, W. J., Jr., "Reaction of the Hydrated Proton with Active Carbon", Adsorption from Aqueous Solution, Advances in Chemistry Series 79, 10, p. 112 (1968).

32. Smith, S. B., Hiltgen, A. X., and Juhola, A. J., "Kinetics of Batch Adsorption of Dichlorophenol on Activated Carbon", Chem. Eng. Prog. Symp. Ser. 24, 55, 25 (1959).

33. Summary Report - The Advanced Waste Treatment Research Program; June 1960 - December 1961, SEC TR W62-9, U. S. Dept. of Health, Education and Welfare, (May 1962).

34. Thomas, H. C., "Chromatography: A Problem in Kinetics", Ann. N.Y. Acad. Sci. 49, 161 (1948).

35. Tien, Chi, "Mathematics of Diffusion for Non Linear Adsorption", J.AIChE 1, 410 (1961).

36. Vermeulen, T., "Separation by Adsorption Methods", Adv. Chem. Eng. 2, 147 (1958), Academic Press, New York.

37. Weber, W. J., Jr., and Gould, J. P., "Sorption of Organic Pesticides from Aqueous Solution", Advances in Chemistry Series, Number 60 "Organic Pesticides in the Environment" 23, (1966).

38. Weber, W. J., Jr., and Morris, J. C., "Kinetics of Adsorption on Carbon from Solution", ASCE, SED, SA 2, 31 (1963).

39. Weber, W. J., Jr., and Morris, J. C., "Adsorption in Heterogeneous Aqueous Systems", J. AWWA 56, 447 (1964).

40. Weber, W. J., Jr., and Morris, J. C., "Equilibria and Capacities for Adsorption on Carbon", ASCE, SED, SA 3, 79 (1964).

41. Weber, W. J., Jr., and Rumer, R. R., Jr., "Intraparticle Transport of Sulfonated Alkylbenzenes in a Porous Solid: Diffusion with Non Linear Adsorption", Water Resources Research 3, 361 (1965).

42. Weisz, P. B., "Sorption - Diffusion in Heterogeneous Systems; Part 1. - General Sorption Behavior and Criteria", Faraday Society Transactions, 63, 1801 (1967).

43. Weisz, P. B., "Sorption - Diffusion in Heterogeneous Systems; Part 3. - Experimental Models of Dye Sorption", Faraday Society Transactions 63, 1815 (1967).

44. Wilke, C. R., and Chang, P., "Correlation of Diffusion Coefficients in Dilute Solutions", J. AICHE 1, 264 (1955).